INVESTIGATION OF LAND SUBSIDENCE AND EARTH FISSURES IN CEDAR VALLEY, IRON COUNTY, UTAH

by Tyler Knudsen, Paul Inkenbrandt, William Lund, Mike Lowe, and Steve Bowman

INVESTIGATION OF LAND SUBSIDENCE AND EARTH FISSURES IN CEDAR VALLEY, IRON COUNTY, UTAH

by Tyler Knudsen, Paul Inkenbrandt, William Lund, Mike Lowe, and Steve Bowman

UTAH
DNR
GEOLOGICAL SURVEY

CONTENTS

FIGURES

TABLES

APPENDICES

INVESTIGATION OF LAND SUBSIDENCE AND EARTH FISSURES IN CEDAR VALLEY, IRON COUNTY, UTAH

by Tyler Knudsen, Paul Inkenbrandt, William Lund, Mike Lowe, and Steve Bowman

ABSTRACT

In May 2009, Enoch City contacted the Utah Geological Survey (UGS) to investigate a possible "fault" that was damaging streets, sidewalks, and curbs and gutters in the Parkview subdivision in north Enoch. During a reconnaissance investigation, the UGS found a 2.5-mile-long (trace length) earth fissure that had formed in response to land subsidence that appeared to be caused by groundwater overdraft of the local aquifer. In the affected subdivision, the fissure crosses several undeveloped lots, and in addition to damaging streets and sidewalks, vertical displacement across the fissure had reversed the flow direction of a sewer line so that it is no longer possible to gravity-drain sewage from the subdivision. The likely relation of the fissure to groundwater pumping was communicated to Enoch City, the Utah Division of Water Rights, Iron County, and the Central Iron County Water Conservancy District. The UGS subsequently conducted a detailed investigation of the Enoch earth fissure, and investigated the remainder of Cedar Valley to determine if land subsidence and earth fissures were also affecting other areas.

Results of the investigation showed that groundwater discharge in excess of recharge has lowered the potentiometric surface in Cedar Valley by as much as 114 feet since 1939. Basin-fill sediments of the Cedar Valley aquifer contain a high percentage of fine-grained material susceptible to compaction upon dewatering. Lowering the potentiometric surface (head decline) by groundwater pumping in excess of annual aquifer recharge has caused permanent compaction of fine-grained sediments of the Cedar Valley aquifer. Currently, the largest identified subsidence at an existing benchmark in Cedar Valley is 0.9 feet near Enoch City; however, vertical displacement across the Enoch-graben-west fissure zone is about 3 feet in some locations. Recently acquired interferometric synthetic aperture radar imagery shows that land subsidence is occurring over a broad area in central Cedar Valley, but a lack of historical accurate benchmark elevation data over much of the valley prevents its detailed quantification.

In response to the land subsidence, a minimum of 8.3 miles (trace length) of earth fissures have formed in the southwestern and northeastern parts of Cedar Valley. The Enoch-graben-west fissures are the most extensive zone of fissuring and include the only fissures that exhibit ongoing vertical offset. Fissure-related infrastructure damage in Cedar Valley is currently limited to the partially developed Parkview subdivision in Enoch City and a stock-watering pond west of Quichapa Lake. Cracked pavement at the north end of the Legacy Estates subdivision, also in Enoch, appears to be fissure-related. The largest of the Enoch-graben-west fissures trends through and has displaced the ground surface in a livestock pasture/feeding area, creating a potential for groundwater contamination. Aerial photographs show that the largest Enoch-graben-west fissure began forming more than 50 years ago, and that the fissure grew approximately 800 feet to the south between 1997 and 2006. Photolineaments of unknown origin and the presence of an isolated sinkhole and fissure south of State Route 56 and generally along trend with the fissures west of Quichapa Lake indicate the possibility of a more extensive zone of fissuring along the western margin of Cedar Valley.

Based on the investigation results, we conclude the following:

1. Long-term groundwater pumping in excess of recharge (groundwater mining) is the cause of the land subsidence and earth fissures in Cedar Valley.

2. The maximum amount of land subsidence and earth fissure formation in Cedar Valley coincide with areas of significant groundwater-level decline and the presence of compressible fine-grained sediment in the subsurface.

3. If groundwater levels in Cedar Valley continue to decline at a rate of approximately 2 feet per year, average basin-wide subsidence will likely continue at a rate of 0.02 to 1.2 inches per year.

4. Continued subsidence will likely cause new fissures to form in the future.

5. The inventory of earth fissures in Cedar Valley is likely incomplete because fissures lacking offset or not enlarged by erosion typically exist as hairline cracks that are rarely visible on aerial photographs and are difficult to identify in the field.

6. Currently unrecognized or new earth fissures may damage existing and future infrastructure in Cedar Valley.

7. Continued southward growth of either the Enoch-graben-west or -east fissures may eventually impact fully developed neighborhoods in Enoch City.

8. Earth fissures could provide a direct path for contaminated surface water to reach the Cedar Valley aquifer, a principal source of potable water in Cedar Valley.

9. Managing basin-fill aquifers as a renewable resource and managing the hazards presented by land subsidence and earth-fissure formation require that subsiding areas and rates of subsidence within those areas (likely variable) be defined (technologies such as InSAR, LiDAR, and high-precision GPS/GNSS surveying are well suited to this task).

10. Site-specific hazard investigations are required for new development, and in some instances for existing development, in areas known or suspected to be subsiding. Recommended guidelines for conducting such investigations are included in appendix H of this report.

INTRODUCTION

Purpose

This report presents the results of an investigation by the Utah Geological Survey (UGS) of land subsidence and earth fissures in Cedar Valley, Iron County, Utah. On May 5, 2009, the UGS received a request from Enoch City to investigate a feature affecting a new subdivision in the northern part of that community. Earl Gibson, Enoch City Public Works Director, thought the feature might be an active fault. UGS geologists responded to the request and subsequently mapped a 2.5-mile-long, generally north-south-trending earth fissure that had formed along the west side of the Enoch graben (Rowley and Threet, 1976; Anderson and Christenson, 1989; Black and others, 2003; Knudsen, 2014a). The affected subdivision is near the south end of the fissure; there the fissure has formed in basin-fill deposits, crosses several undeveloped lots, and has cracked and vertically displaced asphalt concrete street surfaces, concrete curb and gutter, and sidewalks. Mr. Gibson stated that an inspection using a pipeline camera revealed that the flow direction of a sewer line crossing the fissure had been reversed, and that it was no longer possible to gravity-drain sewage from the subdivision. At the time of our reconnaissance, the streets, curb and gutter, and underground utilities in the subdivision were less than 18 months old.

Immediately north of the subdivision on undeveloped rangeland, we observed as much as 3 feet of down-to-the-east vertical displacement across the fissure, clearly indicating that grading for the subdivision had obscured the extent of pre-subdivision displacement to the south. Farther north, the fissure entered irrigated agricultural land; the land owner, Mr. Mike Clark, stated that the fissure had been active for at least

30 years. Continuing north, the fissure passed through a livestock pasture/feeding area before again entering undeveloped rangeland and apparently dying out.

Based on our field reconnaissance, examination of aerial imagery, and discussions with Mr. Gibson and Mr. Clark, we reached the following preliminary conclusions: (1) the feature is likely an earth fissure—not a fault, (2) the location of the fissure is controlled at least in part by a pre-existing Quaternary fault, (3) down-to-the-east displacement is actively occurring across the fissure, and (4) the likely cause of the fissure is aquifer compaction related to long-term groundwater pumping in excess of aquifer recharge.

On May 7, 2009, we presented our preliminary conclusions to Enoch City, the Utah Division of Water Rights, the Iron County Engineer, and the Central Iron County Water Conservancy District (CICWCD). Based on that information, the CICWCD requested that the UGS prepare a proposal and budget for a study to further investigate the Enoch earth fissure, and to expand our reconnaissance to determine if additional earth fissures and land subsidence features are present elsewhere in Cedar Valley. The CICWCD Board approved the UGS proposal, and the UGS and CICWCD entered into a Memorandum of Understanding to conduct the investigation starting in June 2009. We delivered a final report of the investigation results (Knudsen and others, 2012) to the CICWCD in March 2012. This UGS Special Study incorporates the results of the initial investigation prepared for the CICWCD and includes analyses of two new remote sensing datasets (interferometric synthetic aperture radar [InSAR; Katzenstein, 2013; appendix E] and light detection and ranging [LiDAR; Utah Geological Survey, 2011] technologies) that greatly enhance our understanding of the distribution and amplitude of subsidence and extent of fissures in Cedar Valley.

The UGS took the following steps to complete this investigation:

1. Mapped earth fissures and land-subsidence features in Cedar Valley using aerial photography, LiDAR data, and field reconnaissance.

2. Assessed and documented infrastructure and other development affected or potentially affected by earth fissures in Cedar Valley.

3. Quantified changes in land surface elevation in Cedar Valley by comparing historical elevation data measured at a limited number of available bench marks in the valley to newly acquired elevation data measured using global positioning system (GPS) methods, and compared subsidence results with a recently completed InSAR investigation of Cedar Valley.

4. Defined the current potentiometric surface (water table) in Cedar Valley based on existing water-level data and new water-level measurements by the UGS, compared the current potentiometric surface with earlier potentiometric-surface information from available historical water-level data, and prepared a map showing the extent and magnitude of water-level decline for the maximum period of record possible in Cedar Valley.

5. Defined the nature and extent of potentially compressible, fine-grained sediments in the subsurface in Cedar Valley by compiling existing well-log data for the valley, created simplified cross sections of the valley basin fill, and prepared a map of the extent of potentially compressible, fine-grained sediment in Cedar Valley.

6. Provided recommendations regarding additional investigations to better define the extent of subsidence and fissure formation, and possible aquifer management options to help mitigate subsidence and fissure formation.

7. Prepared recommended guidelines for investigating land-subsidence and earth-fissure hazards prior to development.

Principal Sources of Information

Principal sources of information used to evaluate land subsidence and earth fissures in Cedar Valley include:

1. nine 1:24,000-scale geologic quadrangle maps that cover the study area (see appendix A for geologic map references);

2. the 1:100,000-scale *Interim Geologic Map of the Cedar City 30' x 60' Quadrangle, Iron and Washington Counties, Utah* (Rowley and others, 2006);

3. *Geology and Ground-Water Resources of Cedar City and Parowan Valleys, Iron County, Utah* (Thomas and Taylor, 1946);

4. *Ground-Water Resources of the Parowan–Cedar City Drainage Basins, Iron County, Utah* (Bjorklund and others, 1978);

5. *The Geology of Cedar Valley, Iron County, Utah, and Its Relation to Ground-Water Conditions* (Hurlow, 2002);

6. 398 water-well driller's logs on file with the Utah Division of Water Rights (2010a);

7. eight sets of aerial photographs covering all or portions of the study area: (a) stereoscopic 1938 1:20,000-scale U.S. Department of Agriculture (USDA) Soil Conservation Service (Project BPI) photos, (b) stereoscopic 1960 USDA (Project DIE) 1:20,000-scale photos, (c) stereoscopic 1981 (Project 810941) 1:24,000-scale morning and afternoon low-sun-angle photos (Earth Sciences Associates, 1982, and compiled in Bowman and others, 2011), (d) 1993-1997 U.S. Geological Survey (USGS) orthophotography at various scales (Utah Automated Geographic Reference Center [Utah AGRC, 2013]), (e) 2006 National Agriculture Imagery Program (NAIP) orth photography at various scales (Utah AGRC, 2006a), (f) 2006 high-resolution orthophotography (HRO; Utah AGRC, 2006b), (g) 2009 NAIP orthophotography at various scales (Utah AGRC, 2009), and (h) 2011 NAIP orthophotography at various scales (Utah AGRC, 2011);

8. 1-meter LiDAR bare earth imagery (UGS, 2011);

9. a survey performed by a Utah licensed Professional Land Surveyor using real-time kinematic (RTK) GPS methods of 72 historical benchmarks in Cedar Valley having elevation data of varying accuracy (appendix D);

10. *InSAR Analysis of Ground Surface Deformation in Cedar Valley, Iron County, Utah* (Katzenstein, 2013; appendix E).

PREVIOUS WORK

Averitt (1962), Threet (1963a, 1963b), Averitt and Threet (1977), Williams and Maldonado (1995), Mackin and others (1977), and Maldonado and others (1997) studied the geology of the Cedar Valley area. Huntington and Goldthwait (1904), Mackin (1960), Averitt (1962), Hamblin (1970, 1984), Anderson and Mehnert (1979), Anderson (1980), Earth Sciences Associates (1982), Anderson and Christenson (1989), and Lund and others (2007) studied the Hurricane fault zone and discussed its significance as a source of large earthquakes and as a boundary between the Basin and Range and Colorado Plateau physiographic provinces. Blank and Mackin (1967) made a geologic interpretation of an aeromagnetic survey of the southwest part of the study area. Kaliser (1978a, 1978b) investigated ground surface subsidence related to hydrocollapsible soils in Cedar City, Utah.

Meinzer (1911) conducted a reconnaissance investigation of water resources in western Utah, including Cedar Valley, which he called Rush Lake Valley. Thomas and Taylor (1946) completed the first comprehensive investigation of ground-water conditions in Cedar and Parowan Valleys. Thomas and

others (1952) and Barnell and Nelson (in Waite and others, 1954, p. 75–84) provided descriptions of the status of groundwater development in Cedar Valley. Sandberg (1963, 1966) described the groundwater resources for selected basins in southwestern Utah, including Cedar Valley. Barnett and Mayo (1966) made recommendations regarding groundwater management and warned of a potential water-resources crisis in Cedar Valley. Bjorklund and others (1977, 1978) reevaluated groundwater conditions in Cedar and Parowan Valleys and produced water budgets for each valley. Howells and others (2002) provided selected hydrologic data for Cedar Valley collected from 1930 to 2001. Hurlow (2002) evaluated the relation of groundwater to geology in the Cedar Valley drainage basin. Brooks and Mason (2005) evaluated the hydrologic system and water quality in Cedar Valley, and developed a digital groundwater flow model for the basin-fill aquifer.

SETTING

Location and Physiography

Cedar Valley is in eastern Iron County, southwestern Utah (figure 1). It is a northeast-southwest-trending, elongate valley bordered by the Black Mountains to the north, the Markagunt Plateau to the east, the low-lying Eightmile Hills and The Three Peaks to the west, and the Harmony Mountains to the southwest. Cedar Valley is approximately 32 miles long and ranges from 8 miles wide at its northern end to less than 1 mile wide in the south. The floor of Cedar Valley covers 270 square miles; its drainage basin encompasses more than 580 square miles. Elevations range from about 10,750 feet on the west flank of Brian Head on the Markagunt Plateau to about 5350 feet at the valley drainage outlet at Mud Spring Wash in the northwest part of the valley.

Coal Creek, the principal perennial stream in Cedar Valley, flows westward from the Markagunt Plateau and has deposited a large alluvial fan in the Cedar City area (Bjorklund and others, 1978). Shurtz Creek, a smaller perennial stream flowing westward from the Markagunt Plateau, enters Cedar Valley near Hamiltons Fort. Fiddlers Canyon Creek, one of the larger intermittent streams flowing westward from the Markagunt Plateau, enters Cedar Valley in the north part of Cedar City. Quichapa Creek is a perennial stream flowing northeastward into the valley from the Harmony Mountains. Surface water flows westward out of Cedar Valley via Mud Spring Wash and through Iron Springs Gap only during rare flash floods caused by heavy local precipitation (Bjorklund and others, 1978). Spring runoff accumulates in Quichapa and Rush Lakes, which are shallow playa lakes (figure 1).

Population and Land Use

From 2000 to 2007, population in Iron County (most of the people in the county live in Cedar Valley) increased by 29%

from 33,779 to 43,526 (Demographic and Economic Analysis Section, 2008). Five years later, the U.S. Census Bureau estimated that there were 46,750 residents in Iron County in 2012 (most recent estimate available; U.S. Census Bureau, 2013). The projected population of Iron County is expected to be 104,000 by 2050 (Demographic and Economic Analysis Section, 2005).

Government, trade, and the service industry are the principal sources of employment in Iron County (Utah Division of Water Resources, 1995). Although agricultural land is being subdivided for residential and commercial uses, agricultural commodity production, mostly beef, dairy, and irrigated crops, will likely continue to be an important part of Cedar Valley's economy (Utah Division of Water Resources, 1995).

Climate

Cedar Valley's climate is characterized by large daily temperature variations; moderately cold winters; and warm, dry summers (Bjorklund and others, 1978). From 1947 to 2007, temperatures at Cedar City Airport ranged from a maximum of 105°F to a minimum of -26°F (Moller and Gillies, 2008); the maximum daily temperature variation is greatest in summer when fluctuations can be as much as 40°F (Ashcroft and others, 1992). The normal mean annual temperature at the Cedar City Airport was 50.9°F from 1947 to 2008 (Moller and Gillies, 2008). The growing season (the number of consecutive frost-free days) in Cedar Valley averages 133 days at the Cedar City Airport (Moller and Gillies, 2008).

Brian Head averages 35.7 inches (period of record 1991–2007) of precipitation annually (Moller and Gillies, 2008), mostly as snow during winter. Annual precipitation in Cedar Valley ranges from about 8 to 14 inches (Bjorklund and others, 1978). At the Cedar City Airport, normal mean annual precipitation was 11.41 inches and mean annual evapotranspiration was 49.11 inches from 1948 to 2007 (Moller and Gillies, 2008). Most precipitation is generated in winter and spring by humid air masses moving southeastward from the North Pacific (Bjorklund and others, 1978). Appreciable rain from summer thunderstorms results from humid air masses migrating northwestward from the Gulf of Mexico (Bjorklund and others, 1978). Snow is common in Cedar Valley from December through March, but snowstorms are not uncommon during April and even May (Bjorklund and others, 1978).

Geology

Cedar Valley is at the eastern margin of the Basin and Range physiographic province adjacent to the Markagunt Plateau, part of the High Plateaus section of the Colorado Plateau physiographic province (Stokes, 1977). At the latitude of Cedar Valley, the boundary between the Basin and Range and Colorado Plateau physiographic provinces is considered by many geologists to be the late-Quaternary-active, west-dip-
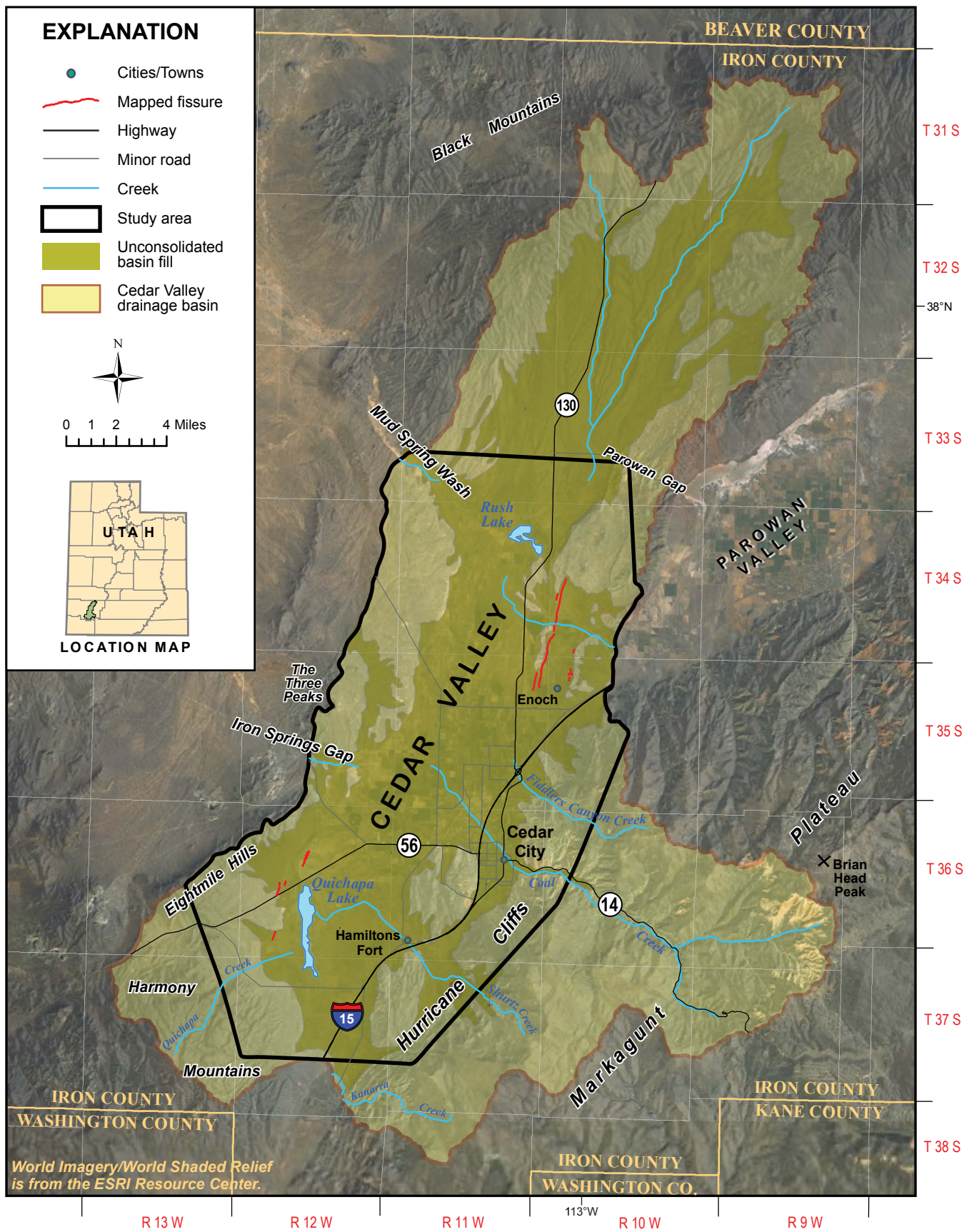
Figure 1. *Cedar Valley study area showing location of known earth fissures in relation to major physiographic features.*

ping, normal-slip Hurricane fault (figure 2) (e.g., Anderson and Mehnert, 1979; Anderson and Christenson, 1989; Lund and others, 2007), although a geologic transition zone up to several miles wide exists between the Basin and Range and Colorado Plateau proper. The trace of the Hurricane fault is marked by the steep Hurricane Cliffs (west face of the Markagunt Plateau), which are up to 2000 feet high (Hamblin, 1970). Total vertical displacement across the Hurricane fault in the vicinity of Cedar Valley is estimated between 1400 and about 5000 feet (Kurie, 1966; Anderson and Mehnert, 1979; Anderson and Christenson, 1989).

Other Quaternary-active, normal-slip faults present in Cedar Valley include the Enoch graben (west- and east-bounding faults), the Cedar Valley west side faults, and the Cross Hollow Hills faults (figure 2) (Black and others, 2003). Hurlow (2002) defined an eastern basin-bounding fault system (EBBFS), a complex zone of west-dipping normal faults that extends from south and west of the Cross Hollow Hills, northward to the western margin of the Red Hills (figure 2). The trace of the EBBFS is buried by young alluvium in Cedar Valley, but is expressed at the surface along the west margin of the Hieroglyph horst (Threet, 1963b; Williams and Maldonado, 1995) and the Red Hills, where it displaces a 1.28 ± 0.4 million-year-old basalt flow down to the west (Anderson and Christenson, 1989). Because it displaces a Quaternary-age basalt flow, the EBBFS is also Quaternary active.

The Hieroglyph horst consists of elevated Tertiary and Quaternary alluvial-fan deposits, and is bounded on its east side by the Enoch-graben-west fault. The EBBFS separates the larger, deeper Cedar Valley basin from the smaller, shallower Enoch graben sub-basin. The Enoch graben is a narrow structural basin along the northeast side of Cedar Valley bounded on the west by the Hieroglyph horst and on the east by the Red Hills (Threet, 1963b; Rowley and Threet, 1976; Anderson and Christenson, 1989; Black and others, 2003; Knudsen, in 2014a) (figure 2). Both the Enoch-graben-west and -east faults have formed fault scarps several to tens of feet high.

Hurlow (2002) and Rowley and others (2006) mapped concealed faults along the east side of the low hills bounding the west side of Cedar Valley (figure 2). Those faults may be coincident to the north with the late-Quaternary-active Cedar Valley west side faults (Black and others, 2003), indicating that the concealed western faults (herein named the western-basin-bounding fault system [WBBFS]) may also be Quaternary active.

Typical of many valleys in the Basin and Range physiographic province, Cedar Valley is an asymmetrical graben formed by vertical displacement along its valley margin faults. The asymmetry is due to greater displacement on the EBBFS (up to 7500 feet) to the east than on the WBBFS to the west. The resulting deep, asymmetric sag extends from west of the

Cross Hollow Hills northward to the western margin of the Red Hills (Hurlow, 2002) (figure 2). Bedrock is shallower east of the EBBFS beneath the Enoch graben and Cedar City. The Cross Hollow Hills are a horst block formed in a complexly faulted zone between the EBBFS on the west and the Hurricane fault on the east (figure 2).

The geomorphic characteristics of Cedar Valley are typical of many basin-and-range valleys. Valley margins consist of coalescing alluvial fans that slope gently basinward into a slightly undulating broad valley bottom. A low divide created by the Coal Creek alluvial fan separates Cedar Valley into two surface-water subbasins. The south basin drains into ephemeral Quichapa Lake and the north basin partly drains into ephemeral Rush Lake (figure 1).

Rock units in the Cedar Valley area range from Triassic to Quaternary in age. Bedrock and semiconsolidated basin-fill units have a maximum combined thickness of more than 16,000 feet (Bjorklund and others, 1978). The Markagunt Plateau east of the Hurricane Cliffs is composed chiefly of gently east-dipping Triassic to Tertiary sedimentary rocks capped locally by younger volcanic rocks (figure 2). Complexly faulted Miocene volcanic and plutonic rocks crop out in the hills west of the valley. Little is known about bedrock beneath Cedar Valley, but it likely consists of down-faulted sedimentary, volcanic, and plutonic rocks similar to those that crop out in the uplands surrounding the valley. Unconsolidated to poorly consolidated basin-fill deposits up to 3900 feet thick fill Cedar Valley (Cook and Hardman, 1967; Hurlow, 2002); these deposits attain their greatest thickness west of the EBBFS near Rush Lake in the northeastern part of Cedar Valley.

GROUNDWATER IN CEDAR VALLEY

Groundwater in the Cedar Valley drainage basin is present in two types of aquifers: fractured bedrock and basin-fill deposits. Fractured bedrock aquifers are recharged primarily from infiltration of precipitation and streamflow, and groundwater flows primarily through fractures. Because bedrock is typically rigid and not subject to compression upon removal of groundwater, we focus only on groundwater in basin-fill aquifers for this investigation.

Occurrence

The Cedar Valley basin-fill aquifer consists primarily of Quaternary and Tertiary alluvial sediments, composed of discontinuous, lenticular, commonly elongated, poorly to well-sorted layers of clay, silt, sand, gravel, and boulders (Thomas and Taylor, 1946), interbedded with volcanics and fine-grained lacustrine and eolian deposits (Bjorklund and others, 1978). Based on water-well data, Thomas and Taylor (1946) and Anderson and Mehnert (1979) estimated that basin fill is at least 1000 feet thick, but a gravity survey indicates basin fill
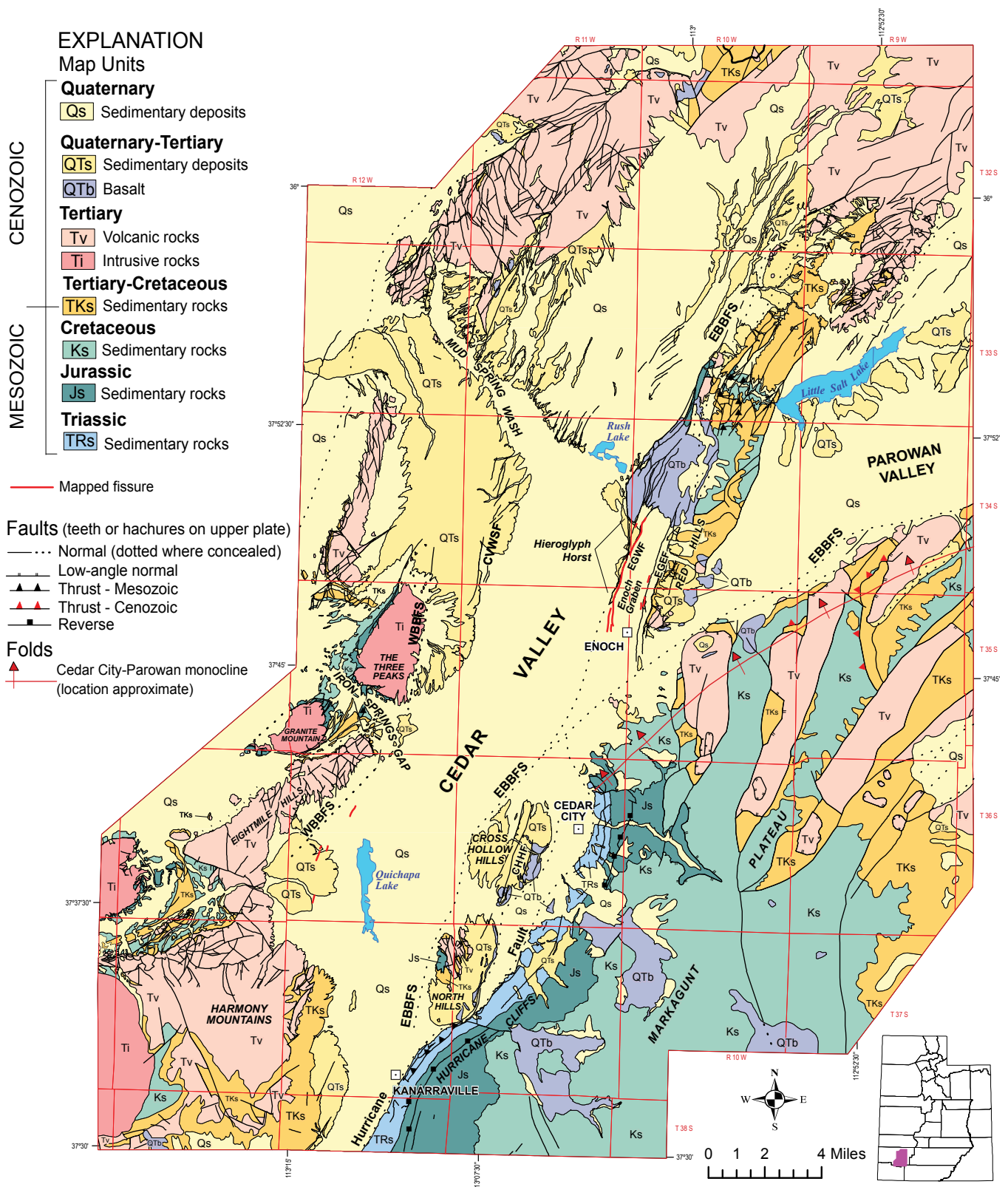
Figure 2. *Simplified geology of Cedar Valley drainage basin and adjacent areas (modified from Hurlow, 2002). WBBFS = western basin-bounding fault system, CVWSF = Cedar Valley west-side faults, EBBFS = eastern basin-bounding fault system, EGWF = Enoch-graben-west faults, EGEF = Enoch-graben-east faults, CHHF = Cross Hollow Hills faults.*

may be as much as 3900 feet thick in the eastern part of Cedar Valley (Cook and Hardman, 1967). Seismic-reflection profiles indicate the basin fill has a maximum thickness of 3800 feet near Rush Lake (Hurlow, 2002).

Groundwater in the basin-fill aquifer occurs under confined, unconfined, and perched conditions (Bjorklund and others, 1978). The basin-fill aquifer is generally unconfined along the upper-elevation margins of Cedar Valley, where it typically consists of coarse granular, permeable alluvial-fan sediments (Thomas and Taylor, 1946; Bjorklund and others, 1978). Low-permeability silt and clay interbeds overlie water-yielding, coarse-grained deposits in the central parts of the valley, creating leaky confined basin-fill aquifer conditions (Sandberg, 1966; Bjorklund and others, 1978). Low-permeability sediments are spatially extensive in the Cedar Valley aquifer (see Aquifer Characteristics section) and locally form effective confining beds or layers, but are not continuous enough to form major layers in the basin fill and cause the groundwater system to act as a single, complex aquifer (Thomas and Taylor, 1946). The boundary between confined and unconfined conditions is gradational, shifting as the potentiometric surface of the basin-fill aquifer system rises and falls with changes in recharge and discharge (Bjorklund and others, 1978). In 1939, upward groundwater gradients in the central, lower-elevation areas of Cedar Valley were sufficient to supply flowing (artesian) wells in an area that covered approximately 50 square miles (Thomas and Taylor, 1946, plate 18), but no flowing wells have existed in Cedar Valley since 1975 (Bjorklund and others, 1978) due to a lowered potentiometric surface resulting from groundwater mining.

Wells completed in alluvial deposits in Cedar Valley yield 1 to 4000 gallons per minute (Bjorklund and others, 1978). The most productive parts of the aquifer consist of beds of clean, well-sorted gravel and sand (Bjorklund and others, 1978). Using data from 10 wells in the Cedar Valley basin-fill aquifer, Sandberg (1966) calculated a range for specific capacity of 10 to 50 gallons per minute per foot of drawdown with an average of 28 gallons per minute per foot of drawdown. Bjorklund and others (1978) compiled data from six multiple-well aquifer tests completed in gravelly aquifer material in Cedar Valley and calculated a range for average hydraulic conductivity of 13 to 251 feet per day (ft/d), a transmissivity range of 2540 to 52,000 ft^2/d, and a storage coefficient range of 0.0005 to 0.2.

Groundwater flow is generally from higher-elevation recharge areas along the mountain front to lower-elevation discharge areas. In southern Cedar Valley, groundwater flows northward from the Kanarraville area, northeastward from the Harmony Mountains, and southeastward from the Eightmile Hills (Bjorklund and others, 1978, plate 5). Groundwater in the vicinity of the Coal Creek alluvial fan moves northward and northwestward from the apex of the fan and then either southward toward Quichapa Lake or westward toward Iron Springs Gap (Thomas and Taylor, 1946). Groundwater in northern Cedar Valley moves northwestward toward Rush Lake and then continues toward Mud Spring Wash (Bjorklund and others, 1978). Hydraulic gradients are generally low (with the exception of pumping-induced cones of depression) in the central, lower-elevation areas of Cedar Valley, such as near Quichapa Lake.

Quality

Because earth fissures can result in water-quality degradation, we present Cedar Valley's current groundwater quality. Groundwater quality in Cedar Valley is generally good and is suitable for most uses (Utah Division of Water Resources, 1995). Groundwater in the basin-fill aquifer is generally classified as calcium- or magnesium-sulfate type. Sodium-chloride-type groundwater is present near Rush Lake and calcium-bicarbonate-type groundwater is present southwest of Quichapa Lake (Bjorklund and others, 1978). Thomas and Taylor (1946) reported total dissolved solids (TDS) concentrations ranging from about 150 mg/L, just west of Quichapa Lake, to more than 1700 mg/L for certain wells on the Coal Creek alluvial fan. Sandberg (1966) reported TDS concentrations in groundwater ranging from 281 to 3750 mg/L. Bjorklund and others (1978, table 5) reported TDS concentrations in groundwater ranging from 166 to 2752 mg/L. Based on water-quality data collected by the USGS (Howells and others, 2002) and from public water-supply wells within the study area (Rachael Cassady, Utah Division of Drinking Water, written communication, 2001) from 1974 to 2000, TDS concentrations range from 184 to 2190 mg/L with an average of 584 mg/L (Lowe and others, 2010).

Nitrate, typically associated with human activities, has been identified in Cedar Valley groundwater. Nitrate concentrations in groundwater have been analyzed and reported in two different ways in the literature for Cedar Valley: nitrate as nitrogen (N) and nitrate as nitrate (NO$_3^-$). Thomas and Taylor (1946, p. 107) reported nitrate-as-nitrate concentrations ranging from 0 to 260 mg/L for wells in Cedar Valley; they noted that the highest nitrate concentration in groundwater was found in the Fiddlers Canyon alluvial-fan area, and that this high-nitrate groundwater also contained high chloride and sulfate concentrations. Water-quality data collected by the USGS (Howells and others, 2002), data from public water-supply wells within the study area (Rachael Cassady, Utah Division of Drinking Water, written communication, 2001), and 1979–81 data reported by Lowe and Wallace (2001) indicate nitrate-as-nitrogen concentrations range from less than 0.06 to 57.4 mg/L (Lowe and others, 2010). The U.S. Environmental Protection Agency (2010a) drinking-water quality (health) standard for nitrate as nitrogen is 10 mg/L, and for nitrate as nitrate is 45 mg/L.

Thomas and Taylor (1946) noted that depths for most of the wells having high nitrate concentration in Cedar Valley exceed 100 feet, suggesting a geologic source of nitrate possibly

associated with soluble salts in the basin fill rather than an anthropogenic origin. Wallace and Lowe (2000) and Lowe and Wallace (2001) also suggested that historically high nitrate concentrations in the Enoch area may be due in part to a geologic source of nitrogen, and documented nitrogen-bearing strata in the Straight Cliffs Formation in Fiddlers Canyon southeast of Enoch.

Recharge and Discharge

Most recharge to the basin-fill aquifer comes from precipitation within the Cedar Valley drainage basin (Sandberg, 1966). Recharge to the Cedar Valley basin-fill aquifer, in order of greatest quantity recharged, is from (1) infiltration of precipitation falling on unconsolidated basin fill, (2) inflow from bedrock aquifers in the surrounding hills and mountains, (3) infiltration of irrigation water from groundwater sources, (4) seepage from streams and major irrigation canals, (5) infiltration of irrigation water from surface-water sources, (6) subsurface inflow from Parowan Valley, (7) infiltration of land-applied wastewater effluent, and (8) infiltration of irrigation water applied to lawns and gardens (table 1) (Brooks and Mason, 2005).

Discharge from the basin-fill aquifer, in order of greatest quantity discharged, occurs through (1) well withdrawals, (2) evapotranspiration, (3) subsurface outflow through Iron Springs Gap and Mud Spring Wash, and (4) spring flows (table 1) (Brooks and Mason, 2005). Because water-well pumping is by far the greatest source of groundwater discharge, groundwater development in Cedar Valley is considered in detail for this study.

Groundwater Development

Pumping from wells is the largest component of groundwater discharge in the Cedar Valley drainage basin, and is a major controlling variable of both long- and short-term groundwater-level fluctuations in the valley (Thomas and Taylor, 1946; Bjorklund and others, 1978; Brooks and Mason, 2005). Groundwater withdrawal and drought are the major causes of long-term water-level decline (Bjorklund and others, 1978; Brooks and Mason, 2005). Seasonal water-level declines occur because most wells are pumped from May to September. From October to April, pumping is reduced and water levels rise, but pumping resumes the next summer before water levels reach the levels of the previous year (Bjorklund and others, 1978).

To examine long-term trends in groundwater withdrawal, we compiled total pumping rates for the following periods: (1) 1938 to 1940 (Thomas and Taylor, 1946), (2) 1945 to 1963 (Brooks and Mason, 2005), and (3) 1964 to 2009 (Utah Division of Water Rights, 2010c; figure 3). We also examined municipal pumping records after 1964, including data from Cedar City and Enoch City between 1979 and 2009. We used simple linear regressions to estimate long-term changes in pumping rates.

Most of the water pumped in Cedar Valley is used for agriculture and the amount of irrigation required partially depends upon the amount of precipitation in the basin area (Brooks

Table 1. *Conceptual groundwater budget for 2000, Cedar Valley, Iron County, Utah (modified from Brooks and Mason, 2005). Compare to table 3, which shows a budget deficit.*

		Cubic Feet/Day	Acre-ft/Year
RECHARGE	Precipitation on unconsolidated basin fill	1,228,000	10,300
	Bedrock inflow from surrounding hills and mountains	1,181,000	9900
	Recharge from irrigation with groundwater	847,000–1,026,000	7100–8600
	Seepage from streams and major irrigation canals	561,000–608,000	4700–5100
	Recharge from irrigation with surface water	584,000	4900
	Subsurface inflow	239,000	2000
	Recharge from land application of wastewater effluent	179,000	1500
	Recharge from irrigation of lawns and gardens	72,000–119,000	600–1000
	Total recharge (rounded)	4,890,000–5,128,000	41,000–43,000
DISCHARGE	Wells	4,293,000	36,000
	Evapotranspiration	358,000	3000
	Subsurface outflow	119,000	1000
	Springs	Negligible	Negligible
	Total discharge (rounded)	4,771,000	40,000
	Amount of storage gained	119,000–358,000	1000–3000
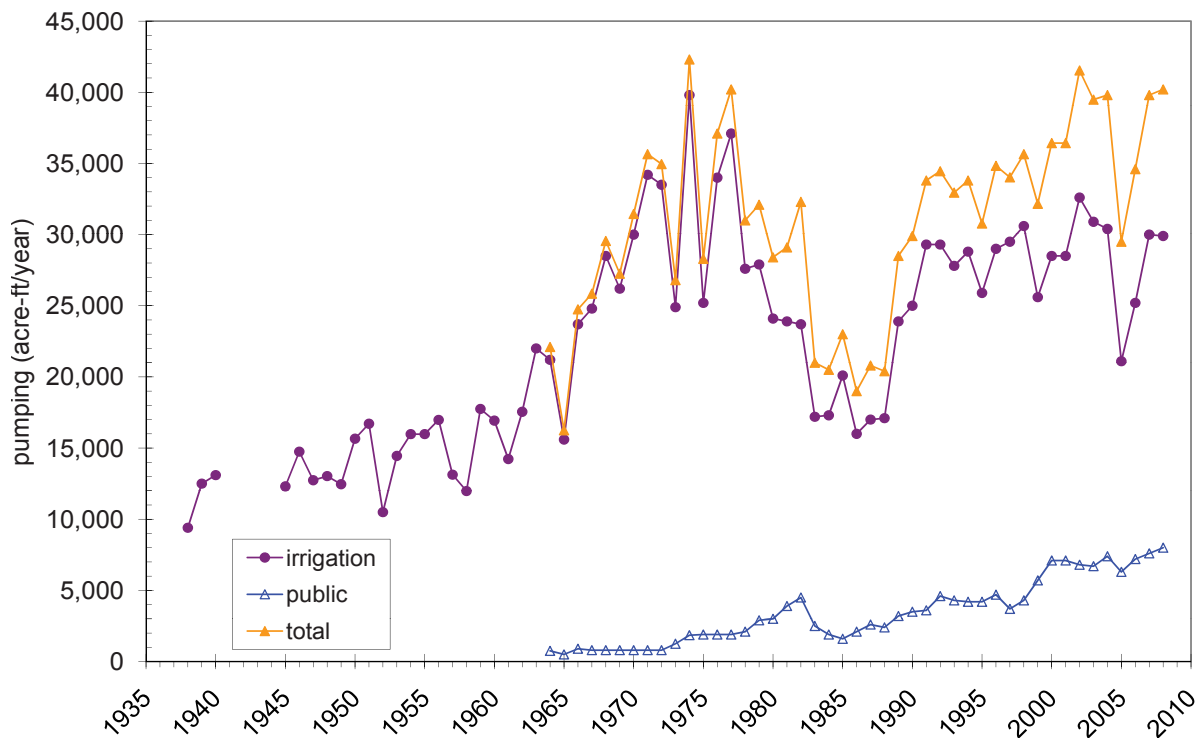
Figure 3. *Annual water usage by category for Cedar Valley from 1938 to 2009 (data from Thomas and Taylor, 1946; Brooks and Mason, 2005; Utah Division of Water Rights, 2010c).*
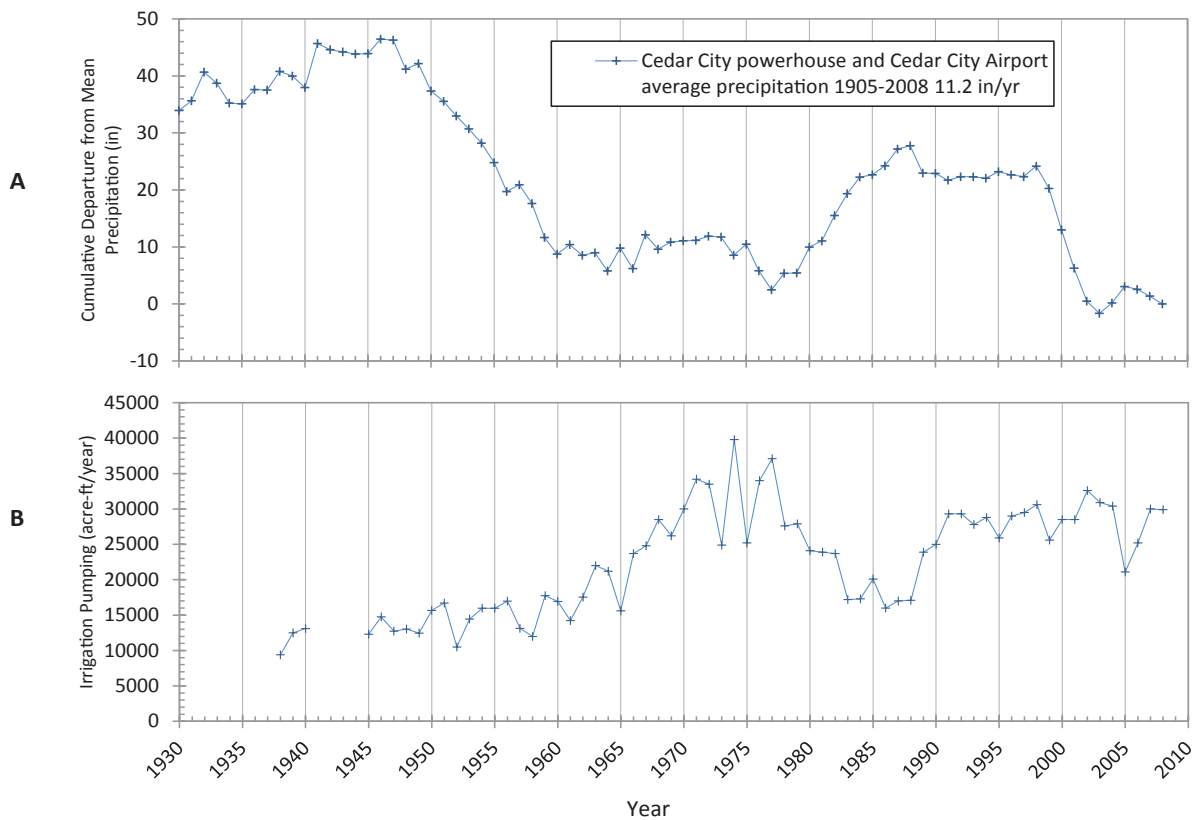
Figure 4. *A. Cumulative departure from mean precipitation (data from Utah Climate Center, 2010), and B. irrigation well pumping in Cedar Valley (data from Utah Division of Water Rights, 2010c).*

and Mason, 2005) (figure 4). The yearly average of precipitation (including snow) from four weather stations (Cedar City Airport, Summit, Cedar City powerhouse, and Parowan powerhouse) from 1945 to 2008 for Cedar Valley is 11 inches per year (Utah Climate Center, 2010). Although the Parowan powerhouse and Summit weather stations are in Parowan Valley, precipitation in the Parowan area contributes to subsurface flow into Cedar Valley (Brooks and Mason, 2005). Departure from average precipitation is the difference between annual precipitation and mean annual precipitation. Cumulative departure from mean is the sum of departures from the average for each year (figure 4A).

Since 1964, total pumping in Cedar Valley has increased at a rate of approximately 600 acre-feet per year (figure 3) (Utah Division of Water Rights, 2010c). As of 2008, agricultural (interpreted as crop cultivation) pumping (74%) and municipal pumping (20%) comprised 94% of all pumping, with private domestic and stock (5%) and industrial wells (1%) comprising the other 6% (Burden, 2009).

Municipal pumping was negligible relative to agricultural pumping before the early 1960s, because municipalities were small and generally relied on springs for their water supply (Brooks and Mason, 2005). Since then, municipal withdrawals have increased at a rate of 160 acre-feet per year (Utah Division of Water Rights, 2010c). Enoch and Cedar City currently operate 13 wells that produce most of the public water

supply in Cedar Valley (table 2). Eight of the wells are within Enoch and Cedar City's boundaries and the other five wells are near Quichapa Lake on the west side of Cedar Valley (figure 5). The two cities have water rights for numerous other wells, but collectively these wells produce less than 1000 acre-feet per year. The wells near Quichapa Lake pump approximately 4000 acre-feet per year collectively. The wells in the Enoch area pump about 3000 acre-feet per year collectively. Municipal pumping occurs year-round, but volume varies by season. Maximum pumping is typically in July (Brooks and Mason, 2005) and minimum pumping is in December (figure 6).

Agricultural pumping is the largest component of well discharge in Cedar Valley (Bjorklund and others, 1978; Brooks and Mason, 2005). In 2008, agricultural wells pumped 30,000 acre-feet (figure 3) (Utah Division of Water Rights, 2010c). However, agricultural pumping as a share of all pumping is decreasing at a rate of about half a percent per year. In 1964, agricultural withdrawals represented 96% of all pumping from the aquifer in the valley (figure 3). By 2008, agricultural pumping was 74% of all pumping. While the percentage of agricultural pumping is decreasing over time, the rate of agricultural and municipal pumping is increasing by 20 and 160 acre-feet per year, respectively (figure 3) (Utah Division of Water Rights, 2010c).

Agricultural pumping increased at a rate of 200 acre-feet per year from 1945 to 1965. From 1965 to 1974, agricultural

Table 2. *Major municipal wells and their yearly average discharge.*

	Well	WIN[1]	CAD[2]	Avg. Yearly Discharge[3] (acre-ft/yr)
Enoch Area	Ravine	30363	(C-35-10)7acd-1	140
	Woolsey	4064	(C-35-10)7ccd-1	180
	Anderson	30360	(C-35-10)7dcc-1	200
	Homestead	3996	(C-35-10)18acb-1	260
	Northfield	27968	(C-35-11)35cbb-1	240
	Cemetery	4006	(C-36-11)11bdb-1	440
	Enoch #1	28692	(C-35-10)18cca-1	440
	Iron Works	24548	(C-35-10)7abd-1	600
Quichapa Lake Area	Quichapa #1 South[4]	3977	(C-36-12)32ccc-1	200
	Quichapa #3 North	3992	(C-36-12)32ccb-1	670
	Quichapa #5	4004	(C-36-12)29abb-1	700
	Quichapa #6	4005	(C-36-12)17ddd-1	1060
	Quichapa #7	13549	(C-36-12)20add-1	1390

[1]*Utah Division of Water Rights well identification number.*

[2]*U.S. Geological Survey well numbering system for Utah. See appendix B. The numbers after the dash at the end refer to the order in which the wells were constructed and labeled for that location.*

[3]*From Utah Division of Water Rights (2010b).*

[4]*This well was not pumped during 2010–2011.*
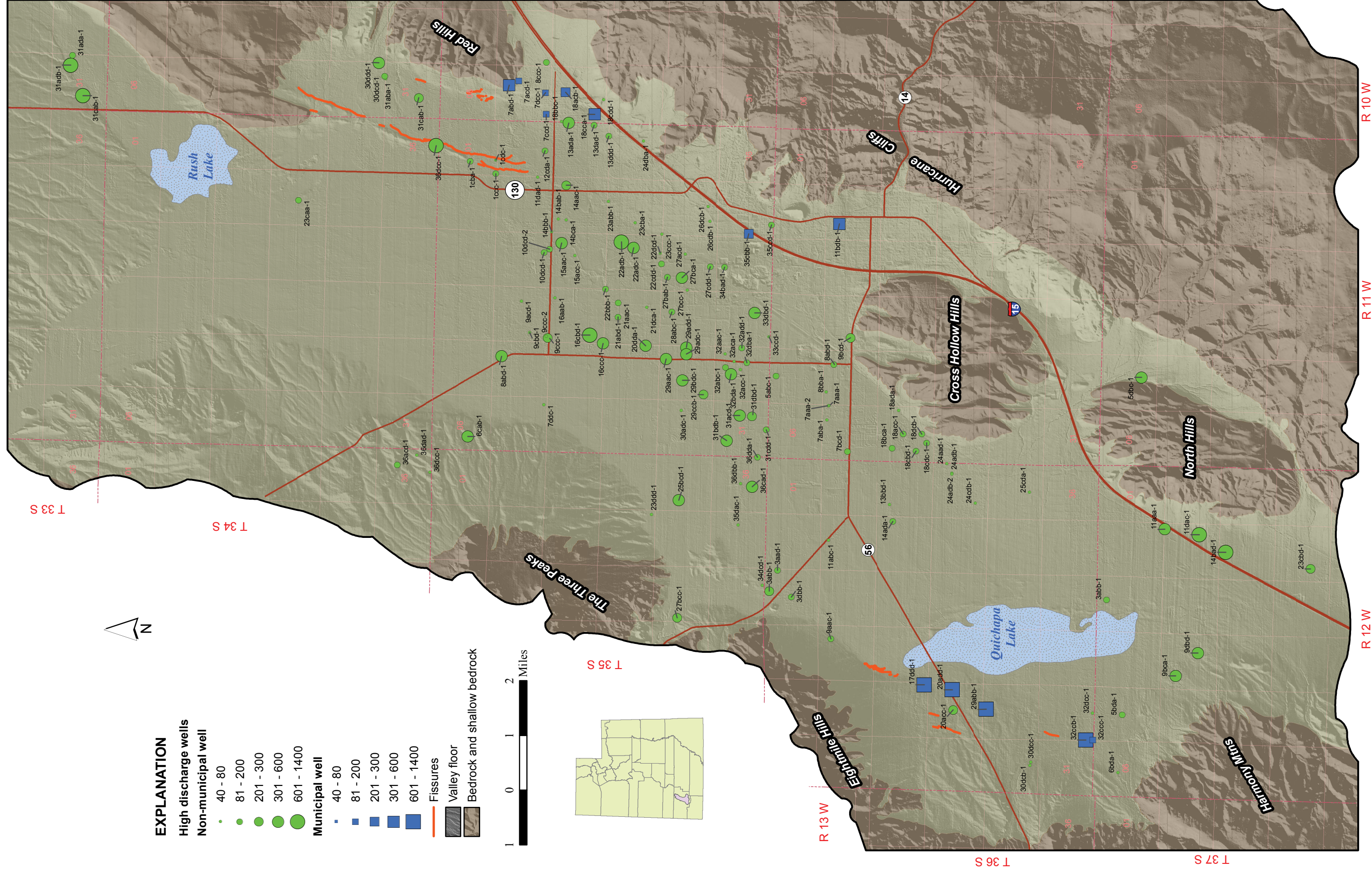
Figure 5. *High-discharge wells in Cedar Valley. Discharge estimates and well locations from Utah Division of Water Rights (2010a, 2010b). Wells are labeled by the end of their cadastral location identification number (CAD ID) (appendix B). Appendix C lists these wells and their approximate discharge.*
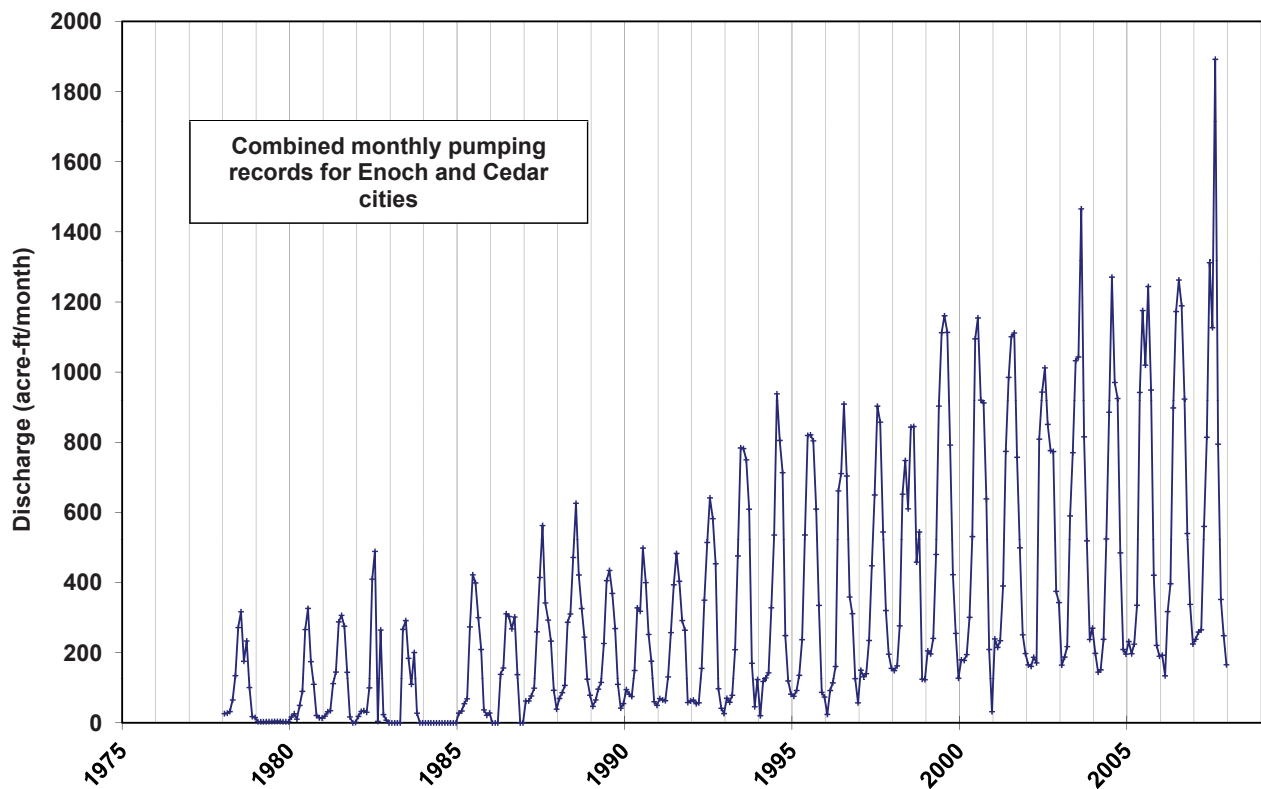
Figure 6. *Monthly mean withdrawal from Cedar City and Enoch City municipal wells from 1978 to 2008 (Utah Division of Water Rights, 2010b). Data prior to 1978 were not available.*

pumping increased by 2800 acre-feet per year, reaching its record high of 39,800 acre-feet in 1974. After 1974, pumping decreased by approximately 2000 acre-feet per year reaching a low of 16,000 acre-feet in 1986. After 1986, pumping rates increased to and maintained a rate of about 30,000 acre-feet per year with an annual increase of less than 20 acre-feet per year.

Bjorklund and others (1978) noted that annual discharge from the Cedar Valley hydrologic system exceeds recharge, resulting in a long-term decline in groundwater levels in Cedar Valley. Using specific yield as an estimate for storativity, Bjorklund and others (1978) estimated groundwater storage decrease by multiplying basin-wide storativity, long-term change in groundwater level, and affected basin area. Specific yield is a measure of the volume of water that can be drained by gravity from a material per unit volume of that material. Assuming a basin-wide storativity of 0.1, they estimated the average annual loss from storage between 1940 and 1974 to be 3300 acre-feet. This estimate depends strongly on the estimate for average valley-wide specific yield and neglects the specific storage of the aquifer—the volume of water released per unit volume of aquifer owing to compressibility of the aquifer skeleton and the water itself. The storage properties of the aquifer are also changing in areas where the aquifer is compacting due to groundwater extraction.

Brooks and Mason (2005) used their calibrated transient-state model to estimate a storage decrease of 9100 acre-feet in 2000 (table 3). While their conceptual (table 1) hydrologic budget shows an increase in storage, localized hydrologic budgets within the valley were likely not balanced to account for observed decreases in groundwater levels. Assuming the estimated average annual (1940–1974) groundwater storage decrease of 3300 acre-feet from Bjorklund and others (1978) is reasonable, the average loss of groundwater from aquifer storage has increased from 3300 acre-feet in 1974, to 9100 acre-feet in 2000.

Using the same technique employed by Bjorklund and others (1978), we estimated a storage decrease of 10,700 acre-feet for 2000, using a storativity estimate of 0.1 (Bjorklund and others, 1978), a basin area of 177,600 acres, and an average annual water-level change of 0.6 feet (table 4). This estimate agrees well with the Brooks and Mason (2005) estimate of 9100 acre-ft of storage change, considering the uncertainty of the variables involved. Both estimates for storage are approximate, and either a more complete hydrologic budget or better estimates of storativity are necessary to more accurately estimate hydrologic imbalances. However, the long-term deficit in Cedar Valley's water budget is well documented and is increasingly expressed as a significant decline in groundwater levels over time.

Table 3. Transient groundwater model budget from Brooks and Mason (2005), representing the model approximated budget for the year 2000.

		Cubic Feet/Day	Acre-ft/Year
RECHARGE	Irrigation and precipitation on irrigated lands, including seepage from Coal Creek	2,330,000	19,500
	Winter precipitation on all areas	700,000	5900
	Subsurface Inflow		
	Parowan Valley[1]	370,000	3100
	North consolidated rock	160,000	1400
	Southeast consolidated rock	36,000	300
	East consolidated rock	84,000	700
	Southwest consolidated rock	190,000	1600
	West consolidated rock	120,000	1000
	Inflow from south of area	9500	80
	Total recharge (rounded)	4,000,000	33,500
DISCHARGE	Wells	4,080,000	34,200
	Evapotranspiration	530,000	4500
	Springs	150,000	1300
	Outflow to other areas	320,000	2700
	Total discharge	5,100,000	42,700
	Water removed from storage[2]	1,100,000	9100

[1]Includes 1100 acre-feet per year recharge from consolidated rock.
[2]Valley-wide water-level declines from March 2000 to March 2001 indicate a removal of water from storage (discharge exceeding recharge).

Table 4. Change in potentiometric surface and rate of groundwater-level decline over various segments of time. Negative values indicate a rise in groundwater levels.

Basin-Wide Water Level Decrease[1]								
	Spring Water Levels					**Fall Water Levels**		
	1940[2]–1974[3]	1974[3]–2000[4]	2000[4]–2010[6]	1940[2]–2000[4]	1940[2]–2010[6]	1939[2]–1974[3]	1974[3]–2009[5]	1939[2]–2009[5]
years	34	26	10	60	70	35	35	70
min (ft)[1]	-22	-56	-10	-19	-1	-16	-28	-3
max (ft)	48	47	75	62	90	58	82	114
mean (ft)	11	14	22	24	47	19	42	63
mean rate (ft/yr)	0.3	0.5	2.2	0.4	0.7	0.5	1.2	0.9

Water-Level Decrease Along Cross Sections[1]								
	Spring Water Levels					**Fall Water Levels**		
	1940[2]–1974[3]	1974[3]–2000[4]	2000[4]–2010[6]	1940[2]–2000[4]	1940[2]–2010[6]	1939[2]–1974[3]	1974[3]–2009[5]	1939[2]–2009[5]
years	34	26	10	60	70	35	35	70
min (ft)[1]	-11	-2	-1	3	5	-3	2	8
max (ft)	35	39	38	58	75	45	80	99
mean (ft)	8	15	22	22	42	16	45	61
mean rate (ft/yr)	0.2	0.6	2.2	0.4	0.6	0.5	1.3	0.9

[1]Negative value indicates an increase in water levels.
[2]November 1939 and April 1940 water levels from Thomas and Taylor (1946) plate 13.
[3]Spring and fall 1974 water levels from Bjorklund and others (1978) plate 5.
[4]March 2000 water levels from Brooks and Mason (2005) figure 5.
[5]October 2009 water levels from figure 7.
[6]March 2010 water levels from figure 8.
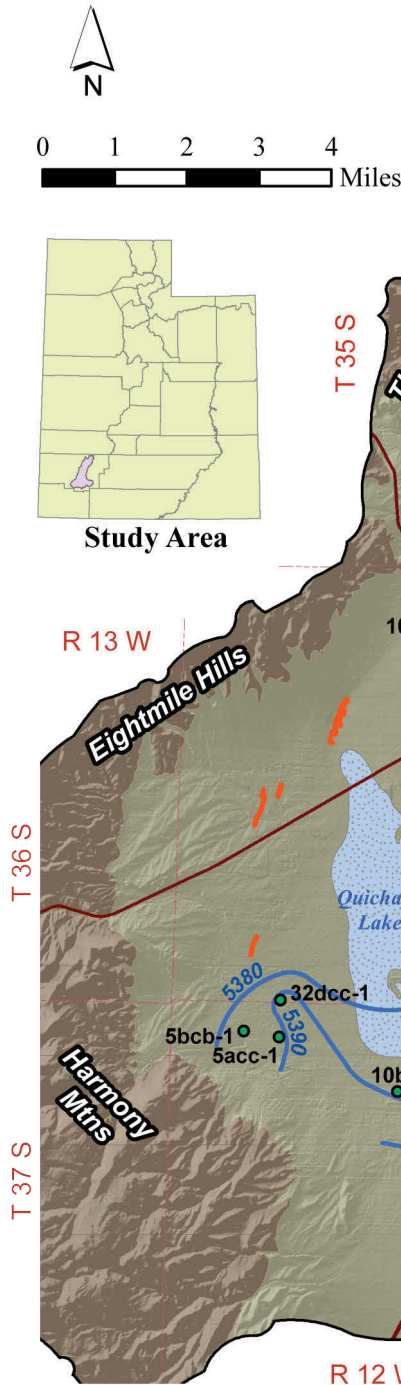
Figure 7. Cedar Valley potentiometric surface during October 2009. Well details and water-level measurements are listed in table 5.

Potentiometric Surface Change Over Time

Since the early 1950s, several authors have reported long-term groundwater-level declines in Cedar Valley (Bjorklund and others, 1978; Lowe and others, 2000; Brooks and Mason, 2005; Burden, 2009). For this study, we measured water levels in 33 wells to produce a potentiometric-surface map for Cedar Valley (figure 7), which we then compared to past water levels to evaluate long-term water-level changes.

Methods

In October 2009, we collected water-level measurements from 33 wells. Water levels in several of those wells are also measured by the USGS every March. We measured water levels in wells near existing earth fissures, Enoch City wells, and CICWCD wells. Cedar City municipal wells did not have access points for accurate water-level measurement.

The field-collected depth to water minus the measured riser height (height of the casing above the ground surface) is the depth to water from the ground surface. We measured the field-collected depth to water using both a USGS standard steel tape and an electric water-level probe. Both instruments have reported accuracies of 0.01 foot. When conditions allowed, we measured water levels multiple times using both methods for greater precision. We measured from the standard USGS measuring point along the casing when marks or USGS directions were available. Stretching of the line and the line moving around obstructions could have introduced less than a foot of error during water-level measurement, but this is negligible relative to errors in the ground-surface elevation measurement for each well.

Ground surface elevations at each well are based on digital elevation models (DEM) derived from the National Elevation Dataset (NED) maintained by the USGS (Gesch and others, 2002; Gesch, 2007) (table 5). The NED consists of data from a variety of sources including digital photogrammetry, aerial photographs, and cartographic contours. The use of combined data sources and careful review by professional cartographers make these data slightly more accurate than elevations obtained from USGS 7.5-minute topographic quadrangle maps. The vertical accuracy of the NED data is 8 feet (as of March 2010), and the relative vertical accuracy for closely spaced data within the larger NED dataset is 2.6 feet (Gesch, 2007). The USGS continuously updates the NED dataset as they collect data. After we completed calculations using the NED data, the USGS updated the NED dataset to include LiDAR data commissioned by the UGS. Although the newer data are more accurate, they would not affect the resulting water level data enough to warrant the expense of the time to recalculate the groundwater elevation. Use of DEMs allows for quick, objective assignment of ground-surface elevations at wellheads.

Because the NED is based on the horizontal North American Datum of 1983 (NAD 83) and the North American Vertical Datum of 1988 (NAVD 88), we projected the horizontal and vertical positions of the wellheads into the datums used on the USGS quadrangles (NAD 27 and NGVD 29) with the National Geodetic Survey's orthometric height conversion calculator VERTCON (National Geodetic Survey, 2010a). The VERTCON conversion is accurate to less than 0.8 inch (Milbert, 1999). We applied the NGVD 29 datum shift to all wellhead elevations assigned from the NED. We then compared the converted NED elevations to the available elevations assigned to the wells by the USGS in the National Water Information System (NWIS; U.S. Geological Survey, 2010) to ensure that the elevations were similar. We did not use NWIS elevations because they were not available for all of the wells measured in the field, and because most of the NWIS elevations are based on elevations derived from USGS 7.5-minute quadrangles (U.S. Geological Survey, 2010). NED-derived elevations are within the margin of error reported by the USGS in the NWIS (usually 5 ft) for each site, unless (1) the site elevation was determined by a method more accurate than scaling from a topographic map, (2) the location of the well is not as reported, or (3) NWIS assigned an incorrect elevation.

We calculated water-level elevation by subtracting depth to water from the ground-surface elevation. We interpolated the resulting water-level-elevation data using a spline technique to create potentiometric surface contours. Spline interpolation applies a smooth, piecewise polynomial (similar to regression) fit to the existing points. We refined the contours by hand to ensure a realistic interpretation of the potentiometric surface (figure 7). USGS-collected water-level data (Burden, 2009) and well-driller-recorded depth to water (Division of Water Rights, 2010a) provided a check on the accuracy of the contour lines. Although the USGS values provide a check, there were not enough fall 2009 water levels from the USGS to independently produce a potentiometric surface map. However, we repeated the same process outlined above for 26 water-level measurements (table 6) taken by the USGS in the spring of 2010, to create a potentiometric surface map for that time (figure 8).

We also used a regularized spline technique to interpolate contours from Thomas and Taylor (1946), Bjorklund and others (1978), and Brooks and Mason (2005) for comparison with the water-level data we collected. The resulting interpolated potentiometric surfaces were limited to the aerial extent of the contours. The contour lines that we compared our elevations to were not likely based on NWIS data, especially the 1939 and 1940 water-level contours from Thomas and Taylor (1946). Although all of the authors (Thomas and Taylor, 1946; Bjorklund and others, 1978; Brooks and Mason, 2005) displayed the well locations used to create their potentiometric surface maps, they did not provide the depth-to-water data they collected. Thomas and Taylor (1946), Bjorklund and others (1978), and Brooks and Mason (2005) used topographic maps with the NGVD 29 vertical datum to assign ground-surface elevations. Had the authors listed the depth to water, we

Table 5. *Wells and measured water levels used for the October 2009 potentiometric surface map of Cedar Valley (figure 7).*

CAD[1]	Method	Measured Twice	Date Measured	Ground Surface Elevation[2] (ft)	Water-Level Elevation (ft)
(C-35-11)10ccd-1	Sounder[3]	Y	10/20/2009	5491	5421
(C-35-11)17ddd-1	Steel tape	Y	10/20/2009	5511	5412
(C-36-11)30acc-3	Sounder	Y	10/20/2009	5619	5338
(C-36-12)24cdb-1	Steel tape	Y	10/23/2009	5504	5394
(C-34-11)16bcc-1	Sounder	Y	10/21/2009	5408	5390
(C-34-11)1daa-1	Steel tape	N	10/21/2009	5400	5375
(C-35-11)4aba-1	Sounder	Y	10/21/2009	5457	5433
(C-35-11)12add-1	Steel tape	N	10/21/2009	5489	5408
(C-35-11)27acc-1	Sounder	Y	10/21/2009	5553	5469
(C-35-11)27bbc-1	Steel tape	Y	10/21/2009	5547	5462
(C-35-11)28aac-2	Sounder	Y	10/21/2009	5549	5458
(C-35-11)21dbd-2	Steel tape	N	10/21/2009	5533	5455
(C-35-11)12dcd-1	Steel tape	Y	10/22/2009	5498	5424
(C-35-11)12ddd-2	Steel tape	Y	10/22/2009	5513	5407
(C-36-11)8abd-1	Sounder	Y	10/21/2009	5566	5438
(C-36-11)7aba-1	Sounder	Y	10/23/2009	5531	5427
(C-35-12)36ddd-1	Both	Y	10/23/2009	5516	5431
(C-37-12)5acc-1	Sounder	Y	10/23/2009	5504	5391
(C-37-12)5bcb-1	Both	Y	10/23/2009	5542	5385
(C-36-12)32dcc-1	Sounder	Y	10/23/2009	5498	5397
(C-37-12)10bba-1	Sounder	Y	10/23/2009	5461	5390
(C-37-12)23abd-1	Sounder	Y	10/24/2009	5530	5416
(C-36-11)18bdd-1	Sounder	Y	10/24/2009	5517	5401
(C-36-11)18bca-2	Sounder	Y	10/24/2009	5513	5403
(C-36-11)18cac-1	Sounder	Y	10/24/2009	5509	5402
(C-36-12)12dba-1	Sounder	Y	10/24/2009	5510	5418
(C-36-12)10aaa-1	Sounder	Y	10/24/2009	5479	5408
(C-35-11)25bcc-1	Sounder	Y	10/24/2009	5740	5447
(C-35-11)14bac-1	Steel tape	Y	10/22/2009	5495	5417
(C-35-11)23bdd-1	Steel tape	Y	10/22/2009	5551	5418
(C-35-10) 7dcc-1	Sounder	Y	10/22/2009	5620	5494
(C-35-10) 7abd-1	Sounder	Y	10/22/2009	5572	5409
(C-35-11) 1cdc-1	Sounder	Y	10/21/2009	5469	5378

[1]*U.S. Geological Survey well numbering system for Utah. See appendix B. The numbers after the dash at the end refer to the order in which the wells were constructed and labeled for that location.*
[2]*Elevation from the National Elevation Dataset (NED) (Gesch and others, 2002; Gesch, 2007) and adjusted for the National Geodetic Vertical Datum of 1929 (NGVD 29).*
[3] *Sounder refers to electric water-level sounder.*

Table 6. NWIS (U.S. Geological Survey, 2010) wells used for the March 2010 potentiometric surface map of Cedar Valley (figure 8).

USGS Site Number	CAD[1]	Date Measured	Water-Level Elevation (ft)	Station Elevation[2] (ft)
373319113120301	(C-37-12)28aac- 1	3/2/2010	5433	5552
373509113101101	(C-37-12)14abc- 1	3/2/2010	5401	5480
373542113122401	(C-37-12) 9acc- 1	3/2/2010	5403	5491
373710113132701	(C-36-12)32dcc- 1	3/2/2010	5400	5500
373742113100801	(C-36-12)35adc- 1	3/11/2010	5415	5511
374038113124501	(C-36-12)16bba- 1	3/2/2010	5394	5472
374105113085001	(C-36-12)12dba- 1	3/2/2010	5432	5509
374130113104801	(C-36-12)10aaa- 1	3/2/2010	5416	5479
374132113063601	(C-36-11) 8aab- 1	1/20/2010	5452	5562
374248113075201	(C-35-11)31dbd- 1	3/2/2010	5447	5527
374249113090701	(C-35-12)36caa- 1	3/2/2010	5425	5505
374304113052901	(C-35-11)33aac- 1	3/3/2010	5467	5578
374345113032301	(C-35-11)26acd- 1	3/3/2010	5456	5665
374423113053301	(C-35-11)27bbc- 1	3/3/2010	5470	5546
374423113053401	(C-35-11)21dbd- 2	3/3/2010	5465	5532
374502113064002	(C-35-11)17dcd- 2	3/2/2010	5455	5509
374521113014801	(C-34-11) 9cdc- 1	3/17/2010	5376	5400
374545113035001	(C-35-11)14bac- 2	3/2/2010	5465	5496
374550113040601	(C-35-11)11ccc- 1	3/2/2010	5448	5493
374554113020801	(C-35-11)12dcd- 1	3/3/2010	5427	5493
374744113055001	(C-35-11) 4aba- 1	3/2/2010	5438	5458
374745113022901	(C-34-11)36dcc- 2	3/3/2010	5390	5456
374927113033401	(C-34-11)23bdd- 1	3/3/2010	5385	5413
374929113053301	(C-34-11)21dcd- 1	3/2/2010	5409	5427
375233113015501	(C-34-11) 1daa- 1	3/12/2010	5377	5401
375341113072502	(C-33-11)31aad- 2	3/17/2010	5315	5352

[1]*U.S. Geological Survey well numbering system for Utah. See appendix B. The numbers after the dash at the end refer to order in which the wells were constructed and labeled for that location.*
[2]*Elevation from the NED (Gesch and others, 2002; Gesch, 2007) and adjusted for NGVD 29.*

could have calculated water-level elevations based on NED elevations and their listed depth to water.

Potentiometric contour maps are based on a limited number of points with a limited areal density, distributed over a limited area. For each point, the water-level-measurement values and assigned elevations have varying degrees of accuracy. Inaccuracies are propagated when these values are interpolated.

We used contours from Thomas and Taylor (1946), Bjorklund and others (1978), and Brooks and Mason (2005) because they are based on a large number of well-distributed wells. Thomas and Taylor (1946) used water levels from 138 wells to create their potentiometric-surface contours for Cedar Val-

ley in fall of 1939 and spring of 1940. Water levels during 1939 and 1940 were stable and the hydrologic budget was balanced (Brooks and Mason, 2005). Because of well-defined potentiometric surfaces and the relative water-level stability, the 1939 and 1940 potentiometric-surface contours are appropriate to compare to more recent water levels. Bjorklund and others (1978) used about 80 wells to delineate Cedar Valley's potentiometric surface for both spring and fall of 1974, and Brooks and Mason (2005) used 134 wells to create their potentiometric-surface contours for spring of 2000.

Water-level elevations from Thomas and Taylor (1946), Bjorklund and others (1978), Brooks and Mason (2005), our 2009 field data (table 5, figure 7), and NWIS data (U.S. Geo-
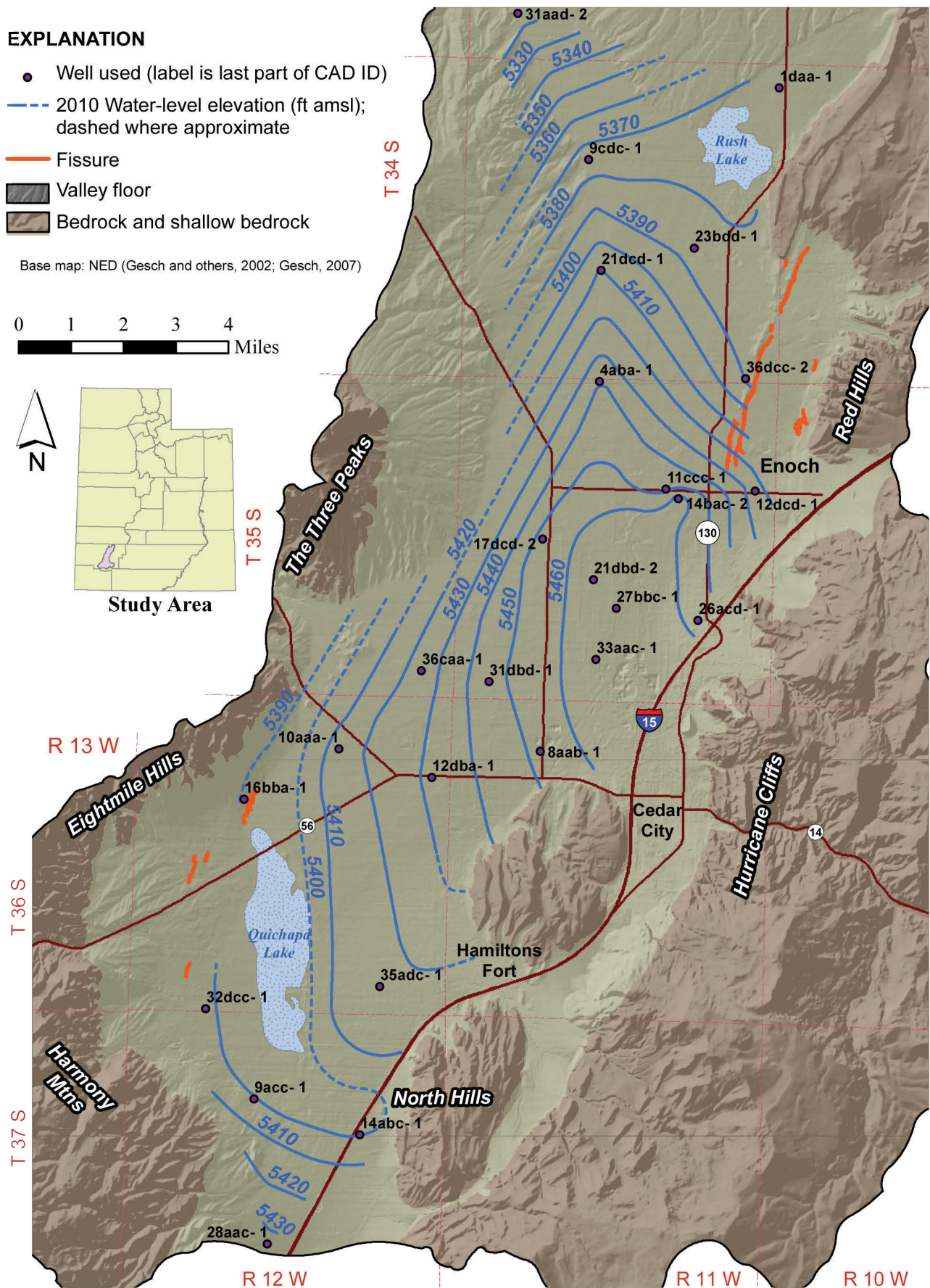
Figure 8. *Cedar Valley potentiometric surface during March 2010 from NWIS data (U.S. Geological Survey, 2010). Wells are listed in table 6.*
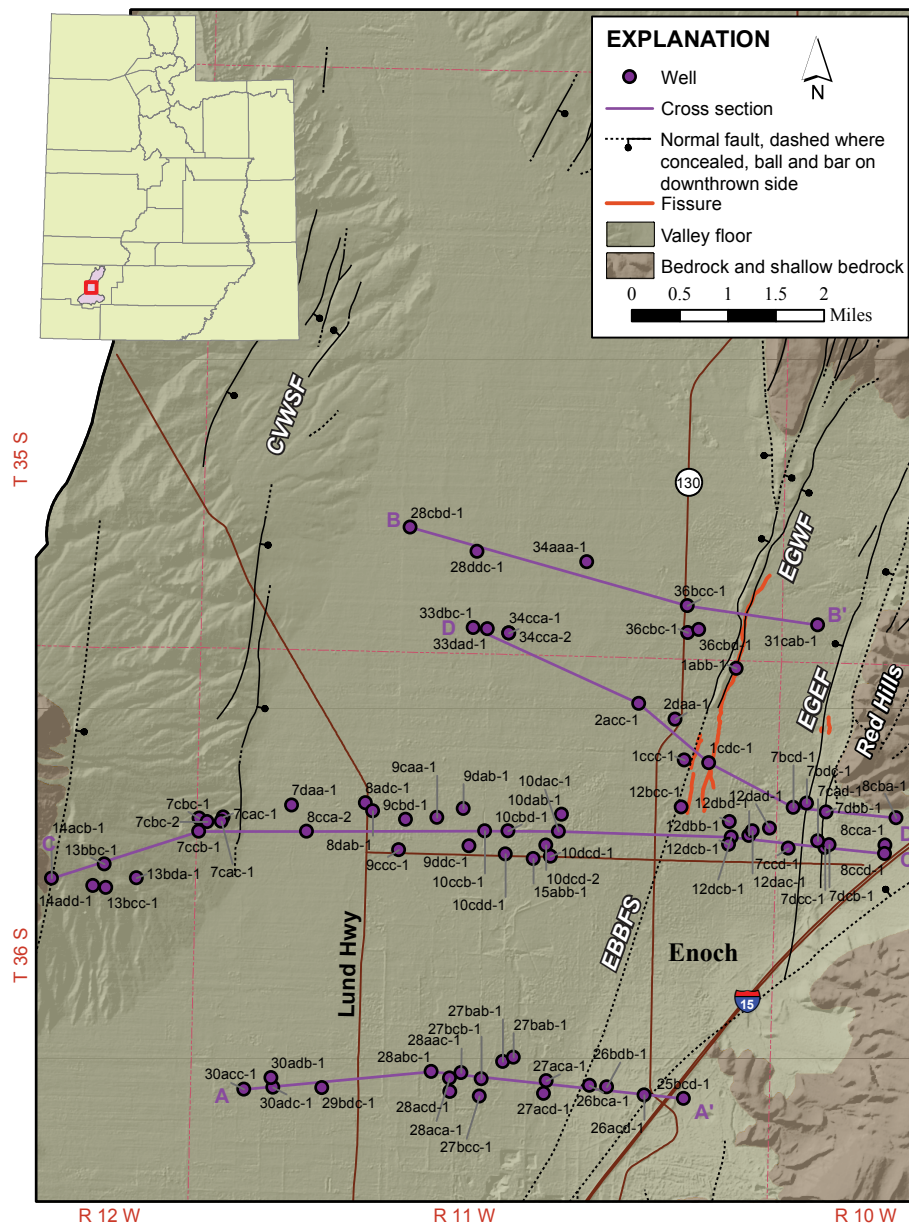
Figure 9. Cross section locations in northern Cedar Valley. The number next to each well is its CAD ID. Table 8 lists the wells in this figure. CVWSF = Cedar Valley west-side faults, EBBFS = eastern basin-bounding fault system, EGWF = Enoch-graben-west faults, EGEF = Enoch-graben-east faults.

logical Survey, 2010) (table 6, figure 8) provided water-level data for potentiometric-surface profiles along six cross sections prepared for this study. Although we created and examined potentiometric-surface profiles for water-level elevations from five different sources, due to scale limitations, we only present the Thomas and Taylor (1946) 1939 data and our 2009 field data in the cross sections (figures 9–16). We created the profiles by assigning values from each of the potentiometric surfaces that we made to 500 evenly spaced points along each cross section. The difference between our 2009 water-level-elevation points along the cross sections and the historical water-level information is the decline for each point. The average of those differences along all of the cross sections is the average decline. The cross sections sample areas of well-defined

potentiometric-surface contours, providing a reliable estimate of water-level changes along the same lines of section where we examined geology.

We used potentiometric-surface changes along the cross sections to determine average water-level decline and rate of water-level decline in Cedar Valley (table 4). Rate of groundwater-level decline is the number of years between observations divided by the amount of water-level decline.

Data

Seasonal variations are significant when comparing potentiometric-surface maps from different years and seasons.
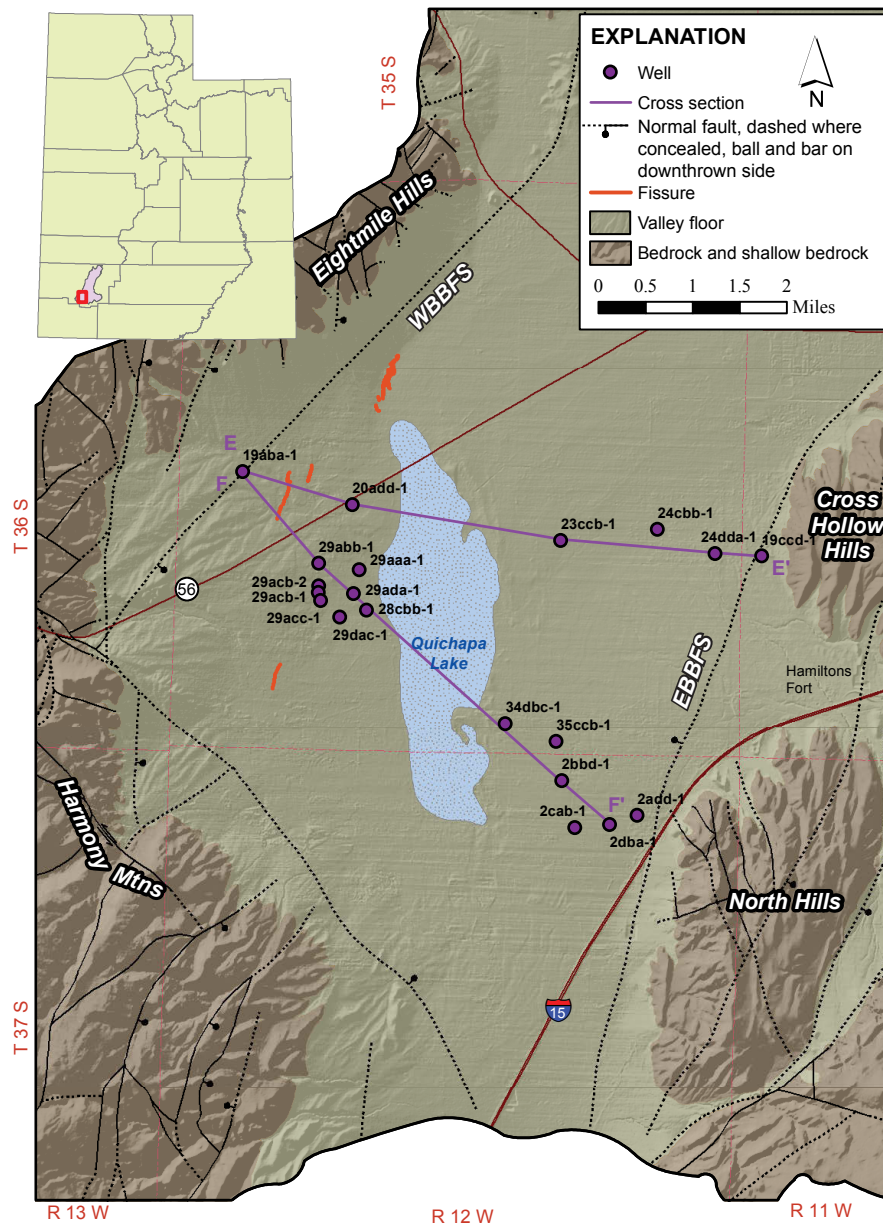
Figure 10. *Cross section locations in southern Cedar Valley. The number next to each well its CAD ID. Table 8 lists the wells in this figure. WBBFS = western basin-bounding fault system, EBBFS = eastern basin-bounding fault system.*

Water-level decline due to summer pumping causes contours to move horizontally toward the margins of the valley on the order of several hundred feet. Once pumping is discontinued or reduced during the winter months, groundwater levels begin to recover to a level near original spring water levels and the contours move back toward the center of the valley (Bjorklund and others, 1978).

Bjorklund and others (1978) showed seasonal water-level variations ranging from 10 to 40 feet. They noted that most seasonal variations were caused by pumping, with additional influence from variations in precipitation. Bjorklund and others' (1978) figure 6 shows seasonal fluctuations of more than 40 feet in some areas. Comparison of Bjorklund and others'

(1978) potentiometric surfaces shows a maximum decrease in groundwater levels from March 1974 to October 1974 of 49 feet. Thomas and Taylor (1946, their plate 14) documented seasonal fluctuations of 2 to 14 feet from April 1939 to September 1939. Comparison of Thomas and Taylor's (1946) September 1939 to April 1940 potentiometric surfaces shows a rise in groundwater levels of 11 feet. The average difference between water-level data during March 2009 taken from hydrographs (Burden, 2009) and October 2009 (this study) (figure 7, table 5) is about 12 feet (table 7).

Comparison of contours from the fall of 2009 (figure 7) to the spring of 2010 (figure 8) shows smoother, less sinuous contours in the spring. Although the troughs are still present
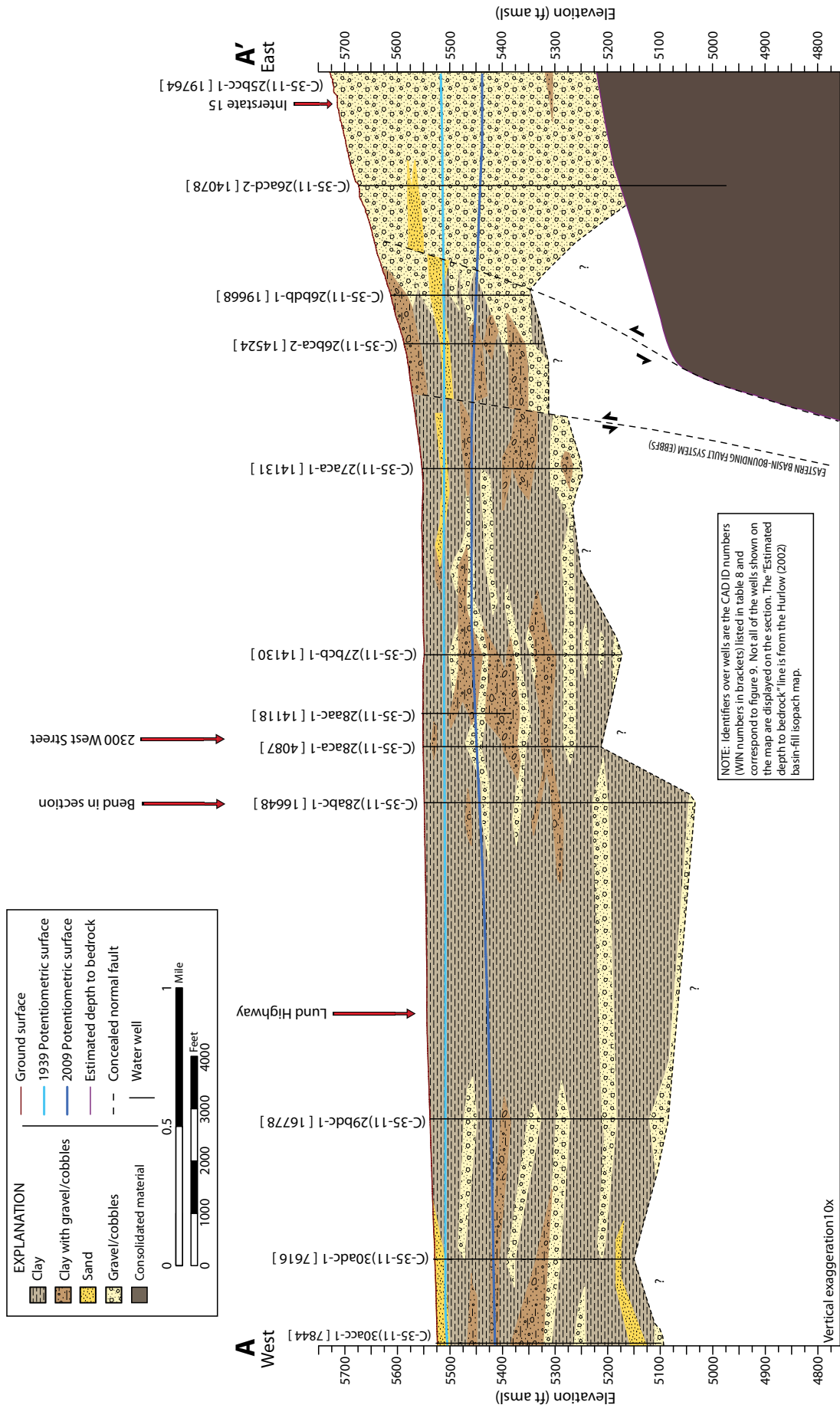
Figure 11. *West-east cross section A–A'. Figure 9 shows the location of this cross section.*
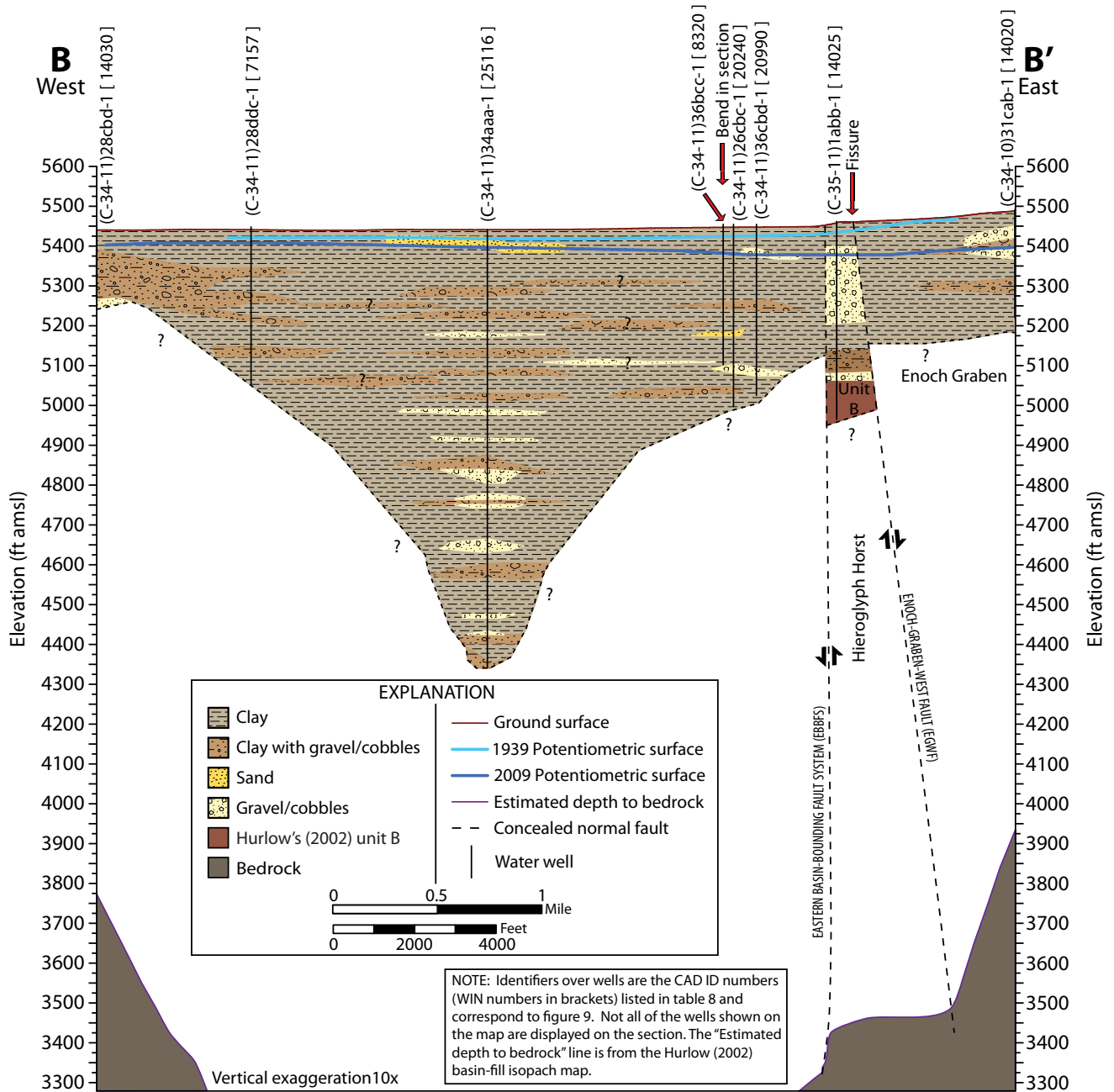
Figure 12. Northwest-southeast cross section B–B'. Figure 9 shows the location of this cross section.
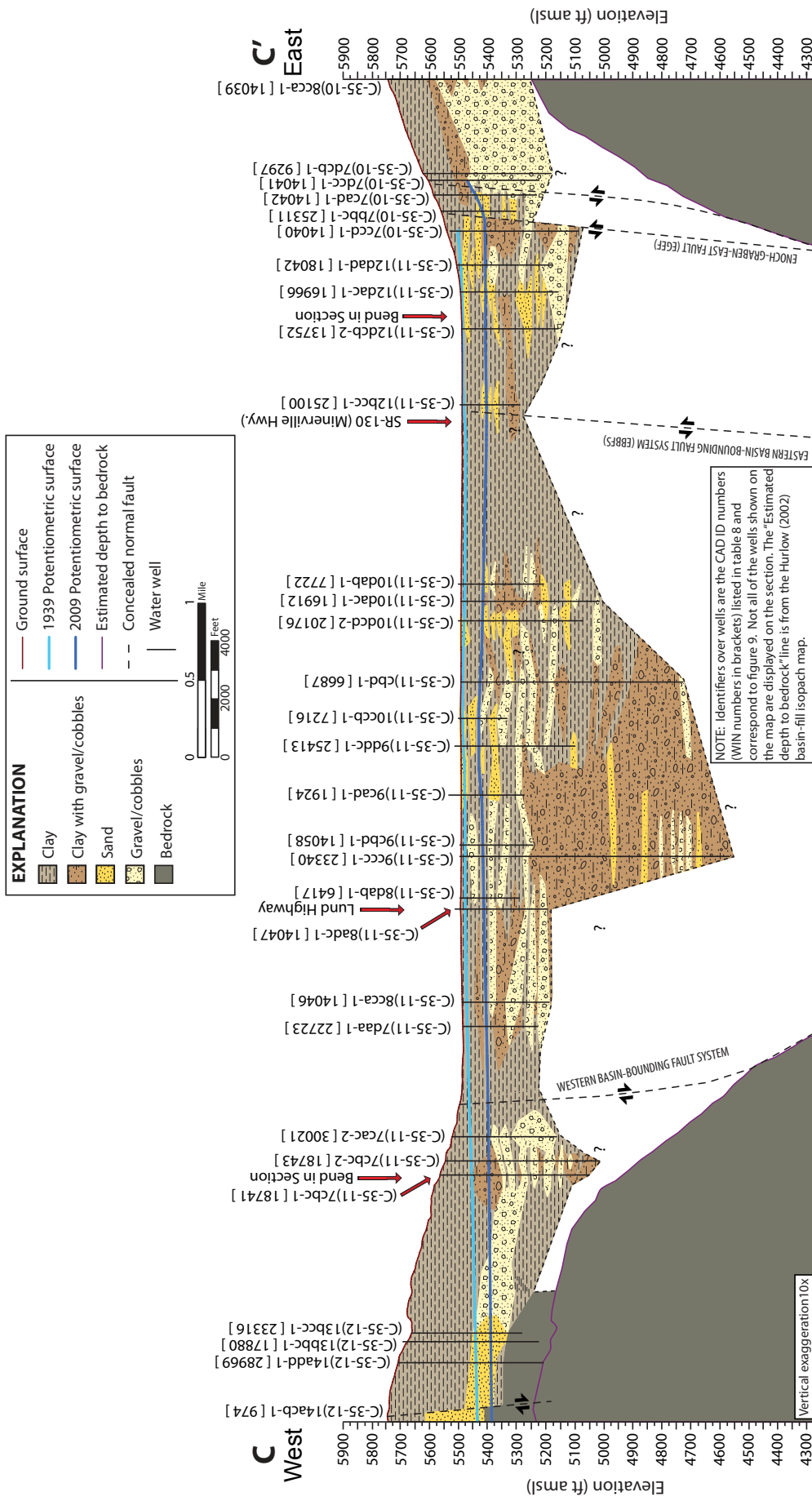
Figure 13. *West-east cross section C–C'. Figure 9 shows the location of this cross section.*
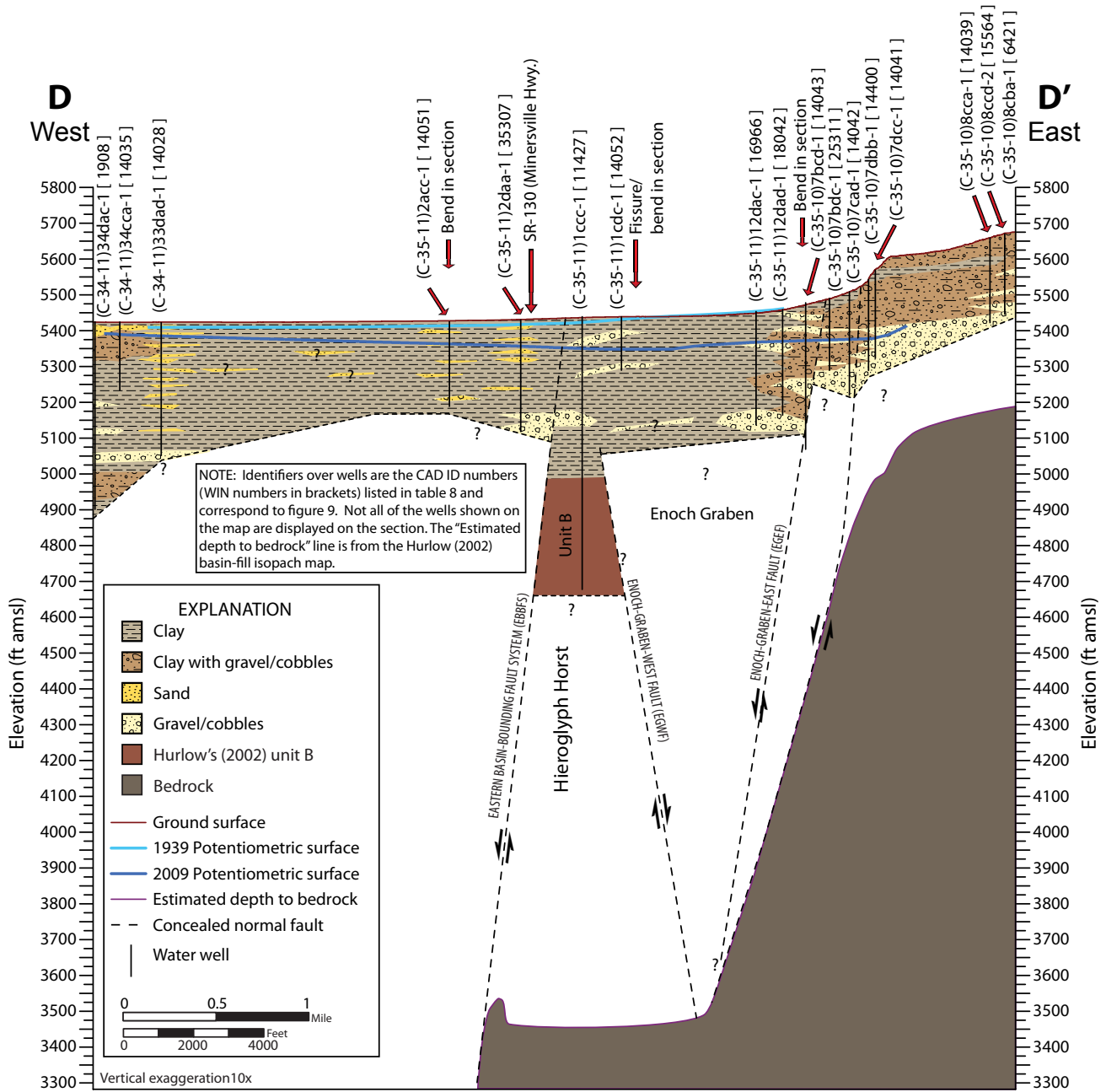
Figure 14. *Northwest-southeast cross section D–D'. Figure 9 shows the location of this cross section.*

EXPLANATION

Clay

Clay with gravel/cobbles

Sand

Gravel/cobbles

Bedrock

Ground surface

1939 Potentiometric surface

2009 Potentiometric surface

Estimated depth to bedrock

Concealed normal fault

Water well

NOTE: Identifiers over wells are the CAD ID numbers (WIN numbers in brackets) listed in table 8 and correspond to figure 9. Not all of the wells shown on the map are displayed on the section. The "Estimated depth to bedrock" line is from the Hurlow (2002) basin-fill isopach map.

Vertical exaggeration 10x

Figure 15. Northwest-southeast cross section E–E'. Figure 10 shows the location of this cross section.
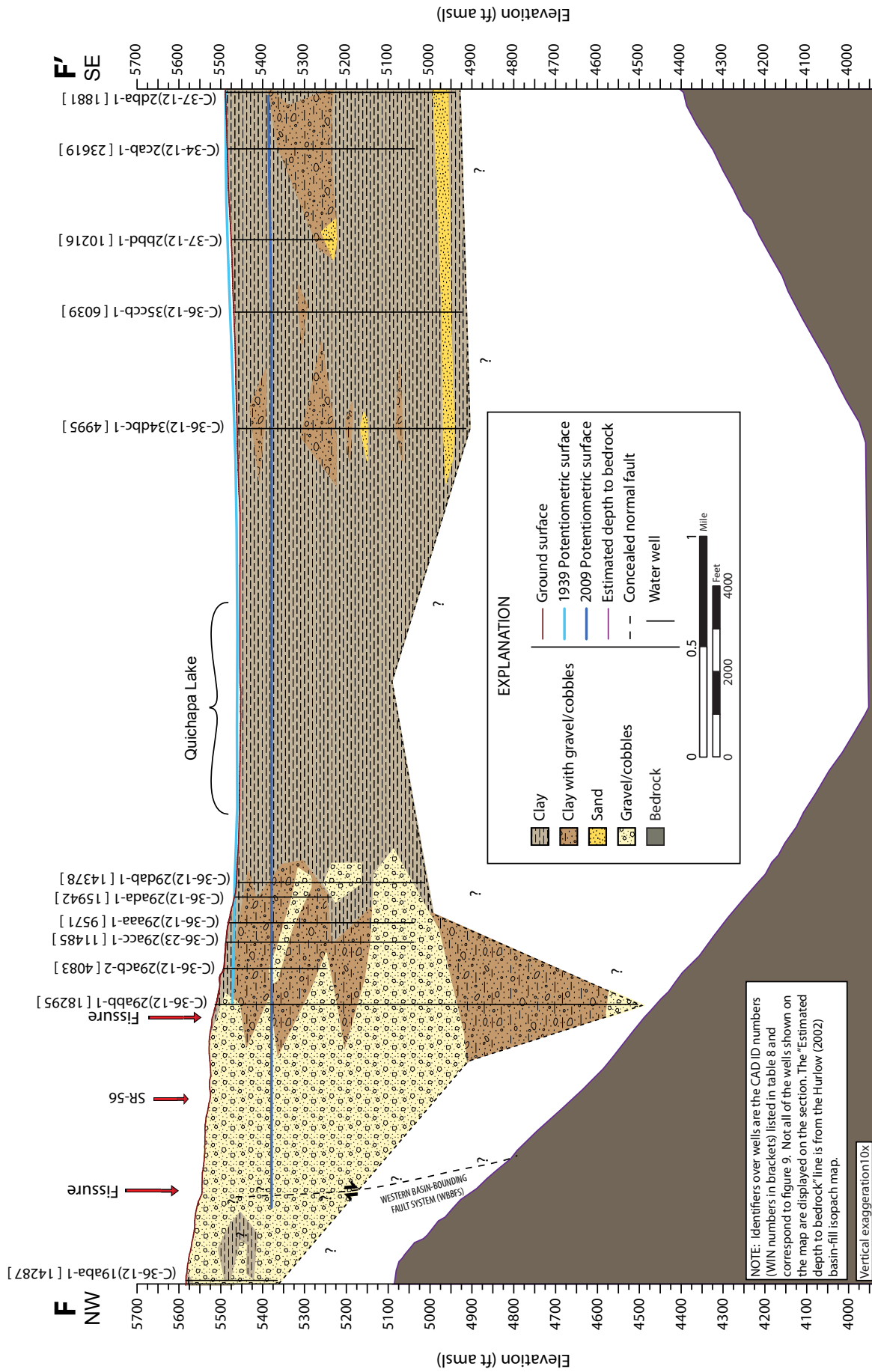
***Figure 16.** Northwest-southeast cross section F–F'. Figure 10 shows the location of this cross section.*

Table 7. *Seasonal variations in groundwater levels from eight wells. See figure 7 for well locations.*

Cadastral Location (CAD)[1]	USGS Site Number	Field Date Measured	Depth to Water (ft)	USGS Date Measured	USGS Depth to Water (ft)	Seasonal Difference (ft)
(C-34-11)1daa-1	375233113015501	10/21/2009	29.2	3/2/2009	28.1	1
(C-35-11)4aba-1	374744113055001	10/21/2009	27.4	3/2/2009	18.7	9
(C-35-11)27bbc-1	374423113053301	10/21/2009	87.4	3/5/2009	73.9	13
(C-35-11)21dbd-2	374423113053401	10/21/2009	81.9	3/5/2009	64.8	17
(C-35-11)12dcd-1	374554113020801	10/22/2009	76.0	3/2/2009	64.7	11
(C-36-12)32dcc-1	373710113132701	10/23/2009	104.2	3/9/2009	96.2	8
(C-36-12)12dba-1	374105113085001	10/24/2009	94.9	3/9/2009	73.0	22
(C-36-12)10aaa-1	374130113104801	10/24/2009	74.6	3/9/2009	59.9	15
					Average Difference	**12**

[1]*U.S. Geological Survey well numbering system for Utah. See appendix B. The numbers after the dash at the end refer to order in which the wells were constructed and labeled for that location.*

in the spring of 2010, they are broader with a lower gradient surrounding them. The greatest amount of rise in the potentiometric surface between fall of 2009 and spring of 2010 was around 40 feet in the areas of Enoch and northwest of Hamiltons Fort. The mean rise over the entire valley from fall 2009 to spring of 2010 was about 15 feet. The least amount of rise from fall of 2009 to spring of 2010 was in the areas of least development, in the northern part of the valley.

Long-term seasonal water-level fluctuations are discernible on NWIS hydrographs (figure 17) and by comparing seasonal fluctuations observed by Thomas and Taylor (1946) and Bjorklund and others (1978). Seasonal variations in water level were smaller in the 1930s and the 1940s and became larger after 1950. NWIS sites 374525113014601 [(C-35-10)18cbb-1], 374105113085001 [(C-36-12)12dba-1], and 373855113130501 [(C-36-12)20ddc-1] show an increase in seasonal variation over time (figure 17). The NWIS sites have identification numbers that consist of a site's latitude and longitude, in degrees, minutes, and seconds followed by a site number (e.g., 374105113085001 = 37º41'05", -113º08'50", site 01), and a cadastral location identifying number (in brackets above; see appendix B).

The contours on the Bjorklund and others (1978) potentiometric-surface map for spring 1974 are similar to those on our 2009 potentiometric-surface map (figure 7). Although water levels have decreased, the general direction of groundwater flow has remained the same. Heads are highest near the head of the Coal Creek alluvial fan and decrease toward the western and northern parts of the valley.

Significant drawdown has occurred throughout most of Cedar Valley from fall of 1939 to fall of 2009 (figure 18, table 4). Mean drawdown from 1939 to 2009 along our cross sections was 61 feet (table 4). Maximum drawdown along the

cross sections was 99 feet in cross section F–F', in the area of Hamiltons Fort. Minimum drawdown observed along the cross sections was 8 feet near the western end of cross section B–B'. Mean drawdown from the change-in-potentiometric-surface map (figure 18) is 63 feet. Maximum decline from the change-in-potentiometric-surface map is 114 feet in the Hamiltons Fort area (figure 18, table 4). The map covers most of Cedar Valley, while the cross sections are focused along just six lines transecting the valley. Potentiometric declines greater than those observed along the cross sections exist in Cedar Valley. Based on the map (figure 18), drawdown is greater than 80 feet in the Enoch graben area.

Six NWIS wells have hydrographs spanning from fall of 1939 to spring of 2009 (figure 17). Well 374132113063601 [(C-36-11)8aab-1] also has a fairly complete record, but it was dry in the fall of 2009. The greatest observed water-level decline of 77 feet was in NWIS well 374105113085001 [(C-36-12)12dba-1], in the central part of the valley, south of State Route 56 (SR-56) (compare figures 17 and 18). The minimum change observed was 2.5 feet in well 374521113014801 [(C-34-11)9cdc-1], in the northwest part of the valley. Most of the hydrographs show a general trend of relatively stable water levels from 1939 to 1949, decreasing water levels from 1950 to 1960, stable water levels from 1961 to 1979, increasing water levels from 1980 to 1985, and generally decreasing water levels from 1985 to present (figure 17). This general trend loosely follows the trends observed in the cumulative departure from mean precipitation data (figure 4).

The NWIS-observed changes in water levels compare reasonably well to our change-in-potentiometric-surface map. Only five NWIS wells are within the map area and have data that span a similar period as the map (figure 18). The NWIS-observed changes average 10 feet smaller than the map observations. The greatest discrepancy is 20 feet less than the map
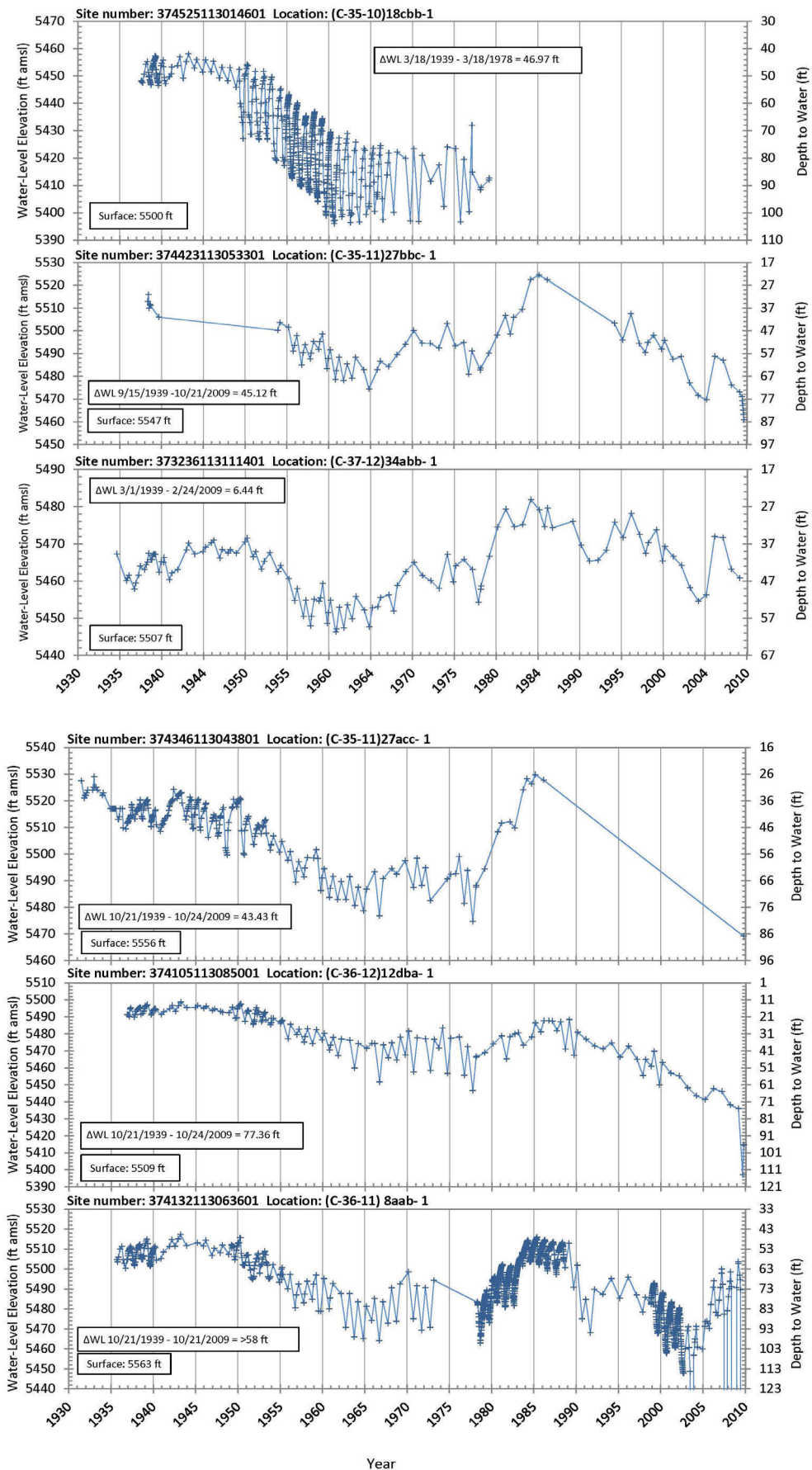
Figure 17. *Hydrographs from selected NWIS (U.S. Geological Survey, 2010) wells. Well locations are shown on figure 18.*
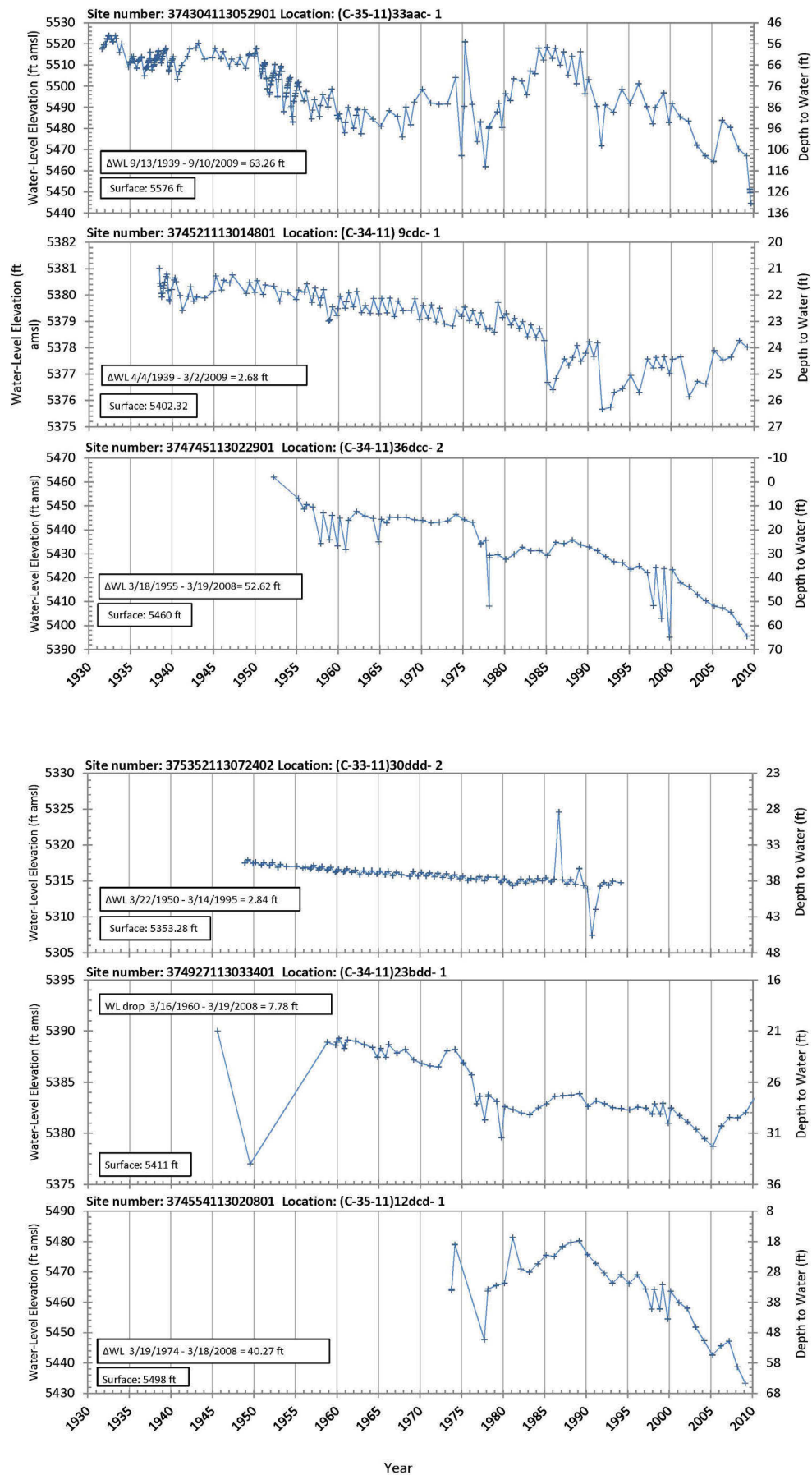
Figure 17. *continued*
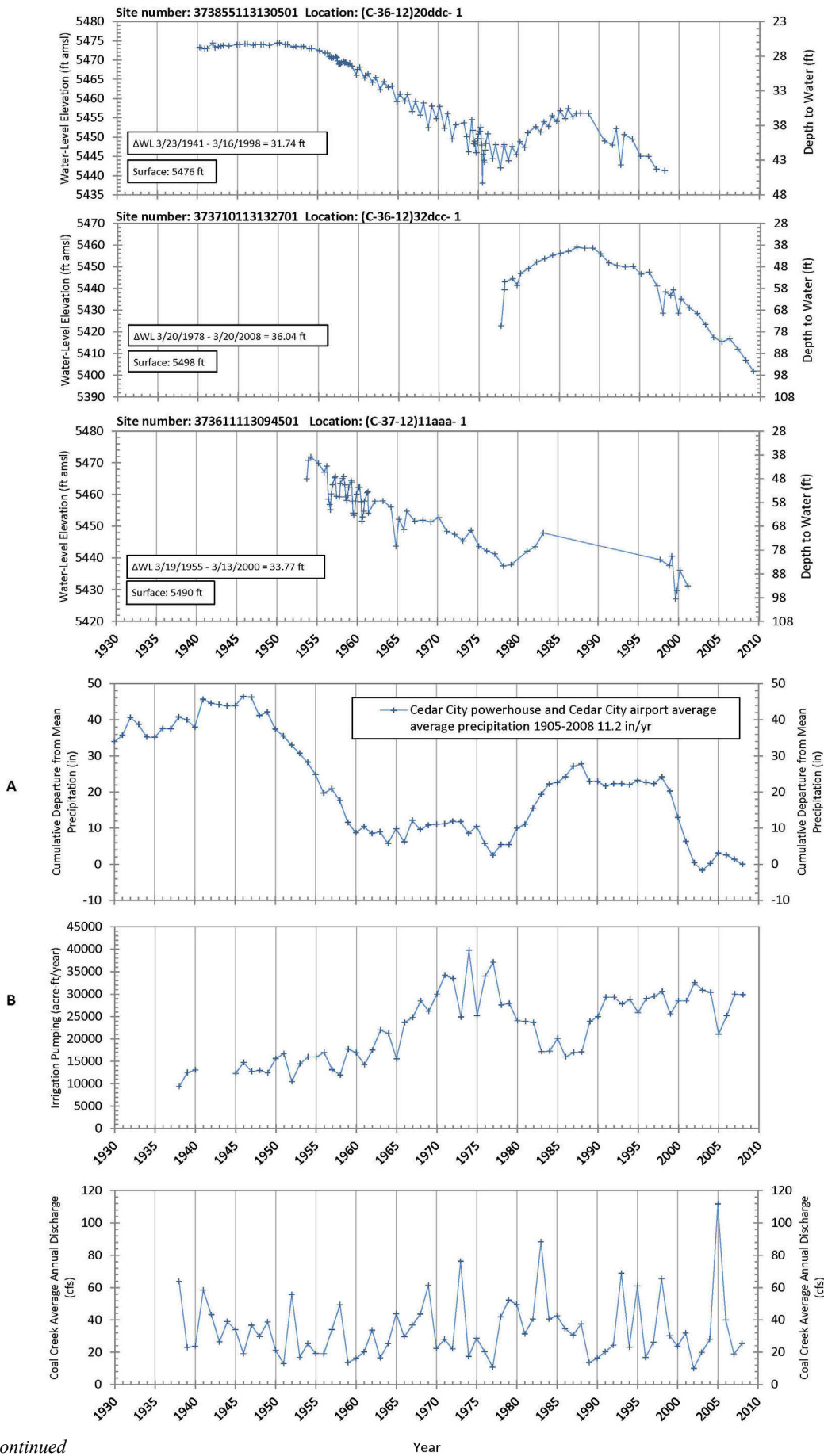
Figure 17. *continued*
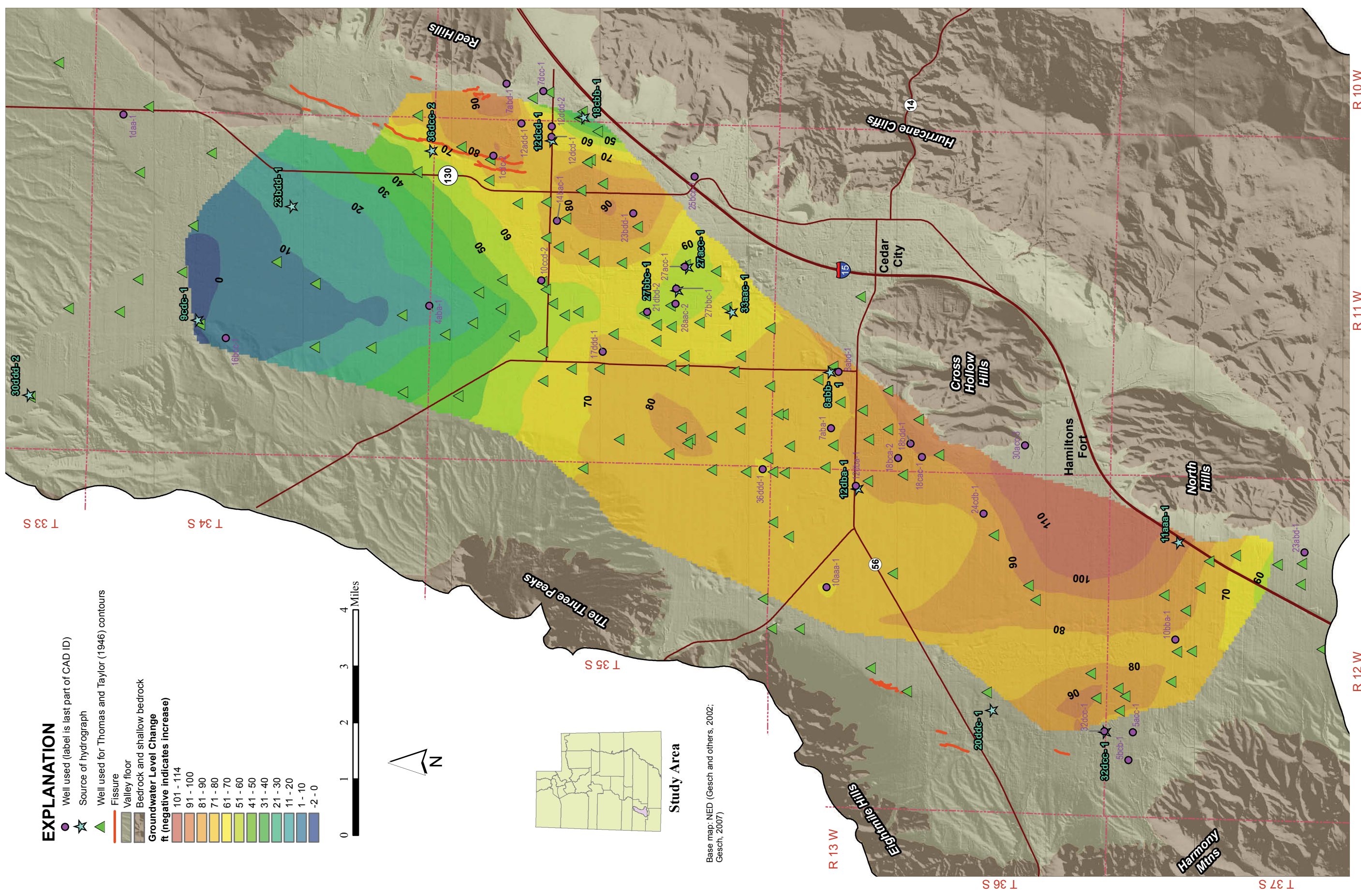
Figure 18. Change in potentiometric surface from September 1939 (Thomas and Taylor, 1946) to October 2009 (this study). Thomas and Taylor (1946) did not provide well identification with their well locations. Hydrographs from selected NWIS (U.S. Geological Survey, 2010) wells (stars) are shown on figure 17.

interpolation at well 374132113063601 [(C-36-11)8aab-1], just west of Cedar City (figure 18). These values are within the error created by possible discrepancies in available ground-surface elevations used in calculating water-level elevations.

Groundwater levels have increased up to 2 feet since 1939, in the far northwestern part of the valley (figure 18). A lack of pumping in this region combined with local recharge may account for this rise in groundwater level. However, the far northwestern part of the valley is an area of few wells and therefore poorly defined water levels; Thomas and Taylor (1946) show several of their contours in this area as "approximate" and figure 7 only shows well 16bbc-1 in that area. Consequently, the rise may be an artifact of inadequate data.

Based on changes shown on the potentiometric-surface maps, the rate of groundwater-level decline in Cedar Valley is increasing over time (table 4). The annual rate of mean basin-wide water-level decline from spring of 2000 to spring of 2010 was 2.2 feet per year. This estimate is similar to that reported by Burden (2009) of 5 feet of decline from March 2008 to March 2009. The rate of 2.2 feet per year is much greater than the decline along the cross sections of 0.6 feet per year from 1974 to 2000, and 0.2 feet per year from 1940 to 1974 (table 4).

CEDAR VALLEY AQUIFER CHARACTERISTICS

Distribution and Composition of Aquifer Sediments

Texture (fine versus coarse grained), distribution, and thickness of aquifer sediments affect aquifer compressibility, and therefore aquifer susceptibility to subsidence. Previous workers have described Cedar Valley basin-fill sediments in varying detail. Thomas and Taylor's (1946) figures 2 and 3; Lowe and others' (2000) figures 8, 14, and 20; and Hurlow's (2002) figure 15 are cross sections that differentiate coarse- and medium-grained deposits along the basin edges from fine-grained basin-fill deposits in Cedar Valley. Brooks and Mason (2005) used water-well drillers' logs to create a map depicting percentages of basin fill composed of sand and gravel. Hurlow (2002, plate 1) shows surface distribution of fine-grained deposits. For this study, we prepared six cross sections (figures 11–16) and a map showing the distribution and percentage of fine-grained sediments (figure 19) to characterize the basin-fill sediments in Cedar Valley.

Methods

We created the six cross sections (figures 11–16) using (1) 98 water-well drillers' logs (figures 9 and 10, table 8; Utah Division of Water Rights, 2010a), (2) cross sections from Lowe and others (2000) and Hurlow (2002), and (3) Hurlow's

(2002) basin-fill isopach map. Existing earth fissures and areas of current or possible future infrastructure development determined cross-section locations. We categorized the water-well drillers' descriptions of the basin-fill sediments into five categories: (1) clay—described as clay, clay with silt or sand, or silt or sand with clay matrix, (2) clay with gravel/cobbles—described as clay with gravel/cobbles, low-permeability gravel, or gravel/cobbles with a clay matrix, (3) sand—described as sand, silt and sand, coarse silt, or permeable silt, (4) gravel/cobbles—described as gravel/cobbles with mention of high permeability or no mention of clay, and (5) bedrock—described as any type of consolidated or cemented material.

Smaller well-to-well cross sections projected to the appropriate vertical and horizontal scales were combined to create the six full cross sections (figures 11–16). We constructed the well-to-well cross sections using Groundwater Modeling System (GMS) 6.0 (AQUAVEO, 2010) software. A NED 30-foot (10-meter) horizontal resolution DEM (Gesch and others, 2002; Gesch, 2007) provided ground-surface elevations for the cross sections and wells. The cross sections included all wells with drillers' logs within 1650 feet of the cross-section lines (table 8). We projected the 98 wells to their respective cross-section lines and edge matched the individual well-to-well cross sections to form the longer cross sections.

We estimated depth to bedrock using the 30-foot (10 meter) DEM and Hurlow's (2002) isopach lines (his figure 10A). We digitized Hurlow's (2002) basin-fill-thickness contours and converted them into a basin-fill-thickness raster. The depth to the contact between basin fill and bedrock is the difference between the resulting raster and the DEM.

We determined the percentages of fine- versus coarse-grained sediment at 298 wells in Cedar Valley using water-well drillers' logs. We classified each described unit on the logs as either "fine" or "coarse." If a majority of the material was clay or silt (i.e., clay, clay-sand, silt, topsoil), we assigned a "fine" designation. Generally, gravelly clay, sandy clay, and similar clay-dominated sediments fit in the "fine" category, whereas gravels and sands having little clay or clay matrix fit into the "coarse" category. Consolidated materials were classified as "bedrock." We calculated the percentage of fine-grained sediment at each point by summing the thicknesses of fine-grained materials over the total depth of the well. We plotted the percentages of fine-grained sediment in each well at the well location, and interpolated between locations using a natural neighbor technique with a cell size of 330 x 330 feet. The natural neighbor method uses sample points near each other to interpolate values guaranteed to be within the range of the samples used, and will not produce trends that are not already represented by the input samples. The result is a map showing the distribution and percentage of fine-grained sediments (figure 19). We used a common depth limit of 200 feet to standardize the percentages. The map is limited to the areal coverage of water wells in Cedar Valley.
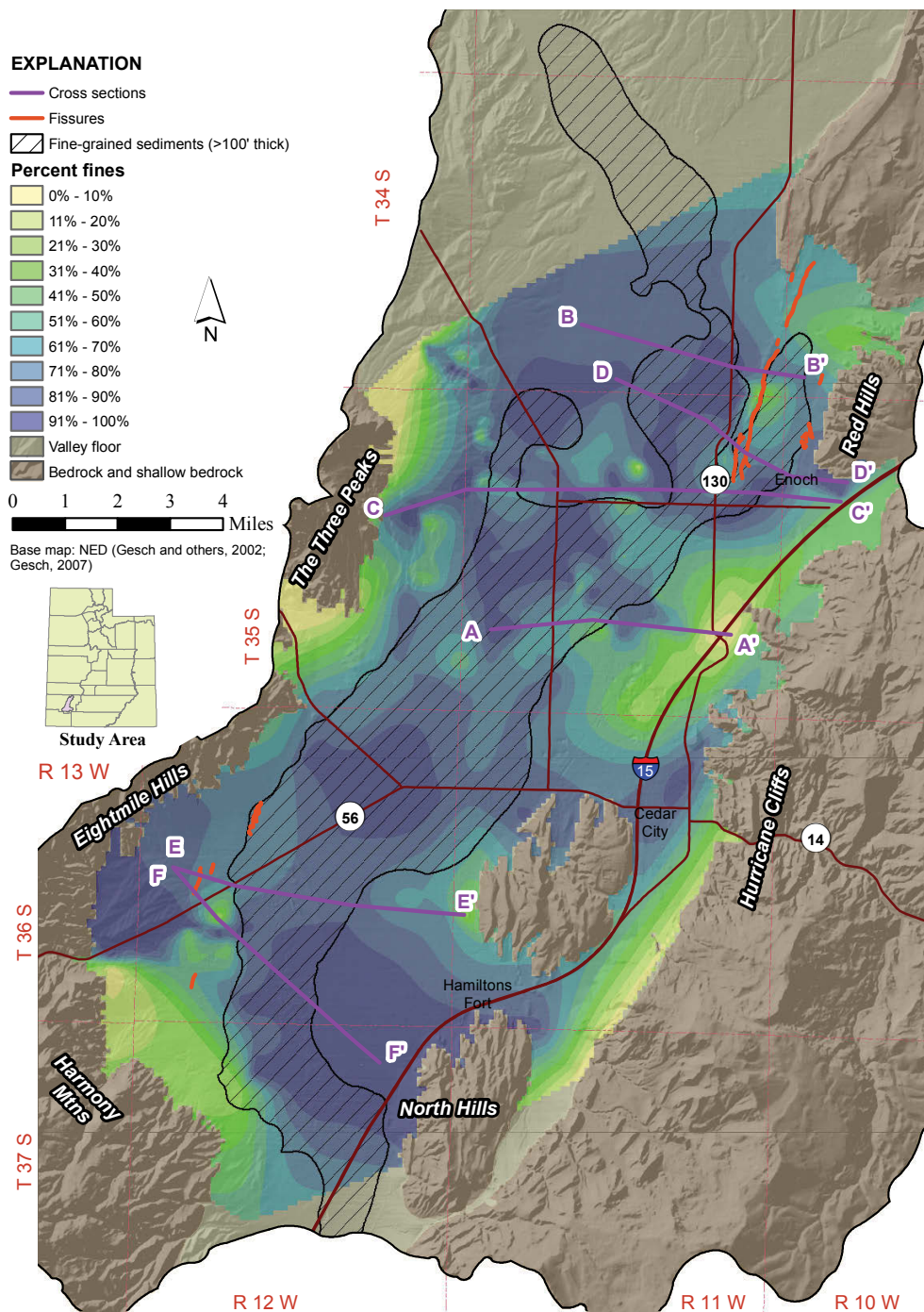
Figure 19. *Distribution and percentage of fine-grained sediments up to 200 feet deep in Cedar Valley. Hachured area delineated using cross sections, Brooks and Mason's (2005) figure 4, Hurlow (2002), and the percent fines map (shown).*

We checked the map values (figure 19) against the percentages of fine-grained sediments from nine detailed geologic well logs in Lowe and others (2000) (table 9). The mean difference between the geologic logs and the map is ± 18%. Considering that the well drillers' descriptions may have considerable inherent error, and that the simplifying process of assigning each described well driller's unit to one of three general sediment categories (fine, coarse, and bedrock) may have also introduced some error, we consider ± 18% error reasonable.

We used our map of the distribution and percentage of fine-grained sediments (figure 19) together with our cross sections, cross sections and isopachs from Hurlow (2002), and a map from Brooks and Mason's (2005) figure 4 to delineate an area of dominantly fine-grained sediment in Cedar Valley (hachured area on figure 19). The delineated area in the central part of Cedar Valley is composed of greater than 90% clay- or silt-sized material where basin-fill sediments are greater than 100 feet thick. Transitional areas in the cross sections (figures 11–16) from dominantly gravel to dominantly clay mark the

Table 8. *Wells used for construction of cross sections.*

CAD[1]	WIN[2]	UTM Easting[3] (m)	UTM Northing[3] (m)	Drilled Depth (ft)	Screen Depth[4] (ft)
(C-37-12)2add-1	140	309159	4164754	590	590
(C-35-12)14acb-1	974	308869	4181394	610	605
(C-36-12)28cbb-1	1466	304535	4168233	377	377
(C-35-11)7cac-1	1801	311714	4182344	151	151
(C-34-11)33dac-1	1908	315935	4185567	530	450
(C-35-11)9cad-1	1924	315328	4182405	205	185
(C-36-12)29acb-1	2737	303714	4168537	338	338
(C-36-12)29acb-2	4083	303718	4168649	270	270
(C-35-11)28aca-1	4087	315543	4178068	276	156
(C-35-11)12dcb-1	4857	320260	4182079	334	254
(C-36-12)34dbc-1	4995	306908	4166309	550	545
(C-35-11)27bcc-2	5621	316042	4177770	335	200
(C-36-12)35ccb-1	6039	307777	4166006	545	542
(C-35-11)8dab-1	6417	314250	4182514	210	160
(C-35-10)8cba-1	6421	323022	4182398	160	120
(C-35-11)10cbd-1	6687	316517	4182182	750	690
(C-34-11)28ddc-1	7157	316003	4186830	350	160
(C-35-11)10ccb-1	7216	316130	4182182	145	120
(C-35-11)30adc-1	7616	312579	4177914	320	320
(C-35-11)10dab-1	7722	317418	4182459	470	435
(C-36-12)24cbb-1	7763	309509	4169607	400	360
(C-35-11)30acc-1	7844	312096	4177886	426	415
(C-35-11)12dbb-1	7951	320229	4182336	320	300
(C-34-11)36bcc-1	8320	319522	4185929	320	280
(C-35-11)27bab-1	8623	316608	4178414	118	78
(C-35-10)7dcb-1	9297	321898	4181952	300	110
(C-36-12)29aaa-1	9571	304411	4168925	413	400
(C-37-12)2bbd-1	10216	307870	4165339	260	220
(C-35-11)30adb-1	10754	312549	4178075	298	275
(C-35-11)1ccc-1	11427	319473	4183362	830	600
(C-36-12)29acc-1	11485	303751	4168401	500	435
(C-36-12)20add-1	13549	304292	4170023	802	162
(C-35-11)12dcb-2	13752	320218	4181960	327	307
(C-34-10)31cab-1	14020	321707	4185608	188	187
(C-35-11)1abb-1	14025	320366	4184895	498	200
(C-34-11)33dad-1	14028	316172	4185545	188	148
(C-34-11)28cbd-1	14030	314882	4187236	160	50
(C-34-11)34cca-1	14035	316533	4185476	360	280
(C-35-10)8cca-1	14039	322833	4181948	232	150
(C-35-10)7ccd-1	14040	321213	4181894	375	220

Table 8. *continued*

CAD[1]	WIN[2]	UTM Easting[3] (m)	UTM Northing[3] (m)	Drilled Depth (ft)	Screen Depth[4] (ft)
(C-35-10)7dcc-1	14041	321832	4181906	300	110
(C-35-10)7cad-1	14042	321713	4181968	250	200
(C-35-10)7bcd-1	14043	321300	4182575	400	150
(C-34-11)34cca-2	14045	316533	4185476	300	200
(C-35-11)8cca-1	14046	313146	4182174	300	260
(C-35-11)8adc-1	14047	314129	4182647	305	205
(C-35-11)2acc-1	14051	318712	4184300	251	223
(C-35-11)1cdc-1	14052	319881	4183318	160	148
(C-35-11)10dcd-1	14056	317231	4181759	700	200
(C-35-11)10ccd-1	14057	316476	4181795	315	275
(C-35-11)9cbd-1	14058	314800	4182372	250	160
(C-35-11)15abb-1	14061	316941	4181723	316	316
(C-35-11)26acd-2	14078	318800	4177791	400	140
(C-35-11)28aac-1	14118	315735	4178160	351	NA
(C-35-11)27bcb-1	14130	316072	4178060	198	182
(C-35-11)27aca-1	14131	317157	4178027	300	220
(C-35-11)27bab-2	14132	316427	4178348	157	NA
(C-36-12)23ccb-1	14286	307854	4169419	228	201
(C-36-12)19aba-1	14287	302415	4170588	116	112
(C-36-11)19ccd-1	14353	311286	4169154	200	125
(C-36-12)29dab-1	14378	304075	4168116	485	200
(C-35-10)7dbb-1	14400	321846	4182498	300	220
(C-35-11)26bca-2	14524	317884	4177948	210	140
(C-35-10)8ccd-2	15564	322830	4181801	276	246
(C-35-11)12dbd-1	15907	320552	4182107	302	262
(C-36-12)29ada-1	15942	304315	4168516	300	260
(C-35-11)28abc-1	16648	315229	4178181	490	310
(C-35-11)29bdc-1	16778	313399	4177908	602	202
(C-35-11)10dac-1	16912	317362	4182173	460	440
(C-35-11)12dac-1	16966	320615	4182183	331	291
(C-35-12)13bda-1	17111	310296	4181401	403	363
(C-35-11)28acd-1	17634	315543	4177848	250	210
(C-35-12)13bbc-1	17880	309754	4181631	380	380
(C-35-11)12dad-1	18042	320899	4182227	305	265
(C-36-12)29abb-1	18295	303715	4169035	1006	162
(C-35-11)7cbc-1	18741	311342	4182394	320	266
(C-35-11)7ccb-1	18742	311339	4182175	420	240
(C-35-11)7cbc-2	18743	311479	4182336	500	460
(C-37-12)2dba-1	18817	308687	4164600	542	531
(C-35-11)26bdb-1	19668	318170	4177925	226	188

Table 8. continued

CAD[1]	WIN[2]	UTM Easting[3] (m)	UTM Northing[3] (m)	Drilled Depth (ft)	Screen Depth[4] (ft)
(C-35-11)25bcc-1	19764	319459	4177732	318	238
(C-35-11)10dcd-2	20176	317154	4181947	400	80
(C-34-11)36cbc-1	20240	319531	4185483	450	410
(C-34-11)36cbd-1	20990	319713	4185533	412	372
(C-35-11)7daa-1	22723	312893	4182612	244	205
(C-35-12)13bcc-1	23316	309784	4181241	400	400
(C-35-11)9ccc-1	23340	314685	4181869	934	630
(C-35-11)9dab-1	23515	315773	4182556	510	490
(C-37-12)2cab-1	23619	308095	4164543	450	410
(C-36-12)24dca-1	24798	310491	4169196	222	197
(C-35-11)12bcc-1	25100	319505	4182382	200	NA
(C-34-11)34aaa-1	25116	317842	4186662	1100	900
(C-35-10)7bdc-1	25311	321520	4182644	196	188
(C-35-11)9ddc-1	25413	315865	4181932	400	320
(C-35-11)27acd-1	27168	317113	4177817	250	170
(C-35-12)14add-1	28969	309562	4181271	358	345
(C-35-11)7cac-2	30021	311748	4182411	307	247
(C-35-11)2daa-1	35307	319316	4184041	340	260

[1]*U.S. Geological Survey well numbering system for Utah. See appendix B. The numbers after the dash at the end refer to order in which the wells were constructed and labeled for that location.*
[2]*Utah Division of Water Rights well identification number.*
[3]*Using NAD 1983 UTM Zone 12 projection.*
[4]*First reported depth to an interval of casing open to aquifer material. NA means screen depth not reported for that well.*

boundary of the area of fine-grained sediment in the central part of the valley (figure 19). We did not include the extent of dominantly fine-grained sediment above areas of shallow bedrock (overlying basin-fill sediments less than 100 feet thick) near the margins of the valley, because these areas will undergo less compaction and also contain fewer wells from which to obtain basin-fill characteristics.

Basin-Fill Sediments

In southern Cedar Valley, thick sequences of fine-grained sediments are centered near Quichapa Lake (figure 19, cross sections E–E' [figure 15] and F–F' [figure 16]). Alluvial-fan deposits emanating from adjacent highlands to the west of Quichapa Lake are present around the edge of the valley (figure 19, cross sections E–E' [figure 15] and F–F' [figure 16]). Water-well drillers' logs show that the most gravel-rich areas are within Hurlow's (2002) Quaternary-Tertiary alluvium unit near the valley margin west of Quichapa Lake (figure 19; cross section F–F' [figure 16]). These deposits fine eastward and northward, transitioning from gravel to gravel-rich clays to clay with intermittent gravel and sand lenses. A similar pattern of coarse alluvial fans is repeated east of Quichapa

Lake. There, basin-fill sediments fine westward from gravely layers adjacent to the Cross Hollow Hills to clay near Quichapa Lake (figure 19; cross section E–E' [figure 15]).

The northern part of the valley has similar sediment distribution trends as the southern part. The eastern side of northern Cedar Valley is bisected by the EBBFS and the Enoch graben faults (figure 2). Aquifer materials on the margins of northern Cedar Valley are coarse and become progressively finer toward the valley center. However, near the center of the valley, northwest of Enoch, there are some areas of coarse material surrounded by fine-grained material (figure 19; cross section C–C' [figure 13]). On the east side of the valley, the abundance of gravel decreases from Cedar City northward toward Enoch.

Faults divide northern Cedar Valley into two subbasins, the Enoch graben and the deeper main Cedar Valley basin to the west (Hurlow, 2002). Basin-fill thickness is 2200 feet in the Enoch graben (Hurlow, 2002). West of the graben near Rush Lake, the main Cedar Valley basin deepens to more than 3800 feet. Cross sections of the area show the narrow Hieroglyph horst between the two faults that separate the adjoining basins (cross section B of plate 2 in Hurlow, 2002; cross section B–B'

Table 9. *Error of percent fines shown on figure 19 checked using percentage logs from Wallace (in Lowe and others, 2000).*

CAD[1]	WIN[2]	Wallace (%)	Map (%)	Difference (%)
(C-35-11)1bbb-1	17989	94.2	93.6	0.5
(C-35-11)14aad-1	23449	50	52	2
(C-35-11)9abb-1	18226	73	78.3	5
(C-35-11)9ccc-1	23340	79	97	17
(C-35-12)24cab-1	18032	8	19	11
(C-35-11)25bdb-1	19668	9	53.3	44
(C-35-11)31ccb-1	24222	77	70	7
(C-35-10)7ccd-1	14040	3	37	34
(C-37-12)2ccd-1	23134	50	88	38

[1]*U.S. Geological Survey well numbering system for Utah. See appendix B. The numbers after the dash at the end refer to order in which the wells were constructed and labeled for that location.*
[2]*Utah Division of Water Rights well identification number.*

[figure 12] this report). The horst likely continues southward beneath the surface toward western Enoch (figure 2; cross section D–D' [figure 14]).

Driller's logs for wells 11427 and 14025 (table 8) show consolidated sediments on the Hieroglyph horst between the Enoch-graben-west fault and the EBBFS (figure 2). The log of well 11427 shows sandstone at 520 feet below the ground surface (cross section D–D' [figure 14]). The driller's log for well 14025 shows conglomerate at a depth of 405 feet (cross section B–B' [figure 12]). The consolidated material is probably Hurlow's (2002) unit B, which consists of consolidated Tertiary-age alluvial and mudflow material. The depths to sandstone from the well-drillers' logs are within 100 feet of unit B as shown on cross sections A and B of Hurlow's (2002) plate 1.

Discussion

Our cross sections and map of the distribution and percentage of fine-grained sediments generally agree with work by others (Taylor and Thomas, 1946; Bjorklund and others, 1978; Lowe and others, 2000; Hurlow, 2002; Brooks and Mason, 2005). Our cross section E–E' (figure 15) does not show as much coarse material as do the Hurlow (2002) and Lowe and others (2000) cross sections. This may be due to differences in how the sediments were grouped. Some sediment defined as "medium grained" by Lowe and others (2000) and Hurlow (2002) may be defined in this study as "fine grained." For example, the Hurlow (2002) cross sections generally show coarse/medium-grained deposits extending farther into the valley than do the cross sections prepared for this study. Because they contain significant amounts of fine-grained matrix material and individual clay strata that are prone to

compaction upon dewatering, we consider many of the sediments categorized as "medium grained" by Lowe and others (2000) and Hurlow (2002) to be compressible, and therefore include them in the "fine" category.

We described matrix-supported units as "coarse" when creating the fine-grained-sediment map. Due to ambiguity in the well drillers' logs, it is possible that we incorrectly categorized some units from the logs as "fine." Since we used various additional sources mentioned above to verify and refine the dominantly fine-grained sediments area (hachured area on figure 19), the hachured area is considered a more reliable estimate of the distribution of potentially compactable material.

CEDAR VALLEY LAND SUBSIDENCE

We evaluated land subsidence in Cedar Valley by comparing historical elevation data of various ages with newly acquired survey elevations measured in 2011 (appendix D). The UGS also contracted for an InSAR analysis of ground surface deformation in Cedar Valley (Katzenstein, 2013) which is presented in its entirety in appendix E.

Benchmarks in Cedar Valley with historical elevation data are limited in number and are of varying accuracy. Dozens of benchmarks were installed and measured in Cedar Valley by the USGS and the Utah State Engineer (USE) during the period 1905–1948 in support of topographic quadrangle mapping. We discovered that the majority of these benchmarks have been destroyed by agricultural and development activities in recent decades. We were able to locate 12 benchmarks in Cedar Valley that were spirit leveled prior to 1949, and an additional 12 monuments installed or rehabilitated by Enoch

City and measured using GPS methods in 1998.

An additional 48 monuments distributed throughout Cedar Valley were measured during the 2011 survey, but lack accurate historical elevation data. The monuments are chiefly section corner markers erected in recent decades by the Iron County Engineer. Unfortunately, elevations for the Iron County (IC) monuments are not available (Steve Platt, Iron County Engineer, verbal communication, 2009). Although these monuments coincide with published elevations (rounded to the nearest foot) on USGS 7.5-minute topographic quadrangles, the published elevations are deemed too inaccurate for use in determining subsidence. The USGS estimates supplemental elevations such as section corners, wells, road intersections, etc. (i.e., not benchmarks) on their topographic quadrangles using photogrammetric methods rather than precise leveling. Accuracy requirements for these supplemental elevations are roughly one-third the map contour interval (D. Benson, USGS, written communication, 2011), which for Cedar Valley quadrangles ranges from ± 3.3 to 13.3 feet (one-third of a 10- or 40-foot contour interval, respectively). Due to the inaccuracy of these reported elevations, the newly measured elevations in appendix D for those locations should only be used as a reference for future subsidence monitoring purposes. However, these monuments are not well distributed throughout the valley and are generally not coincident with the areas identified on InSAR imagery (Katzenstein, 2013; appendix E) as having the greatest magnitudes of subsidence. Additional new survey monuments would be required to adequately monitor subsidence throughout the valley.

The survey data presented in this report were collected by a Utah licensed Professional Land Surveyor (appendix D). Geographic location and ellipsoid heights were measured during the period September 24–November 4, 2011, using real-time kinematic (RTK) GPS methods. See appendix D for a complete description of survey methods and results.

Subsidence for the Pre-1949–2011 Period

U.S. Geological Survey topographic quadrangles for Cedar Valley show two types of pre-1949 benchmarks. The USGS installed four of the pre-1949 benchmarks in support of their topographic quadrangle mapping (stations USGS1, USGS3, USGS4, and USGS5 on figure 20). The USGS leveled benchmark USGS3 to 1st-order accuracy standards; the remaining three were leveled to 3rd-order accuracy standards (USGS, 1965, 1969). The original USGS leveling results, reported to the nearest thousandth of a foot (0.012 inch), are available in unpublished level-line notes on file at the USGS National Geospatial Technical Operations Center (USGS, 1965, 1969). The remaining eight pre-1949 benchmarks are USE benchmarks (USE1-8 on figure 20) that have elevations rounded to the nearest thousandth of a foot stamped on their disks. Few details are known about the installation of the USE benchmarks, or how they were measured. All elevations reported

for the USGS and USE benchmarks agree with the rounded benchmark elevations reported on USGS quadrangle maps for Cedar Valley. All pre-1949 leveled elevations are reported relative to the NGVD 29.

Methods

Orthometric elevations reported in this study are relative to the NAVD 88 and were produced by subtracting the NGS GEOID09 separation from GPS-measured ellipsoid heights (appendix D). To compare the historical leveled elevations measured relative to the NGVD 29 with the newly acquired GPS elevations, we converted the historical elevations to the NAVD 88 using the NGS online orthometric height conversion calculator VERTCON (National Geodetic Survey, 2010). Once in the same datum, the elevations were then directly compared to determine subsidence for the pre-1949–2011 period.
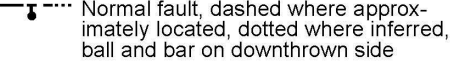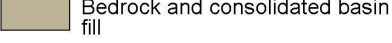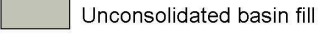
Data Accuracy

The allowable closure errors for 1st- and 3rd-order leveling are 0.05 foot $* D^{1/2}$ and 0.017 foot $* D^{1/2}$, respectively, where D is the total distance in miles of the level circuit or line (Marshall, 1911; U.S. Army Corps of Engineers, 2007). Since the lengths of the USGS level lines that were run through Cedar Valley are not known, we could not calculate accuracies for the historical elevations, although generally, even surveys of lower order accuracy have routinely been used to measure 0.05-foot changes in elevation over several miles (Galloway and others, 1999). The accuracy of elevations stamped on the USE benchmarks is not known, but since the elevations are published on USGS quadrangles as benchmark elevations, they likely at least meet USGS 3rd-order leveling accuracy standards.

With limited time and budget constraints, we contracted for an RTK GPS survey campaign which is less accurate compared to more time-consuming and therefore more expensive static GPS surveys. The manufacturer's published RTK vertical accuracy (Trimble, 2013) for the GPS unit used (Trimble 5800) is ± 20 millimeters (0.8 inch) + 1 part per million (ppm); 1 ppm is equal to 0.063 inch of error per mile from the base station. Baseline lengths for benchmarks used in our subsidence calculations were less than 5.5 miles, therefore the RTK instrument vertical accuracy is 0.8 inch + (0.063 inch * 5.5) = ± 1.1 inch. GPS measurement error may be greater depending on accuracies of ellipsoidal height and published elevations of vertical control stations.

Other sources of error for our subsidence calculations include (1) the NGS VERTCON orthometric height conversion (a modeled accuracy of 0.8 inch or less [1 sigma], although locally, errors may be greater; Milbert, 1999), and (2) the GEOID09 model used to convert GPS-derived ellipsoid heights into orthometric elevations (about ± 0.6 inch; Roman and

EXPLANATION

▲ Benchmark, elevation change (feet) in bold, station name in parentheses

— Fissure

⊢•⊣ Normal fault, dashed where approx-imately located, dotted where inferred, ball and bar on downthrown side

Bedrock and consolidated basin fill

Unconsolidated basin fill

Shaded relief base map from the Utah AGRC ArcGIS Image Service
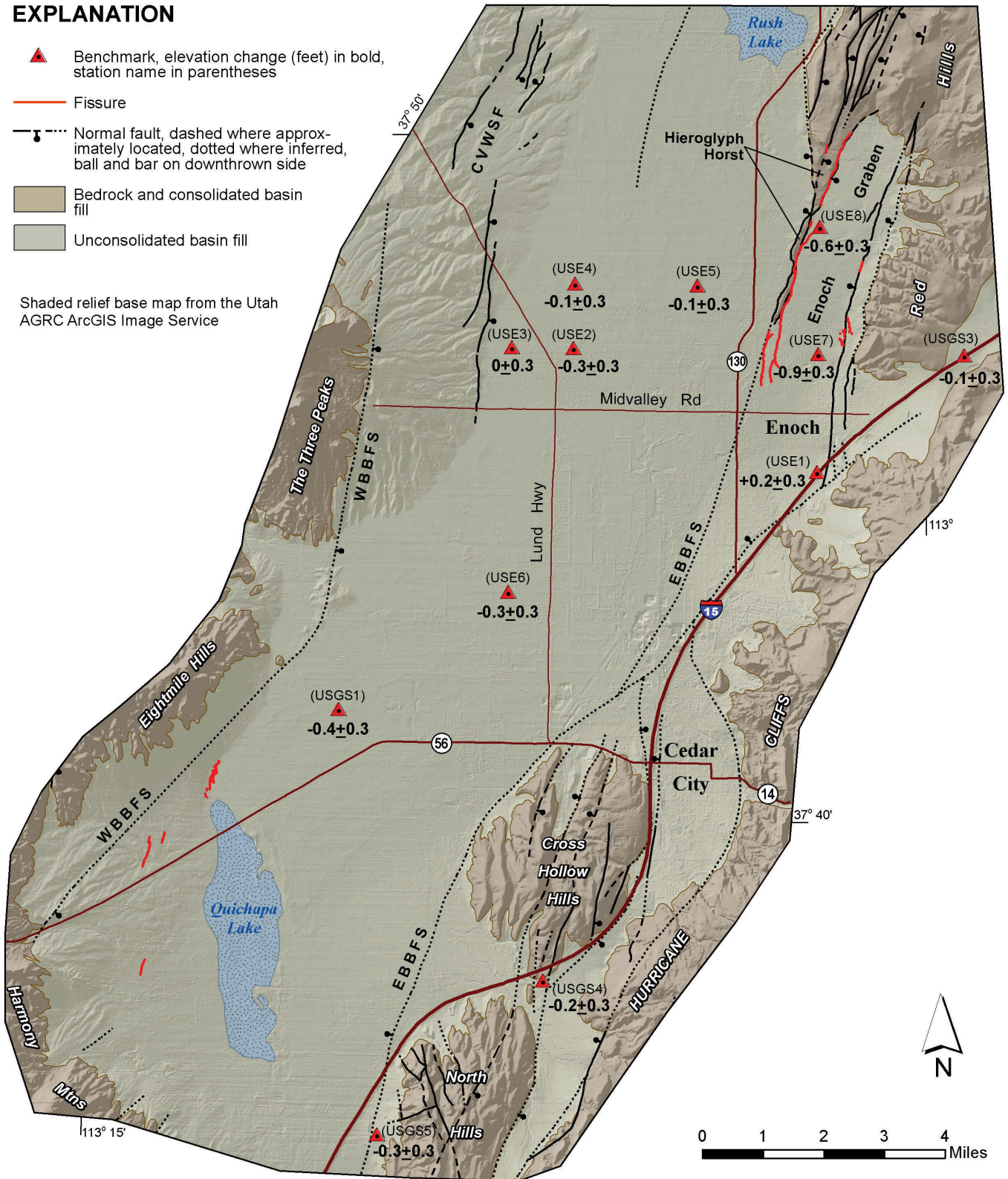
Figure 20. *Subsidence for the period pre-1949–2011, based on comparison of historical leveling and modern GPS data. Table 10 lists survey data, subsidence calculation results, and estimated errors. Geology from Rowley and others (2006); CVWSF = Cedar Valley west-side faults, WBBFS = western basin-bounding fault system, and EBBFS = eastern basin-bounding fault system.*

others, undated). The combined error from all above sources is approximately ± 0.3 foot.

Uncertainties in leveling techniques and modeled transformations between the NGVD 29 and the NAVD 88 datums (VERTCON) are illustrated by comparing historical leveling elevation data for benchmark USGS4 (figure 20), which is in a geologically stable area. The USGS leveled that benchmark in 1928 to 3rd-order accuracy, and adjusted the results to the NGVD 29 datum (elevation = 5794.57 feet). The NGS re-leveled benchmark USGS4 in the mid-1980s to 1st-order accuracy and adjusted the height to the NAVD 88 datum (elevation = 5798.09 feet). Adding the VERTCON shift value (3.701 ft) to the older USGS-leveled elevation to adjust it to the NAVD 88 (Geoid09) datum yields an elevation of 5798.27 feet, 0.18 foot higher than the elevation relative to the NAVD 88 datum. Since benchmark USGS4 is founded in bedrock, the apparent 0.18 foot of subsidence reflects the combined inaccuracies of leveling and the VERTCON conversion.

Results

Subsidence results for the pre-1949–2011 period are in table 10 and plotted on figure 20. Only three (USE7, USE8, and USGS1) of the 12 benchmarks have calculated subsidence greater than the expected uncertainty of ± 0.3 foot. Benchmarks USE7 and USE8, both within the Enoch graben, experienced the greatest elevation decline—0.9 and 0.6 foot ± 0.3 foot, respectively. Benchmark USGS1 in the southwestern

part of Cedar Valley subsided 0.4 foot ± 0.3 foot. Calculated elevation changes at the remaining nine monuments did not exceed the expected uncertainty, indicating that the vertical position changes at these monuments have either been less than ± 0.3 foot or static.

Figure 20 shows an elevation change of as much as 0.18 foot at benchmarks USGS3 and USGS4 despite being in geologically stable areas. The apparent subsidence indicated at these benchmarks is within our estimated uncertainty (± 0.3 foot) and reflects the combined errors of leveling techniques, GPS-derived elevations, and the VERTCON transformation (see Data Accuracy above) rather than a physical change in elevation. The subsidence data may be normalized (held fixed) to stable benchmark USGS4 by adding 0.18 foot (i.e., the difference between the 1928 and 2011 elevations at benchmark USGS4) to all subsidence values. However, such a correction would show apparent, but statistically insignificant uplift at several benchmarks (USE3, USE4, USE5, and USGS3) of 0.1 to 0.2 foot where uplift is not reasonable. An exception is benchmark USE1 which would show a significant and unreasonable uplift of 0.4 foot. Since normalizing the subsidence data to USGS4 results in apparent uplift at several benchmarks in the northern part of Cedar Valley, we do not consider the normalization correction demonstratively more accurate across the study area. For these reasons, we made no further changes to the subsidence results in table 10.

Due to the absence of benchmarks with historical elevation

Table 10. *Summary of survey data and calculated subsidence in Cedar Valley for the period pre-1949–2011.*

Benchmark Name	Latitude (NAD 83)	Longitude (NAD 83)	pre-1949 elevation (ft) (NGVD 29)	pre-1949 elevation source	pre-1949 elevation (ft) (NAVD 88)	2011 elevation[1] (ft) (NAVD 88)	pre-1949–2011 elevation change (ft)
USE1	37°45'02.89513"N	113°01'55.21873"W	5589.228	Stamped on disk	5592.971	5593.2	0.2 ± 0.3
USE2	37°46'46.58577"N	113°06'21.18172"W	5475.371	Stamped on disk	5478.957	5478.7	-0.3 ± 0.3
USE3	37°46'46.64312"N	113°07'28.02633"W	5472.694	Stamped on disk	5476.277	5476.3	0.0 ± 0.3
USE4	37°47'42.28742"N	113°06'20.26504"W	5456.960	Stamped on disk	5460.543	5460.4	-0.1 ± 0.3
USE5	37°47'41.97424"N	113°04'07.49607"W	5452.561	Stamped on disk	5456.147	5456.0	-0.1 ± 0.3
USE6	37°43'16.06975"N	113°07'28.11268"W	5536.041	Stamped on disk	5539.621	5539.3	-0.3 ± 0.3
USE7	37°46'44.44311"N	113°01'55.82384"W	5471.308	Stamped on disk	5474.973	5474.1	-0.9 ± 0.3
USE8	37°48'33.93808"N	113°01'55.79890"W	5482.922	Stamped on disk	5486.528	5485.9	-0.6 ± 0.3
USGS1	37°41'33.12338"N	113°10'30.04815"W	5485.899	USGS 3rd order	5489.469	5489.1	-0.4 ± 0.3
USGS3	37°46'44.85196"N	112°59'17.53782"W	5808.597	USGS 1st order	5812.423	5812.3	-0.1 ± 0.3
USGS4	37°37'41.76511"N	113°06'45.13994"W	5794.570	USGS 3rd order	5798.271	5798.09	-0.18 ± 0.3[2]
USGS5	37°35'27.67231"N	113°09'42.21564"W	5552.758	USGS 3rd order	5556.397	5556.1	-0.3 ± 0.3

[1]*See appendix D for details of 2011 GPS survey.*
[2]*Elevation change assumed to be zero since benchmark is located in a geologically stable area.*
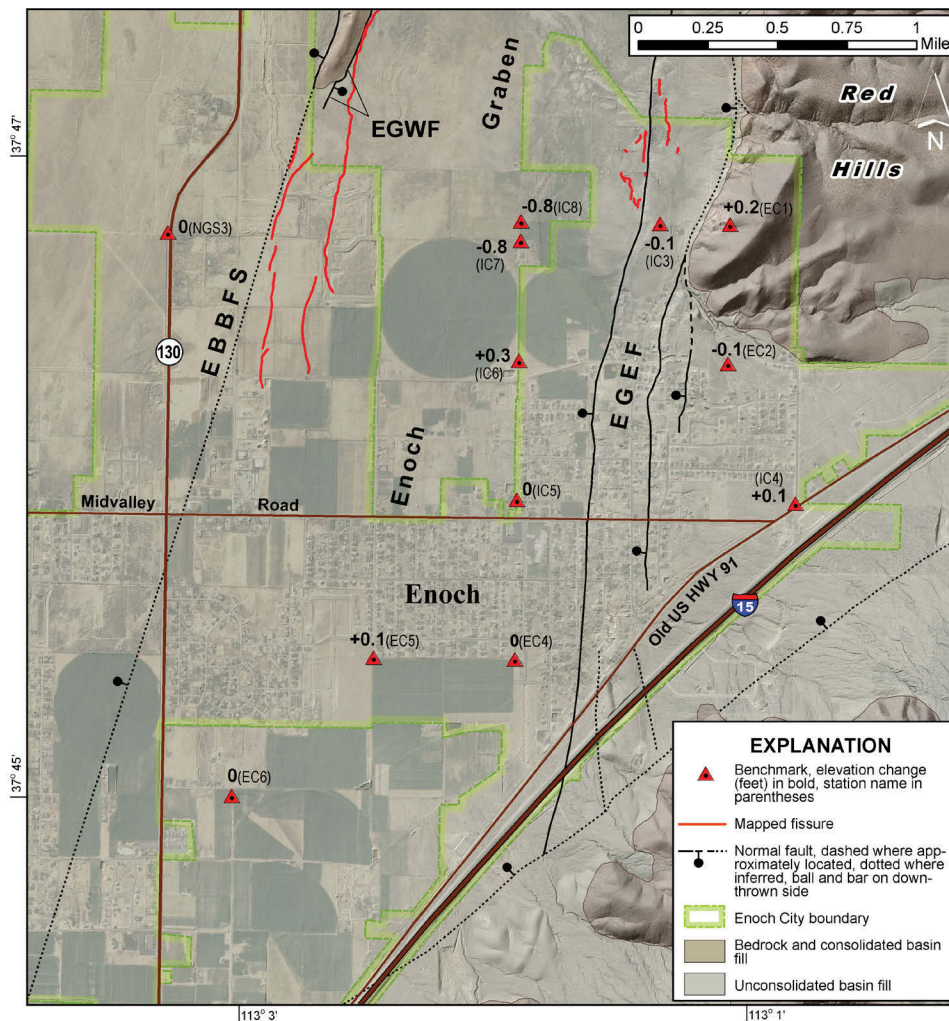
Figure 21. *Subsidence for the period 1998/1999–2009/2010 in Enoch City. Table 11 lists survey data, subsidence calculation results, and estimated error. Geology is from Rowley and others (2006); EBBFS = eastern basin-bounding fault system, EGWF = Enoch-graben-west faults, and EGEF = Enoch-graben-east faults. Base map consists of 2009 NAIP imagery (Utah AGRC, 2009) and shaded relief derived from 1-meter LiDAR data (UGS, 2011).*

data in the southern part of the valley, including the Quichapa Lake area, subsidence amplitude and distribution for the pre-1949–2011 period there are unknown.

Subsidence for the Period 1998–2011

Enoch City restored 29 permanent benchmarks at section corners within the city limits in 1998. The restoration campaign consisted of resurveying existing IC markers; damaged or destroyed benchmarks were replaced with Enoch City (EC) brass caps. Survey work was performed by a Utah licensed Professional Land Surveyor using a Trimble 4400 GPS system and RTK methods. Enoch City provided the survey map with geographic coordinates and ellipsoid heights to the UGS for this study. The survey narrative attached to the map indicates ellipsoid heights could vary by as much as 0.4 feet. A nearby NGS High Accuracy Reference Network station (HARN [NGS Permanent Identifier HO0468]; benchmark NGS3 on figure 21) was the basis for geographic coordinates and

ellipsoid heights. Many of the benchmarks measured in 1998 have subsequently been destroyed; however, we successfully located 12 benchmarks and had them resurveyed during the period September 24–November 4, 2011, using RTK GPS methods (appendix D).

Methods

Comparison of the measured ellipsoid heights from the 1998 and 2011 surveys required additional analysis. Both the 1998 and 2011 surveys utilized the NGS NAD 83 network, as reported by the NGS in its datasheets for NGS3 and other nearby NGS-network benchmarks, as the ellipsoid-height basis. The NGS has published various adjustments or realizations of the NAD 83 network over past decades. The 1998 Enoch survey was based on the 1994 realization of the NAD 83 datum, commonly expressed as NAD 83(1994). The NGS has since adjusted its network and, in 2007, published a new realization of the NAD 83 datum (NAD 83[2007]). The NAD 83(2007)

datum is the datum used for the 2011 survey in this report (appendix D). The NAD 83(2007) datum is 0.314 foot lower in height compared to the NAD 83(1994) datum at NGS3. Therefore, to compare measurements made in the two different datums, 0.314 foot was subtracted from the ellipsoid heights reported in the 1998 Enoch survey (table 11). Since benchmark NGS3 is founded in unconsolidated deposits in an area that newly acquired InSAR imagery (Katzenstein, 2013; appendix E) shows has subsided, it is possible that a component of the minus-0.314-foot elevation change in the NGS datasheets may reflect subsidence. However, separating physical monument movement from regional network adjustments used to produce the station's published coordinates is not possible with currently available data (M. Vorhauer, NGS, written communication, 2010). Survey data and calculated subsidence are listed in table 11. Figure 21 shows monument locations and calculated subsidence for the period 1998–2011.

Results

Two benchmarks experienced elevation change within the margin of error of our calculations (approximately ± 0.4 ft). Benchmarks IC7 and IC8 in the central Enoch graben subsided 0.8 feet. The remaining monuments were relatively stable. The nearly equal amounts of subsidence in the central Enoch graben for the periods 1998–2011 (0.8 ft) and ~1949–2011 (0.9 ft) indicates that the onset of significant subsidence there likely began in the late 1990s.

Discussion

Our subsidence calculations document as much as 0.9 foot of subsidence in the Enoch graben, and that measurable subsidence (0.1–0.4 ft) has likely occurred in other parts of central Cedar Valley. However, the number of existing benchmarks with accurate historical elevation data in Cedar Valley is insufficient to adequately characterize the distribution, amplitude, and rate of subsidence in the valley. Newly acquired InSAR imagery shows that a broad area of central Cedar Valley has experienced varying amounts of subsidence during the periods 1992–2000 and 2004–2010 (Katzenstein, 2013; appendix E). Additionally, we have documented significant groundwater drawdown in areas of Cedar Valley that also have thick accumulations of compaction-prone, fine-grained sediments in the subsurface (see Cedar Valley Aquifer Characteristics section above); however, the absence of historical benchmarks in those areas prevents documenting absolute subsidence amounts. For example, in the Quichapa Lake area, we have documented 70 to 90 feet of groundwater decline between 1939 and 2009 (figure 18), thick zones of compressible fine-grained sediments in the subsurface (figure 19), and active zones of earth fissures north and west of the lake (see Cedar Valley Earth Fissures section below). Although benchmarks with accurate historical elevation data are not available in the vicinity of Quichapa Lake, the Katzenstein (2013) InSAR study documents significant subsidence in that area (appendix E). The up to 3 feet of down-to-the-east displacement across the Enoch-graben-west fissures (see following section) indicates that local areas of subsidence greater than 0.9 foot are present within the graben, but are inadequately identified due to the sparse distribution of historical benchmarks.

Periodic re-observations of a well-distributed GPS network across Cedar Valley and repeated applications of sat-

Table 11. Summary of survey data and calculated subsidence for the period 1998–2011 in Enoch City.

Benchmark Name	Latitude (NAD 83)	Longitude (NAD 83)	1998 Ellipsoid Height (ft) (NAD 83[1995])	1998 Ellipsoid Height[1] (ft) (NAD 83[2007])	2011 Ellipsoid Height[2] (ft) (NAD 83[2007])	1998–2011 Elevation Change (ft)
NGS3	37°46'46.04416"N	113°03'19.33709"W	5400.763	5400.449	5400.449	0 ± 0.4
EC1	37°46'48.80003"N	113°01'06.37349"W	5600.8	5600.5	5600.7	0.2 ± 0.4
EC2	37°46'22.71841"N	113°01'06.48633"W	5571.3	5571.0	5570.9	-0.1 ± 0.4
EC4	37°45'26.76050"N	113°01'55.99013"W	5466.2	5465.9	5465.9	0.0 ± 0.4
EC5	37°45'26.71690"N	113°02'29.37889"W	5436.4	5436.1	5436.2	0.1 ± 0.4
EC6	37°45'00.44218"N	113°03'02.46518"W	5468.3	5468.0	5468.0	0.0 ± 0.4
IC3	37°46'48.85339"N	113°01'22.94053"W	5456.6	5456.3	5456.2	-0.1 ± 0.4
IC4	37°45'56.66699"N	113°00'50.05357"W	5654.9	5654.6	5654.7	0.1 ± 0.4
IC5	37°45'56.65732"N	113°01'55.98034"W	5456.7	5456.4	5456.3	0 ± 0.4
IC6	37°46'22.78492"N	113°01'55.91456"W	5424.7	5424.4	5424.7	0.3 ± 0.4
IC7	37°46'45.30800"N	113°01'55.82556"W	5404.0	5403.7	5402.9	-0.8 ± 0.4
IC8	37°46'48.95056"N	113°01'55.80365"W	5401.5	5401.2	5400.4	-0.8 ± 0.4

[1]*From 1998 survey control map for Enoch City.*
[2]*See appendix D for details of 2011 GPS survey.*

ellite-based techniques such as InSAR can better define the distribution and rate of subsidence in Cedar Valley. The GPS-measured network of monuments in this study (appendix D) is limited, but provides an initial basis for future monitoring. An expanded network of better distributed new benchmarks would be required to fully quantify subsidence in Cedar Valley. New benchmarks should be constructed to minimize near-surface influences from shrink/swell soils, etc. Additional information on a high-precision benchmark network is included in the High-Precision GPS/GNSS Survey Network section.

CEDAR VALLEY EARTH FISSURES

To identify subsidence-related features in Cedar Valley, we (1) examined eight sets of aerial imagery (see Sources of Information section) covering all or parts of the study area for the period 1938 to 2011, (2) examined 2011 1-meter LiDAR imagery covering Cedar Valley (Utah Geological Survey, 2011b), (3) made a field reconnaissance of possible earth-fissure lineaments identified on aerial photographs and LiDAR, and (4) investigated reports of possible earth fissures received in response to a press release asking the public to report possible fissures.

To ensure that the study area was fully scrutinized on aerial photography, we created a quarter-section grid overlay of Cedar Valley for viewing in Google Earth, and systematically reviewed each grid for photolineaments of unknown origin on mid-1990s (Utah AGRC, 2013), 2006 (Utah AGRC, 2006a, 2006b), 2009 (Utah AGRC, 2009), and 2011 (Utah AGRC, 2011) orthophotography. Photolineaments identified on the Google Earth imagery were then checked against older stereoscopic photo sets (1938, 1960, 1981; see Sources of Information section) and recent LiDAR imagery (Utah Geological Survey, 2011), to remove lineaments related to abandoned roads, buried utilities, stock trails, etc. We then investigated the remaining photolineaments of unknown origin in the field. Fieldwork consisted of locating, mapping (with a hand-held, recreational-grade GPS unit), describing, and photographing confirmed earth fissures. Additionally, we investigated several reports of possible earth fissures received from the public in response to a press release placed in a local newspaper, and identified two previously unrecognized fissures.

Our initial inventory of Cedar Valley fissures (Knudsen and others, 2012), which relied almost entirely on aerial-photography analysis and word-of-mouth reports from citizens, yielded 3.9 miles (trace length) of fissures. With the advantage of newly acquired (2011), valley-wide LiDAR coverage, our current investigation more than doubled the total length of mapped fissures in Cedar Valley to 8.3 miles. While it is possible that new fissures may have formed during the short period between our investigations (about 2 years), the significant increase of mapped fissures is most likely due to the greater resolution of LiDAR compared to aerial photography

as a reconnaissance tool.

Fissures in Cedar Valley are concentrated along the east and west margins of the Enoch graben and north and west of Quichapa Lake in the southwestern part of the valley (figure 22). Mapped fissures are described in detail in the following sections.

Enoch-Graben-West Fissures

The Enoch-graben-west fissures are the most extensive zone of fissures in Cedar Valley. The fissure zone is as much as 0.25 mile wide and is closely aligned with the western margin of the Enoch graben—a narrow structural basin bounded by the Red Hills to the east and the narrow Hieroglyph horst to the west (figures 22 and 23). The fissures closely parallel and commonly coincide with the Enoch-graben-west faults. The 4.4-mile-long fissure zone extends from near 5200 North in Enoch City to the middle of section 19, T. 34 S., R. 10 W., Salt Lake Base Line and Meridian (SLBM) (figure 23). Knudsen and others (2012) mapped the most prominent fissure (EGWF1) as part of their reconnaissance study of subsidence and fissures in Cedar Valley, and supposed that the 2.5-mile-long EGWF1 was the extent of fissuring along the western margin of the Enoch graben. However, subsequently acquired LiDAR imagery revealed an additional 2.9 miles of fissures along the western side of the Enoch graben, resulting in a total of 5.4 miles of fissures in that area. Enoch-graben-west fissures formed in generally fine-grained sediment, mapped by Knudsen (2014a) as distal alluvial-fan deposits (map units Qaf_1 and Qafc, figure 23), or are localized near the contact between the younger fine-grained sediment (Qaf_1 and Qafc) and older fan alluvium (QTaf). The Enoch-graben-west fissures (numbered EGWF1–6) are described in detail in the following sections.

Description of Fissure EGWF1

The largest fissure in Cedar Valley, in terms of length and vertical displacement, EGWF1 extends for 2.5 miles (trace length) north from near the southern border of the Parkview subdivision in Enoch City to the NE1/4 section 36, T. 34 S., R. 11 W., SLBM (figure 23). Sinuous in detail, EGWF1 is generally arcuate at map scale with an average trend of N. 15° E. The fissure exhibits down-to-the-east displacement along nearly its entire length, creating a prominent, near-vertical deflection (scarp) in the ground surface (figure 24) that has a maximum height of about 3 feet near the center point of the fissure. The fissure consists of a single continuous strand, except for two short sections (less than 25 feet long) of closely spaced parallel strands where the fissure exhibits its maximum displacement. Sinkholes and elongate depressions up to 5 feet long, 3 feet wide, and 2.5 feet deep are common along and near the fissure (figure 25).

The southern 0.5 mile of EGWF1 crosses the Parkview subdi-
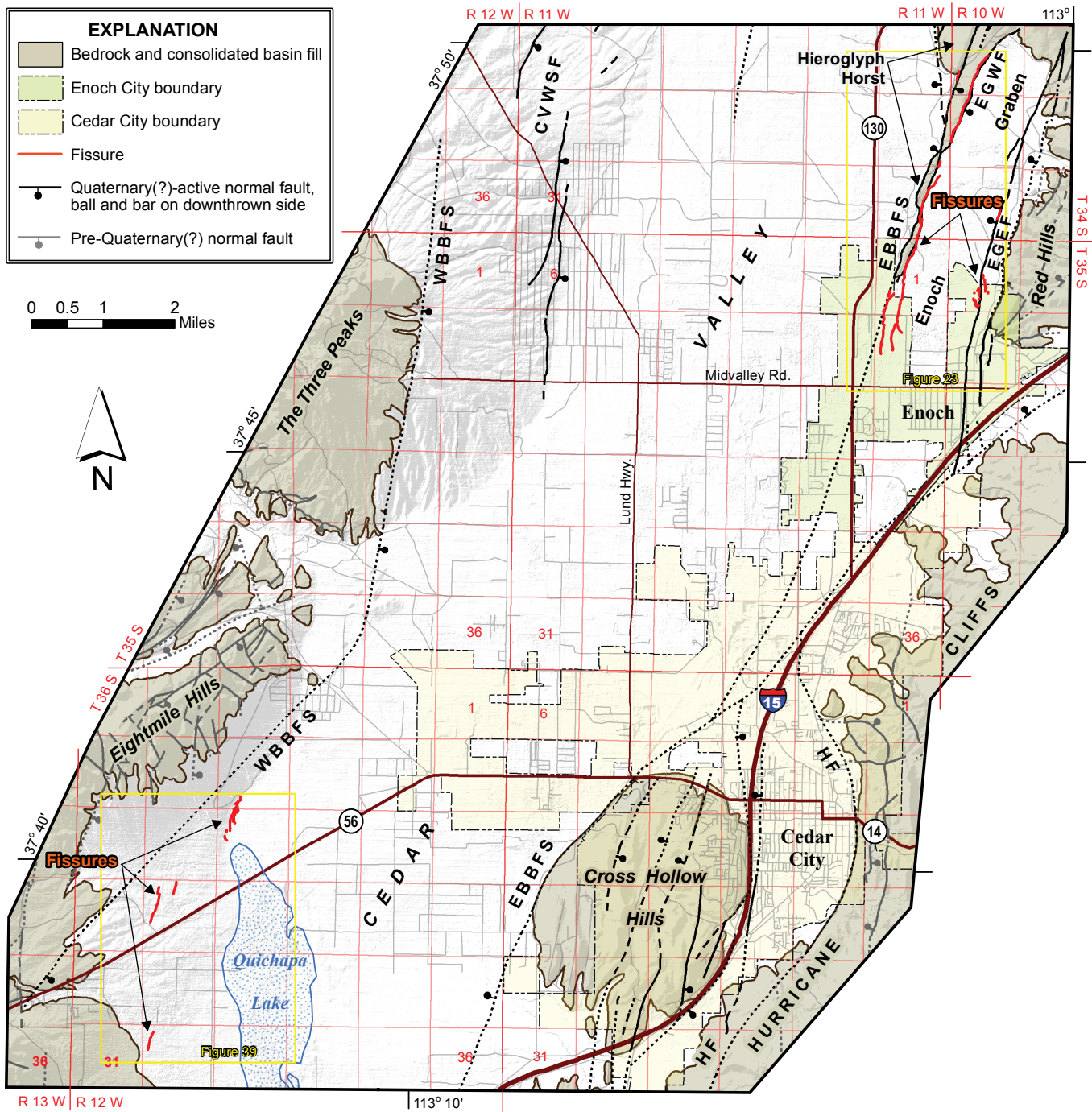
Figure 22. *Fissures in Cedar Valley and their relations to Quaternary faults. CVWSF = Cedar Valley west-side faults, WBBFS = western basin-bounding fault system, EBBFS = eastern basin-bounding fault system, EGWF = Enoch-graben-west faults, EGEF = Enoch-graben-east faults, and HF = Hurricane fault. Shaded relief base map from the Utah AGRC ArcGIS Image Service.*

vision (figures 23 and 26E). The fissure exhibits about 3 feet of vertical surface displacement where it enters the subdivision from rangeland to the north (figure 24). Grading and construction for the subdivision began in late 2006, and destroyed evidence for the fissure within the 475-lot development. Paved roads, sidewalks, curb and gutter, and underground utilities were completed in the summer of 2007, as was a single model home that remained unoccupied as of November 2013. Fissure-related damage to street pavement was first

noticed about a year after completion of paving (Earl Gibson, Enoch City Public Works Director, verbal communication, 2009). We originally observed the road damage in May 2009, where EGWF1 intersects 5700 North, and where it crosses a roundabout at the intersection of 850 East and 5600 North. Periodic visits to the subdivision since May 2009 have revealed continued damage to road surfaces (figure 27) due to additional vertical displacement across the fissure and subsequent piping of road-section aggregate base by infiltrating surface
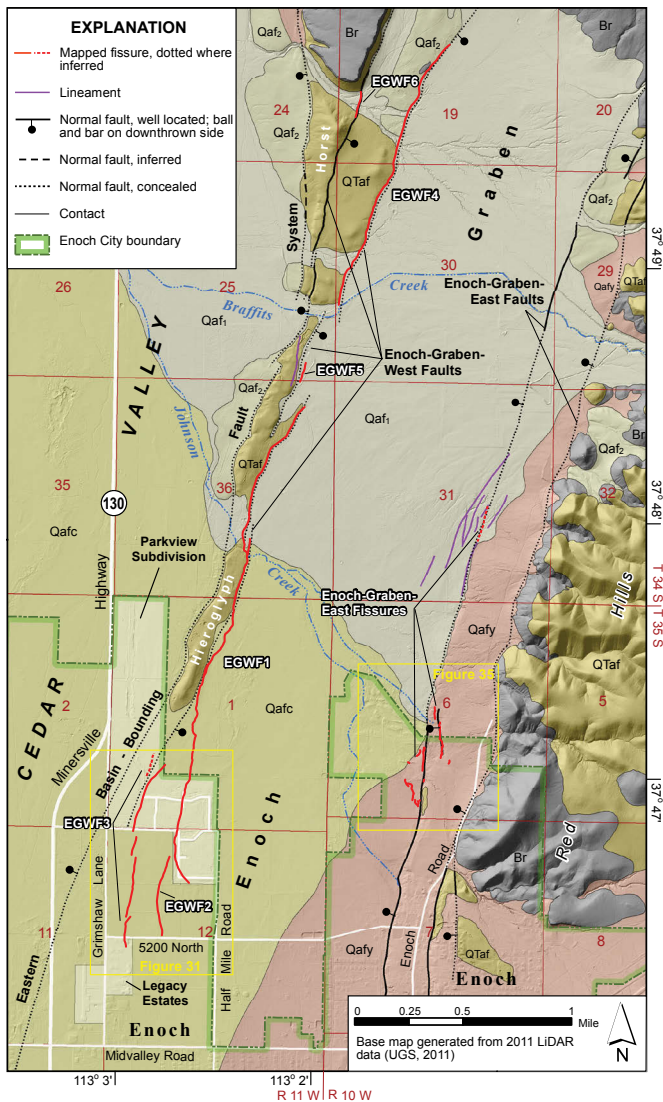
Figure 23. Fissures near and within Enoch City (as of July 2013). Geology modified from Knudsen (2014a); Qaf_1 = Holocene to upper Pleistocene level-1 fan alluvium, Qaf_2 = lower Holocene to upper Pleistocene level-2 fan alluvium, $Qafy$ = Holocene to upper Pleistocene undivided fan alluvium (includes both Qaf_1 and Qaf_2 alluvium), $Qafc$ = Holocene and upper Pleistocene coalesced fan alluvium, $QTaf$ = Pleistocene to Pliocene older fan alluvium, Br = bedrock.

Figure 24. Scarp produced by down-to-the-east displacement across the EGWF1 fissure immediately north of the Parkview subdivision in Enoch City (view is to the northeast). Photo taken in May 2009.

Figure 25. Sinkholes aligned along the EGWF1 fissure (view is to the northwest). Photo taken in May 2009.

water. Since the street was paved in 2007, vertical displacement across EGWF1 has cracked, warped, and displaced pavement several inches. Repeat measurements of the cracked pavement yielded an average slip rate of about 1.7 in/yr. Down-to-the-east vertical displacement has also reversed the flow direction of the main subdivision sewer line installed in 2007 (Earl Gibson, Enoch City Public Works Director, verbal communication, 2009). South of 5600 North, EGWF1 traverses several undeveloped graded lots on the west side of 850 East (figure 26E). Displacement across the fissure is not yet apparent on the lots, although surface water has eroded a thin, discontinuous ground crack 0.25–2 inches wide with several small sinkholes along its length. Near 5500 North, the fissure

bends to the southeast and crosses 850 East, creating a 3-foot-wide zone of en echelon hairline cracks in the pavement with about 3 to 4 inches of vertical surface displacement across the zone. The fissure was not detected beyond 850 East during our July 2013 field reconnaissance. However, the fissure is visible
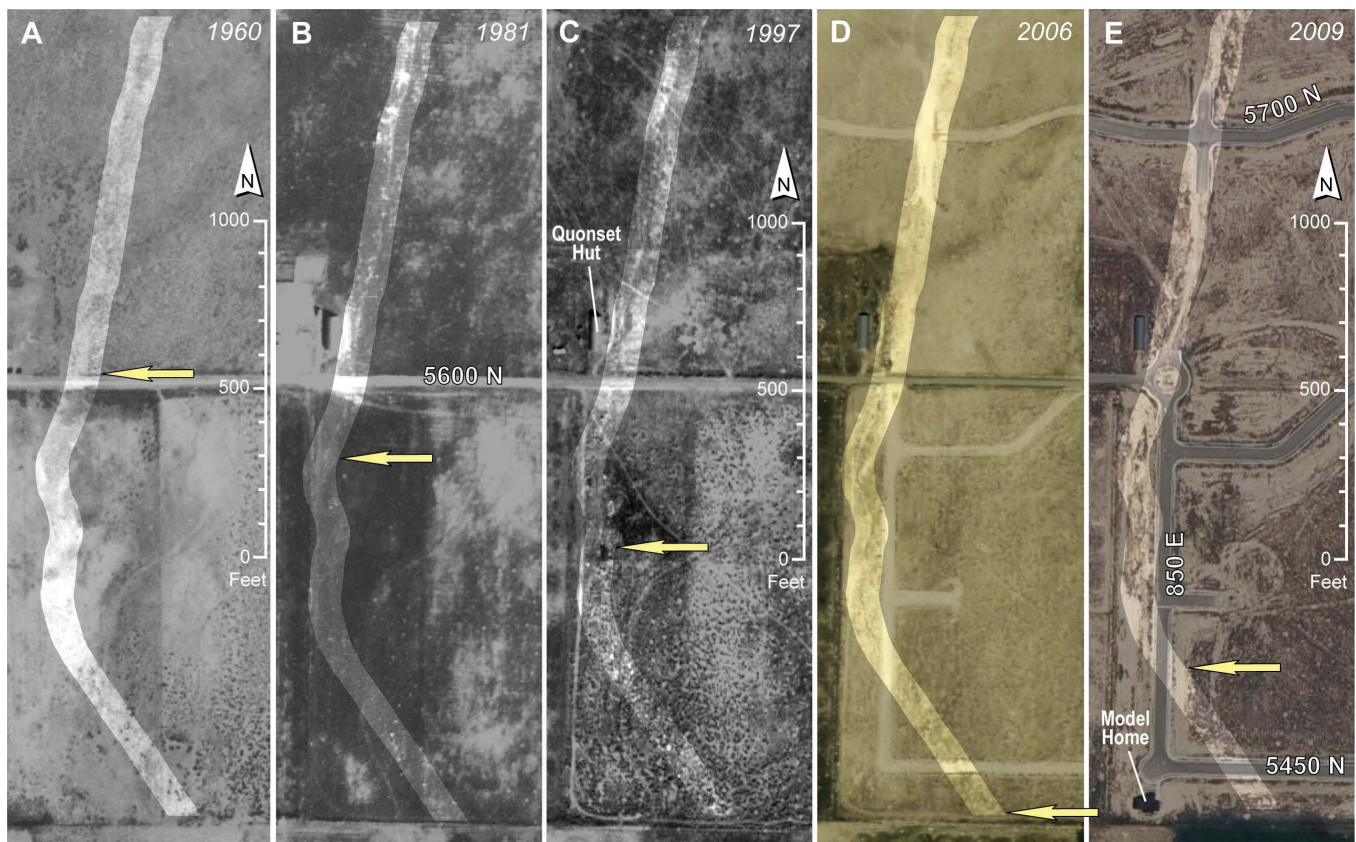
Figure 26. *Historical aerial-photograph analysis of the southern extent (yellow arrow) of the EGWF1 fissure. Area surrounding the 2006 fissure extent is highlighted in each photo. A. 1960 USDA photo showing a faint lineament that does not appear to have vertical displacement. B. 1981 low-sun-angle photo showing a well-developed fissure that dies out just south of 5600 N. C. 1997 USGS photo indicating 250 feet of southward lengthening since 1981. D. 2006 NAIP imagery showing the fissure extending to the southern property boundary prior to major earthwork for the Parkview subdivision. E. 2009 NAIP photo showing the destruction of many portions of the fissure due to earthwork and paving.*
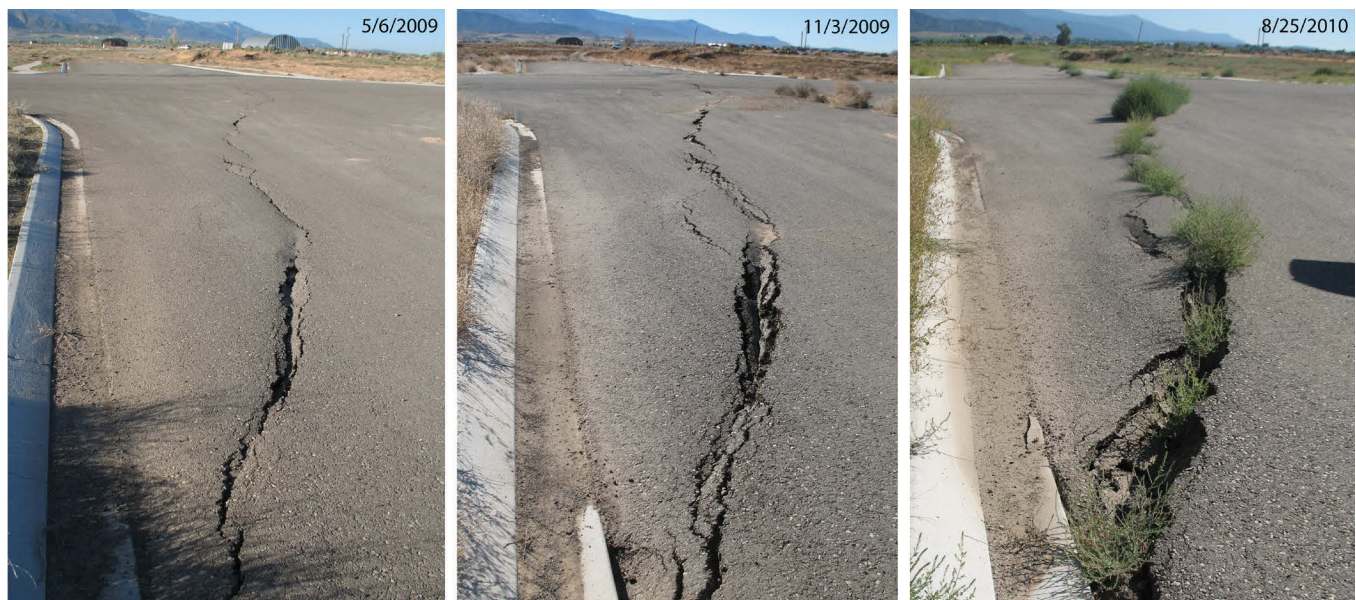
Figure 27. *Time sequence photo comparison showing progressive damage to pavement in the Parkview subdivision by the EGWF1 fissure. View is to the south toward the intersection of 5700 North and 850 East. Quonset hut in middle distance of first photo was removed before remaining photos were taken.*

Figure 28. Repair to irrigation pivot track where it crosses the scarp of the EGWF1 fissure (view is to the northwest). Photo taken in May 2009.

on 2006 NAIP orthophotos that predate major earthwork for the subdivision (figure 26D and E). On the photos, the fissure extends to the development's southern boundary and passes within 250 feet of the model home.

North of the subdivision, EGWF1 traverses undeveloped rangeland and irrigated farmland. Approximately 1800 feet of the fissure crosses an agricultural field irrigated by a pivoting sprinkler irrigation system. Ranch operator Mike Clark indicated (verbal communication, 2009) that the rate of vertical displacement across the fissure requires the annual addition of material to the irrigation system's tire track to create a ramp that allows the pivot wheel to cross the growing fissure scarp (figure 28).

The USGS Enoch 7.5-minute topographic quadrangle shows Johnson Creek—a minor drainage that collected runoff from once-perennial springs emanating from the east side of the Enoch graben—passing through a low point in the narrow Hieroglyph horst and continuing westward toward Rush Lake. Although the springs are now dry, storm and irrigation water still occasionally fill Johnson Creek. Our field observations and review of aerial photography showed that at the intersection of EGWF1 and Johnson Creek, the fissure traverses

a heavily used livestock pasture/feeding area. Animal waste covers the livestock area, and the intermittent flow in Johnson Creek passes through the waste before ponding against the fissure scarp, which now blocks the stream drainage (figure 29).

It is unknown when EGWF1 began to form, although USDA 1960 aerial photographs show a few short (less than 2000 feet long), discontinuous lineaments coinciding with the modern fissure location, indicating initial fissure development by that time (figure 26A). Mr. Clark stated (verbal communication, 2009) that he noticed fissure-related features, including sinkholes, on his ranch as a child in the 1970s. The fissure is clearly visible on 1981 low-sun-angle photos as a continuous lineament, although it appears about 1150 feet shorter at its southern end than it is today (figure 26B). USGS 1997 (Utah AGRC, 2013) orthophotos show the fissure extended southward about an additional 250 feet since 1981 (figure 26C). NAIP 2006 (Utah AGRC, 2006a) orthophotos show the fissure at roughly the extent it has today (figure 26D), indicating approximately 800 feet of southward lengthening between 1997 and 2006. On currently available 2011 NAIP imagery, the southern extent of the fissure has been obscured by grading for the Parkview subdivision in Enoch City.

Descriptions of Fissures EGWF2–EGWF6

The EGWF2 fissure extends 2000 feet to the north from 5200 North in Enoch City to nearly join EGWF1 where it traverses the Parkview subdivision (figure 23). The fissure is apparent on 2011 LiDAR (Utah Geological Survey, 2011; figure 30), but because it crosses land that is regularly plowed, the fissure is not always evident along its entire length in the field. However, we observed a well-developed ground crack (figure 31) and small (< 1 ft. diameter), aligned sinkholes after a significant rain storm in August 2012. Although scarp formation is subdued due to agricultural activities, we estimate as much as 6 inches of down-to-the-east surface displacement across the fissure. The fissure has an average trend of N. 5° E., and can be traced to within 350 feet of the southern part of EGWF1 which shares a similar orientation (figures 23 and 30). Due to similar trends and a closely overlapping relationship, EGWF2 may be considered to be the southern extension of EGWF1.

EGWF3 consists of five en echelon fissures that parallel the combined EGWF1/EGWF2 fissure between 600 and 1000 feet to the west (figure 30). EGWF3 trends an average of N. 8° E. and extends from near 5200 North in Enoch City northward across the central part of the Parkview subdivision (figure 30). The total trace-length sum of the fissures is 5160 feet. Individual fissure segments range from 480 to 1800 feet long and are separated by narrow (< 150 feet) dextral step-overs. Despite being in an area that has been significantly disturbed by development and agricultural activities, we observed substantial evidence for the fissures in the field including 1–4-centimeter-wide ground cracks, numerous elongate sinkholes up to 2 feet long and 1 foot deep, and down-to-the-east ground-surface displacement (figure 32). The central fissure segments south
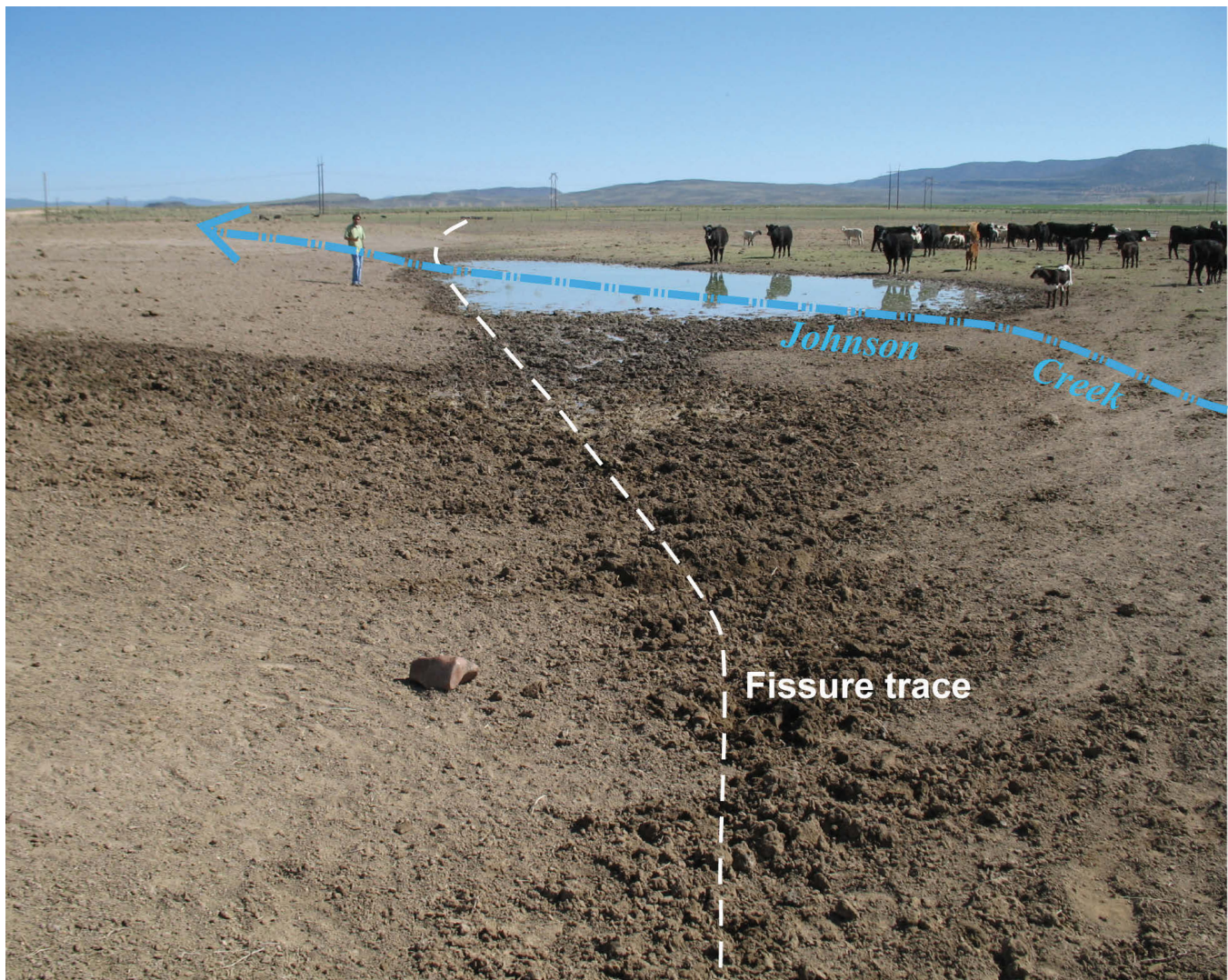
Figure 29. *Scarp of the EGWF1 fissure blocking the Johnson Creek drainage and allowing water to pond along the fissure (view is to the northwest). Photo taken in May 2009.*

of the Parkview subdivision exhibit the greatest vertical surface displacement of 5 to 6 inches. Although EGWF3 crosses 5600 North and 5700 North (paved in 2007) in the Parkview subdivision, we have not detected any definitive cracks in pavement due to fissures as of July 2013.

2011 LiDAR data show the southern approximately 240 feet of EGWF3 extending into the Legacy Estates subdivision (figure 30) and within 50 feet of a home. Ongoing construction at Legacy Estates, which began in 2006, and ongoing agricultural activity have obscured field evidence of the fissure near and within the subdivision, but following a severe rain event on July 27, 2013, we documented a well-defined ground crack within 100 feet north of 5200 North. Developing cracks across the asphalt concrete pavement (figure 33) of 5200 North are coincident with the mapped fissure trace determined from LiDAR data. Although there is not yet any discernible vertical displacement of pavement, the lengthening of cracks and addition of cracks in this area are likely caused by move-

ment along EGWF3.

The EGWF4 fissure extends 1.3 miles along the western margin of the Enoch graben in the western parts of sections 30 and 19, T. 34 S., R. 10 W., SLBM (figure 23). Although easily identified on 2011 LiDAR data, the fissure is not everywhere well developed in the field. The EGWF4 fissure, like other subdued fissures in the northwestern part of the Enoch graben, is best viewed following accelerated erosion events caused by an abundance of surface water from heavy-precipitation storms. We mapped the extent of EGWF4 following a severe cloudburst storm in August 2012 that caused localized flooding in Enoch City. The fissure trends N. 21° E. and is expressed as eroded linear ground cracks as much as 4 inches wide and 2 feet deep (figure 34), and thinner cracks (~1–2 in wide) that link elongate sinkholes which are up to 3 feet long and 2 to 3 feet deep. Although hillshade terrain models of the LiDAR data indicate possible vertical offset of the ground surface across EGWF4, we could not definitively
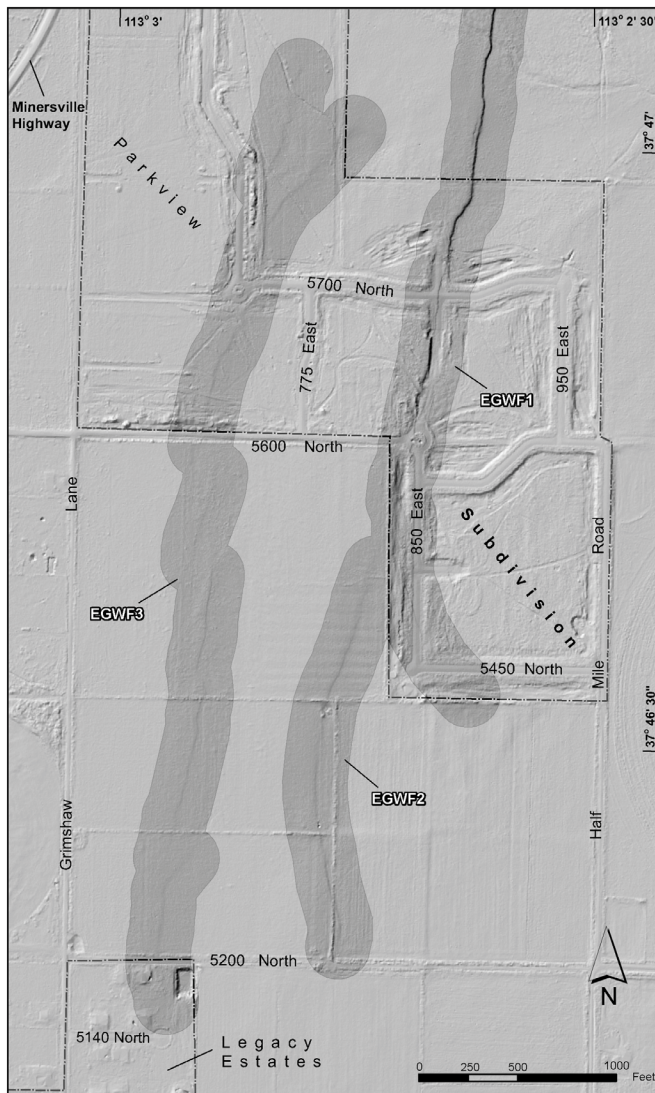
Figure 30 (above). 2011 Bare-earth LiDAR image (UGS, 2011) showing where Enoch-graben-west fissures intersect the Parkview and Legacy Estates subdivisions. Shading added to highlight fissure traces.

Figure 31 (top right). The EGWF2 fissure on August 23, 2012, shortly after a significant rainfall event. View is to the south.

Figure 32 (right). The EGWF3 fissure on August 23, 2012, exhibits down-to-the-east ground-surface displacement of 6 inches. View is to the north.

distinguish if low escarpments we observed along and near the fissure were related to the fissure, surface faulting, or if they are slight elevation inflexions across geologic contacts between older (and higher) alluvial fan deposits (Qaf$_2$ and QTaf) and younger fine-grained fan deposits (unit Qaf$_1$) (figure 23). We mapped the southern extent of EGWF4 to Braffits Creek, where evidence of the fissure is likely obscured by the construction of channels and dikes.

We mapped the N. 8° E.-trending EGWF5 fissure for 480 feet

Figure 33 (above). *Progression of crack formation on asphalt concrete pavement at 5200 North in the Legacy Estates subdivision in Enoch City. Cracks are coincident with the mapped EGWF3 fissure. View is to the south.*

Figure 34 (right). *Trace of the EGWF4 fissure on August 23, 2012, shortly after a significant rainfall event. View is to the south.*

in an area modified by dike construction and that is occasionally inundated by heavy runoff from Braffits Creek (figure 23). EGWF5 is similar in appearance to EGWF4 with discontinuous linear cracks generally less than 1 inch wide and sparse sinkholes less than 1 foot in diameter. We detected no ground-surface displacement across the fissure. Subparallel to, and about 200 feet west of EGWF5 is a 1200-foot-long lineament visible in 2011 LiDAR data (Utah Geological Survey, 2011) and 2006 HRO aerial photography (Utah AGRC, 2006b). Although the lineament looks similar to nearby fissures in the LiDAR and aerial photography, we found little evidence in the field for a fissure, and could not rule out the possibility that the lineament could be an eroded fault scarp.

Fissure EGWF6 traverses a narrow deposit of fine-grained alluvial-fan deposits (Qaf$_1$) where an unnamed drainage passes through the Hieroglyph horst in the SW1/4 section 19, T. 34 S., R. 10 W., SLBM (figure 23). The 635-foot-long fissure trends N. 12° E. and is characterized by discontinuous linear cracks at the surface that are less than 2 inches wide. Elongate sinkholes with fissure-aligned long dimensions as much as 2 feet, and with depths as much as 2 feet, are common in the
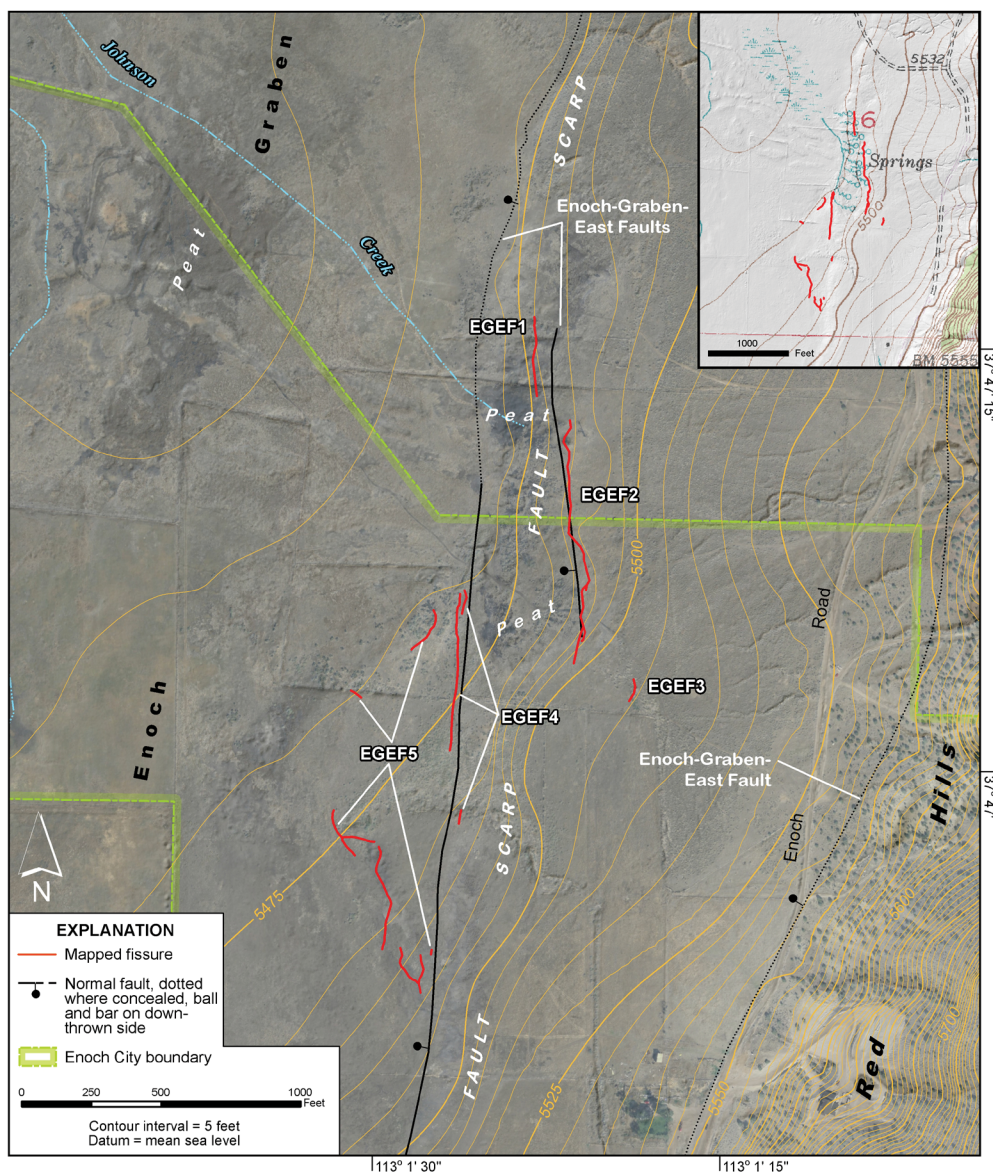
Figure 35. *Extent of the Enoch-graben-east fissures as of July 2013; fault locations from Knudsen (2014a). Base map consists of 2006 HRO imagery (Utah AGRC, 2006b). Inset is a portion of the 1950 USGS Enoch 7.5-minute quadrangle showing mapped springs and marsh in relation to the Enoch-graben-east fissures; inset map contour interval is 10 feet.*

bottom of two east-west-trending gullies that carry significant runoff during cloudburst storms. We detected a subdued scarp (< 1 ft high) along portions of EGWF6, but the scarp could be an eroded fault scarp produced by surface rupture of the Quaternary-active fault that is coincident with the fissure. We found evidence for the fissure within a few feet on both sides of a moderately used gravel road that accesses a cinder quarry about 1.5 miles to the northeast. Damage to the road was not evident, likely because the road is regularly graded.

Enoch-Graben-East Fissures and Desiccation Cracks

We mapped several poorly defined, discontinuous fissures (numbered EGEF1 through EGEF5 on figure 35) north of

Enoch City along the eastern margin of the Enoch graben in the S1/2 section 6, T. 35 S., R. 10 W., SLBM (figure 23). We also mapped several prominent lineaments visible on aerial photography and LiDAR imagery approximately 1 mile to the north in the S1/2 section 31, T. 34 S., R. 10 W., SLBM (figure 23). However, we could not gain access to the lineaments that are on private property, and therefore we could not verify if fissures are present there. The main group of fissures in section 6 forms a diamond-shaped zone approximately 1000 feet wide and 2500 feet long. The long axis of the zone trends N. 10° E., roughly parallel with a west-facing, 6- to 10-foot-high scarp created by the westernmost Enoch-graben-east fault (figure 35; Knudsen, 2014a; Rowley and Threet, 1976; Black and others, 2003). The fissures vary from aligned sinkholes (figure 36) to eroded fissure-aligned gullies; we did not detect
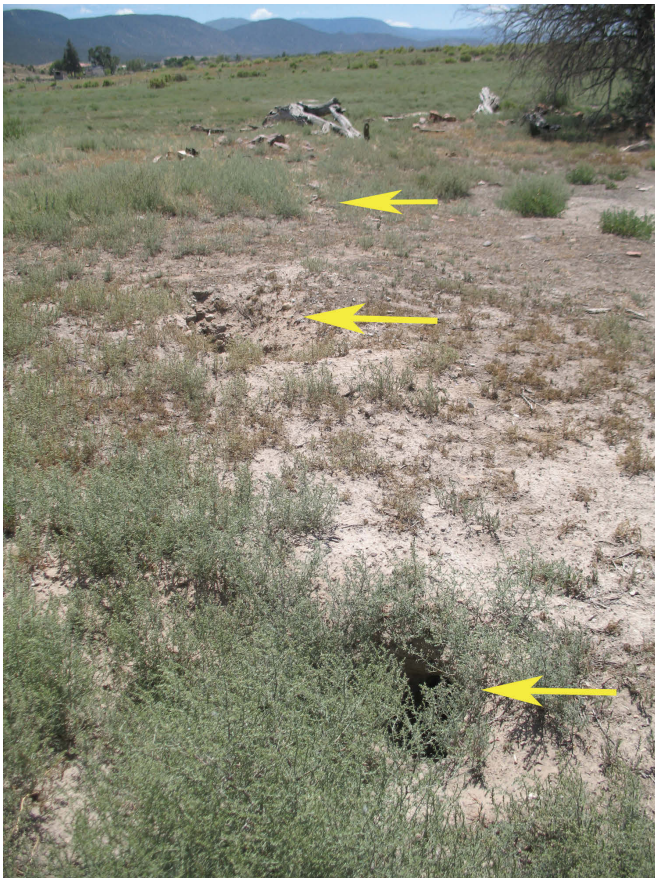
Figure 36. *Trace of the EGEF2 fissure expressed as aligned sinkholes in fine-grained alluvium (yellow arrows indicate sinkholes; view is to the southeast). Photo taken in June 2009.*

Figure 37. *Vertical desiccation cracks developed in dried peat deposits on the east side of the Enoch graben in a former marsh area (view is to the northwest). Photo taken in June 2009.*

any vertical displacement across any of the Enoch-graben-east fissures. The fissures are formed on coarse- to fine-grained Holocene to late Pleistocene alluvial-fan deposits (Knudsen, 2014a), and near the now-dry springs, on thick dried peat deposits (figure 35) and organic clay associated with a formerly extensive marsh. Some fissures in this zone are partially obscured by a dense network of polygonal desiccation cracks in the dried peat. Individual polygons, defined by deeply eroded cracks up to 15 inches wide and 22 inches deep, range from 2 to 5 feet across (figure 37).

Fissures EGEF1 and EGEF2 extend for 300 and 930 feet, respectively, and form a 100-foot-wide left step-over pattern (figure 35). Both fissures trend about N. 5° W., and are characterized by numerous elongate sinkholes and depressions up to 20 inches long, 14 inches wide, and 36 inches deep related to the collapse of pipes along the fissure plane. North-south-trending primary cracks are commonly visible in sinkhole walls, but rarely at the surface. EGEF1 and EGEF2 intersect an area of deep polygonal cracks developed in dried peat and clay-rich deposits, but can be distinguished from the desiccation cracks by the linear alignment of deep sinkholes. The fissures formed along a 6- to 10-foot-high, gently west-sloping (~4°) scarp created by one of the Enoch-graben-east

faults (Knudsen, 2014a; Black and others, 2003); EGEF2 in particular is closely aligned with the mapped trace of the fault (figure 35).

About 200 feet east of EGEF2 and the Enoch-graben-east fault scarp, EGEF3 is the easternmost fissure of the Enoch-graben-east fissures. We mapped 85 feet of fissure, although we suspect it may be longer but is partially obscured by heavy brush and the accumulation of tumbleweeds. Despite its short mapped length, a deep gully and sinkholes (both as much as 4 feet deep and 4 feet wide) make the fissure conspicuous in the field.

Three linear fissures that closely parallel the mapped trace of the Enoch-graben-east fault zone are grouped together as EGEF4 on figure 35. The fissures are expressed as mostly continuous, linear depressions less than 14 inches wide and 12 inches deep in organic-rich, clayey silt and sand deposits. The depressions have rounded walls, and slightly eroded cracks less than 2 inches wide are commonly visible in the depression bottoms. Combined, the fissures are 705 feet long and trend an average of N. 3° E. The southernmost EGEF4 fissure is partially obscured by wind-blown sand deposits.

Figure 38. *Trace of an EGEF5 fissure formed on fine-grained alluvial-fan deposits. View is to the south. Photo taken in April 2013.*

We combined a group of sinuous and branching ground cracks occupying flat ground west of the Enoch-graben-east fault scarp into fissure group EGEF5 (figure 35). The fissures are typically expressed as isolated, hairline cracks with sparse sinkholes less than 10 inches wide and 8 inches deep. Shorter (< 15 ft long), more heavily eroded sections form linear gullies up to 1 foot deep and 1 foot wide (figure 38). Most branches generally trend to the northwest, but the northernmost EGEF5 fissure trends northeast. The EGEF5 fissures are developed in fine-grained, clay-rich alluvial-fan deposits.

Due to a lack of surface displacement and a generally minor degree of erosion, the main Enoch-graben-east fissures are not visible on aerial photographs; therefore, we could not estimate the time of fissure formation by looking at photos of different ages. However, analysis of geomorphic and hydrologic features on aerial photographs and topographic maps, combined with verbal reports from long-time Enoch residents provide insight on when the springs on the east side of the Enoch graben dried up, and significantly reduced groundwater recharge to the Enoch graben aquifer. Spring water is apparent on USDA 1960 aerial photos, and several springs and a marsh are shown on both the 1950 USGS 15- and 7.5-minute Enoch topographic quadrangles. Spring and marsh symbols remain on a 1978 photo-revised edition of the Enoch quadrangle (figure 35 [inset]), although the map states that revisions were not

field-checked. The area adjacent to the springs appears dry on 1981 low-sun-angle photos, indicating perennial spring flow had ceased sometime between 1960 and 1981. The exact timing of the drying of the springs and marsh within that period is unknown; however, a local, long-time rancher indicated that it occurred sometime in the mid- to late 1970s (Norman Grimshaw, verbal communication, 2009). This is in agreement with Bjorklund and others' (1978) report of the springs near Enoch City being dry at the time of their study. Earth-fissure formation likely commenced along the east side of the Enoch graben following desiccation of the springs and marsh.

Enoch-Graben-East Lineaments

We mapped several prominent lineaments visible on aerial photography and 1-meter LiDAR imagery (USGS, 2011) about 1 mile north of the main Enoch-graben-east fissures (figure 23). The lineaments are on private property and we could not gain access to the area. Most lineaments are deep gullies up to 6 feet deep (estimated from LiDAR-derived 3-foot contours). The unusually linear gullies trend an average N. 21° E. and closely parallel the Enoch-graben-west fault zone (figure 23). We assume the gullies could be localized along fissures until proven otherwise in the field. We mapped a single lineament that is roughly coincident with a strand of the Enoch-graben-east fault zone as an inferred fissure (figure 23), because the lineament's appearance in LiDAR imagery is strikingly similar to the appearance of other mapped fissures in Cedar Valley, including the alignment of prominent sinkholes.

Quichapa-North Fissures

A group of eroded fissures create a branching and en echelon pattern in a 3300 x 400-foot zone in western Cedar Valley, about 0.5 mile north of Quichapa Lake (figures 39 and 40). Many of the longer fissure segments trend between due north and N. 10° W., although the zone as a whole trends N. 20° E., closely paralleling the topographic break in slope defined by the intersection of gently east-sloping (2–3°) alluvial-fan deposits and the generally flat valley floor. The fissures also parallel an inferred concealed strand of the western basin-bounding fault system (figures 39 and 40). The fissures formed near the mapped contact between coarse- to fine-grained alluvial-fan deposits (map unit Qafy on figure 39) sourced from the Eightmile Hills and fine-grained coalesced alluvial deposits (map unit Qafc) on the valley floor.

Fissures in the northern part of the zone, grouped together and labeled QNF1 on figure 40, create a complex branching pattern where sinuous segments commonly splay or intersect, but do not cross. Most of the longer continuous strands generally trend north; shorter branches commonly splay off to the northeast or northwest, but a few trend east-west. QNF1 fissures are typically greatly enlarged by inflow of surface water that eroded vertical-walled gullies up to 5 feet deep
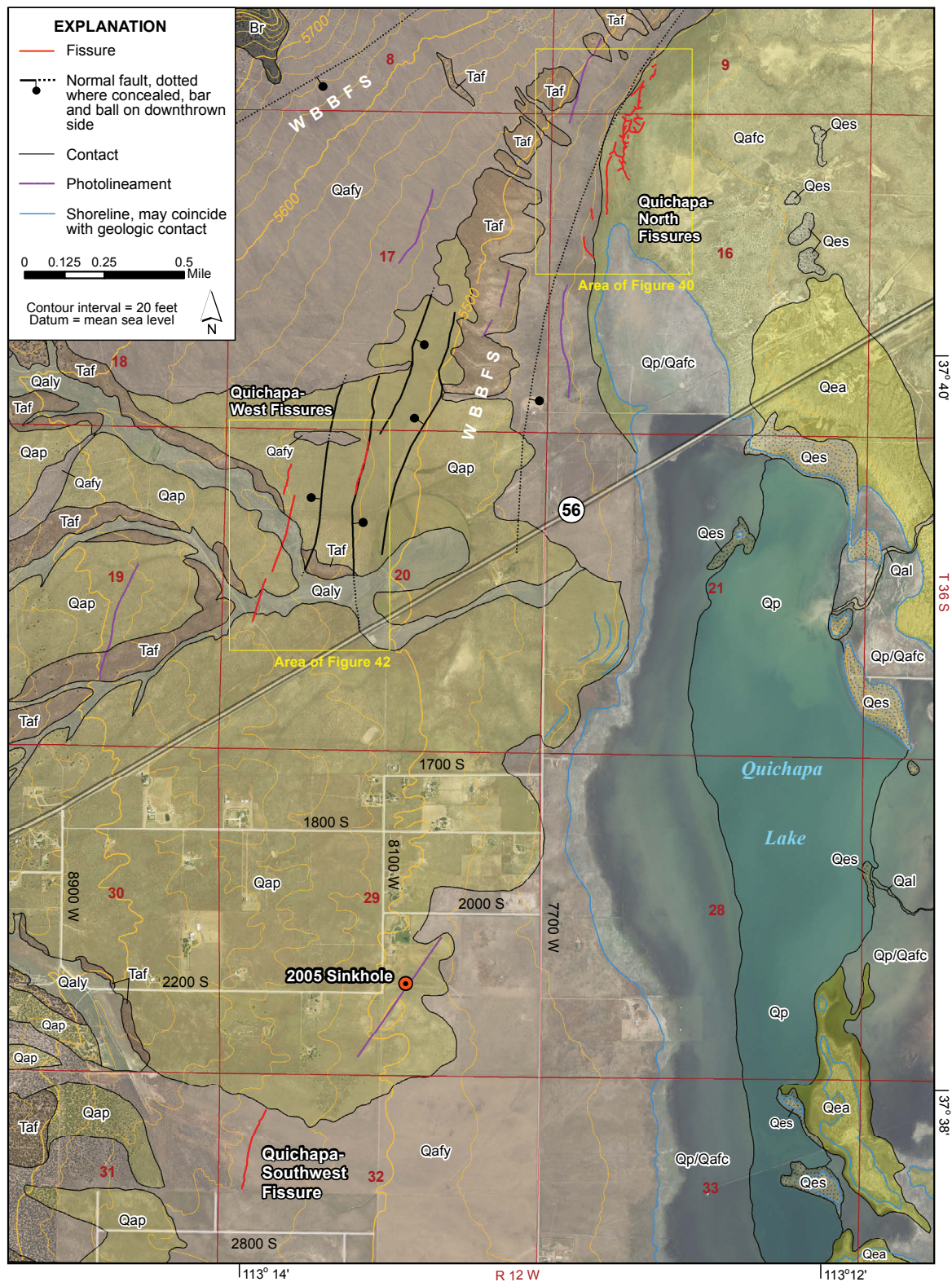
Figure 39. *Fissures near Quichapa Lake as of July 2013. Base map consists of 2011 NAIP imagery (Utah AGRC, 2011). Geology modified from Knudsen and Biek (2014); WBBFS = western basin-bounding fault system, Qaly = Holocene to upper Pleistocene alluvium deposited in low-relief stream channels and floodplains, Qafy = Holocene to upper Pleistocene alluvial-fan deposits; Qafc = Holocene to upper Pleistocene low-gradient, coalesced alluvial-fan deposits in central Cedar Valley, Qap = Holocene to middle Pleistocene(?) alluvium covering gently-sloping erosional surfaces, Qes = Holocene wind-blown sand deposits, Qp = Holocene to upper Pleistocene Quichapa Lake playa deposits, Qp/Qafc = thin (< 1 ft thick) playa deposits over low-relief alluvial-fan deposits, Qea = Holocene to upper Pleistocene eolian sand reworked by alluvial processes, Taf = Pliocene to Miocene moderately consolidated alluvial-fan deposits, and Br = Tertiary volcanic bedrock.*
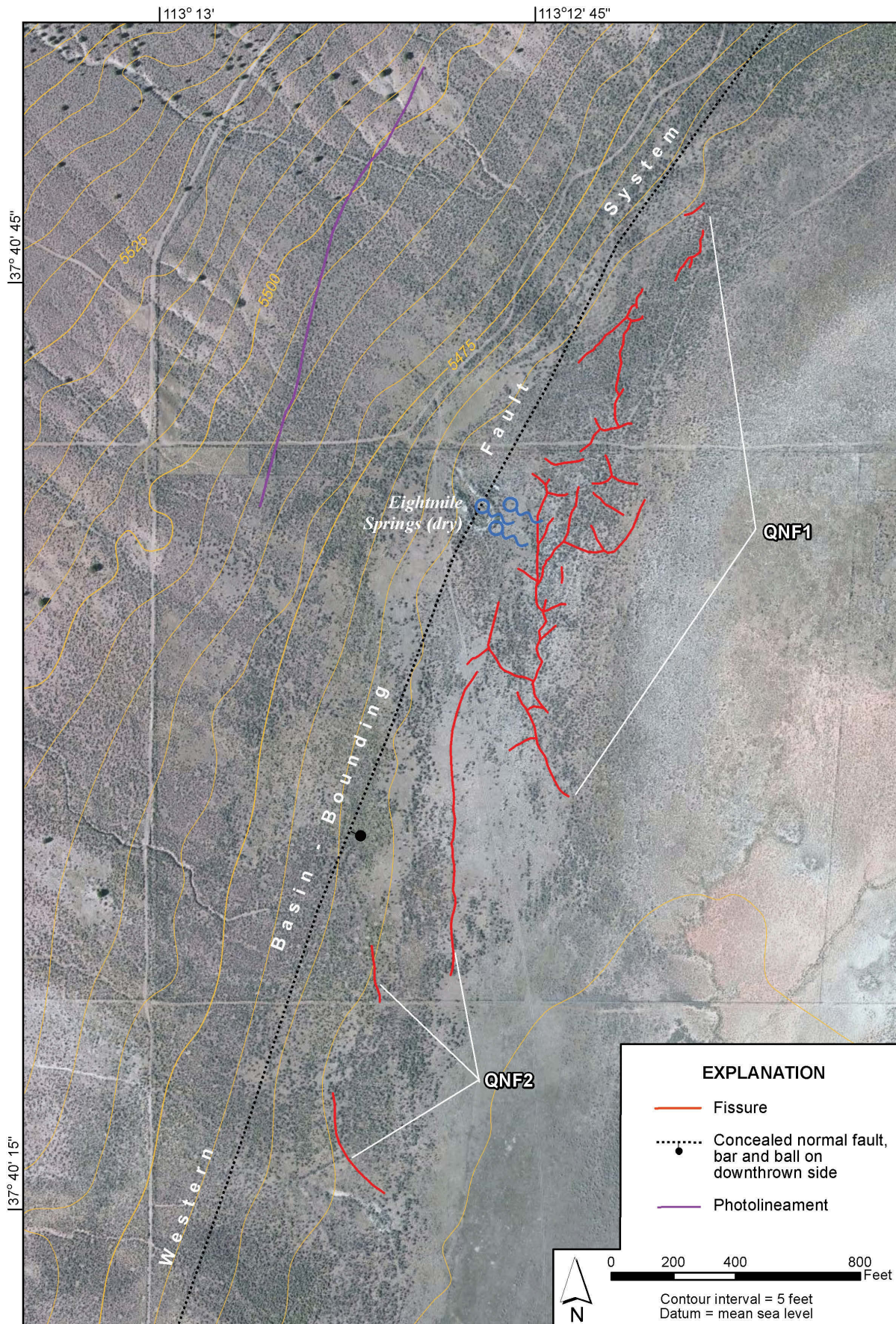
Figure 40. *Extent of Quichapa-north fissures as of July 2013. Undated aerial-photography base from Microsoft Bing Maps.*

Figure 41. *Vertical-walled gully eroded along a QNF1 fissure. Note branching pattern and soil bridging across the fissure (view is to the north). Photo taken in August 2009.*

and 3 feet wide (figure 41). Some 8- to 15-foot-long gullied sections are bridged by 8 to 20 inches of undisturbed surface sediment that disguise the large void below. Deeply gullied sections alternate with shorter sections of shallow (less than 12 inches deep) fissure-aligned depressions, uneroded hairline cracks, and unfissured ground. The total trace length of all QNF1 fissures is about 4900 feet. Near Eightmile Springs (now dry) (figure 40), two dirt roads used by ranchers have been rerouted and repaired to mitigate the effects of fissure damage.

The three southernmost fissures mapped north of Quichapa Lake, QNF2 on figure 40, are spaced about 200 feet apart, lack branches, and form an en echelon pattern. The fissures generally trend north-northwest and have a total trace length of 1560 feet. The longest fissure is about 1000 feet long and is arcuate at its northern end. Similar in appearance to the QNF1 fissures, surface-water inflow has enlarged sections of the QNF2 fissures up to 4 feet deep and 1.5 feet wide; however, intervening sections of uneroded primary cracks and uneroded ground are longer.

The timing of fissure development north of Quichapa Lake is unknown. Portions of the fissure complex are visible on 2006 HRO imagery (Utah AGRC, 2006b), indicating that the fissure existed prior to 2006. Fissures are not visible on older orthophotos, likely due to insufficient photo resolution rather than the absence of fissures.

Quichapa-West Fissures

Four linear fissures (QWF1-QWF4 on figure 42) trending N. 13° W. to N. 17° W. form a 0.6-mile-long zone in western Cedar Valley about 1 mile west of Quichapa Lake. The fissures formed in fine- to coarse-grained alluvial deposits sourced from the Eightmile Hills (map units Qap and Qaly of Knudsen and Biek, 2014; figure 39). The fissures closely parallel, and in one case, coincide with Quaternary-active normal faults of the western basin-bounding fault system (figure 42).

The easternmost Quichapa-west fissure, QWF1, is the only fissure identified in Cedar Valley that is expressed as an uneroded primary ground crack (figure 43) over its entire
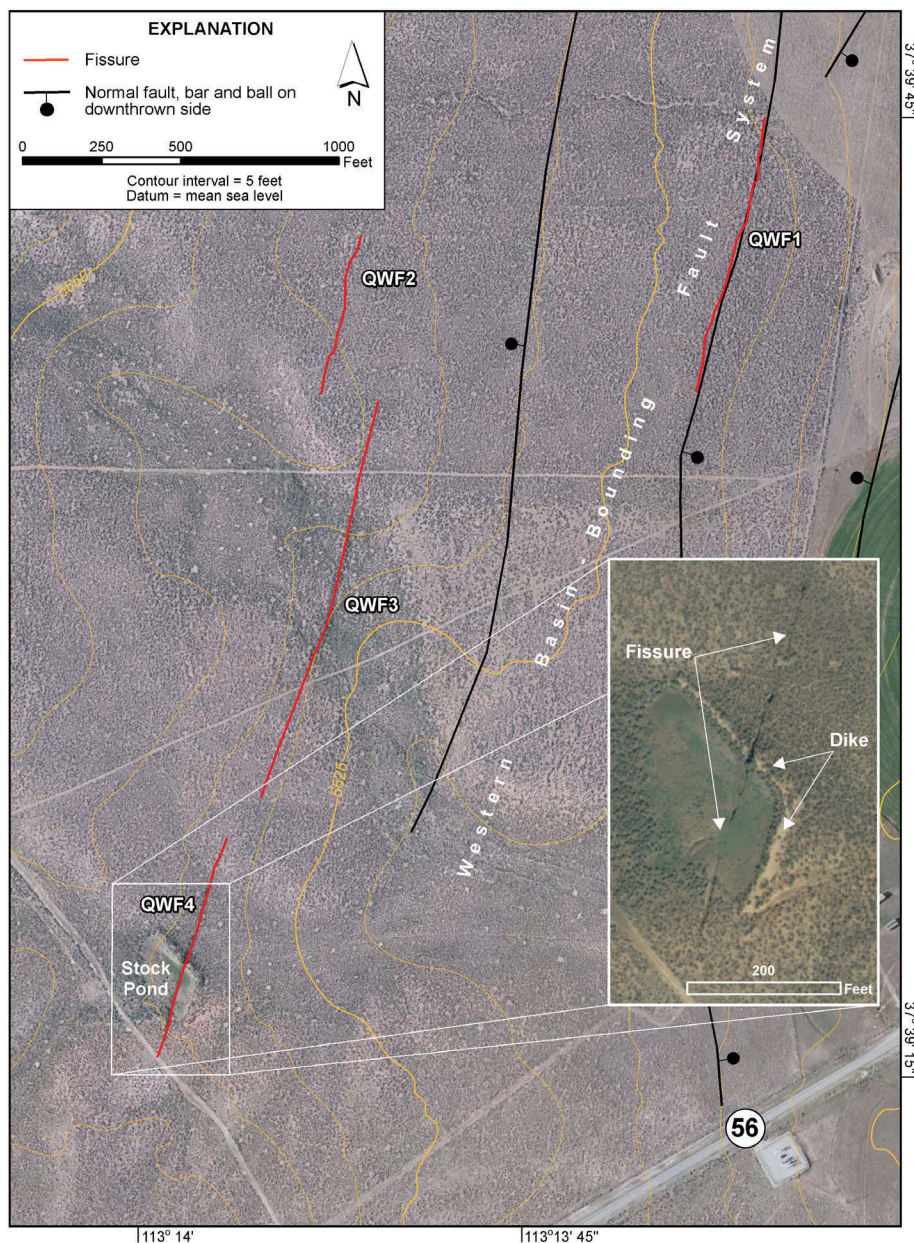
Figure 42. *Quichapa-west fissures as mapped in July 2013. Base map consists of undated aerial imagery from Microsoft Bing Maps. Inset is 2006 HRO photography (Utah AGRC, 2006b) showing fissure damage to stock pond and dike.*

length. The crack is commonly less than 0.4 inch wide, and in places was difficult to distinguish from shallow, centimeter-scale desiccation cracks in the clay-rich soil. We traced the crack to the north for 900 feet until it intersected a freshly scarified field being prepared for installation of a pivoting irrigation system; any further evidence of the crack was destroyed by the plowing. Sinuous in detail, the crack is remarkably linear at map scale. Curiously, despite its extremely narrow width, QWF1 is one of the few fissures on the west side of Cedar Valley that we detected on aerial photographs. A distinct color contrast across the fissure is visible on 2006 HRO imagery (Utah AGRC, 2006b) that is not apparent in the field, but may be related to a subdued fault scarp that is coincident with the fissure.

Fissure QWF2 is 520 feet long and is expressed as sparse sinkholes and open pipes separated by up to 30 feet of unfissured ground aligned along a N. 13° W. trend. The individual elongate holes are less than 3 feet long and taper downward into deep (at least 5 feet), inclined pipes eroded along the vertical fissure plane. We encountered evidence for this fissure only in ephemeral stream washes where surface flow has eroded and widened the fissure.

We traced fissure QWF3, expressed as a discontinuous deep gully up to 2 feet wide and 2.5 feet deep, for 210 feet across the bottom of a low wash. Evidence for the fissure gradually dies out to the north and south beyond the wash. We infer that QWF3 extends an additional 150 feet to the north and

Figure 43. *Fissure QWF1 expressed as an uneroded primary ground crack. This fissure could be traced for 900 feet before becoming obscured by recent agricultural activity. Photo taken in August 2009.*

Figure 44. *Gullied Quichapa-west fissure QWF4 where it crosses a stock pond (view is to the north). Photo taken in August 2009.*

up to 1300 feet to the south based on the presence of a strong photo lineament, most likely caused by preferential vegetation growth along an uneroded primary crack not yet well expressed at the surface.

The southern end of the 200-foot-long QWF4 fissure is marked by a 6-foot-deep elongate sinkhole just north of a two-wheel dirt track. A vertical crack in the sinkhole's southern wall indicates the primary crack continues southward without surface expression, under the track and toward SR-56, which is about 0.5 mile away along the crack trend (figure 39). North of the dirt track, intermittent elongate sinkholes transition into a continuous 3-foot-deep vertical-walled gully as the fissure traverses a broad ephemeral wash. Here, the fissure crosses a stock pond created by a 4- to 10-foot-high, L-shaped earthen dike constructed across the wash (figure 42). Impounded water behind the dike severely eroded and enlarged the fissure up to 6 feet wide and 4.5 feet deep (figure 44). The resultant gully extends across the pond and intersects and breaches the north arm of the dike, where an estimated 350 cubic feet of dike-fill material washed down the fissure. After passing through the dike, the fissure begins to cut the north side of the wash where it transitions into aligned sinkholes and deep pipes before dying out.

Timing of fissure development west of Quichapa Lake is unknown, but the rancher on whose property the stock pond is located indicated that the stock pond was constructed sometime in the 1940s–1950s and never held water well (Craig Jones, verbal communication, 2009). Although the poor water retention of the stock pond could be due to a variety of reasons, water infiltration into the fissure is a likely explanation. However, the deep gullying and removal of the dike embankment above the fissure appears to have occurred after June 1993; the fissure is not apparent on 1993 aerial photos (Utah AGRC, 2013) or earlier available photos, but is clearly visible on 2006 HRO imagery (Utah AGRC, 2006b; figure 42 [inset]) at nearly the same extent as today.

Quichapa-Southwest Fissure

We mapped a single 1400-foot-long fissure about 1.5 miles southwest of Quichapa Lake. The Quichapa-southwest fissure is prominent on LiDAR imagery and aerial photographs, but is quite subdued in the field (figure 45). The fissure is expressed as a shallow linear gully that, unlike other gullied fissures in Cedar Valley, lacks steep walls. The fissure-aligned gully is as much as 20 feet wide and rarely exceeds about 2 feet deep. The fissure's southern end is marked by a few shallow, poorly

Figure 45. *Linear depression 4 to 5 feet wide developed along the Quichapa-southwest fissure (view is to the north). Ticks point toward depression. Photo taken in December 2012.*

defined sinkholes less than 1 foot deep. The fissure formed in mostly fine-grained distal alluvial-fan deposits (map unit Qafy on figure 39), but near its midpoint it can also be traced for about 200 feet through a relatively recent cobble and boulder-rich debris-flow deposit. The fissure formed more than 20 years ago since it is visible on 1993 USGS orthophotography (Utah AGRC, 2013).

Extent of Fissures Near Quichapa Lake

Based on several lines of evidence, we suspect that the earth fissures north and west of Quichapa Lake may be more extensive than is apparent at the ground surface. The Quichapa-west fissures in particular are evident only in low areas that are periodically inundated with surface water during storms; the fissures may extend farther than their mapped traces as uneroded hairline cracks yet to be widened by erosion. We encountered several small (less than 1.5 feet wide) isolated sinkholes and short hairline cracks near the Quichapa-north and Quichapa-west fissures that may be related to additional fissure formation, but due to their discontinuity and lack of

alignment with known earth fissures, we could not definitively classify them as fissure-related features. Additionally, several photolineaments subparallel to mapped fissures (figure 39) were either not detectible in the field or could not be distinguished from possible shorelines, fault scarps, or other geomorphic features.

In 2005, the UGS received a request from a homeowner at 2049 South 8100 West (west of Quichapa Lake and south of SR-56; figure 39) to investigate a sinkhole that had formed on his property. The sinkhole was about 5 feet wide and 4 feet deep, and within 0.75 mile of the Quichapa-southwest fissure (figure 39). At that time, the cause of the sinkhole was not readily apparent; however, based on its location along the trend of nearby mapped fissures and the presence of nearby photolineaments of uncertain origin, the possibility that the sinkhole developed on or near an earth fissure cannot be discounted.

DISCUSSION

Land Subsidence and Earth Fissure Formation

In the United States, more than 17,000 square miles in 45 states have been directly affected by land subsidence, and more than 80 percent of the subsidence has occurred because of groundwater overdraft (Galloway and others, 1999). Land subsidence due to groundwater withdrawal in thick, unconsolidated sediments results from a decrease in fluid (pore water) pressure as the water in fine-grained sediments moves into adjacent coarser grained sediments (Leake, 2010). The decrease in pressure increases the effective stress in the dewatered portion of the aquifer and transfers the entire overburden stress (weight) to the aquifer matrix. The change in effective stress causes the aquifer matrix to change volume (compact) (Galloway and others, 1999). Initial matrix compaction is elastic and will recover if the aquifer is recharged. However, once collapse exceeds the elastic limit of the matrix material, compaction becomes permanent, aquifer storage is reduced, and land subsidence ensues (Galloway and others, 1999).

Most subsidence results from draining fine-grained sediment layers (aquitards) into adjacent coarser grained aquifer material because silt and clay have higher porosities and lower matrix strength than coarse-grained sediment (Galloway and others, 1999). Granular materials (sand and gravel) may settle almost instantaneously after dewatering, but because of their much lower permeability, fine-grained material (silt and clay) may require decades to fully compact and may continue to compress even after groundwater withdrawals are brought into equilibrium with recharge or cease altogether (Bell and others, 2002; Budhu and Shelke, 2008). The relation between groundwater-level decline and land subsidence is complex and varies as a function of total aquifer thickness, composition, and compressibility. In some areas of Arizona, about 300 feet of groundwater decline produced only 0.6 foot of subsidence. In other areas, a similar water-level decline generated land subsidence of as much as 18 feet (Arizona Land Subsidence Group, 2007).

Earth fissures are linear cracks in the ground that initiate at depth due to differential basin-fill compaction and eventually extend to the ground surface (Galloway and others, 1999). Earth fissures form in response to horizontal stresses that develop when land subsidence causes different parts of an aquifer to compact by different amounts (Leake, 2010; Arizona Division of Emergency Management, 2007). Earth fissures may range from a few feet to several miles long and from hairline cracks to tens of feet wide where they intercept surface flow and are enlarged by erosion (Carpenter, 1999). Earth fissures typically form along the edge of basins, usually parallel to mountain fronts; above subsurface bedrock highs often coincident with pre-existing faults; or over zones of changing sediment characteristics and density (Arizona Land Subsidence Group, 2007). Some earth fissures exhibit differential displacements of several inches to several feet as

aquifers compact across them.

Land Subsidence Hazards

Hazards caused by land subsidence include (1) changes in elevation and slope of streams, canals, and drains, (2) damage to bridges, roads, railroads, storm drains, sanitary sewers, water lines, canals, airport runways, and levees, (3) damage to private and public buildings, and (4) failure of well casings from forces generated by compaction of fine-grained materials in aquifer systems (Leake, 2010; Lin and others, 2009). Over half of the area of the San Joaquin Valley in California has subsided due to groundwater withdrawals resulting in one of the largest human-caused alterations of the Earth's surface topography (Galloway and others, 1999). Near Mendota, California, in the San Joaquin Valley, subsidence in excess of 28 feet necessitated expensive repairs to two major central California water projects (California Aqueduct and Delta-Mendoda Canal; Galloway and others, 1999). In Mexico City, rapid land subsidence caused by groundwater withdrawal and associated aquifer-system compaction has damaged colonial-era buildings, buckled highways, and disrupted water supply and wastewater drainage (Viets and others, 1979; Galloway and others, 1999). Early oil and gas production and a long history of groundwater pumping in the Houston-Galveston area, Texas, have created severe and costly coastal-flooding hazards (Galloway and others, 1999; Harris-Galveston Subsidence Districts, 2010). Lin and others (2009) reported significant land subsidence and earth fissure damage related to groundwater mining in the Beijing area, including damage to the new Capital International Airport.

Earth Fissure Hazards

Impacts on expanding urban areas in the southwestern United States from land subsidence, differential compaction, and earth fissures are increasing (Shlemon, 2004). Earth fissures related to groundwater mining may be tens to hundreds of feet deep, and may connect nonpotable or contaminated surface and near-surface water to the principal aquifer (Pavelko and others, 1999; Bell, 2004) used for public water supply. Infiltration of contaminated surface water into fissures could negatively impact groundwater quality. Additionally, earth fissures can change runoff/flood patterns, deform or break buried utilities and well casings, cause buildings and other infrastructure to deform or collapse, endanger livestock and wildlife, and may pose a life-safety hazard (Arizona Division of Emergency Management, 2007). Although known earth fissures are currently limited to chiefly rural areas in Utah (Escalante Desert—Lund and others, 2005; Cedar Valley—this study), elsewhere in the western United States, earth fissures related to land subsidence have become a major factor in land development. The following examples from Arizona and Nevada show how much damage earth fissures related to long-term groundwater mining can cause if not mitigated.

Earth fissures were first recognized in Arizona in 1927; since that time their number and frequency has increased as land subsidence due to groundwater pumping has likewise increased (Arizona Division of Emergency Management, 2007). More than 1100 square miles of Arizona, including portions of the Phoenix and Tucson metropolitan areas, are now affected by subsidence and numerous associated earth fissures (Arizona Land Subsidence Group, 2007; Conway, 2013). Damage caused by earth fissures in Arizona currently totals in the tens of millions of dollars, and includes cracked, displaced, or collapsed freeways and secondary roads; broken pipes and utility lines; damaged and breached canals; cracked building foundations; deformed railroad tracks; collapsed and sheared well casings; damaged dams and flood-control structures; and livestock deaths (Viets and others, 1979; Arizona Division of Emergency Management, 2007; Arizona Land Subsidence Group, 2007).

Likewise, long-term groundwater pumping in excess of recharge in Nevada's Las Vegas Valley has produced water-table declines of 100 to 300 feet (Pavelko and others, 1999) and up to 6 feet of land subsidence (Bell and others, 2002; Bell and Amelung, 2003). By the early 1990s, the Windsor Park subdivision in North Las Vegas was so impacted by earth fissures that 135 homes had to be abandoned and removed at a cost of about $20 million, and another 105 homes required significant repairs (Bell, 2003; Saines and others, 2006). Most earth fissures in Las Vegas Valley are associated with pre-existing Quaternary faults (Bell and Price, 1991; Bell and others, 2002; Bell and Amelung, 2003; Bell, 2004). Artificial aquifer recharge has caused a decline in subsidence rates in Las Vegas Valley of 50 to 80%, depending upon location since 1991 (Bell and others, 2002).

Cause of Land Subsidence and Earth Fissures in Cedar Valley

Our investigation included an evaluation of the historical potentiometric surface (water table) decline; distribution, thickness, and texture of basin-fill deposits; lateral changes in basin-fill texture and density; changes in benchmark elevations; InSAR study results; and the locations of Quaternary faults in Cedar Valley. Unfortunately, the limited number of benchmarks with reliable elevation data in the study area prevents adequately characterizing the distribution and rate of subsidence in Cedar Valley. However, available data indicate that land subsidence and earth fissures in Cedar Valley coincide with areas of significant potentiometric surface decline; the presence of compressible, fine-grained, basin-fill sediment in the subsurface; and the presence of planar discontinuities either in the bedrock beneath the valley or in basin-fill deposits. All of the above conditions are characteristic of numerous areas in the arid southwestern United States where land subsidence and earth-fissure formation have occurred in response to groundwater-level decline (e.g., Bell and Price, 1991; Galloway and others, 1999; Leake, 2010; Harris and Allison, 2006; Arizona Land Subsidence Group, 2007). We conclude that the land subsidence and earth fissures in Cedar Valley are likewise directly related to groundwater pumping in excess of aquifer recharge.

Because the aquifer in Cedar Valley is fairly heterogeneous (Thomas and Taylor, 1946; Bjorklund and others, 1978; Hurlow, 2002), localized pressure decline caused by pumping near highly compressible sediments likely has a greater influence on nearby fissure development than valley-wide groundwater-level declines. The fissures documented in this report are near high-yield wells (figure 5). Two agricultural wells in the Enoch graben seasonally pump more than 300 acre-feet. On the western margin of the graben, near the Enoch-graben-west fissures, an irrigation well pumps more than 600 acre-feet per year. Along the eastern margin of the graben are Enoch municipal wells. Three large-capacity Cedar City municipal wells are close to fissure zones north and west of Quichapa Lake. A single fissure southwest of Quichapa Lake is likewise near another large-capacity Cedar City municipal well.

Depending on the compressibility and thickness of aquifer sediments, a base estimate of 0.01 to 0.6 inch of subsidence may occur per foot of drop in groundwater level (Poland and Davis, 1969; Bouwer, 1977). Reduction in hydraulic pore pressure (water level) in the aquifer from pumping allows water to be released from clay layers into surrounding coarser grained aquifer material. The dewatered clays then compact under the weight of the overlying material (Poland and Davis, 1969). In aquifers where the ratio of subsidence to head decline is high (0.05), the volume of water released from clay compaction can be 50 times greater than water derived from elastic compression of the aquifer and expansion of water. This assumes that the ratio of subsidence to head decline is much greater than the coefficient of storage from the compressed portion of the aquifer (Poland and Davis, 1969), which is common in confined or leaky confined aquifers. Unconsolidated aquifer systems with many fine-grained interbeds of silty clay and clay are highly compressible relative to mostly coarse-grained aquifers. Due to low permeability of clay-rich interbeds and confining units, pore pressure equilibrium may require years to decades to achieve (Poland and Davis, 1969). This means that once subsidence has begun, it can continue long after water-level declines have ceased.

If pore pressure is reduced by pumping, stress on the aquifer skeleton must increase to compensate. If pressure decline is sufficient to create effective stresses that surpass the pre-consolidation stress of the aquifer, the aquifer becomes permanently compacted and its porosity is reduced (Poland and Davis, 1969). Compaction of an aquifer depends on sediment compressibility within a range of effective stresses and the magnitude of change in head creating the range of effective stresses. The duration of head change, dimensions and permeability of compactable beds, clay mineralogy, water chemistry, and particle size also play a role in aquifer compaction (Poland and Davis, 1969).

Table 12. *Estimates of potential subsidence from groundwater-level decline.*

Water-level Decline		Minimum Subsidence (ft)	Maximum Subsidence (ft)
Ratio of subsidence to head change[1]		0.001	0.05
Basin-wide water level decline			
Mean decline (ft)	63	0.06	3
Minimum decline (ft)	-3	0	0
Maximum decline (ft)	114	0.1	6
Water level change along cross section			
Mean decline (ft)	61	0.06	3
Minimum decline (ft)	8	0.008	0.4
Maximum decline (ft)	99	0.1	5
Annual water-level decline (ft/yr)	2	0.002	0.1

[1]*From Bouwer (1977).*

Maximum, minimum, and average basin-wide groundwater-level decline from 1939 to 2009 were 114, -3, and 63 feet, respectively (table 4). Based on the groundwater-level decline along our lines of cross section (figures 11 through 16) and the basic range of subsidence to head change ratios from Bouwer (1977), basin-wide subsidence could range from 0.1 inch to 5 feet from 1939 to 2009 (table 12). The rate of decline has been increasing since at least the 1950s due to increasing pumping rates, and the potentiometric surface has, on average, decreased 2 feet per year from 2000 to 2010 (table 4). Continued aquifer pressure declines will continue to cause subsidence and related effects. To stop water-level decline, the hydrologic budget (recharge versus discharge) throughout the valley must be balanced. Even if pressure decline is halted, there may be a significant time lag before subsidence stops.

Long-term groundwater-level changes are greatest near Quichapa Lake (figure 18) and in the Enoch graben, where earth fissures are known to exist. New InSAR data (Katzenstein, 2013; appendix E) shows that these same areas also have experienced significant ground subsidence over the past two decades. The Enoch graben and Quichapa Lake areas contain several large agricultural wells and the greatest density of large-capacity municipal wells in Cedar Valley (figure 5).

Earth fissures are frequently associated with abrupt changes in basin-fill thickness caused by bedrock surface irregularities and/or planar discontinuities within the subsiding sediments themselves. These conditions contributed to the formation of both the Enoch-graben-west and -east fissures, which are localized along known Quaternary faults in areas where the potentiometric surface has declined 80 feet or more (compare figures 18 and 23). Both the Quichapa-north and -west fissures are close to and subparallel with strands of the east-dipping WBBFS (figure 39). The Quichapa-north fissures also are present at the interface between coarse-grained fan deposits to the west and fine-grained basin-fill deposits to the east

(figures 19 and 39). The difference in texture between these two deposits likely provides a density contrast across which differential compaction and fissure formation are localized.

Both the Quichapa-north fissures grouped as QNF1 (figure 40) and the Enoch-graben-east fissures grouped as EGEF5 (figure 34) are unique compared to the remaining fissures in Cedar Valley. Both fissure groups exhibit a significant branching pattern with many branches that have atypical trends (i.e., some branches trend east-west while most nearby fissures trend north-south) and form polygonal patterns. The QNF1 and EGEF5 fissure groups are also both formed on fine-grained, clay- and silt-rich deposits in topographically low, flat areas. The former presence of springs (Eightmile Springs near QNF1 [figure 40] and numerous springs near EGEF5 [figure 35]—all now dry) close to these fissures indicates that the deposits where the branching fissures formed were likely saturated at or near the surface. The water table that once intersected the ground surface creating the springs is now as much as 90 feet below the surface in these areas (see Potentiometric Surface Change Over Time section above). For these reasons, we consider it possible that these fissures are at least in part localized desiccation cracks formed by the dewatering of near-surface, clay-rich sediment due to significant groundwater declines. DuRoss and Kirby (2004) documented similar features formed on clay- and silt-rich sediment near the Little Salt Lake playa margin in Parowan Valley. In particular, the QNF1 fissures resemble giant desiccation cracks mapped by Harris (2004) at several locations in Arizona. In general, giant desiccation cracks are shorter, less straight, and significantly less deep than earth fissures related to pumping-induced subsidence (Harris, 2004).

Effect of Land Subsidence and Earth Fissures in Cedar Valley

This investigation documents groundwater-pumping-induced land subsidence of about 0.9 foot in the Enoch area with smaller amounts (0.1–0.4 ± 0.3 foot) in parts of the central Cedar Valley over a 60-year period (figure 20). However, this subsidence was documented over a sparse benchmark network and the valley lacks monuments with historical elevation data in many areas that are suspected to have experienced the greatest amount of subsidence. Recently acquired InSAR imagery (Katzenstein, 2013; appendix E) shows that a broad area within Cedar Valley, including the Quichapa Lake area, has experienced varying amounts of subsidence between 1992–2000 and 2004–2010. The maximum cumulative subsidence observed in the Quichapa Lake area was 2.0 inches and 4.7 inches during the 1992–2000 and 2004–2010 time periods, respectively (Katzenstein, 2013; appendix E). In central Cedar Valley, the maximum observed subsidence was 1.5 inches and 2.4 inches during the 1992–2000 and 2004–2010 time periods, respectively (Katzenstein, 2013; appendix E).

Additionally, we identified numerous subsidence-related earth fissures within the southwestern and northeastern parts of the valley (figure 22). The combined length of the fissures is presently 8.3 miles (August 2013). Most of the fissures are restricted to undeveloped range- and agricultural land where their impacts are limited to a breached stock pond embankment, ongoing displacement of a pivoting irrigation system wheel track, and creating a hazard for livestock and wildlife. However, portions of the Enoch-graben-west fissures (figure 23) traverse the partially developed Parkview subdivision, and may be affecting part of the Legacy Estates subdivision in the north part of Enoch City.

In response to periods of heavy precipitation or snow melt, Johnson Creek (figure 23), an intermittent stream, flows into a livestock area from the east and periodically ponds water contaminated with fecal waste against the east side of the scarp produced by the EGWF1 fissure (figure 29). If the fissure extends to or near the groundwater table, it could provide a potential pathway for contaminated surface water to reach the underlying aquifer, which is used extensively as a source of both municipal and agricultural water.

Within the Parkview subdivision, continuing down-to-the-east displacement across the EGWF1 fissure has damaged streets, curb and gutter, and sidewalks; bisected several lots making them unsuitable for development; and reversed the flow direction of a sewer trunk line. The Parkview subdivision represents the first extensive earth-fissure-related damage to the built environment in Utah. The damage in the Parkview subdivision is significant because (1) a geotechnical engineering firm determined that site conditions (soil and geology) were suitable for the proposed development, but missed the predevelopment presence of earth fissures clearly visible on aerial

photographs, (2) the subdivision was subsequently designed by an engineering firm in accordance with applicable building codes, (3) a bank provided financing to develop the property, and (4) the Enoch City Planning Commission and City Council approved the subdivision. However, because of fissure-related problems, Enoch City has withheld final approval of the subdivision and has placed a moratorium on any further development there (Earl Gibson, Enoch City Public Works Director, verbal communication, 2009). In short, established procedures for investigating and approving new development were followed, and yet the end result is a development moratorium and a subdivision in distress. The Parkview subdivision demonstrates the potential for future earth-fissure-related infrastructure problems in both Cedar Valley and other Utah basins where groundwater pumping exceeds recharge.

In addition to affecting new development, the formation and growth of earth fissures in Cedar Valley represent a hazard to existing infrastructure. Four sets of aerial photographs covering a 46-year period (1960–2006) document the progressive growth of the EGWF1 fissure (figure 26). The photographs show the fissure extending farther to the south over time, and that the fissure grew about 800 feet longer in the decade between 1997 and 2006. The southern tip of the fissure is now within 1800 feet of an established residential neighborhood in Enoch City. Continued southward growth of the EGWF1 and EGWF2 fissures could adversely impact homes and utilities in that area. The southern end of the EGWF3 fissure may already be impacting a road at the north end of the Legacy Estates subdivision. Likewise, if the Enoch-graben-east fissures (figure 23) extend to the south, it could also impact existing Enoch City neighborhoods. Presently unrecognized or future earth fissures may appear with little or no warning within Cedar Valley where conditions are conducive to fissure formation, particularly during major precipitation or flooding events.

Additionally, if uneroded and presently unrecognized ground cracks extend south of the Quichapa-west earth fissures along the western margin of Cedar Valley, crack widening due to infiltrating surface water may adversely affect SR-56 (currently, within 0.5 mile of the mapped southern end of Quichapa-west fissure QWF4), buried utilities along the highway corridor, and homes and other structures west of Quichapa Lake.

LAND SUBSIDENCE AND EARTH FISSURE MITIGATION

Land subsidence and earth fissures related to groundwater withdrawal are human-caused geologic hazards. Because they result from human activity, the land subsidence and earth fissures are also subject to human management. Subsidence occurs and fissures form because groundwater is being pumped from an aquifer at a rate greater than aquifer recharge (groundwater mining). Reducing pumping to bring recharge and discharge into balance will slow or stop land subsidence and earth fissure formation—a process successfully imple-

mented in other areas experiencing land subsidence and earth fissure problems (Ingebritsen and Jones, 1999; Bell and others, 2002). Both the cause and cure for groundwater-mining-related land subsidence and earth-fissure hazards are typically societal in nature. It is rare that a single groundwater producer (individual or organization) causes land subsidence and earth fissure formation, and it is equally rare that a single producer can affect a cure. This is particularly true of Utah's alluvial valleys, each with many stakeholders, where only collective action by all involved (producers, consumers, managers, and regulators) can prevent groundwater mining.

Recommendations related to mitigating land-subsidence and earth-fissure issues in Utah's alluvial valleys, including Cedar Valley, fall into three broad categories:

1. Identify existing earth fissures, and define the distribution, amount, and rate of land subsidence in valley areas.

2. Implement best aquifer management practices to bring basin-fill aquifers into balance between groundwater discharge and recharge to stop groundwater mining.

3. Conduct best hazard-characterization practices in areas subject to land subsidence and earth-fissure formation to prevent damage to existing and future infrastructure, limit reductions in real estate values and other economic impacts, ensure public safety, and minimize land-use restrictions.

Identify Existing Earth Fissures and Define the Distribution, Amount, and Rate of Land Subsidence

We recommend three principal methods to better identify earth fissures and determine the distribution, amount, and rate (likely non-uniform) of land subsidence in Utah's alluvial valleys. The three methods are InSAR, LiDAR, and establishing and monitoring a high-precision GPS/GNSS (global navigation satellite system) network of survey benchmarks, preferably sited using the results of the other two technologies.

InSAR

Synthetic aperture radar (SAR) is a side-looking, active (produces its own illumination) radar imaging system that transmits a pulsed microwave signal toward the earth and records both the amplitude and phase of the back-scattered signal that returns to the antenna (Arizona Department of Water Resources [ADWR], no date; Zebker and Goldstein, 1986; Zebker and others, 1994). InSAR utilizes interferometric processing to compare the amplitude and phase signals received during one pass of the SAR platform (typically earth orbiting satellites) over a specific geographic area with the amplitude and
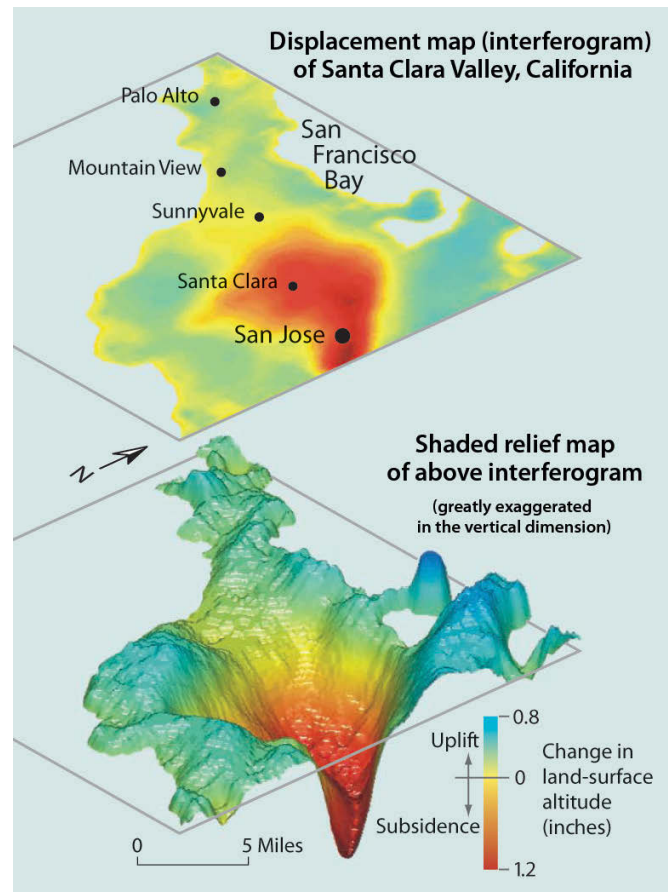
Figure 46. *Unwrapped interferogram (upper image) of Santa Clara Valley, California, showing patterns of subsidence (with local uplift) that occurred from January to August 1997. The shaded-relief map (lower image) translates the color-zonation pattern of the interferogram (based on cycles of phase) into three-dimensional topography. Vertical dimension greatly exaggerated. From Galloway and others (2000).*

phase signals received during a second pass of the platform over the same area, but at a different time (ADWR, no date). Surface displacement measurements of less than a half inch over an area of several tens of square miles have been routinely demonstrated worldwide in subsidence applications using InSAR technology. More advanced applications of InSAR can measure local displacement rates on the order of a few millimeters per year (Skaw, 2005). The amount and pattern of deformation in an interferogram are shown by using the color spectrum to indicate areas of greater or lesser deformation. Figure 46 shows an example of an interferogram documenting subsidence in Santa Clara Valley, California (upper image), and a shaded-relief map (lower image) that correlates the color bands with the deformation pattern (USGS, 2000).

The ADWR routinely uses InSAR to monitor active land subsidence basins in Arizona (ADWR, no date; Conway, 2013). Repeated InSAR applications show the spatial extent, deformation rates, and time-series history of the basins. The subsidence measurements assist the ADWR in educating the

public and local government agencies on the reality and severity of the land-subsidence hazard in Arizona. County and local governments have realized the importance of InSAR to their own monitoring efforts, and have entered into agreements with ADWR to ensure that SAR data are collected, processed, and analyzed for areas critical to each group's monitoring needs (ADWR, no date; Conway, 2013). In addition, water resource managers, engineers, hydrologists, geologists, and other scientists routinely use InSAR data to identify and evaluate areas of subsidence, uplift, earth fissures, faults, and other features related to groundwater mining (Skaw, 2005).

Forester (2006, 2012) demonstrated that long-term subsidence in southwest Utah is detectable and measurable with InSAR. Of three regions analyzed (Escalante Valley, Milford, and Parowan), the greatest subsidence was detected in Escalante Valley with subsidence rates as high as 2.4 inches per year (Forester, 2012). Katzenstein (2013; appendix E) used InSAR to identify an approximately 100-square-mile area in Cedar Valley, Utah, affected by subsidence due to groundwater mining. He further stated that the InSAR data indicate the rate of subsidence appears to be increasing with time. Other subsidence-related InSAR applications include measuring land subsidence and uplift in Las Vegas Valley related to groundwater withdrawal and recharge (Amelung and others, 1999), investigating the application of interferometric techniques to the measurement and interpretation of vertical deformation over pumped aquifers in Las Vegas Valley (Bell and others, 2002; Hoffmann, 2003), and mapping subsidence and/or uplift attributed to groundwater-level changes in Albuquerque Basin, New Mexico (Heywood and others, 2002); Antelope Valley, California (Galloway and others, 1998; Hoffmann and others, 2003); San Luis Obispo County, California (Valentine and others, 2001); Coachella Valley, California (Sneed and others, 2001; 2002); Houston–Galveston Bay area, Texas (Stork and Sneed, 2002; Buckley and others, 2003); Santa Ana Basin, California (Bawden and others, 2001); Santa Clara Valley, California (Ikehara and others, 1998; Schmidt and Bürgmann, 2003); and Yucca Flat, Nevada (Laczniak and others, 2003; Halford and others, 2005).

InSAR's chief advantage for subsidence monitoring is that it offers wide-area continuous coverage at a reasonable level of accuracy at better cost efficiency than traditional surveying techniques (Skaw, 2005; note Skaw reports measurements in the metric system) that only reports positions at a few discrete points. A typical InSAR frame covers an area of approximately 10,000 km^2 (~3861 mi^2) at a pixel resolution of about up to 10 meters (~33 ft)—or > 8,000,000 discrete point measurements within the 100 km by 100 km (62 mi by 62 mi) frame. Skaw (2005) reports that the cost to perform static GPS/GNSS surveys with the same vertical accuracy, but at 1/1000th the resolution would conservatively cost $500,000 for the two surveys required to measure change, making the cost per point measurement to produce an InSAR change map using currently available satellite data less costly by many orders of magnitude than conventional surveying technolo-

gies. In short, InSAR provides an accurate, rapid, and cost-efficient way to determine the horizontal and vertical extent of land subsidence and subsidence rate variability over a large area to an accuracy of about 1 centimeter. Appendix F presents additional detailed information about the InSAR technique, satellite imagery acquisition and processing, and cost.

LiDAR

LiDAR is an airborne, remote sensing, laser system that measures the properties of scattered light to accurately determine the distance to a target (reflective surface). LiDAR is similar to radar, but uses laser pulses instead of radio waves, and commonly is collected from fixed-wing aircraft or helicopters. LiDAR produces a rapid collection of points (typically more than 70,000 per second) that results in very dense and accurate elevation data over a large area (National Oceanic and Atmospheric Administration [NOAA], 2008). The resulting highly accurate, georeferenced elevation points can be used to generate three-dimensional representations of Earth's surface and its features (NOAA, 2008). After processing, LiDAR data can be used to produce a "bare-earth" terrain model (figure 47), in which vegetation and manmade structures have been removed. LiDAR has several advantages over traditional photogrammetric methods; chief among them are high accuracy, high point density, large coverage area, and the ability to resample areas quickly and efficiently, which creates the ability to map discrete elevation changes over time at a very high resolution (NOAA, 2008).

LiDAR is used extensively in base mapping, natural resource management, floodplain mapping, transportation and utility corridor mapping, urban planning, and in many kinds of geologic investigations. For example, LiDAR has been used to identify previously unrecognized faults (Harding and Berghoff, 2000) and landslides (Oregon Department of Geology and Mineral Industries, 2006; Schulz, 2007), and to measure subtle amounts of uplift at Mount St. Helens (National Aeronautics and Space Administration, 2004; U.S. Geological Survey, 2004). LiDAR offers two important advantages over conventional aerial photography for mitigating land-subsidence and earth-fissure hazards. First, high-resolution, bare-earth LiDAR images can be used to identify and map currently unrecognized earth fissures that are not apparent on conventional aerial photography. For example, analysis of color aerial photographs by the UGS identified 3.9 miles (trace distance) of subsidence-related earth fissures in Cedar Valley, Utah. The UGS subsequently obtained LiDAR imagery for Cedar Valley and was able to identify an additional 4.4 miles (trace distance) of fissures (total 8.3 miles) that were not apparent on the aerial photographs (see Cedar Valley Earth Fissures section). Second, repeat LiDAR surveys can be used to generate displacement maps to define the boundaries of subsidence areas, and may allow monitoring of existing earth fissure growth and new fissure formation.

LiDAR costs vary based on project specifications. For exam-

Figure 47. *UGS (2011) bare-earth LiDAR image of the south end of the Enoch-graben-west fissures. These fissures exhibit vertical down-to-the-east displacement and are well expressed on LiDAR imagery.*

ple, 2-meter LiDAR data acquired in 2006 for the Wasatch Front area cost $141,000 for ~1300 square miles (~$108/mi²) (Rick Kelson, Utah Automated Geographic Reference Center, verbal communication, 2011), whereas 0.5-meter LiDAR data acquired in 2013 for Salt Lake and Utah Valleys and the Wasatch fault zone cost $510,000 for ~1353 square miles (~$377/mi²). These estimates assume a contiguous, roughly rectangular project block. The location, type of terrain, vegetation cover, and time of year can also affect pricing. Appendix G presents additional detailed information about LiDAR technology, imagery acquisition, and processing, and cost.

High-Precision GPS/GNSS Survey Network

The accuracy and coverage of benchmark networks in Utah's alluvial valleys are variable. In many areas, benchmarks, particularly older monuments, have been destroyed or disturbed by subsequent agricultural or development activities.

For example, the current network of benchmarks with well-constrained historical elevation data in Cedar Valley, Utah (an area of over 100 square miles) consists of only 24 benchmarks with varying periods of record and varying levels of elevation accuracy (see Cedar Valley Land Subsidence section). Constraints on the number and locations of existing benchmarks may allow for only a general determination of the areal and vertical extent of land subsidence in valley areas, and may not permit adequate monitoring of either the rate or distribution of ongoing subsidence.

Where accurate, periodic monitoring of subsidence is important for aquifer management or hazard avoidance, the UGS recommends that following acquisition of InSAR and Li-DAR data to better define the boundaries of subsiding areas and earth fissure locations, those data be used to help site a network of high-precision GPS/GNSS survey monuments in subsidence and fissure "hot spots." Periodic resurveying of the benchmarks using GNSS methods would permit repeated high-precision (1–5 mm horizontal/vertical) subsidence monitoring in areas most important to best aquifer management practices and hazard mitigation. For increased accuracy, detailed subsidence studies typically employ static GPS survey methods rather than RTK surveys (http://www.azwater.gov/AzDWR/Hydrology/Geophysics/GPS.htm). GPS surveys should generally follow the latest versions of the NGS guidelines for establishing ellipsoid (Zilkoski and others, 1997) and orthometric (Zilkoski and others, 2008) heights. High-quality floating sleeved rod or other appropriate monuments are recommended for precise vertical measurements that significantly reduce near-surface soil movements, such as from expansive soils. For bedrock sites, UNAVCO has developed stable mounting structures to isolate GPS/GNSS instruments from near-surface soil movements (http://pbo.unavco.org/instruments/gps/monumentation).

Best Aquifer Management Practices

In valleys where groundwater mining is occurring, dewatering of fine-grained layers in basin-fill aquifers is the principal cause of aquifer compaction and associated land subsidence and earth-fissure formation. If aquifer compaction is to be avoided, basin-fill aquifers should be managed to balance groundwater recharge and discharge at both local and basin-wide scales. There are several ways to accomplish this goal, including (1) increasing overall water resources by importing water from other basins, (2) increasing groundwater recharge to the basin-fill aquifer through conjunctive management of ground- and surface-water resources, (3) dispersing high-discharge wells to reduce localized land subsidence, and (4) reducing overall groundwater withdrawals in a basin.

Increasing Overall Water Resources

Importing water from one basin to another may be feasible, assuming the necessary water rights can be obtained. Importing water has been one of the initial responses to land-subsidence

problems caused by groundwater-mining-induced aquifer compaction in other areas including California (Holzer, 1989; Johnston, 1989; Onsoy and others, 2005), Nevada (Swanson, 1996), Arizona (Arizona Land Subsidence Group, 2007), and central Iran (Solaimani and Mortazavi, 2008). Imported water can be used to minimize or eliminate the need to withdraw groundwater locally. In some areas, imported water has also been used to recharge the aquifers undergoing compaction (Reichard and Bredehoeft, 1985; Galloway and others, 1999; Onsoy and others, 2005). It should be noted that importing water from other basins may reduce land-development opportunities and/or may cause subsidence and other related issues in the basins from which the water is obtained, and may simply move the problem from one basin to another or create problems in both basins.

Increasing Recharge to the Basin-Fill Aquifer

Increasing groundwater recharge to aquifers with historically declining water levels through conjunctive management of groundwater and surface-water resources has proven to be a powerful tool in preventing or reducing aquifer compaction (Reichard and Bredehoeft, 1985; Holzer, 1989; Swanson, 1996; Galloway and others, 1999; Onsoy and others, 2005; Utah Division of Water Resources, 2005). Conjunctive management of ground- and surface-water resources through aquifer storage and recovery (ASR) projects offers a potential partial solution to problems associated with water-level declines in basin-fill aquifers. Not only can such projects help stabilize water-level declines, they can also provide water planners and managers with increased flexibility to managing a basin's water supply and provide a source of supplemental water.

Artificial groundwater recharge has long been used to enhance groundwater quality, reduce pumping lifts, store water, salvage storm-water runoff, and reduce aquifer compaction in subsiding areas (Clyde and others, 1984; Pyne, 1995; Galloway and others, 1999). ASR projects involve storing water in an aquifer by artificial groundwater recharge when water is available, and recovery of the stored water from the aquifer when water is needed (Pyne, 1995). Basically, groundwater aquifers are used as water-storage facilities rather than constructing surface-water reservoirs. Artificial groundwater recharge can be accomplished by surface spreading or ponding (such as in rapid infiltration basins) where surficial deposits are highly permeable, or by using wells to inject surface water into an aquifer where surface deposits are less permeable (Clyde and others, 1984). Although loss of stored water through artificial groundwater recharge does occur, principally due to water moving vertically or laterally out of the target aquifer before recovery, the sometimes significant loss of water through evaporation in surface-water storage facilities is avoided (Clyde and others, 1984).

The most beneficial areas for artificial groundwater recharge

using either surface-spreading/ponding techniques or injection wells are areas experiencing the greatest land subsidence. Water imported from other basins could also be used as a source of artificial groundwater recharge. If the basin-fill aquifer is recharged via surface spreading or ponding, the recharge sites should be in primary recharge areas (Lowe and others, 2010), where thick clay layers that may inhibit subsurface water flow are absent in the basin fill. Injection wells may be located where needed.

Dispersing High-Discharge Wells

Aquifer compaction and associated land subsidence and earth fissures may be stopped or reduced by locating new or relocating existing high-discharge wells in areas that will minimize subsidence. Optimization models, developed by groundwater hydrologists, coupled with groundwater-flow models can be used to determine where these wells would best be located (Leake, 2010). Campbell and Jensen (1975, as reported in a Water Well Journal editorial) recommended evaluating the feasibility of redistributing pumping loads in the Houston, Texas, area from the vicinity of subsidence areas to more distant locations. In the Owari Plain of Japan, short-term and local changes in head are considered when regulating groundwater pumping to prevent land subsidence (Daito and others, 1991). This option requires properly designing and drilling new wells and constructing associated infrastructure in areas where subsidence can be minimized.

Reducing Groundwater Withdrawals

Limiting the amount of groundwater extracted from an aquifer so that stored water will not be significantly depleted is the basis for the water-resource management concept known as "safe yield" (Galloway and others, 1999). To avoid groundwater mining, the volume of water withdrawn from an aquifer cannot significantly exceed natural and artificial recharge to the aquifer—the concept of safe yield is usually applied using average annual values of recharge and discharge. Given climatic variability, it may be necessary to manage subsidence-prone areas even more conservatively to avoid increasing the rate and/or area of subsidence during drought periods. Managing subsidence-prone areas may be possible using the "optimal yield" concept, in which groundwater discharge is allowed to vary from year to year, or even seasonally, depending on the state of the aquifer system and the availability of local and imported water supplies. This concept incorporates the dynamic nature of the groundwater system and allows water managers to adapt to variations in water supply and use (Galloway and others, 1999).

Valley-wide groundwater withdrawals could be reduced by acquiring and retiring existing water rights, although we did not find any case histories of this being done in areas with aquifer-compaction problems. However, groundwater withdrawals have been reduced in other areas by regulating

groundwater pumping (Holzer, 1989) and/or by groundwater pricing (Bangkok City, 2001). Current statutory authority to implement groundwater management in Utah is contained in Utah Code Ann §73-5-15. Regarding provisions for "local districts" to seek cooperative agreements among water users and undertake quasi-governmental management of groundwater, see Utah Code Ann §17B, et al.

In Texas, which applies the principles of English common law, groundwater is the absolute property in perpetuity of the overlying private landowner (Brah and Jones, 1978), unlike in Utah where groundwater is considered a public resource and the Utah State Engineer grants individuals the right to use allotted amounts. When land subsidence due to groundwater mining developed in coastal areas of the Houston-Galveston region beginning in the 1950s, there was little incentive for private groundwater users to reduce reliance on relatively inexpensive groundwater resources and arrest the subsidence, as they themselves did not incur the subsidence-related costs (Holzer, 1989). In the 1970s, individuals and groups affected by the land subsidence attempted to mitigate the subsidence problem by focusing on ways to turn incentives for groundwater pumping into disincentives (Holzer, 1989). They considered four alternatives: (1) implementation of a surcharge on groundwater pumping, (2) creation of a regional water authority through legislation, (3) formation of a regional underground water conservation district under the Texas Water Code, and (4) creation of a local government agency to regulate pumping (Brah and Jones, 1978). Alternative four was implemented in 1975 by authorization of the Harris-Galveston Subsidence District (HGSD) by the Texas State Legislature. The HGSD was authorized to regulate groundwater pumping by issuing 1- to 5-year permits to all major production wells in the district. The objective of awarding the permits, for which fees are collected to fund the district, was to reduce groundwater withdrawal to an amount that would restore and maintain sufficient artesian pressure in the aquifer to halt subsidence (Holzer, 1989). Conversion of water users from groundwater to surface-water sources made available by local water agencies, as encouraged by the HGSD, has contributed to water-level recoveries and the slowing of the rate of subsidence in coastal areas of the Houston-Galveston region (Strause, 1984).

The first generally recognized occurrence of subsidence caused by groundwater withdrawal in the United States was in the 1920s in Santa Clara Valley, California (Tolman and Poland, 1940; Ingebritsen and Jones, 1999); subsidence in this formerly agricultural (now largely metropolitan) area eventually affected more than 230 square miles of land (Poland and Green, 1962) and locally reached a maximum of 12.9 feet (Poland, 1977). Initial response to the subsidence included formation of the Santa Clara Valley Water Conservation District (SCVWCD) in 1929, which was chartered under California law with responsibility for mitigating the groundwater overdraft problem. Subsequently, the SCVWCD constructed groundwater recharge facilities along the valley margins in

1935 and 1936 (Holzer, 1989). These facilities, combined with abnormally high rainfall, temporarily halted water-level declines and slowed subsidence during the early 1940s (figure 3 in Poland, 1977), but groundwater withdrawals largely associated with industrial and urban activities following World War II resulted in new groundwater-level declines and associated subsidence (Holzer, 1989; Ingebritsen and Jones, 1999). These new water-level declines led to the recognition that major imports of water were needed to meet long-term water demands in Santa Clara Valley, and the South Bay Aqueduct System was constructed as a result (Holzer, 1989). Groundwater users were encouraged to switch to this new surface-water source by a tax on groundwater pumping implemented in 1964 that removed the economic incentive to use groundwater (Holzer, 1989). The SCVWCD has since used the approach of combining all water resources into a common pool and distributing water costs according to water use rather than water source (Holzer, 1989). This approach led to the recovery of water levels in the 1970s (figure 3 in Poland, 1977) and the halting of subsidence as of 1974–75 (Poland, 1977).

Groundwater withdrawals can also be reduced by implementing water conservation measures. Such measures could include (1) incentive pricing, (2) outdoor watering guidelines and ordinances, (3) landscape guidelines and ordinances, (4) commercial and residential water audits, (5) installation of meters on water connections, (6) retrofit, rebate, and incentive programs, and (7) leak detection and repair programs (Utah Division of Water Resources, 2001). Incentive pricing (for the public supply consumer rather than the groundwater supplier) should be designed to reward efficiency and discourage waste of groundwater resources. The Utah Division of Water Resources (2001) outlines several strategies for accomplishing this goal. Because 67% of residential water is consumed for outdoor use, overall water consumption could be reduced significantly by implementing strategies such as supplying only the amount of water needed by plants to produce maximum growth and maintaining a sprinkler uniformity of 60% (Utah Division of Water Resources, 2001). Requiring xeriscaping through ordinances or legislation (as implemented in Florida, Texas, and Nevada) or through monetary incentives (as implemented in Las Vegas, Nevada, and Glendale, Arizona) can significantly reduce overall water use (U.S. Environmental Protection Agency, 2010b). Water audits, metering, retrofitting (such as replacing standard toilets, urinals, and faucets with low-flow fixtures), and leak detection and repair are also important ways to reduce groundwater withdrawals by reducing water use (Utah Division of Water Resources, 2001).

Aquifer Management Recommendations

Based largely on mitigation measures employed in other areas experiencing land subsidence and earth fissures caused by groundwater-withdrawal-related aquifer compaction, we have presented a variety of aquifer management alternatives which local and state government agencies may consider

implementing based on local needs. Best management practices for Utah's basin-fill aquifers will likely include the application of an assortment of the aquifer management practices summarized above. If water is imported from other basins, the best use of the water, to bring average annual recharge and discharge in basin-fill aquifers into balance, may be through ASR projects provided the imported water is of suitable quality. Even if water from other basins is not available, implementing ASR projects using spring runoff from within valley drainage basins would be beneficial. Aquifer storage and recovery projects would be most beneficial in areas with the greatest water-level declines and greatest amount of subsidence. ASR-like activities are generally governed by Utah Code Ann § 73-3b, provided there is the intent to "recover" the stored water. Proposals to "recharge" only using spring runoff and flood flows are generally implemented under the authority of flood control. If such projects are proposed explicitly for artificial groundwater recharge (without recovery), Utah Department of Environmental Quality regulations would have to be considered.

Eliminating groundwater mining, both basin-wide and in local areas experiencing the greatest subsidence, is required to prevent or halt land subsidence and earth fissure formation. Because the areas of greatest water-level decline generally correspond to clusters of existing high-discharge wells, consideration should be given to discontinuing pumping of some of these wells and dispersing new wells into areas where subsidence is not occurring or is occurring at a slower rate. Additionally, water conservation measures should either be encouraged or required basin-wide, but such measures will likely not be sufficient to halt declining water levels in basin-fill aquifers where groundwater mining is occurring, especially in view of likely future population growth in many of Utah's alluvial valleys. Following Santa Clara Valley's policy of taxing groundwater pumping to discourage groundwater depletions may be an option in developing areas. A tax on groundwater pumping could be varied annually, seasonally, or by location, depending on the rate at which water-level/head in the basin-fill aquifer is rising or falling. A network of monitoring wells should be established and monitored at regular intervals to determine the rate and direction of water-level/head change in basin-fill aquifers; this monitoring network could be used as the basis for varying the tax on groundwater pumping. Taxing groundwater pumping or requiring conservation measures are likely outside the current authority of local governments. Legal advice should be obtained if such measures are considered.

Bringing discharge in basin-fill aquifers subject to groundwater mining into balance with recharge so the aquifer can be managed using either "safe yield" or "optimal yield" concepts may be difficult both economically and politically in the short term. However, the long-term cost of not managing aquifers and accepting the damage associated with land subsidence and earth fissures is much greater. Even if best aquifer management practices are implemented in areas subject to ground subsidence, aquifer compaction may continue for some time into the future, and hazard-characterization procedures in areas subject to ground subsidence, as discussed below, will likely be necessary.

Best Land-Subsidence and Earth-Fissure Hazard Investigation and Mitigation Practices

Land subsidence and earth fissures related to groundwater mining are geologic hazards, and as such are geotechnical issues that must be addressed during land development in subsiding areas. Because land subsidence and earth-fissure formation related to groundwater mining are human-caused, the most effective mitigation method is to bring long-term aquifer recharge and discharge into balance, so that groundwater mining ceases and land subsidence and earth fissure growth/formation stop. Strategies for achieving balance between aquifer recharge and discharge are presented in the Best Aquifer Management Practices section above.

Although bringing aquifer recharge and discharge into balance is our recommended long-term hazard-mitigation strategy, we recognize that achieving that goal will take time (possibly decades), during which land subsidence and earth-fissure formation may continue. Given the low permeability of the fine-grained sediment layers in many basin-fill aquifers, subsidence may continue for some time (again, possibly decades) even after recharge and discharge balance is achieved as dewatered fine-grained deposits continue to drain and compact (Galloway and others, 1999). Additionally, under groundwater-mining conditions, still-saturated fine-grained deposits may also compact. Lowering the potentiometric surface reduces overall aquifer head, which in turn reduces pore-water pressure throughout the aquifer. The pressure reduction decreases the buoyant effect of the groundwater, and allows saturated fine-grained units to compact (Galloway and others, 1999). Considering all of the above, land subsidence and earth fissures may remain hazards in valley areas undergoing subsidence for a considerable time even after groundwater mining ceases, and will be permanent hazards if groundwater mining continues.

Our recommendations for site characterization and hazard mitigation in subsiding areas fall into two categories—basin-wide and site-specific.

Basin-Wide Recommendations

The first consideration when dealing with land subsidence and earth fissures as geologic hazards is to determine as precisely as possible whether a proposed site and/or project is inside or outside of a subsiding area. If outside, land subsidence and earth fissures do not present a hazard; if inside or if in an adjacent area that may become subject to subsidence and fissuring over time, a variety of consequences related to subsidence and earth fissures become possible and require careful evaluation.

Within a subsiding area, the rate of subsidence and location of existing earth fissures are critical considerations for hazard evaluation. Therefore, periodically documenting valley-wide subsidence area boundaries (subject to change over time with ongoing groundwater mining), subsidence amount and rate (likely variable) within those boundaries, and locating all existing earth fissures are first-order, basin-wide priorities for land-subsidence- and earth-fissure-hazard mitigation.

Necessary detailed information on subsidence boundaries, subsidence rates, and earth-fissure locations can be obtained by application of the InSAR, LiDAR, and high-precision GPS/GNSS survey technologies discussed above. Therefore, our basin-wide hazard-mitigation recommendation reiterates the implementation of those technologies, including establishing a long-term monitoring program (chiefly a combination of InSAR and high-precision GPS/GNSS surveying) to track the distribution, magnitude, and growth of subsidence areas and earth fissures. Repeat collection of LiDAR imagery is significantly more costly, but new imagery should be obtained as frequently as funding permits. The UGS is able to assist local governments and other state agencies with establishing a long-term land-subsidence and earth-fissure monitoring program.

Site-Specific Recommendations

The cost of groundwater-mining-induced land subsidence and earth-fissure damage to the built environment in other southwestern states (chiefly Arizona, Nevada, and California) has been substantial (hundreds of millions of dollars) and has frequently resulted in litigation (Corwin and others, 1991; Shlemon, 2004). Deleterious effects associated with land subsidence include reduced aquifer storage capacity, change in both natural and irrigation runoff/flood patterns, deformation or collapse of well casings, tilting of long-baseline gravity-flow infrastructure (sewer and water lines, pipelines, canals, irrigation ditches, collector/storm drains), and damage to rigid or precisely leveled structures (building and equipment foundations, dams, canals, railroads, roadways, airport runways) (Gelt, 1992; Galloway and others, 1999; Ingebritsen and Jones, 1999; Pavelko and others, 1999; Skaw, 2005; Arizona Land Subsidence Group, 2007; Baum and others, 2008). Hazards associated with earth fissures include providing a direct conduit for contaminated surface water to reach groundwater aquifers; cracked, displaced, or collapsed highways and secondary roads; broken pipes and utility lines; damaged and breached canals; cracked and displaced building foundations; deformed railroad tracks; damaged dams and flood-control structures; and livestock and wildlife injury or death (Viets and others, 1979; Gelt, 1992; Arizona Division of Emergency Management, 2007; Arizona Land Subsidence Group, 2007). Therefore, it is prudent to carefully evaluate sites proposed for new development in areas of known or suspected land subsidence to ensure that the most damaging effects of land subsidence and earth fissures are avoided or mitigated.

Literature review: We reviewed published land-subsidence and earth-fissure related literature to identify guidelines or county/municipal ordinances for evaluating and/or mitigating land-subsidence and earth-fissure hazards. We identified two sets of guidelines pertaining directly to land subsidence and earth fissures. The first, published by the Nevada Bureau of Mines and Geology (Price and others, 1992), presents "alternatives and realistic options" for mitigating the subsidence hazard in Las Vegas Valley. The second, published by the Nevada Earthquake Safety Council (NESC) (1998), is titled *Guidelines for Evaluating Potential Surface Fault Rupture/Land Subsidence Hazards in Nevada.* Price and others (1992) listed six general recommendations for mitigating land-subsidence hazards, but did not provide detailed implementation guidance. The recommendations include reducing net groundwater withdrawals, defining potential hazard zones, restricting the use of applied water in already developed areas, establishing a regional subsidence district to set water policy and priorities, establishing long-term monitoring programs, and encouraging research into the cause and process of earth-fissure formation. The NESC (1998) guidelines provide specific guidance for evaluating surface-fault rupture and land subsidence, and are intended to "provide a standardized minimum level of investigation for fault rupture and fissuring in Nevada." The guidelines are based on previously published surface-fault-rupture-evaluation guidelines in California and Utah (see appendix H), but do not provide hazard-mitigation recommendations. Additionally, California Geological Survey Note 48 (2011), *Checklist for the Review of Engineering Geology and Seismology Reports for California Public Schools, Hospitals, and Essential Services Buildings,* includes "Regional Subsidence" in its list of "Other Geologic Hazards or Adverse Site Conditions" that must be considered when performing a geologic-hazard assessment for the above critical facilities.

Our review of county and municipal building codes focused on areas of known land subsidence and earth-fissure formation (table 13). The purpose of the review was to determine what land-subsidence- and earth-fissure-hazard investigations and mitigation measures are required in those jurisdictions. The review showed that most jurisdictions only require a general geotechnical/soil/engineering geology report, in which presumably land subsidence and earth fissures would be identified and evaluated if present at a site. Two municipalities, the City of Murrieta, California, and the City of North Las Vegas, Nevada, specifically require that land subsidence and/or earth fissures be considered prior to permitting new development. The City of Murrieta Grading Manual (table 13) requires an engineering geology report and states (bold text added for emphasis):

> *Engineering geology reports shall be required for all developments where geologic conditions are considered to have a substantial effect on existing and/or future site stability. This requirement may be*

Table 13. *Review of municipal and county building codes in jurisdictions that have experienced problems related to land subsidence and earth fissures.*

Counties				
Jurisdiction	**Fissure**	**Subsidence**	**Geologic Hazards**	**Geotechnical Report**
Clark County, NV[1]	30.28.130.3.X	30.20.110.a4C	30.16.240.a.16.D	30.16.240.a.16.D
Imperial County, CA[1]	None	8.76.020 92201.040	91502.01 Surface fault rupture	Geothermal only
Maricopa County, AZ	None	None	None	None
Pinal County, AZ[1]	None	8.20.150.B.4	None	18.81.060.D.1 Soils report/site grading
Riverside County, CA[1]	None	None	16.60.030 Surface fault rupture	15.60.050 Geologic report
San Joaquin County, CA[1]	None	5-8335	9-905.11.(c)	9-905.11.(c)

Cities				
Jurisdiction	**Fissure**	**Subsidence**	**Geologic Hazards**	**Geotechnical Report**
El Paso, TX[1]	None	None	19.24.010 Mountain development	19.24.040 Soils report
Glendale, AZ[1]	None	Sec. 31-24(c)(5)	None	None
Las Vegas, NV[1]	None	19.06.170.B(3)(b) Hillside development	19.06.170.D(8)(a) Hillside development	19.80.050.E.(1) Landscaping
Murrieta, CA[2]	Grading Manual 5.4 Soil and Engineering Geology Report Content	Grading Manual 5.4 Soil and Engineering Geology Report Content	Grading Manual Appendix B Technical Guidelines for Soil and Geology Reports	Grading Manual Appendix B Technical Guidelines for Soil and Geology Reports
North Las Vegas, NV[1]	16.12.030.AA 17.20.220.C.2.e.(5) 17.28.040.C.2.a.xiv	17.28.060.D.1.d.v	16.12.030.AA 17.20.220.C.2.e.(5)	15.72.150.D 16.16.070.D.4
Phoenix, AZ[1]	None	None	Sec.32A-22.(a).(3) Engineering geology Sec. 32-32.A Hillside development	None
Riverside, CA[3]	None	None	None	None
Temecula, CA[4]	None	None	None	18.06.060.C Seismic hazard
Tucson, AZ[5]	None	None	Development Standards 11-01.0.E	Development Standards 11-01.0.D

[1]*Municode Library (http://www.municode.com/Library/Library.aspx).*
[2]*City of Murrieta Grading Manual (http://www.murrieta.org/uploads/forms/publicworks/Grading_Manual_2005.pdf#search="subsidence").*
[3]*City of Riverside municipal code (http://www.riversideca.gov/municode/query.asp).*
[4]*Online Codes (http://www.qualitycodepublishing.com/codes.htm).*
[5]*Land Use Code of the City of Tucson (http://cms3.tucsonaz.gov/sites/default/files/planning/Complete%20LUC.pdf).*

*extended to other sites suspected of being potentially adversely affected by faulting, **fissuring, or differential settlement.***

*The preliminary (initial) engineering geology report shall include a comprehensive description of the site topography and geology; an opinion and supporting technical data as to the adequacy of the proposed development from an engineering geologic standpoint; an opinion and supporting technical data as to the potential for hydrocollapse to occur should the water table rise; **an opinion and supporting technical data as to the potential for differential settlement and fissuring from ground water pumping; an opinion as to the presence of steep subsurface geologic contacts that may contribute to fissuring**; an opinion and supporting technical data concerning the potential for onsite faulting or liquefaction; an opinion as to the extent that instability on adjacent properties may adversely affect the project; an opinion and supporting technical data concerning the potential for debris flows or mud flows engendered by regional land use changes; a description of the field investigation and findings; conclusions regarding the effect of geologic conditions on the proposed development; **and specific recommendations for plan modification, corrective grading and/or special techniques and systems to facilitate a safe and stable development**, and shall provide other recommendations as necessary, commensurate with the project grading and development. The preliminary engineering geology report may be combined with the soil engineering report.*

The City of North Las Vegas, Nevada, has experienced tens of millions of dollars in damage to buildings and infrastructure (Bell, 2003) due to land subsidence and earth fissures associated with groundwater mining. The North Las Vegas Code of Ordinances (table 13) specifies that "areas of fissuring and/or subsidence" be analyzed when evaluating site conditions and submitting preliminary plans for new development. Additionally, preliminary maps of proposed development sites must comply with the following (bold text added for emphasis):

*All known geologic hazards shall be shown. Geological hazards such as fault lines and/or **fissures** affecting residential structures may substantially alter the tentative map layout and require the submission of a revised tentative map which must be approved by the city prior to acceptance of the civil improvement plans. The footprint of proposed residential structures shall be plotted on all lots impacted by faults and/or **fissures**.*

Neither the Murrieta Grading Manual nor the North Las Vegas Code of Ordinances specifies mitigation measures once areas of subsidence and earth fissures are identified.

Consultation: To better understand site-specific land-subsidence and earth-fissure identification and mitigation issues, we consulted with Ken Euge (Geological Consultants Inc., Phoenix, Arizona), Ken Fergason (AMEC Earth and Environmental, Inc., Flagstaff, Arizona), and Ralph Weeks (GeoSouthwest, LLC, Phoenix, Arizona). All are registered Professional Geologists in Arizona and have extensive experience with land-subsidence and earth-fissure identification and mitigation. Due to the extensive area in Arizona affected by land subsidence and earth fissures (thousands of square miles), numerous hazard evaluation investigations have been conducted and subsidence/fissure mitigation strategies implemented. Those efforts were largely conducted in response to land subsidence and/or fissures affecting existing infrastructure, or were part of site investigations for the construction or retrofit of high-value infrastructure such as dams, canals, pipelines, and major transportation facilities (Sergent, Hauskins, and Beckwith, 1984a, 1984b, 1985a, 1985b, 1985c; Sandoval and Bartlett, 1991; Schumann, 1995; Rucker and Keaton, 1998; Rucker and Fergason, 2009; Euge, written communication, 2010).

In the absence of general guidelines that establish minimum technical site-characterization standards for land subsidence and earth fissures in Arizona (the Arizona Geological Survey published suggested guidelines by the Arizona Land Subsidence Interest Group [2011]), site investigations there were conducted on a case-by-case basis. Investigation methods have been dictated by site-specific geologic and hydrologic conditions, extent of local land subsidence and/or fissures, and investigation budget, which tend to be larger and more flexible for high-value infrastructure such as dams. Investigation techniques employed include remote sensing analysis and interpretation (stereoscopic aerial photographs, InSAR, and LiDAR), field reconnaissance and mapping, surface and subsurface geophysical investigations, test pits, drilling, borehole instrumentation, and trenching. Mitigation measures have included relocating proposed infrastructure away from earth-fissure hazard zones, reinforcing structures that bridge fissures, use of reinforced geotextiles and lean concrete to prevent infiltration into fissures, cutoff trenches and berms to divert water away from fissures, and increasing canal/dam freeboard.

Hazard-mitigation recommendations: The following recommendations to reduce the impact of land subsidence and earth fissures are modified from Price and others (1992) and Euge (written communication, 2010):

- Define land-subsidence and earth-fissure hazard zones and require that land-subsidence and earth-fissure hazards be carefully investigated on a site-specific basis in those areas prior to new development.

- Avoid land-subsidence and earth-fissure areas where possible.

- Disclose the presence of land subsidence and earth

fissures during real-estate transactions.

- If avoidance is not possible, integrate subsidence and fissures in project design to provide a factor of safety for development.

- Promote water conservation practices to reduce the impact on groundwater aquifers, either through reduced groundwater pumping and/or artificial recharge.

- Keep water out of earth fissures—control surface runoff.

- Landscape earth fissure areas with drought-resistant native vegetation—limit irrigation.

- Prevent construction of retention basins, dry wells, or effluent disposal (including on-site wastewater disposal) in earth-fissure affected areas.

- Establish a long-term monitoring program (InSAR, LiDAR, and high-precision GPS/GNSS surveying) to track the occurrence, magnitude, and growth of subsidence areas and earth fissures.

- Establish an interagency subsidence abatement district responsible for setting water policy and priorities, and to be responsible for developing continued subsidence mitigation strategies. Such agencies may be a natural extension of already-existing water conservancy districts.

- Recognize that it may be necessary to limit certain kinds of land use (e.g., water conveyance or retention structures, on-site wastewater disposal systems, pipelines, hazardous materials processing or storage) in areas of rapid, ongoing subsidence or extensive earth fissuring.

Hazard investigation guidelines: The purpose of guidelines for investigating land-subsidence and earth-fissure hazards is to (modified from Christenson and others, 2003):

- protect the health, safety, welfare, and property of the public by minimizing the potentially adverse effects of land subsidence and earth fissures;

- assist local governments in regulating land use and provide standards for ordinances;

- assist property owners and developers in conducting reasonable and adequate investigations;

- provide engineering geologists and geotechnical engineers with a common basis for conducting hazard investigations; and

- provide an objective framework for the preparation and review of reports.

Appendix H provides recommended guidelines for investigating land-subsidence and earth-fissure hazards. The purpose, scope, and methods of investigation for land-subsidence and

earth-fissure hazards will vary depending on site-specific conditions, and the type and scope of individual projects. For a given site, some topics may be addressed in more detail than at other sites because of differences in the geologic and/or hydrologic setting and/or intended site use. Although not all investigative techniques need to be or can be employed in all instances, the guidelines in appendix H provide minimum standards for conducting site investigations and preparing complete and well-documented reports. Reports on land-subsidence- and earth-fissure-hazard investigations should be reviewed by local or state government agencies that employ or retain Utah licensed Professional Geologists experienced in land subsidence and earth-fissure issues prior to project approval, and if mitigation measures are proposed, they should be reviewed by a Utah licensed Professional Engineer specializing in geotechnical or geological engineering. Therefore, all reports should be adequately documented and carefully written according to the guidelines to facilitate those reviews.

The scope of an investigation depends not only on the type, complexity, and economics of a project, but also on the level of risk acceptable for the proposed structure or development. A more detailed investigation is required for critical, sensitive, or high-occupancy structures than is necessary for less critical or costly infrastructure. The conclusion drawn from any given set of data, however, must be consistent and unbiased. Recommendations must be clearly separated from conclusions, because recommendations are not totally dependent on geologic factors. The final decision as to whether, or how, a given project should be developed is the responsibility of the owner and the governing body that must review and approve the project (Christenson and others, 2003).

Mitigation Practices Summary

1. Land subsidence and earth fissures due to groundwater mining are human-caused hazards caused by pumping more groundwater from a basin-fill aquifer than is recharged on a long-term basis.

2. Land subsidence and earth-fissure formation will continue until average annual recharge and discharge are brought into balance (safe yield).

3. Land subsidence and earth-fissure formation may continue for some time (perhaps decades) after recharge and discharge are balanced as fine-grained, basin-fill deposits continue to slowly drain and compact, and as pore-water pressure in the still-saturated portion of the aquifer re-equilibrates.

4. Managing basin-fill aquifers as a renewable resource and managing the hazards presented by land subsidence and earth-fissure formation requires that subsiding areas and rates of subsidence within those areas (likely variable) be defined. Technologies such as

InSAR, LiDAR, and high-precision GPS/GNSS surveying are well suited to this task.

5. Recommendations for dealing with land subsidence and earth fissures in alluvial valleys include:

    a. Stop mining groundwater and manage basin-fill aquifers as renewable resources. Adopt best aquifer management practices to bring long-term recharge of basin-fill aquifers into balance with long-term discharge. Possible strategies for achieving safe yield include:

        1. Import water from other basins.

        2. Recharge aquifers artificially, including aquifer storage and recovery projects.

        3. Relocate concentrations of high-discharge wells to dispersed locations away from subsiding areas.

        4. Establish a subsidence abatement district responsible for setting water policy and priorities (such as reducing water rights, permitting production wells, or taxing groundwater pumping) and for developing continued subsidence mitigation strategies. This function may naturally fall to existing water conservancy districts, where such districts already exist.

        5. Implement water conservation practices to reduce groundwater consumption over time to achieve safe yield.

    b. Better define the distribution, amount, and rate of subsidence and the location of as-yet unidentified earth fissures through the application of InSAR, LiDAR, and high-precision GPS/GNSS survey technologies. Establish a long-term monitoring program (chiefly a combination of repeated InSAR and high-precision GPS/GNSS surveying with LiDAR as available) to track the occurrence, distribution, and growth of subsidence areas and earth fissures until safe yield is achieved and subsidence/fissure formation stops.

    c. Institute both basin-wide and project-specific characterization and mitigation of land-subsidence and earth-fissure hazards in areas subject to groundwater mining by:

        1. Using InSAR, LiDAR, and high-precision GPS/GNSS survey results to better define the area and rates of subsidence and create land-subsidence and earth-fissure hazard-zone maps.

        2. Adopting building codes or sensitive land ordinances that require site-specific land-subsidence and earth-fissure hazard investigations for all new development in and adjacent to subsiding areas and for existing infrastructure as necessary.

        3. Adopting as guiding principles/action items the 11 recommendations contained in the Hazard Mitigation Recommendations section above.

SUMMARY

1. The potentiometric surface in Cedar Valley has been lowered by as much as 114 feet by groundwater pumping in excess of recharge since 1939.

2. The basin-fill sediments that comprise the Cedar Valley aquifer contain a high percentage of fine-grained, compressible material (silt and clay horizons), particularly in the central part of the valley that is susceptible to compaction upon dewatering or lowering of aquifer pore water pressure. Most subsidence in Cedar Valley has likely occurred where the percentage of fine-grained, basin-fill sediment is greater than 50 percent.

3. Lowering the potentiometric surface (head decline) has caused permanent compaction of fine-grained sediments in the Cedar Valley aquifer, which in turn has produced subsidence of the valley floor. Currently, the largest amount of measurable subsidence recorded at a benchmark in Cedar Valley is 0.9 foot in the Enoch graben over the ~1949–2011 time period; however, displacement across the differentially subsiding Enoch-graben-west fissures away from nearby benchmarks with accurate elevation data is about 3 feet in some places. Significant subsidence has occurred in other parts of Cedar Valley (Katzenstein, 2013; appendix E), although a lack of accurate historical benchmark elevation data prevented measuring absolute subsidence in those areas.

4. In response to the land subsidence, earth fissures have formed in the southwestern and northeastern parts of Cedar Valley; total length of the fissures is presently about 8.3 miles.

5. The Enoch-graben-west earth fissures are the most extensive zone of fissures, and include the only fis-

sures that exhibit vertical differential displacement. The rate of down-to-the-east displacement across the EGW1 fissure has been about 1.7 inches/year.

6. Significant fissure-related damage in Cedar Valley is currently limited to the partially developed Parkview residential subdivision in Enoch City. There, Enoch-graben-west fissures have displaced street surfaces, curb and gutter, and sidewalks, and has reversed the flow direction of a subdivision sewer line. Cracked street pavement at the north end of the Legacy Estates subdivision also appears to be fissure-related.

7. The EGW1 fissure also trends through and has displaced the ground surface in a livestock pasture/feeding area. Johnson Creek, an intermittent stream that flows into this area from the east, periodically ponds water contaminated with livestock fecal waste against the east side of the fissure scarp, creating a potential groundwater-contamination hazard.

8. Multiple sets of aerial photographs show that the EGW1 fissure began forming more than 50 years ago, and that the fissure grew approximately 800 feet to the south between 1997 and 2006. The southern tip of the fissure is obscured on more recent photography by grading for the Parkview subdivision.

9. Photolineaments of unknown origin and the presence of an isolated sinkhole and fissure south of SR-56 and generally along-trend with the fissures west of Quichapa Lake indicate the possibility of a more extensive zone of fissuring along the western margin of Cedar Valley.

CONCLUSIONS

Based on the investigation results, we conclude the following:

1. Long-term groundwater pumping in excess of recharge (groundwater mining) has dewatered the upper part of the Cedar Valley aquifer, and simultaneously lowered pore water pressure in the remaining saturated aquifer. The combination of dewatering and lower aquifer pressure is allowing high-porosity, low-permeability, fine-grained sediment beds in the aquifer to permanently compact. Compaction of the fine-grained sediments is the principal cause of the land subsidence and subsequent earth fissure formation in Cedar Valley.

2. Aquifer compaction has permanently reduced the storage capacity of the Cedar Valley aquifer; further reduction will occur if compaction continues.

3. Based on the estimated ratio of subsidence to head change for the basin-fill aquifer, if the potentiometric surface in Cedar Valley continues to decline 2 feet per year, average basin-wide subsidence will likely continue at a rate between 0.02 and 1.2 inches per year.

4. The inventory of earth fissures in Cedar Valley is likely incomplete because fissures not undergoing differential displacement or enlarged by erosion typically exist as hairline cracks which are rarely visible on aerial photographs, and not always apparent on LiDAR data. In agricultural or heavily vegetated areas, hairline fissures can be difficult to identify even at the ground surface.

5. Because the earth-fissure inventory is likely incomplete, currently unrecognized earth fissures may appear in other areas of Cedar Valley, particularly if enlarged by erosion.

6. If groundwater overdraft of the Cedar Valley aquifer continues, land subsidence will also continue and new earth fissures may form in the future, which could damage existing or future infrastructure in Cedar Valley. The exact location where new fissures may form is unknown without additional detailed geologic and hydrologic investigations. However, in general, new fissures are most likely to develop where deep basin-fill deposits comprising 50% or greater fine-grained, compressible sediments are experiencing declining water levels and either planar discontinuities in the sediments, or abrupt changes in basin-fill thickness cause differential compaction of the dewatering aquifer.

7. Continued southward growth of either the Enoch-graben-west or -east fissures may eventually impact existing neighborhoods in Enoch City.

8. If presently unrecognized ground cracks extend south of SR-56 along the western margin of Cedar Valley, crack widening due to infiltrating surface water may adversely affect the SR-56 right-of-way, buried utilities along the highway corridor, and homes and other structures west of Quichapa Lake.

9. Earth fissures may now or in the future provide a direct path for contaminated surface water to reach the Cedar Valley aquifer, which is a source of culinary water to area residents.

10. Managing basin-fill aquifers as a renewable resource and managing the hazards presented by land subsidence and earth-fissure formation requires that subsiding areas and rates of subsidence within those

areas (likely variable) be defined. Technologies such as InSAR, LiDAR, and high-precision GPS/GNSS surveying are well suited to this task.

11. Site-specific hazard investigations are required for new development, and in some instances for existing development, in areas known or suspected to be subsiding. Recommended guidelines for conducting such investigations are included in appendix H of this report.

REFERENCES

Amelung, F., Galloway, D.L., Bell, J.W., Zebker, H.A., and Laczniak, R.J., 1999, Sensing the ups and downs of Las Vegas—InSAR reveals structural control of land subsidence and aquifer-system deformation: Geology, v. 27, no. 6, p. 483–486.

Anderson, R.E., 1980, The status of seismotectonic studies of southwestern Utah, *in* Proceedings, Special Conference on Earthquake Hazards Along the Wasatch-Sierra Nevada Frontal Fault Zones: U.S. Geological Survey Open-File Report 80-801, p. 519–547.

Anderson, R.E., and Christenson, G.E., 1989, Quaternary faults, folds, and selected volcanic features in the Cedar City 1° x 2° quadrangle, Utah: Utah Geological and Mineral Survey Miscellaneous Publication 89-6, 29 p., 1 plate, scale 1:250,000.

Anderson, R.E., and Mehnert, H.H., 1979, Reinterpretation of the history of the Hurricane fault in Utah, *in* Newman, G.W., and Goode, H. D., editors, 1979 Basin and Range Symposium: Rocky Mountain Association of Geologists, p. 145–165.

AQUAVEO, 2010, Groundwater Modeling System v. 7.1.5: Provo, Utah, accessed February 2010.

Arizona Department of Water Resources, no date, Fact Sheet—Monitoring the state's water resources, InSAR—ADWR's satellite based land subsidence monitoring program: Arizona Department of Water Resources, 2 p.

Arizona Division of Emergency Management, 2007, Hazards and prevention—Earth fissures: Arizona Division of Emergency Management, 1 p.: Online, http://www.dem. azdema.gov/operations/mitigation/hazprevent/fissures. html, accessed October 10, 2010.

Arizona Land Subsidence Group, 2007, Land subsidence and earth fissures in Arizona—Research and information needs for effective risk management: Arizona Geological Survey Contributed Report CR-07-C, 24 p.

Arizona Land Subsidence Interest Group, 2011, Suggested guidelines for investigating land-subsidence and earth-fissure hazards in Arizona: Arizona Geological Survey, Contributed Report CR-11-D, 7 p.: Online, http://repository.azgs.az.gov/sites/default/files/dlio/files/nid1272/cr-11-d_az_ef_guidelines_final_0.pdf, accessed March 8, 2012.

Ashcroft, G.L., Jensen, D.T., and Brown, J.L., 1992 Utah climate: Utah Climate Center, 31 p.

Averitt, P., 1962, Geology and coal resources of the Cedar Mountain quadrangle, Iron County, Utah: U.S. Geological Survey Professional Paper 389, 72 p., 3 plates, scale 1:24,000.

Averitt, P., 1967, Geologic map of the Kanarraville quadrangle, Iron County, Utah: U.S. Geological Survey Geologic Quadrangle Map GQ-1120, scale 1:24,000.

Averitt, P., and Threet, R.L., 1973, Geologic map of the Cedar City quadrangle, Iron County, Utah: U.S. Geological Survey Geologic Quadrangle Map GQ-694, scale 1:24,000.

Bangkok City, 2001, Land subsidence, *in* Bangkok City state of the environment report, 2001: Online, http://www. rrcap.unep.org/pub/soe/bangkok_land.pdf, accessed November 4, 2010.

Barnett, J.A., and Mayo, F.M., 1966, Groundwater conditions and related water administration problems in Cedar City Valley, Iron County, Utah: Utah State Engineer Information Bulletin No. 15, 21 p.

Baum, R.L., Galloway, D.L., and Harp, E.L., 2008, Landslide and land subsidence hazards to pipelines: U.S. Geologi-

cal Survey Open-File Report 2008-1164, 192 p.

Bawden, G.W., Thatcher, W., Stein, R.S., Hudnut, K.W., and Peltzer, G., 2001, Tectonic contraction across Los Angeles after removal of groundwater pumping effects: Nature, v. 412, p. 812–815.

Bell, J.B., 2003, Las Vegas Valley—Land subsidence and fissuring due to ground-water withdrawal: U.S. Geological Survey, 5 p.: Online, http://geochange.er.usgs.gov/sw/impacts/hydrology/vegas_gw, accessed March 29, 2010.

Bell, J.B., 2004, Fissure evolution—what we know after 30 years of observation, *in* Shlemon Specialty Conference—Earth Fissures, El Paso, Texas, April 1–3, 2004, Conference Materials: The Association of Engineering Geologists and Engineering Geology Foundation, not paginated, CD.

Bell, J.B., and Amelung, F., 2003, The relation between land subsidence, active Quaternary faults, and earth fissures in Las Vegas, Nevada [abs.]: Geological Society of America Cordilleran Section 99th Annual Meeting.

Bell, J.B., Amelung, F., Ramelli, A.R., and Blewitt, G., 2002, Land subsidence in Las Vegas, Nevada, 1935–2000—New geodetic data show evolution, revised spatial patterns, and reduced rates: Environmental & Engineering Geoscience, v. VIII, no. 3, p. 155–174.

Bell, J.B., and Price, J.G., 1991, Subsidence in Las Vegas Valley: Nevada Bureau of Mines and Geology Open-File Report 93-5, 182 p.

Bjorklund, L.J., Sumsion, C.T., and Sandberg, G.W., 1977, Selected hydrologic data, Parowan Valley and Cedar City Valley drainage basins, Iron County, Utah: Utah Basic Data Release No. 28, 55 p.

Bjorklund, L.J., Sumsion, C.T., and Sandberg, G.W., 1978, Ground-water resources of the Parowan—Cedar City drainage basins, Iron County, Utah: Utah Department of Natural Resources Technical Publication No. 60, 93 p., scale 1:250,000.

Black, B.D., Hecker, S., Hylland, M.D., Christenson, G.E., and McDonald, G.N., 2003, Quaternary fault and fold database and map of Utah: Utah Geological Survey Map 193DM, scale 1:50,000.

Blank, H.R., Jr., and Mackin, J.H., 1967, Geologic interpretation of an aeromagnetic survey of the Iron Springs district, Utah: U.S. Geological Survey Professional Paper 516-B, 14 p., scale 1:48,000.

Bouwer, H., 1977, Land subsidence and cracking due to ground-water depletion: Groundwater, no. 15, v. 5, p. 358–364.

Bowman, S.D., Young, B.W., and Unger, C.D., 2011, Paleoseismology of Utah Volume 21—Compilation of 1982 seismic safety investigation reports of eight SCS dams in southwestern Utah (Hurricane and Washington faults) and low-sun-angle aerial photography, Washington and

Iron Counties, Utah and Mohave County, Arizona: Utah Geological Survey Open-File Report 583, 4 p., 2 plates, six DVDs.

Brah, W.J., and Jones, L.L., 1978, Institutional arrangements for effective ground-water management to halt land subsidence: Houston, Texas A&M University, Texas Water Resources Institute Technical Report 95, 194 p.

Brooks, L.E., and Mason, J.L., 2005, Hydrology and simulation of ground-water flow in Cedar Valley, Iron County, Utah: U.S. Geological Survey Scientific Investigations Report 2005-5170, 127 p.

Buckley, S.M., Rosen, P.A., Hensley, S., and Tapley, B.D., 2003, Land subsidence in Houston, Texas, measured by radar interferometry and constrained by extensometers: Journal of Geophysical Research, 108(B11), 2542, doi: 10.1029/2002JB001848.

Budhu, M., and Shelke, A., 2008, The formation of earth fissures due to groundwater decline, in 12th International Conference, Goa, India, 1–6 October, 2008: International Association for Computer Methods and Advances in Geomechanics, p. 3051–3059.

Burden, C.B., compiler, 2009, Ground-water conditions in Utah, spring of 2009: Utah Department of Natural Resources, Division of Water Resources, Cooperative Investigations Report No. 50, 120 p.

California Geological Survey, 2011, Checklist for the review of engineering geology and seismology reports for California public schools, hospitals, and essential services buildings: California Geological Survey Note 48, 2 p.: Online, http://www.consrv.ca.gov/cgs/information/publications/cgs_notes/note_48/note_48.pdf, accessed March 16, 2012.

Campbell, M.D., and Jensen, O.F., Jr., 1975, Texas land subsidence: Water Well Journal, v. 29, no. 10, p. 52–53.

Carpenter, M.C., 1999, South-Central Arizona—Earth fissures and subsidence complicate development of desert water resources, *in* Galloway, D., Jones, D.R., and Ingebritsen, S.E., editors, Land subsidence in the United States: U.S. Geological Survey Circular 1182, p. 65–78.

Christenson, G.E., Batatian, L.D., and Nelson, C.V., 2003, Guidelines for evaluating surface-fault-rupture hazards in Utah: Utah Geological Survey Miscellaneous Publication 03-6, 14 p.

Clyde, C.G., Duffy, C.J., Fisk, E.P., Hoggan, D.H., and Hansen, D.E., 1984, Management of groundwater recharge areas in the mouth of Weber Canyon: Utah Water Research Laboratory Hydraulics and Hydrology Series UWRL/H-84/01, 101 p.

Conway, B.D., 2013, Land subsidence and monitoring report, Number 1: Arizona Department of Water Resources, 30 p.: Online, http://www.azwater.gov/AzDWR/Hydrology/Geophysics/documents/ADWRLandSubsidenceMonitoringReport_Number1_Final.pdf, accessed September

10, 2013.

Cook, K.L., and Hardman, E., 1967, Regional gravity survey of the Hurricane fault area and Iron Springs district, Utah: Geological Society of America Bulletin, v. 78, p. 1063–1076.

Corwin, E.J., Alhadeff, S. C., Oggel, S. P., and Shlemon, R.J., 1991, Earth fissures, urbanization, and litigation—A case study from the Temecula area, southwestern Riverside County, California: Land Subsidence, Proceedings of the Fourth International Symposium on Land Subsidence, International Association of Hydrological Sciences Publication 200, p. 291–299.

Daito, K., Mizuno, M., and Ueshita, K., 1991, Control of groundwater withdrawal for preventing land subsidence in the Owari Plain, Japan, *in* Proceedings of the Fourth International Symposium on Land Subsidence, May 1991: International Association of Hydrological Sciences Publication No. 200, p. 533–542.

Demographic and Economic Analysis Section, 2005, Utah data guide, summer/fall 2005: Salt Lake City, Utah Governor's Office of Budget and Planning, 12 p.

Demographic and Economic Analysis Section, 2008, Utah data guide, summer 2008: Salt Lake City, Utah Governor's Office of Budget and Planning, 12 p.

DuRoss, C.B., and Kirby, S.M., 2004, Reconnaissance investigation of ground cracks along the western margin of Parowan Valley, Iron County, Utah: Utah Geological Survey Report of Investigation RI-253, 16 p.

Earth Sciences Associates, 1982, Seismic safety investigation of eight SCS dams in southwestern Utah: Portland, Oregon, unpublished consultant's report for the U.S. Soil Conservation Service, 2 volumes, variously paginated.

Forester, R.R., 2006, Land subsidence in southwest Utah from 1993 to 1998 measured with Interferometric Synthetic Aperture Radar (InSAR): Utah Geological Survey Miscellaneous Publication 06-5, 35 p.

Forester, R.R., 2012, Evaluation of Interferometric synthetic aperture radar (InSAR) techniques for measuring land subsidence and calculated subsidence rates for the Escalante Valley, Utah, 1998 to 2006: Utah Geological Survey, Open-File Report 589, 25 p.

Galloway, D.L., Hudnut, K.W., Ingebritsen, S.E., Phillips, S.P., Peltzer, G., Rogez, F., and Rosen, P.A., 1998, Detection of aquifer system compaction and land subsidence using interferometric synthetic aperture radar, Antelope Valley, Mojave Desert, California: Water Resources Research, v. 34, no. 10, p. 2573–2585.

Galloway, D., Jones, D.R., and Ingebritsen, S.E., editors, 1999, Land subsidence in the United States: U.S. Geological Survey Circular 1182, 177 p.

Galloway, D.L., Jones, D.R., and Ingebritsen, S.E., editors, 2000, Measuring land subsidence from space: U.S. Geological Survey Fact Sheet 51-04, 4 p.: Online, http://water.usgs.gov/pubs/FS/fs-051-00, accessed October 11, 2010.

Gelt, J., 1992, Land subsidence, earth fissures change Arizona's landscape: Arroyo, Summer 1992, v. 6, no. 2, University of Arizona.

Gesch, D.B., 2007, Chapter 4—The National Elevation Dataset, *in* Maune, D., editor, Digital Elevation Model Technologies and Applications: The DEM Users Manual, 2nd edition: Bethesda, Maryland, American Society for Photogrammetry and Remote Sensing, p. 99–118.

Gesch, D., Oimoen, M., Greenlee, S., Nelson, C., Steuck, M., and Tyler, D., 2002, The National Elevation Dataset: Photogrammetric Engineering and Remote Sensing, v. 68, no. 1, p. 5–11.

Halford, K.J., Laczniak, R.L., and Galloway, D.L., 2005, Hydraulic characterization of overpressured tuffs in central Yucca Flat, Nevada Test Site, Nye County, Nevada: U.S. Geological Survey Scientific Investigations Report 2005-5211, 36 p.

Hamblin, W.K., 1970, Structure of the western Grand Canyon region, *in* Hamblin, W.K., and Best, M.G., editors, The western Grand Canyon region: Utah Geological Society Guidebook to the Geology of Utah, no. 23, p. 3–20.

Hamblin, W.K., 1984, Direction of absolute movement along the boundary faults of the Basin and Range—Colorado Plateau margin: Geology, v. 12, p. 116–119.

Harding, D.J., and Berghoff, G.S., 2000, Fault scarp detection beneath dense vegetation cover—Airborne LiDAR mapping of the Seattle fault zone, Bainbridge Island, Washington State: Proceedings of the American Society of Photogrammetry and Remote Sensing Annual Conference, Washington, D.C., May, 2000, 11 p.

Harris, R., 2004, Giant desiccation cracks: Arizona Geological Survey Open-File Report 04-01, 93 p.

Harris, R., and Allison, M.L., 2006, Hazardous cracks running through Arizona: Alexandria, VA, American Geological Institute, Geotimes, August 2006, p. 24–27.

Harris-Galveston Subsidence Districts, 2010, Web page: Online, http://www.hgsubsidence.org/, accessed March 31, 2010.

Heywood, C.E., Galloway, D.L., and Stork, S.V., 2002, Ground displacements caused by aquifer-system water-level variations observed using interferometric synthetic aperture radar near Albuquerque, New Mexico: U.S. Geological Survey Water-Resources Investigation Re-

port 2002-4235, 18 p.

Hoffmann, J., 2003, The application of satellite radar interferometry to the study of land subsidence over developed aquifer systems: Palo Alto, Stanford University, Ph.D. dissertation, 211 p.

Hoffman, J., Galloway, D.L., and Zebker, H.A., 2003, Inverse modeling of regional aquifer-system compaction based on land subsidence measurements, Antelope Valley (Mojave Desert), California, *in* Prince, K.R., and Galloway, D.L., 2003, U.S. Geological Survey subsidence interest group conference, proceedings of the technical meeting, Galveston, Texas, November 27–29, 2001: U.S. Geological Survey Open-File Report 03-308, p. 103–113.

Holzer, T.L., 1989, State and local response to damaging land subsidence in United States urban areas: Engineering Geology, v. 27, p. 449–466.

Howells, J.H., Mason, J.L., and Slaugh, B.A., 2002, Selected hydrologic data for Cedar Valley, Iron County, southwestern Utah, 1930–2001: U.S. Geological Survey Open-File Report 2001-419, 81 p.

Huntington, E., and Goldthwait, J.W., 1904, The Hurricane fault in the Toquerville district, Utah: Harvard Museum Camp Zoology Bulletin, v. 42, p. 199–259.

Hurlow, H.A., 2002, The geology of Cedar Valley, Iron County, Utah and its relation to ground-water conditions: Utah Geological Survey Special Study 103, 74 p., 2 plates, scale 1:100,000.

Ikehara, M.E., Galloway, D.L., Fielding, E., Bürgmann, R., Lewis, A.S., and Ahmadi, B., 1998, InSAR imagery reveals seasonal and longer-term land-surface elevation changes influenced by groundwater levels and fault alignment in Santa Clara Valley, California [abs.]: EOS (supplement) Transactions, American Geophysical Union, no. 45, November 10, 1998, p. F37.

Ingebritsen, S.E., and Jones, D.R., 1999, Santa Clara Valley, California—A case of arrested subsidence, *in* Galloway, D., Jones, D.R., and Ingebritsen, S.E., editors, Land subsidence in the United States: U.S. Geological Survey Circular 1182, p. 15–22.

Johnston, R.H., 1989, The hydrologic response to development in regional sedimentary aquifers: Ground Water, v. 27, no. 3, p. 316–322.

Kaliser, B.N., 1978a, Ground surface subsidence in Cedar Valley, Utah: Utah Geological and Mineral Survey Report of Investigation 124, 22 p., 1 plate, scale 1:24,000.

Kaliser, B.N., 1978b, Map of ground surface subsidence in Cedar City, Utah: Utah Geological and Mineral Survey Map 46, scale 1:24,000.

Katzenstein, K., 2013, InSAR analysis of ground surface deformation in Cedar Valley, Iron County, Utah: Utah Geological Survey Miscellaneous Publication 13-5, 43 p.

Knudsen, T.R., 2014a, Interim geologic map of the Enoch quadrangle, Iron County, Utah: Utah Geological Survey Open-File Report 628, 12 p., 2 plates, scale 1:24,000.

Knudsen, T.R., 2014b, Interim geologic map of the Cedar City 7.5-minute quadrangle, Iron County, Utah: Utah Geological Survey Open-File Report 626, 20 p., 2 plates, scale 1:24,000.

Knudsen, T.R., and Biek, R.F., 2014, Interim geologic map of the Cedar City NW quadrangle, Iron County, Utah: Utah Geological Survey Open-File Report 627, 18 p., 2 plates, scale 1:24,000.

Knudsen, T., Inkenbrandt, P., Lund, W., and Lowe, M., 2012, Investigation of land subsidence and earth fissures in Cedar Valley, Iron County, Utah: Utah Geological Survey contract report prepared for the Central Iron County Water Conservancy District, 118 p.

Kurie, A.E., 1966, Recurrent structural disturbance of the Colorado Plateau margin near Zion National Park, Utah: Geological Society of America Bulletin, v. 77, p. 867–872.

Laczniak, R.J., Galloway, D.L., and Sneed, M., 2003, InSAR detection of post-seismic and coseismic ground-surface deformation associated with underground weapons testing, Yucca Flat, Nevada Test Site, *in* Prince, K.R., and Galloway, D.L., editors., 2003, U.S. Geological Survey subsidence interest group conference, proceedings of the technical meeting, Galveston, Texas, November 27–29, 2001: U.S. Geological Survey Open-File Report 2003-308, p. 121–128.

Leake, S.A., 2010, Human impacts on the landscape—land subsidence from ground-water pumping, *in* Impact of climate change and land use in the southwestern United States: Online, http://geochange.er.usgs.gov/sw/changes/anthropogenic/subside/, accessed September 29, 2010.

Lin, Z., Huili, G., Lingling, J., Yaoming, S., Xiaojaun, L., and Jun, J, 2009, Research on evolution of land subsidence induced by nature and human activity by utilizing remote sensing technology: Urban Remote Sensing Event, Shanghai, 5 p., doi 10.1109/URS.2009.5137693.

Lowe, M., and Wallace, J., 2001, Evaluation of potential geologic sources of nitrate contamination in groundwater, Cedar Valley, Iron County, Utah, with emphasis on the Enoch area: Utah Geological Survey Special Study 100, 50 p., scale 1:48,000.

Lowe, M., Wallace, J., and Bishop, C.E., 2000, Analysis of septic-tank density for three areas in Cedar Valley, Utah—a case study for evaluations of proposed subdivisions in Cedar Valley: Utah Geological Survey Water Resource Bulletin 27, 66 p.

Lowe, M., Wallace, J., Sabbah, W., and Kneedy, J.L., 2010, Science-based land-use planning tools to help protect ground-water quality, Cedar Valley, Iron County, Utah: Utah Geological Survey Special Study 134, 125 p.

Lund, W.R., DuRoss, C.B., Kirby, S.M., McDonald, G.N.,

Hunt, G., and Vice, G.S., 2005, The origin and extent of earth fissures in Escalante Valley, southern Escalante Desert, Iron County, Utah: Utah Geological Survey Special Study 115, 30 p.

Lund, W.R., Hozik, M.J., and Hatfield, S.C., 2007, Paleoseismology of Utah Volume 14— Paleoseismic investigation and long-term slip history of the Hurricane fault in southwestern Utah: Utah Geological Survey Special Study 119, 81 p.

Mackin, J.H., 1960, Structural significance of Tertiary volcanic rocks in southwestern Utah: American Journal of Science, v. 258, p. 81–131.

Mackin, J.H., Nelson, W.H., and Rowley, P.D., 1976, Geologic map of the Cedar City NW quadrangle, Iron County, Utah: U.S. Geological Survey Geologic Quadrangle Map GQ-1295, scale 1:24,000.

Mackin, J.H., and Rowley, P.D., 1976, Geologic map of The Three Peaks quadrangle, Iron County, Utah: U.S. Geological Survey Geologic Quadrangle Map GQ-1297, scale 1:24,000.

Maldonado, F., Sable, E.G., and Nealey, L.D., 1997, Cenozoic low-angle faults, thrust faults, and anastomosing high-angle faults, western Markagunt Plateau, southwestern Utah, *in* Maldonado, F., and Nealey, L.D., editors, Geologic studies in the Basin and Range-Colorado Plateau transition in southeastern Nevada, southwestern Utah, and northwestern Arizona, 1995: U.S. Geological Survey Bulletin 2153-G, p. 125–149.

Maldonado, F., and Williams, V.S., 1993, Geologic map of the Parowan Gap quadrangle, Iron County, Utah: U.S. Geological Survey Geologic Quadrangle Map GQ-1712, scale 1:24,000.

Marshall, R.B., 1911, Results of spirit leveling in Utah 1897 to 1910, inclusive: U.S. Geological Survey Bulletin 489, 38 p.

Meinzer, O.E., 1911, Ground water in Juab, Millard, and Iron Counties, Utah: U.S. Geological Survey Water-Supply Paper 277, 162 p.

Milbert, D.G., 1999, National Geodetic Survey (NGS) height conversion methodology: Online, http://www.ngs.noaa. gov/TOOLS/Vertcon/vert_method.html, accessed March 2012.

Moller, A.L., and Gillies, R.R., 2008, Utah Climate (second edition): Logan, Utah, Utah Climate Center, Utah State University, 109 p.

National Aeronautics and Space Administration, 2004, Laser technology helps track changes in Mount St. Helens: National Aeronautics and Space Administration, 1 p.: Online, http://www.nasa.gov/vision/earth/lookingatearth/ mshelensLiDAR.html, accessed October 11, 2010.

National Geodetic Survey, 2010, VERTCON orthometric height conversion: Online, http://www.ngs.noaa.gov/cgi-bin/VERTCON/vert_con.prl, accessed March 2012.

National Oceanic and Atmospheric Administration, 2008, LiDAR 101—An introduction to LiDAR technology, data, and applications: Charleston, South Carolina, National Oceanic and Atmospheric Administration Coastal Services Center, 62 p.

Nevada Earthquake Safety Council, 1998, Guidelines for evaluating potential surface fault rupture/land subsidence hazards in Nevada: Nevada Earthquake Safety Council, 7 p.: Online, http://www.nbmg.unr.edu/nesc/guidelines. htm, accessed October 10, 2010.

Onsoy, Y.S., Bonds, C.L., Petersen, C.R., Aikens, C., and Burke, S.M., 2005, Groundwater management for Yuba County Water Agency—a conjunctive use pilot project, *in* Proceedings of the Water Environment Federation, session 61 through 70, p. 5675-5692: Online, http://www.ingentaconnect.com/content/wef/wef-proc/2005/00002005/00000010/art00046, accessed September 23, 2010.

Oregon Department of Geology and Mineral Industries, 2006, Seeing landslides with LiDAR: Oregon Department of Geology and Mineral Industries Cascadia, v. 4, no. 2, 3 p.

Pavelko, M.T., Woods, D.B., and Laczniak, R.J., 1999, Las Vegas, Nevada—Gambling with water in the desert, *in* Galloway, D., Jones, D.R., and Ingebritsen, S.E., editors, Land subsidence in the United States: U.S. Geological Survey Circular 1182, p. 49–64.

Poland, J.F., 1977, Land subsidence stopped by artesian head recovery, Santa Clara Valley, California, *in* Proceedings of the Second International Symposium on Land Subsidence, Anaheim, December 1976: International Association of Hydrological Sciences Publication No. 121, p. 124–132.

Poland, J.F., and Davis, G.H., 1969, Land subsidence due to withdrawal of fluids: Geological Society of America, Reviews in Engineering Geology no. 2, 83 p.

Poland, J.F., and Green, J.H., 1962, Subsidence in Santa Clara Valley, a progress report: U.S. Geological Survey Water Supply Paper 1619-C, 16 p.

Price, J.G., Bell, J.W., and Helm, D.C., 1992, Subsidence in Las Vegas Valley: Nevada Bureau of Mines and Geology Quarterly Newsletter, Fall 1992, 2 p.: Online, http:// www.nbmg.unr.edu/dox/nl/nl16a.htm, accessed October 10, 2010.

Pyne, R.D.G., 1995, Groundwater recharge and wells— a guide to aquifer storage and recovery: New York, Lewis Publishers, 376 p.

Reichard, E.G., and Bredehoeft, J.D., 1985, Incorporating groundwater modeling into cost-benefit analyses of aquifer recharge, *in* Proceedings of the NWWA (National Water Well Association) Conference on Groundwater Management, October 29–31, 1984, Orlando, Florida: Worthington, Ohio, Water Well Journal Publishing Com-

pany, p. 343–355.

Roman, D.R., Wang, Y.M., Saleh, J., and Li, X., undated, Final national models for the United States: Development of GEOID09: National Geodetic Survey: Online, http://www.ngs.noaa.gov/GEOID/GEOID09/GEOID09_tech_details.pdf, accessed March 2012.

Rowley, P.D., 1975, Geologic map of the Enoch NE quadrangle, Iron County, Utah: U.S. Geological Survey Quadrangle Map GQ-1301, scale 1:24,000.

Rowley, P.D., 1976, Geologic map of the Enoch NW quadrangle, Iron County, Utah: U.S. Geological Survey Quadrangle Map GQ-1302, scale 1:24,000.

Rowley, P.D., and Threet, R.L., 1976, Geologic map of the Enoch quadrangle, Iron County, Utah: U.S. Geological Survey Quadrangle Map GQ-1296, scale 1:24,000.

Rowley, P.D., Williams, V.S., Vice, G.S., Maxwell, D.J., Hacker, D.B., Snee, L.W., and Mackin, J.H., 2006, Interim geologic map of the Cedar City 30' x 60' quadrangle, Iron and Washington Counties, Utah: Utah Geological Survey Open-File Report 476DM, scale 1:100,000.

Rucker, M.L. and Fergason, K.C., 2009, Geophysics in geotechnical investigations and mitigations of distressed flood control dams: FastTimes, v. 14, no. 1, pp. 33–42.

Rucker, M.L., and Keaton, J.R., 1998, Tracing an earth fissure using refraction-seismic methods with physical verification, *in* Borchers, J.W., editor, Land subsidence, case studies and current research, Proceedings of the Joseph F. Poland Symposium on Land Subsidence: Association of Engineering Geologists Special Publication No.8, p. 207–216.

Saines, M., Bell, J.B., Ball, S., and Hendrickx, C., 2006, Formation of earth fissures over the past half century at the Las Vegas Earth Fissure Preserve, Las Vegas, Nevada [abs.], Seminar on Environmental Impacts of Growth, and Mitigation Measures in Southern Nevada, Las Vegas, Nevada, May 24–25, 2006: Las Vegas, Air and Waste Management Association, 1 p.: Online, http://www.ae-gweb.org/docs/section-and-chapters/lv_earth_fissures_preserve_saines.pdf?sfvrsn=2, accessed March 29, 2009.

Sandberg, G.W., 1963, Ground-water data, Beaver, Escalante, Cedar City, and Parowan Valleys, parts of Washington, Iron, Beaver, and Millard Counties, Utah: Utah State Engineer Basic Data Report No. 6, 26 p.

Sandberg, G.W., 1966, Ground-water resources of selected basins in southwestern Utah: Utah State Engineer Technical Publication 13, 43 p.

Sandoval, J.P., and Bartlett, S.R., 1991, Land subsidence and earth fissuring on the Central Arizona Project, Arizona: Land Subsidence, Proceedings of the Fourth International Symposium on Land Subsidence, International Association of Hydrological Sciences Publication 200, p. 249–260.

Schmidt, D.A., and Bürgmann, R., 2003, Time dependent land uplift and subsidence in the Santa Clara Valley, California, from a large InSAR data set: Journal of Geophysical Research, 108(B9), 2416, doi: 10.1029/2002JB002267.

Schulz, W.H., 2007, Landslide susceptibility revealed by LiDAR imagery and historical records, Seattle, Washington: Engineering Geology, v. 89, p. 67–87.

Schumann, H.H., 1995, Land subsidence and earth fissure hazards near Luke Air Force Base, Arizona, *in* Prince, K.R., Galloway, D.L., and Leake, S.A., editors, U.S. Geological Survey subsidence interest group conference, Edwards Air Force Base, Antelope Valley, California [abstract with summary]: U.S. Geological Survey Open-File Report No. 94-532, p. 841–851.

Sergent, Hauskins, & Beckwith, 1984a, City of Phoenix—Study of subsidence effects on sanitary sewers, northeast Phoenix, Arizona—Phase II, field survey: Phoenix, unpublished consultant's report, 2 vol., 21 p., 3 appendices, 24 sheets, scales 1:7,200 and 1:7,800.

Sergent, Hauskins, & Beckwith, 1984b, City of Phoenix—Study of subsidence effects on sanitary sewers, northeast Phoenix, Arizona—Phase I, initial studies: Phoenix, unpublished consultant's report, 32 p., 2 appendices, 22 sheets, scale 1:7,800.

Sergent, Hauskins, & Beckwith, 1985a, City of Phoenix—Study of subsidence effects on sanitary sewers, northeast Phoenix, Arizona—executive summary: Phoenix, unpublished consultant's report, 28 p.

Sergent, Hauskins, & Beckwith, 1985b, City of Phoenix—Study of subsidence effects on sanitary sewers, northeast Phoenix, Arizona—Phase IV, subsidence predictions and mitigating measures: Phoenix, unpublished consultant's report, 49 p., 2 appendices, 53 sheets, scales 1:7,800 and 1:24,000.

Sergent, Hauskins, & Beckwith, 1985c, City of Phoenix—Study of subsidence effects on sanitary sewers, northeast Phoenix, Arizona—Phase III, subsidence model: Phoenix, unpublished consultant's report, 55 p., 2 appendices, 28 sheets, scales 1:7,800 and 1:24,000.

Shlemon, R.J., 2004, Fissure impact on the built environment, *in* Shlemon Specialty Conference—Earth Fissures, El Paso, Texas, April 1–3, 2004, Conference Materials: The Association of Engineering Geologists and Engineering Geology Foundation, unpaginated, CD.

Skaw, J., 2005, A sinking feeling in Arizona—Subsidence is significant: Imaging Notes Magazine, Summer 2005, 3 p.

Sneed, M., Ikehara, M.E., Galloway, D.L., and Amelung, F., 2001, Detection and measurement of land subsidence using Global Positioning System and interferometric synthetic aperture radar, Coachella Valley, California, 1996–98: U.S. Geological Survey Water-Resources Investigations Report 01-4193, 26 p.

Sneed, M., Stork, S.V., and Ikehara, M.E., 2002, Detection

and measurement of land subsidence using Global Positioning System and interferometric synthetic aperture radar, Coachella Valley, California, 1998–2000: U.S. Geological Survey Water-Resources Investigations Report 2002-4239, 29 p.

Solaimani, K., and Mortazavi, S.M., 2008, Investigation of the land subsidence and its consequences of large groundwater withdrawal in Rafsanjan, Iran: Pakistan Journal of Biological Sciences, v. 11, no. 2, p. 265–269.

Stokes, W.L., 1977, Subdivisions of the major physiographic provinces in Utah: Utah Geology, v. 4, no. 1, p. 1–17.

Stork, S.V., and Sneed, M., 2002, Houston-Galveston Bay area, Texas, from space—a new tool for mapping land subsidence: U.S. Geological Survey Fact Sheet 11002, 6 p.

Strause, J.L., 1984, Approximate water-level changes in wells in the Chicot and Evangeline aquifers 1977-84 and 1983-84, and measured compaction 1973-84, in the Houston-Galveston region, Texas: U.S. Geological Survey Open-File Report 84-140, 6 p., scale 1:380,160.

Swanson, G.J., 1996, Water is the key to Las Vegas growth: Water Well Journal, v. 50, no. 11, p. 71–73.

Thomas, H., Nelson, W.B., Lofgren, B.E., and Butler, R.G., 1952, Status of development of selected ground-water basins in Utah: Utah State Engineer Technical Publication 7, p. 22–34.

Thomas, H.E., and Taylor, G.H., 1946, Geology and ground-water resources of Cedar City and Parowan Valleys, Iron County, Utah: U.S. Geological Survey Water Supply Paper 993, 210 p., scale 1:312,500.

Threet, R.L., 1963a, Structure of the Colorado Plateau margin near Cedar City, Utah, *in* Heylmun, E.B., editor, Guidebook to the geology of southwestern Utah: Intermountain Association of Petroleum Geologists, 12th Annual Field Conference, 1963, p. 104–117.

Threet, R.L., 1963b, Geology of the Parowan Gap area, Iron County, Utah, *in* Heylmun, E.B., editor, Guidebook to the geology of southwestern Utah: Intermountain Association of Petroleum Geologists, 12th Annual Field Conference, 1963, p. 136–145.

Tolman, C.F., and Poland, J.F., 1940, Ground-water infiltration, and ground surface recession in Santa Clara Valley, Santa Clara County, California: Transactions of the American Geophysical Union, v. 21, p. 23–24.

Trimble, 2013, Datasheet for the Trimble 5800 GPS system: Online, http://trl.trimble.com/docushare/dsweb/Get/Document-32185/022543-016E_5800_GPS_DS_0708_LR.pdf, accessed September 24, 2013.

U.S. Army Corps of Engineers, 2007, Engineer manual, engineering and design, control and topographic surveying: U.S. Army Corps of Engineers, EM 1110-1-1005, Washington D.C. 20314-1000, 498 p.

U.S. Census Bureau, 2013, State and county quick facts—Iron County, Utah: U.S. Department of Commerce, United States Census: Online, http://quickfacts.census.gov/qfd/states/49/49021.html, accessed September 10, 2013.

U.S. Environmental Protection Agency, 2010a, Current drinking water standards: Online, http://www.epa.gov/safewater/mcl.html, accessed June 8, 2010.

U.S. Environmental Protection Agency, 2010b, Water-efficient landscaping: Online, http://www.epa.gov/watersense/docs/water-efficient_landscaping_508.pdf, accessed November 2, 2010.

U.S. Geological Survey, 1965, Retyped unpublished leveling in support of the Cedar City 15-minute quadrangle, Book B 4782: U.S. Geological Survey National Geospatial Technical Operations Center, Denver, Colorado, variously paginated.

U.S. Geological Survey, 1969, Retyped unpublished leveling in support of the Parowan 15-minute quadrangle, Book B 4777-8: U.S. Geological Survey National Geospatial Technical Operations Center, Denver, Colorado, variously paginated.

U.S. Geological Survey, 2000, Measuring land subsidence from space: U.S. Geological Survey Fact Sheet 051-00, 4 p.

U.S. Geological Survey, 2004, Mount St. Helens, Washington eruption 2004—LiDAR September 2003 to November 20, 2004: USGS Cascade Volcano Observatory, 2 p.: Online, http://vulcan.wr.usgs.gov/Volcanoes/MSH/Eruption04/LiDAR/, accessed October, 7, 2010.

U.S. Geological Survey, 2010, National Water Information System: Online, http://waterdata.usgs.gov/nwis, accessed June, 2010.

Utah Automated Geographic Reference Center, 2006a, 2006 National Agriculture Imagery Program 1 meter orthophotography: Online, http://gis.utah.gov/data/aerial-photography/2006-naip-1-meter-color-orthophotography/, accessed August 14, 2013.

Utah Automated Geographic Reference Center, 2006b, 2006 High resolution orthophotography (HRO): Online, http://gis.utah.gov/data/aerial-photography/2006-hro-1-foot-color-orthophotography/, accessed August 14, 2013.

Utah Automated Geographic Reference Center, 2009, 2009 National Agriculture Imagery Program 1 meter orthophotography: Online, http://gis.utah.gov/data/aerial-photography/2009-naip-1-meter-orthophotography/, accessed August 14, 2013.

Utah Automated Geographic Reference Center, 2011, 2011 National Agriculture Imagery Program 1 Meter orthophotography: Online, http://gis.utah.gov/data/aerial-photography/2011-naip-1-meter-orthophotography/, accessed August 14, 2013.

Utah Automated Geographic Reference Center, 2013, U.S.

Geological Survey mid 1990's 1 meter black and white orthophotography: Online, http://gis.utah.gov/data/aerial-photography/mid-1990s-1-meter-black-white-orthophotography/, accessed August 14, 2013.

Utah Climate Center, 2010, Utah climate data: Online, http://climate.usurf.usu.edu/products/data.php, accessed March, 2010.

Utah Division of Water Resources, 1995, Water use report: Salt Lake City, Utah Department of Natural Resources, p. 36–37.

Utah Division of Water Resources, 2001, Utah's water resources—planning for the future: Salt Lake City, Utah Division of Water Resources, 115 p.

Utah Division of Water Resources, 2005, Conjunctive management of surface and groundwater in Utah: Salt Lake City, Utah Division of Water Resources, 72 p.

Utah Division of Water Rights, 2010a, Well information program: Online, http://www.waterrights.utah.gov/cgi-bin/wellview.exe?Startup, accessed March 2010.

Utah Division of Water Rights, 2010b, Public water supply water use data: Online, http://www.waterrights.utah.gov/cgi-bin/wuseview.exe?Startup, accessed March, 2010.

Utah Division of Water Rights, 2010c, Utah water use program: Online, http://www.waterrights.utah.gov/distinfo/wuse.asp, accessed March, 2010.

Utah Geological Survey, 2011, LiDAR elevation data Cedar and Parowan Valleys: Utah Geological Survey: Online, http://geology.utah.gov/databases/LiDAR/LiDAR.htm.

Valentine, D.W., Densmore, J.L., Galloway, D.L., and Amelung, F., 2001, Use of InSAR to identify land-surface displacements caused by aquifer-system compaction in the Paso Robles area, San Luis Obispo County, California, March to August 1997: U.S. Geological Survey Open-File Report 00-447, poster report.

Viets, V.F., Vaughan, C.K., and Harding, R.C., 1979, Environmental and economic effects of subsidence: Berkeley, California, Lawrence Berkeley Laboratory Geothermal Subsidence Research Management Program, 251 p.

Waite, H.A., Nelson, W.B., Lofgren, B.E., Barnell, R.L., and Butler, R.G., 1954, Status of ground-water development in four irrigation districts in southwestern Utah, *in* Progress report on selected ground-water basins in Utah: Utah State Engineer Technical Publication No. 9, 128 p.

Wallace, J., and Lowe, M., 2000, Geologic evaluation of potential natural sources of nitrate in ground water—An example from southwestern Utah [abs]: Geological Society of America Abstracts with Programs, v. 32, no. 7, p. A–35.

Williams, V.S., and Maldonado, F., 1995, Quaternary geology and tectonics of the Red Hills area of the Basin and Range-Colorado Plateau transition zone, Iron County, Utah, *in* Scott, R.B., and Swadley, W.C., editors, Geo-

logic studies in the Basin and Range-Colorado Plateau transition in southeastern Nevada, southwestern Utah, and northwestern Arizona, 1992: U.S. Geological Survey Bulletin 2056, p. 255–275.

Zebker, H.A., and Goldstein, R.M., 1986, Topographic mapping from interferometric synthetic aperture radar observations: Journal of Geophysical Research, v. 91, p. 4993–4999.

Zebker, H.A., Rosen, P.A., Goldstein, R.M., Gabriel, A., and Werner, C.L., 1994, On the derivation of coseismic displacement fields using differential radar interferometry—The Landers earthquake: Journal of Geophysical Research, v. 99, no. B10, p. 19,617–19,634.

Zilkoski, D.B., Carlson, E.E., and Smith, C.L., 2008, Guidelines for establishing GPS-Derived orthometric heights, version 1.5: Silver Spring, Md., National Geodetic Survey, 15 p.

Zilkoski, D.B., D'Onofrio, J.D., and Frakes, S.J., 1997, Guidelines for establishing GPS-derived ellipsoid heights (Standards: 2 cm and 5 cm), version 4.3: Silver Spring, Md., National Geodetic Survey, 10 p.

APPENDICES

APPENDIX A

Baboon Peak	Dry Willow Peak	Jack Henry Knoll

Enoch NW	Enoch NE	Parowan Gap	Paragonah
USGS GQ-1302 (Rowley, 1976)	USGS GQ-1301 (Rowley, 1975)	USGS GQ-1712 (Maldonado and Williams,1993b)	

The Three Peaks	Enoch	Summit	Parowan
USGS GQ-1297 (Mackin and Rowley, 1976)	UGS (Knudsen, in preparation[a])		

Desert Mound	Cedar City NW	Cedar City	Flanigan Arch	Brian Head
	UGS (Knudsen and Biek, in preparation)	UGS (Knudsen, in preparation[b])		

Stoddard Mt	Kanarraville	Cedar Mountain	Webster Flat	Navajo Lake
	USGS GQ-694 (Averitt, 1967)	USGS P-389 (Averitt, 1962)		

N

0 1 2 3 4 Miles

Surface-Drainage Boundary

Names and boundaries of USGS 7.5-minute quadrangles covering the Cedar City drianage basin, with references for the geologic maps used for this study.

APPENDIX B

Numbering system for wells in Utah following U.S. Geological Survey convention.

Sections within a township

R. 12 W.

6	5	4	3	2	●Well 1
7	8	9	10	11	12
18	17	16	15	14	13
19	20	21	22	23	24
30	29	28	27	26	25
31	32	33	34	35	36

T. 36 S.

6 miles
9.7 kilometers

Tracts within a section

Section 2

b   a

b   a

c   ● Well
b   a

c   d

c   d

1 mile
1.6 kilometers

(C-36-12) 2adb-1

B   A

SALT LAKE ● BASE LINE
Salt Lake City

C   D

SALT LAKE MERIDIAN

■
T. 36 S. R. 12 W.
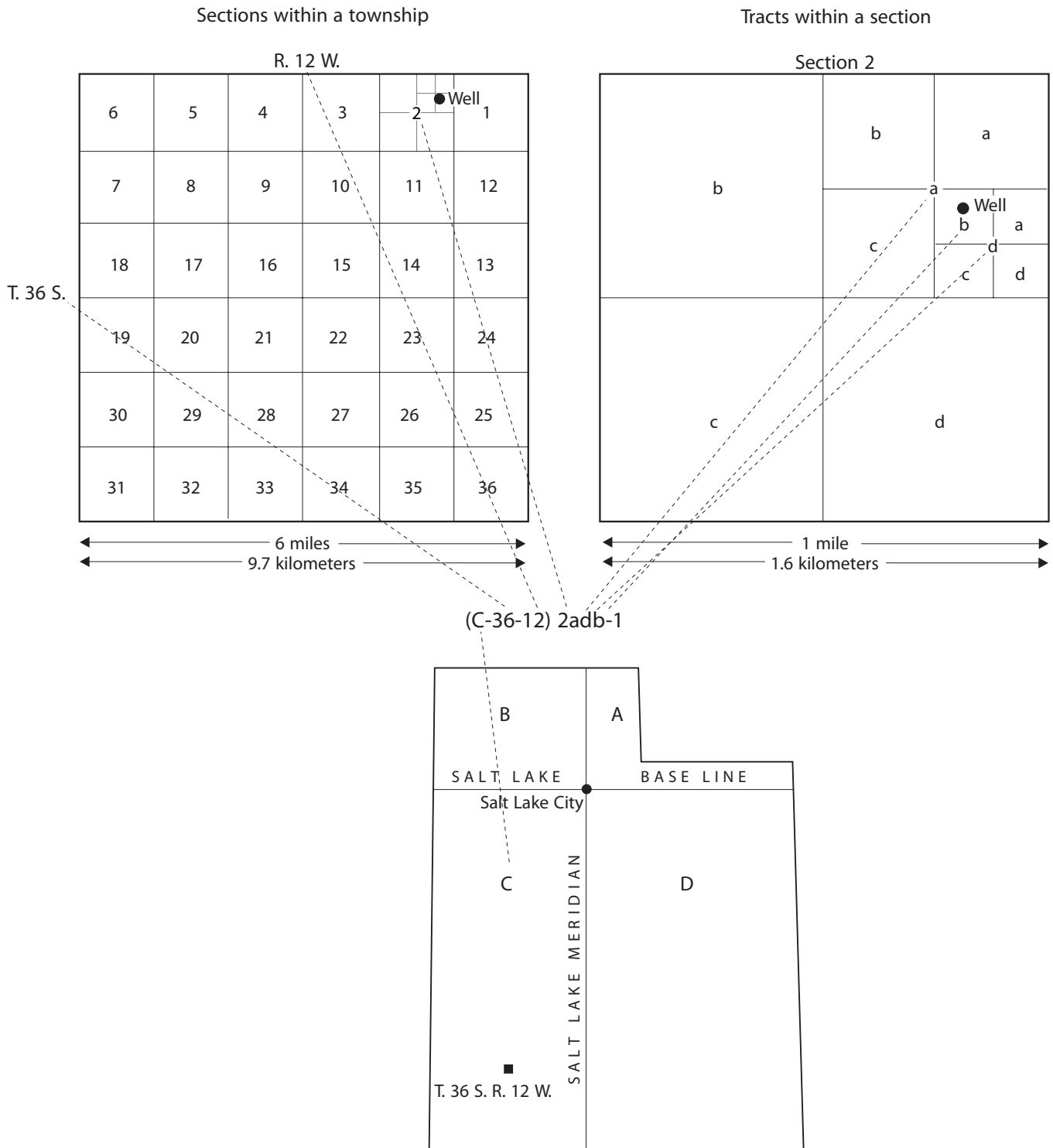
APPENDIX C

Approximate annual pumping of wells with discharges of greater than or equal to 40 acre-feet per year (Utah Division of Water Rights 2010a, 2010b). Figure 5 in main report is a map of these wells.

Cadastral Location (CAD)[1]	Approx. Pumping (acre-ft/yr)[2]	Owner	Well Name[3]
(C-35-11)11dad-1	40	--	--
(C-35-11)14bab-1	40	--	--
(C-35-11)14bbb-1	40	--	--
(C-35-11)14bca-1	40	--	--
(C-35-11)1cdc-1	40	--	--
(C-35-12)36dbb-1	40	--	--
(C-36-11)18ada-1	40	--	--
(C-36-11)7aba-1	40	--	--
(C-36-11)8bba-1	40	--	--
(C-36-12)30dcb-1	40	--	--
(C-36-12)30dcc-1	40	--	--
(C-36-11)7aaa-2	40	Monte Vista Community	Well (10')
(C-35-10)18cdd-1	50	--	--
(C-35-11)16aab-1	50	--	--
(C-35-11)22dcd-1	50	--	--
(C-35-11)23abb-1	50	--	--
(C-35-11)23cba-1	50	--	--
(C-35-11)32aac-1	50	--	--
(C-35-11)32aca-1	50	--	--
(C-35-11)9cbd-1	50	--	--
(C-35-12)34dcd-1	50	--	--
(C-36-11)7aaa-1	50	--	--
(C-36-12)24aad-1	50	--	--
(C-36-12)24adb-1	50	--	--
(C-36-12)24adb-2	50	--	--
(C-36-12)25cda-1	50	--	--
(C-35-11)23ccc-1	60	--	--
(C-35-11)24dba-1	60	--	--
(C-35-11)27bcc-1	60	--	--
(C-35-11)32acc-1	60	--	--
(C-35-11)33ccd-1	60	--	--
(C-35-11)7ddc-1	60	--	--
(C-36-12)11abc-1	60	--	--
(C-36-12)32dcc-1	60	--	--
(C-34-10)31aba-1	70	--	--

Cadastral Location (CAD)[1]	Approx. Pumping (acre-ft/yr)[2]	Owner	Well Name[3]
(C-34-12)36dcc-1	70	--	--
(C-35-11)21dca-1	70	--	--
(C-35-11)26cdb-1	70	--	--
(C-35-11)26dcb-1	70	--	--
(C-35-11)27acd-1	70	--	--
(C-35-11)30adc-1	70	--	--
(C-35-11)9acd-1	70	--	--
(C-36-12)13bbd-1	70	--	--
(C-34-12)36dad-1	80	--	--
(C-35-11)15acc-1	80	--	--
(C-35-11)21aac-1	80	--	--
(C-35-12)23ddd-1	80	--	--
(C-35-12)35dac-1	80	--	--
(C-36-11)7bcd-1	80	--	--
(C-36-12)24cdb-1	80	--	--
(C-37-12)6bda-1	80	--	--
(C-35-11)9ccc-2	80	Midvalley Estates	Existing 12' Well
(C-37-12)3abb-1	90	--	--
(C-35-11)10dcd-1	100	--	--
(C-35-11)10dcd-2	100	--	--
(C-35-11)32abc-1	100	--	--
(C-36-12)3dbb-1	100	--	--
(C-35-10)8ccc-1	110	--	--
(C-35-11)27cdd-1	110	--	--
(C-35-11)28abc-1	110	--	--
(C-35-11)34bad-1	110	--	--
(C-36-11)8abd-1	110	--	--
(C-34-10)30dcd-1	120	--	--
(C-35-11)1cba-1	120	--	--
(C-35-11)22bbb-1	120	--	--
(C-35-11)27bab-1	120	--	--
(C-35-11)35ccd-1	120	--	--
(C-35-11)13ddd-1	130	--	--
(C-33-10)31ada-1	140	--	--
(C-34-11)23caa-1	140	--	--
(C-35-11)22cdd-1	140	--	--
(C-35-11)32add-1	140	--	--
(C-36-11)18dcb-1	140	--	--
(C-36-12)14ada-1	140	--	--
(C-35-10)7acd-1	140	Enoch City	Ravine Well

Cadastral Location (CAD)[1]	Approx. Pumping (acre-ft/yr)[2]	Owner	Well Name[3]
(C-35-11)12cda-1	150	--	--
(C-35-11)21abd-1	150	--	--
(C-35-12)36dda-1	150	--	--
(C-35-11)31cdd-1	160	--	--
(C-36-11)5abc-1	160	--	--
(C-36-12)3aad-1	160	--	--
(C-36-12)9aac-1	160	--	--
(C-35-11)13dad-1	170	--	--
(C-35-10)7ccd-1	180	Enoch City	Woolsey Well
(C-34-12)36acd-1	190	--	--
(C-35-11)1ccc-1	190	--	--
(C-35-11)32dba-1	190	--	--
(C-36-11)18acc-1	190	--	--
(C-36-11)18bca-1	190	--	--
(C-36-11)18cbd-1	190	--	--
(C-36-11)18cdc-1	190	--	--
(C-35-10)7dcc-1	200	Enoch City	Anderson Well
(C-37-12)5bda-1	200	--	--
(C-36-12)32ccc-1	200	Cedar City	Quichapa Well #1 South
(C-35-11)9ccc-1	220	Midvalley Estates	Well (12')
(C-34-10)31cab-1	210	--	--
(C-36-12)3abb-1	210	--	--
(C-35-11)35cbb-1	240	Cedar City	Northfield Well
(C-35-12)27bcc-1	250	--	--
(C-36-11)9bcd-1	250	--	--
(C-36-12)20acc-1	250	--	--
(C-35-10)18acb-1	260	Enoch City	Homestead Well
(C-35-11)14aac-1	270	--	--
(C-35-11)29ccb-1	270	--	--
(C-35-11)31dbd-1	270	--	--
(C-37-12)23cbd-1	290	--	--
(C-35-11)29aac-1	320	--	--
(C-34-10)30ddd-1	340	--	--
(C-35-12)25bcd-1	360	--	--
(C-35-11)15aac-1	370	--	--
(C-35-11)22adc-1	370	--	--
(C-35-11)32bda-1	370	--	--
(C-37-12)9bca-1	370	--	--
(C-37-12)9dbd-1	370	--	--
(C-37-11)5dbc-1	380	--	--

Cadastral Location (CAD)[1]	Approx. Pumping (acre-ft/yr)[2]	Owner	Well Name[3]
(C-35-11)27bca-1	390	--	--
(C-35-11)29adc-1	400	--	--
(C-35-11)29bdc-1	400	--	--
(C-35-11)8abd-1	400	--	--
(C-35-11)31acd-1	430	--	--
(C-35-11)31bdb-1	430	--	--
(C-36-11)11bdb-1	440	Cedar City	Cemetery Well
(C-35-10)18cca-1	440	Cedar City	Enoch Well # 1 (Replacement Well)
(C-35-11)20dda-1	470	--	--
(C-35-11)29add-1	470	--	--
(C-35-11)33dbd-1	480	--	--
(C-35-11)6cab-1	510	--	--
(C-37-12)11aaa-1	540	--	--
(C-35-11)13ada-1	550	--	--
(C-35-11)16ccc-1	560	--	--
(C-35-12)36cad-1	560	--	--
(C-33-10)31adb-1	600	--	--
(C-33-10)31cab-1	600	--	--
(C-35-10)7abd-1	600	Enoch City	Iron Works Well
(C-37-12)11dac-1	640	--	--
(C-36-12)32ccb-1	670	Cedar City	Quichapa Well #3 North
(C-36-12)29abb-1	700	Cedar City	Quichapa #5
(C-35-11)16cbd-1	700	--	--
(C-35-11)22adb-1	800	--	--
(C-37-12)14bad-1	800	--	--
(C-34-11)36dcc-1	980	--	--
(C-36-12)17ddd-1	1060	Cedar City	Quichapa #6
(C-36-12)20add-1	1390	Cedar City	Quichapa Well #7

APPENDIX D

ROSENBERG r ASSOCIATES™
CIVIL ENGINEERS   LAND SURVEYORS

Survey Narrative:

This survey was conducted at the request of the Utah Geological Survey. (U.G.S.)

The purpose of this survey was to prepare an Elevation Certification of the monuments designated by the client for the purpose of subsidence monitoring in and around the Cedar City, Utah valley.

Correspondence with the client in the research and due diligence phase of this project revealed that several survey campaigns had been performed by the Utah Geological Survey prior to Rosenberg Associates involvement in this project. Later evaluation of these campaigns by the U.G.S., Local Cedar City, Utah Licensed Professional Land Surveyors and the Cedar City, Utah City Surveyor's Office revealed questionable methodology, project benchmarks and final findings.

The U.G.S requested Rosenberg Associates perform a certified survey campaign of designated benchmarks throughout the Cedar City, Utah valley. It was requested that the vertical basis of control for this campaign be a benchmark deemed geologically sound, and also that the Geographic coordinates of this campaign be relative to each other and share a common reference datum.

Rosenberg Associates met with Curt Neilson, the Cedar City, Utah Surveyor on October 18, 2011 to ascertain the history of available control in the valley, prior findings of historical surveys by his office and local surveyors, and his knowledge of the U.G.S.'s campaigns to date.

Various control options were considered prior to beginning field work, but after consulting with the client, Mr. Neilson and various other local Professional Land Surveyors, the methodology as described below was deemed to be the best available local option. Multiple survey sessions were conducted throughout the course of this project to verify the published quality of control used and to verify the stability of the project vertical benchmarks as described below.

Field work was conducted on September 24 through November 4, 2011.The resulting orthometric heights, ellipsoid heights, projection coordinates and geographic positions are included on sheets 3 through 5 herein.

The geographic control datum is the North American Datum of 1983 (National Spatial Reference System 2007).

Three National Geodetic Survey monuments were utilized with published P.I.D. designations: HO0468 (Federal Base Network Control Station - R 376), AI5820 (Cooperative Base Network Control Station - NORTH CEDAR CITY), and AI5822 (Cooperative Base Network Control Station - SOUTH CEDAR CITY). Resulting positions as included in this certification coincide with the current published values of these marks at the time the survey was conducted.

The initial meeting with Mr. Nelson revealed that the geographic positions of these three stations were established in a combined static G.P.S. survey campaign conducted by the National Geodetic Survey in conjunction with the Cedar City, Utah Surveyor's Office in 1999. Current published values for these stations were adjusted by the National Geodetic Survey in February 2007.

Stations AI5820 (Cooperative Base Network Control Station - NORTH CEDAR CITY), and AI5822 (Cooperative Base Network Control Station - SOUTH CEDAR CITY) are published as horizontal control stations and as such, N.A.V.D.88 orthometric heights are listed to the nearest foot. Upon ascertaining the origins of these stations geographic coordinates, the actual orthometric heights were calculated by subtracting the published 2009 geoid separation value from the current published ellipsoid height.

Multiple R.T.K./G.P.S. observations were made throughout this survey to verify published values and all were found to coincide with each other to a suitable degree as expected. After field verifying the calculated and published values for the three control stations listed above, these stations were determined to be the most desirable control option available and were utilized throughout the survey campaign as described.

ROSENBERG ⓡ **ASSOCIATES**™
CIVIL ENGINEERS   LAND SURVEYORS

Survey Narrative (Continued):

The orthometric elevation datum is the North American Vertical Datum of 1988 as measured at a 1928 United States Geological Survey brass cap with National Geodetic Survey P.I.D. designation: HO0210 (H 28) Elevation = 5798.08. HO0210 (H 28) was selected by the U.G.S. as the project benchmark for it's location, and preferred stability for future monitoring purposes. Multiple R.T.K. G.P.S. observations were made on this monument and it was found to coincide with the published N.A.V.D. 88 orthometric heights of stations HO0468, AI5820 and AI5822.
Survey was conducted on the above stated dates utilizing a Trimble 5800 G.P.S. Receiver. Orthometric Heights were propagated utilizing the National Geodetic Survey 2009 geoid model.
Projection System and Zone are U.S. State Plane 1983, Utah South 4303. As horizontal locations were the least significant factor of this survey no elevation factor was applied to reflect ground distances. Projection coordinates as included herein are at state plane grid.
At the request of the U.G.S., multiple Utah State Engineer benchmarks were located during this survey. Said benchmark monuments did not contain stamped dates and no information pertaining to their origins could be located. Stamped elevation information as described on the face of the monuments is included in Sheets 3-5 herein.

Surveyor's Certificate:

I, Brandon E. Anderson, St. George, Utah, do hereby certify that I am a Professional Land Surveyor as prescribed by the laws of the State of Utah and that I hold certificate of registration (license) number 4938716. I further certify that the survey described herein has been made by me or under my direct supervision and is a true and correct representation of conditions existing on the ground.

PROFESSIONAL LAND SURVEYOR
CERTIFICATE NO.
4938716
BRANDON E.
ANDERSON
STATE OF UTAH
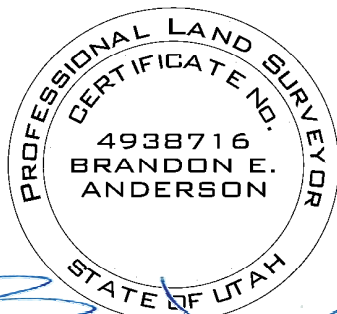
Brandon E. Anderson
License No. 4938716

January 17, 2012

Sheet 2 of 7

ROSENBERG **ASSOCIATES**™
CIVIL ENGINEERS   LAND SURVEYORS

Date: 11/4/2011
Project Name: U.G.S. Subsidence Survey
Project No.: 7183-11
Page: 3 of 7

No.	U.G.S. Designation	Northing U.S. State Plane 1983 Utah South 4303	Easting U.S. State Plane 1983 Utah South 4303	Elevation N.A.V.D. 88 GEOID 09	Latitude N.A.D. 1983 N.S.R.S. 2007	Longitude N.A.D. 1983 N.S.R.S. 2007	Elliptical Height	U.G.S. Designation/ Monument Description/Date Located	
1001	June 2011N Base	10236120.23	1193914.49	5693.7	37°44'15.24082"N	113°02'38.87945"W	5623.404	June 2011N Base 1999 NCDC/CBN AC (AI5820)	
1002	June 2011S Base	10204193.27	1177869.70	6171.5	37°38'56.96771"N	113°05'51.80580"W	6101.061	June 2011S Base 1999 NCDC/CBN AC (AI5822)	
1003	Mar 2010 S Base	10224802.04	1150640.54	5560.1	37°42'15.95355"N	113°11'34.96967"W	5487.971	Mar 2010 S Base 2" BC 110211	
1004	BLM1	10246133.02	1208386.20	5973.6	37°45'56.54513"N	112°59'40.73234"W	5903.989	BLM1 2002 BLMAC CC 16-17 35S 10W 110411	
1005	BLM2	10199141.64	1127519.76	5839.4	37°37'58.06501"N	113°16'16.57897"W	5766.697	BLM2 1990 BLM AC 25-26-35-36 26S 13W 102611	
1006	EC1	10251528.52	1201596.31	5670.9	37°46'48.80003"N	113°01'06.37349"W	5600.689	EC1 1998 ECBC 1/4 6-7 110311	
1007	EC2	10248890.94	1201544.42	5641.1	37°46'22.71841"N	113°01'06.48633"W	5570.895	EC2 1998 ECBC CE 1/16 35S 10W 110311	
1008	EC3							EC3 DESTROYED	
1009	EC4	10243296.56	1197477.67	5536.1	37°45'26.76050"N	113°01'55.99013"W	5465.853	EC4 1998 ECBC 1/4 13 35S 11W 110311	
1010	EC5	10243336.21	1194796.69	5506.6	37°45'26.71690"N	113°02'29.37889"W	5436.205	EC5 1998 ECBC CEN 13 35S 11W 110311	
1011	EC6	10240722.9	1192096.01	5538.5	37°45'00.44218"N	113°03'02.46518"W	5468	EC6 1998 ECBC RM 42.63 13-14-23-24 110311	
1012	EC7	10251297.54	1194934.29	5473.7	37°46'45.43913"N	113°02'29.29973"W	5403.106	EC7 2007 ECBC 1/4 1-12 35S 11W 110311	
1016	IC2	10256907.76	1197731.42	5459.1	37°47'41.35201"N	113°01'55.60751"W	5388.544	IC2 2000 ICBC 1-6-31-36 10-11W 34-35S 110411	
1017	IC3	10251555.55	1200266.58	5526.5	37°46'48.85339"N	113°01'22.94053"W	5456.176	IC3 1984 ICBC 1/4 6-7 110411	
1018	IC4	10246234.87	1202820.94	5724.7	37°45'56.66699"N	113°00'50.05357"W	5654.725	IC4 1984 ICBC 7-8-17-18 110311	
1019	IC5	10246320.11	1197528.00	5526.7	37°45'56.65732"N	113°01'55.98034"W	5456.34	IC5 1984 ICBC 1/4 7-18 110311	
1020	IC6	10248962.39	1197576.58	5495.1	37°46'22.78492"N	113°01'55.91456"W	5424.694	IC6 1984 ICBC 1/4 7 110311	
1021	IC7	10251240.11	1197621.05	5473.4	37°46'45.30800"N	113°01'55.82556"W	5402.92	IC7 1984 ICBC 1-12 110411	
1022	IC8	10251608.47	1197628.84	5470.9	37°46'48.95056"N	113°01'55.80365"W	5400.384	IC8 1984 ICBC 6-7 110411	
1023	IC9	10245988.21	1194836.74	5494.7	37°45'52.93916"N	113°02'29.42462"W	5424.239	IC9 2007 ICBC 1/4 12-13 35S 11W 110311	
1024	IC10	10267669.22	1192601.19	5432.8	37°49'26.89525"N	113°03'01.73843"W	5361.761	IC10 2002 ICBC 23-24-25-26 110311	
1025	IC13	10240831.87	1186704.97	5522.8	37°45'00.63022"N	113°04'09.60440"W	5451.975	IC13 ICBC 14-15-22-23 110211	
1026	IC14	10257132.32	1187118.08	5455.8	37°47'41.83214"N	113°04'07.86617"W	5384.674	IC14 BC LS4100 2-3-34-35 110311	
1027	IC17	10257493.3	1171162.11	5463.6	37°47'42.70754"N	113°07'26.70806"W	5391.933	IC17 1988 ICBC 5-6-31-32 35-36S 11W 110211	
1028	IC18	10209756.43	1148896.55	5473.4	37°39'46.91333"N	113°11'53.26829"W	5401.223	IC18 1983 ICBC 15-16-21-22 102511	
1030	IC20							IC20 DESTROYED	
1031	IC21	10214826.2	1159680.96	5495.9	37°40'38.94378"N	113°09'40.28600"W	5424.116	IC21 1999 ICAC 50OS RM 11-12-13-14 102511	
1032	IC22							IC22 DESTROYED	
1033	IC25	10219928.73	1180920.76	5648.6	37°41'33.03164"N	113°05'17.19563"W	5577.958	IC25 1981 ICBC 3-4-9-10 110111	

ROSENBERG r ASSOCIATES™
CIVIL ENGINEERS   LAND SURVEYORS

Date: 11/4/2011
Project Name: U.G.S. Subsidence Survey
Project No.:   7183-11
Page: 4 of 7

No.	U.G.S. Designation	Northing U.S. State Plane 1983 Utah South 4303	Easting U.S. State Plane 1983 Utah South 4303	Elevation N.A.V.D. 88 GEOID 09	Latitude N.A.D. 1983 N.S.R.S. 2007	Longitude N.A.D. 1983 N.S.R.S. 2007	Elliptical Height	U.G.S. Designation/ Monument Description	
1034	IC26	10241163.1	1170832.84	5508.6	37°45'01.22516"N	113°07'27.27621"W	5437.106	IC26 2007 ICBC 35S 11W 110211	
1035	IC27	10278489.92	1187510.78	5398.3	37°51'13.01980"N	113°04'07.43777"W	5327.042	IC27 1989 ICBC 10-11-13-14 34S 11W 110311	
1036	IC28	10267805.27	1187293.35	5426.1	37°49'27.36489"N	113°04'07.91352"W	5354.867	IC28 1983 ICBC 22-23-26-27 110311	
1037	IC30	10246137.4	1208130.69	5973.1	37°45'56.54805"N	112°59'43.91500"W	5903.424	IC30 2000 ICBC 8-9 35S 10W 110411	
1038	IC31	10190118.1	1153880.59	5471.8	37°36'33.67465"N	113°10'46.90615"W	5400.141	IC31 1999 ICAC 1/4 2-3 37S 12W 102511	
1039	IC32	10193702.95	1153995.87	5470.3	37°37'09.13217"N	113°10'46.27372"W	5398.57	IC32 1999 ICAC 2-3-34-35 36S \12W 102511	
1040	IC33	10198999.29	1154076.23	5473.8	37°38'01.50197"N	113°10'46.45740"W	5402.01	IC33 2002 BBE AC 26-27-34-35 36S 12W 102511	
1041	IC34	10193536.12	1164637.21	5605.6	37°37'09.35177"N	113°08'33.99162"W	5534.463	IC34 ICBC 1-6-31-36 36-37S 11-12W 102511	
1042	IC35	10230747.04	1159904.95	5498.8	37°43'16.36311"N	113°09'41.01841"W	5426.951	IC35 1997 ICBC 25-26-35-36 35S 12W 110111	
1043	IC36	10214848.13	1164932.54	5515.0	37°40'40.07784"N	113°08'34.97529"W	5443.461	IC36 1983 ICBC 7-12-13-19 102511	
1045	LS6	10257085.6	1192421.79	5454.0	37°47'42.24480"N	113°03'01.78715"W	5383.135	LS6 BRADSHAW RLS R&C 110311	
1046	LS8	10262343.81	1192546.35	5444.1	37°48'34.24363"N	113°03'01.32153"W	5373.147	LS8 BBE AC 110311	
1047	LS14	10251303	1192289.35	5472.8	37°46'45.06084"N	113°03'02.24240"W	5402.012	LS14 LOOSE WOOD HUB 110211	
1048	LS15	10268010.2	1176735.32	5431.0	37°49'27.61919"N	113°06'19.53131"W	5359.438	LS151993 BBEAC 20-21-28-29 110311	
1049	LS17							LS17 DESTROYED	
1052	NGS3	10251425.24	1190918.82	5471.3	37°46'46.04416"N	113°03'19.33709"W	5400.449	NGS3 1984 NGS VCM HO0468	
1058	SE1	10200111.95	1141002.71	5505.7	37°38'10.14821"N	113°13'29.21340"W	5433.359	SE1 UGS/GHP R&C 102611	
1059	SE2	10197786.79	1150693.28	5471.3	37°37'48.91343"N	113°11'28.23434"W	5399.325	SE2 UGS/GHP R&C 102511	
1060	USE1	10240881.97	1197500.06	5593.2	37°45'02.89513"N	113°01'55.21873"W	5523.049	USE1 USEBM E-5589.228 110311	
1061	USE2	10251726.75	1176323.23	5478.7	37°46'46.58577"N	113°06'21.18172"W	5407.252	USE2 USEBM E-5475.371 110211	
1062	USE3	10251825.23	1170957.82	5476.3	37°46'46.64312"N	113°07'28.02633"W	5404.725	USE3 USEBM E-5472.694 110211	
1063	USE4	10257358.72	1176493.55	5460.4	37°47'42.28742"N	113°06'20.26504"W	5388.949	USE4 USEBM E-5456.960 110211	
1064	USE5	10257146.19	1187148.02	5456.0	37°47'41.97424"N	113°04'07.49607"W	5384.863	USE5 DIST USEBM E-5452.561 110311	
1065	USE6	10230529.78	1170580.92	5539.3	37°43'16.06975"N	113°07'28.11268"W	5467.896	USE6 USEBM E-5536.041 110111	

ROSENBERG **r** ASSOCIATES™
CIVIL ENGINEERS LAND SURVEYORS

Date: 11/4/2011
Project Name: U.G.S. Subsidence Survey
Project No.: 7183-11
Page: 5 of 7

No.	U.G.S. Designation	Northing U.S. State Plane 1983 Utah South 4303	Easting U.S. State Plane 1983 Utah South 4303	Elevation N.A.V.D. 88 GEOID 09	Latitude N.A.D. 1983 N.S.R.S. 2007	Longitude N.A.D. 1983 N.S.R.S. 2007	Elliptical Height	U.G.S. Designation/ Monument Description	
1066	USE7	10251152.64	1197619.75	5474.1	37°46'44.44311"N	113°01'55.82384"W	5403.665	USE7 USEBM E-5471.308 110411	
1067	USE8	10262226.25	1197803.20	5485.9	37°48'33.93808"N	113°01'55.79890"W	5415.229	USE8 USEBM E-5482.922 110411	
1068	USGS1	10220376.7	1155779.32	5489.1	37°41'33.12338"N	113°10'30.04815"W	5417.181	USGS1 USGS BC E-5495 102611	
1069	USGS2	10207674.85	1173545.73	6114.9	37°39'30.65048"N	113°06'46.31064"W	6044.06	USGS2 1948 USGSBC CEDAR 110111	
1070	USGS3	10250988.79	1210326.14	5812.3	37°46'44.85196"N	112°59'17.53782"W	5742.647	USGS3 1931 USGSBM H63 E-5809 110411	
1071	USGS4	10196661.65	1173449.96	5798.08	37°37'41.76511"N	113°06'45.13994"W	5727.509	USGS4 1928 USGS BC H28 E-5794 (HO0210)	
1072	USGS5	10183350.39	1158966.44	5556.1	37°35'27.67231"N	113°09'42.21564"W	5484.806	USGS5 1928 USGSBC H1 E-5553 102511	
1073	USGLO1	10220433.68	1149070.00	5474.0	37°41'32.49034"N	113°11'53.52280"W	5401.865	USGLO1 1925 GLOBC 3-4-9-10 36S 12W 102611	
1074	USGLO2	10215207.81	1138375.95	5696.5	37°40'38.89169"N	113°14'05.34593"W	5624.088	USGLO2 1925 USGLOBC 7-8-17-18 36S 12W 102611	
1075	USGLO3	10209927.28	1138271.66	5566.0	37°39'46.67423"N	113°14'05.42451"W	5493.508	USGLO3 1925 USGLO3 1925 GLOBC 17-18-19-20 36S 12W 10261	
1076	USGLO4	10215106.88	1143679.71	5507.5	37°40'38.86149"N	113°12'59.35944"W	5435.145	USGLO4 1925 GLOBC 8-9-16-17 36S 12W 102611	
1077	USGLO5	10215086.3	1148960.86	5468.4	37°40'39.61131"N	113°11'53.67230"W	5396.237	USGLO5 2" BC NO MARK 102611	
1078	USGLO6	10262946.75	1160655.44	5672.0	37°48'34.79083"N	113°09'38.79594"W	5600.12	USGLO6 1909 GLOBC 25-26-35-36 34S 12W 110211	
1079	USGLO7	10225675.93	1149070.71	5559.2	37°42'24.31051"N	113°11'54.69843"W	5487.082	USGLO7 1925 GLOBC CC 3-4 36S 12W 102611	
1080	USGLO8	10225678.66	1149167.56	5571.3	37°42'24.35494"N	113°11'53.49412"W	5499.203	USGLO8 1925 USGLOBC 33-34 35S 12W 102611	
1081	USGLO9	10220383.83	1143808.93	5852.3	37°41'31.04799"N	113°12'58.95704"W	5779.96	USGLO9 1925 USGLOBC 4-5-8-9 36S 12W 110111	
1082	USGLO10	10194048.35	1132731.35	5645.1	37°37'08.68837"N	113°15'10.61437"W	5572.531	USGLO10 1936 GLOBC 6-31 36S 12-13W 102611	
1083		10254084.76	1199527.32	5461.8	37°47'13.73620"N	113°01'32.66179"W	5391.41	NEW HORIZON R&C LS 954372 110411	
1084		10262224.14	1197816.05	5485.5	37°48'33.91929"N	113°01'55.63835"W	5414.854	BBE AC 25-30-31-36 110411	

EXHIBIT "A"
FOR
U.G.S. SUBSIDENCE SURVEY

APPENDIX E

**INSAR ANALYSIS OF GROUND DEFORMATION
IN CEDAR VALLEY, IRON COUNTY, UTAH**

on CD: Appendix E_ MP-13-5

APPENDIX F

InSAR BACKGROUND AND APPLICATION

by Steve D. Bowman

INTRODUCTION

Radar interferometry is a process of using phase differences between two or more correlated radar images over the same area to measure surface displacements or topography. Interferometric synthetic aperture radar (InSAR) may now be applied worldwide, due to the availability of high-quality interferometric datasets from various spaceborne (ERS-1, ERS-2, JERS-1, ALOS, Radarsat-1, Radarsat-2, ENVISAT, SRTM, SIR-C, TerraSAR-X, TanDEM-X, and COSMO-SKYMED) and airborne platforms. Only Radarsat-2, TerraSAR-X, TanDEM-X, and COSMO-SKYMED satellites are still operational; ERS-1, ERS-2, ENVISAT, Radarsat-1, ALOS, and JERS-1 have failed.

The United States does not have operating synthetic aperture radar (SAR) satellites and relies on research and academic data access agreements with the European Space Agency (ESA) for their legacy ERS-1, ERS-2, and ENVISAT satellite data and the Canadian Space Agency (CSA) for their legacy Radarsat-1 satellite data. Commercial users must purchase all SAR data. However, the United States (National Aeronautics and Space Administration [NASA]) operated the Shuttle Radar Topographic Mission (SRTM) during 11 days in February 2000, and the Shuttle Imaging Radar (SIR-C) mission during 11 days in April 1994, and again in September-October 1994, that flew aboard the Space Shuttle (Jet Propulsion Laboratory, 2010a, 2010b), along with several other radar satellite platforms that are no longer operational. NASA is investigating developing the DESDynl radar satellite, but it has not been funded and approved by Congress.

The ESA has a long history of SAR satellites, beginning with the launch of ERS-1 in July 1991, followed by a second edition of the satellite, the ERS-2, in April 1995 (ESA, 2008). During 1995 to 1996, the ERS-1 and ERS-2 satellite tandem mission was developed where the satellite space orbits were adjusted to support InSAR between ERS-1/2 image pairs. The ERS-1 and ERS-2 satellites failed in March 2000 (ESA, 2008) and September 2011 (ESA, 2012), respectively. ESA launched the next-generation radar satellite ENVISAT (which also included other sensors) in March 2002 (ESA, 2010), that failed on April 8, 2012 (ESA, 2012).

Japan, through their Japan Aerospace Exploration Agency (JAXA), developed the JERS-1 satellite that was launched on February 11, 1992, and ended operation on October 12, 1998 (JAXA, 2010a). JAXA launched the next-generation radar satellite ALOS on January 24, 2006, and ended operation in May 2011 (JAXA, 2010b). JAXA is planning to launch ALOS-2, the successor to ALOS, in late 2013 (JAXA, undated). Canada, through the CSA and a partnership with a private company, developed the Radarsat-1 and Radarsat-2 satellites with launches in November 1995 and December 2007, respectively (CSA, 2010). Radarsat-1 failed on March 29, 2013 (CSA, 2013). Germany, through the German Aerospace Center (DLR) and a partnership with a private company, developed the TerraSAR-X satellite that was launched on June 15, 2007 (DLR, 2009), and a tandem, almost identical satellite, TanDEM-X that was launched on June 21, 2010 (DLR, 2010).

InSAR BACKGROUND AND PROCESSING TECHNIQUES

First developed by Richman (1971) and Graham (1974) with very limited datasets, InSAR for mapping surface displacements and topography was later investigated by Zebker and Goldstein (1986), Gabriel and others (1989), Goldstein and others (1993), and many others who contributed new processing techniques. The mapping of coseismic displacements resulting from the 1992 Landers earthquake (Zebker and others, 1994) was one of the early applications of InSAR. Later applications included glacier monitoring, volcano deformation monitoring, landslide detection, subsidence monitoring, and other applications. Hanssen (2001) used InSAR to map the displacement field of the Cerro Prieto geothermal field in Mexico, and documented about 8 cm/year (3.1 inches/year) of subsidence resulting from the extraction of water and steam for geothermal power production. Rosen and others (2000) gave an in-depth review and discussion of InSAR concepts, theory, and applications.

Use of InSAR requires an interferometric dataset, a suitable temporal and spatial baseline, and images that correlate together (matching similar locations in each image). InSAR may be applied in one of two methods: differential or topographic interferometry. Differential InSAR measures small-
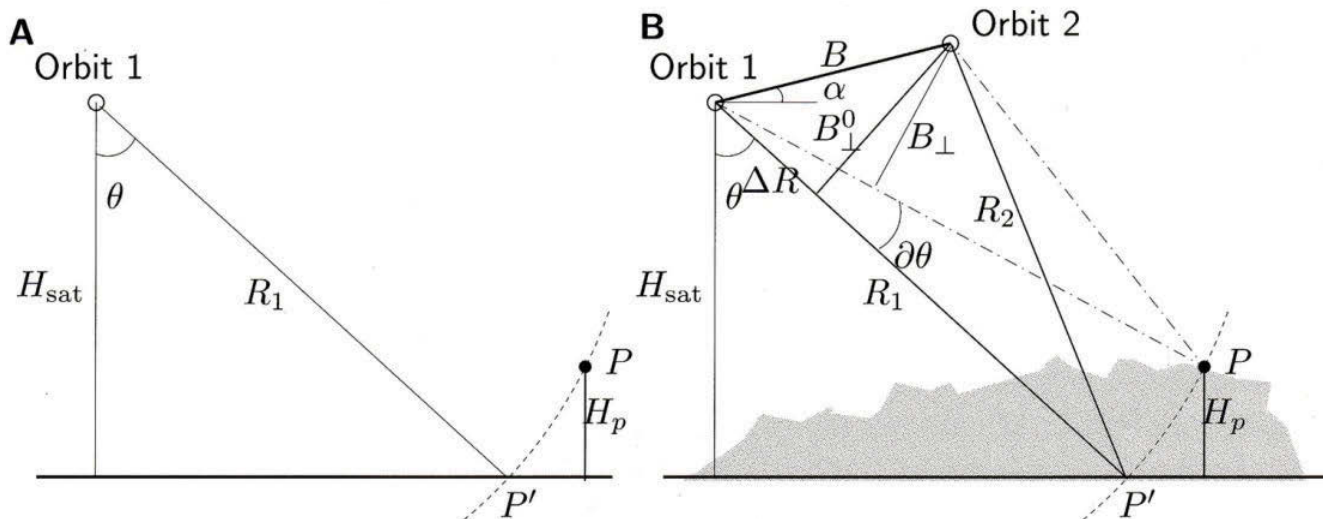
Figure F1. *Satellite geometry for single-pass (A) and interferometric (B) radar acquisition. Using two different satellite space positions allows for the height difference, H_p to be determined (modified from Hanssen, 2001).*

scale ground displacements due to subsidence, earthquakes, glacier movements, landslides, and other ground movement with the effects of topography removed. Topographic InSAR measures ground topography with no ground displacement, resulting in a digital elevation model (DEM). A DEM can be thought of as a three-dimensional topographic map. Differential InSAR can measure displacements to sub-centimeter accuracy and topographic InSAR can measure topography to 10s of meters, depending on sensor and platform characteristics. As shown on figure F1, two satellite image acquisitions with slightly different satellite locations (defined as Orbit 1 and Orbit 2 locations) are needed for InSAR.

Radar interferometry works by measuring the phase differences of two complex-format radar images or images that retain phase information (real and imaginary electrical components of the reflected radar signal). Standard radar images do not retain phase information and cannot be used in InSAR processing and analysis. The interferometric phase, ϕ is defined as:

$$\phi = \varphi_1 - \varphi_2 = \frac{4\pi}{\lambda}\left(\rho_2 - \rho_1\right)$$

where ϕ_1 = phase of Image #1, ϕ_2 = phase of Image #2, λ = radar wavelength, ρ_1 = range of Image #1, and ρ_2 = range of Image #2 (Rosen and others, 2000). Figure F2 shows the imaging geometry of a radar satellite during data acquisition, including the range direction.

The two complex-format radar images typically have short temporal and spatial baselines—the time between the two image acquisitions and the distance between the imaging locations (satellite three-dimensional position) of the two images, respectively. The two images must also cover nearly the same area on the ground surface. The critical baseline, B_c or maximum baseline distance that can be processed, is defined as:

$$B_c = \frac{\lambda r}{2 * R\cos\theta}$$

where λ = radar wavelength, r = radar path length, R = ground range resolution, and θ = local incidence angle (Hanssen, 2001). Table F1 shows the common spaceborne radar platforms and operating radar bands. For C-band systems, $B_c \sim$ 1100 m; L-band systems, $B_c \sim$ 4500 m; and X-band systems, $B_c \sim$ 100 m. The actual usable baseline for ERS-1/2 and Radarsat-1/2 (C-band platforms) is typically 500–600 m or less. Two radar images that generally match the above characteristics can form an interferometric pair.
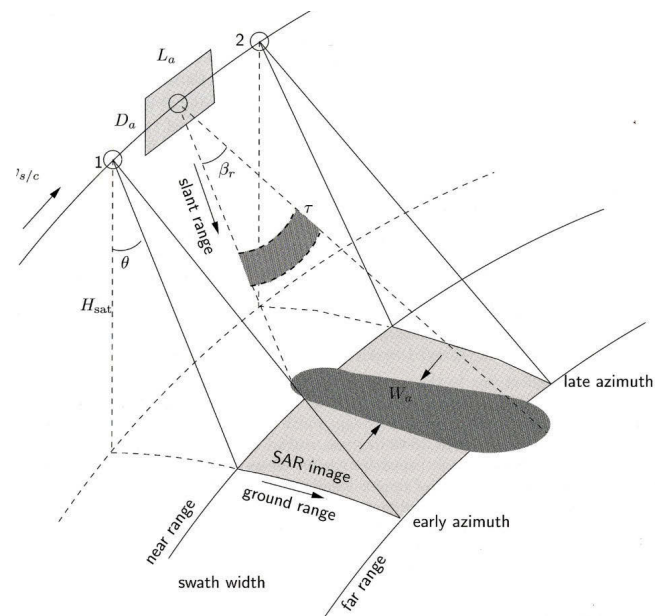

Figure F2. *Imaging geometry of a radar satellite. As the satellite moves in a forward direction (to the upper right in the figure), the satellite images the light gray swath on the ground surface. The dark gray area on the ground surface indicates the area covered by a single radar pulse (modified from Hanssen, 2001).*

Table F1. *Radar bands, wavelengths, and satellite platforms (modified from Avery and Berlin, 1992).*

Radar Band	Wavelength Range (cm)	Satellite Platforms
X	2.4–3.8	X-SAR (SIR-C), SRTM, TerraSAR-X, TanDEM-X
C	3.8–7.5	ERS-1, ERS-2, SIR-C, Radarsat-1, Radarsat-2, ENVISAT
L	15–30	JERS-1, ALOS, ALOS-2, SIR-C

InSAR data processing generally begins with raw sensor data, or single-look complex (SLC) data, and involves raw data processing and co-registering two or more images. The second image (and others if used) must be precisely aligned with the first image with sub-pixel accuracy; otherwise, additional error is introduced into the process and later processing steps will fail. After co-registration, the complex phase information of the first image is multiplied by the conjugate (inverse) phase of the second image to generate an interferogram or interference image.

The interferogram contains topographic and ground displacement information with each cycle of phase (or phase change of 0 to 2π radians) representing a specific quantity of change. At this point in the processing chain, the interferogram is in radar coordinates, which later must be registered to ground coordinates (such as latitude/longitude, Universal Transverse Mercator [UTM], or other coordinate system).

One of the most difficult steps in InSAR processing is the phase unwrapping process. This process utilizes the phase information from the interferogram to determine the magnitude of surface displacements or topography (depending on the analysis method) present in the image. Phase unwrapping may use branch-cut, least squares, and error minimization criteria methods (Rosen and others, 2000). Branch-cut methods utilize phase differences and integrating that difference. The phase-unwrapped solution should be independent of the path of integration (Madsen and Zebker, 1998); however, this may not always be the case. Phase residues may result from this process, across which phase unwrapping is not possible. If an area is enclosed by these errors, the area will not be unwrapped, and no information will be obtained. Many of the branch-cut algorithms are automated and do not require user intervention during processing. An existing DEM, which must cover all of the ground area covered in the radar image, is often used to generate seed points to help in automatic guiding of the phase unwrapping process. Least squares phase unwrapping follows the general procedures of the branch-cut methods, but with least-squares estimation. Figure F3 shows a final, unwrapped, geocoded interferogram from Envisat data of the Cedar Valley and surrounding region. Specific color fringes in the Beryl-Enterprise area, Quichipa Lake, and Enoch graben show vertical displacement directly related to ground subsidence. The variable colors in the rest of the image are the result of incomplete removal of topography and/or atmospheric noise in the data.

After phase unwrapping of the interferogram and depending on the analysis method used, a displacement map may be generated if the effects of topography are removed using an existing DEM, or a DEM may be created if the interferogram contains little to no surface displacements.

ISSUES WITH InSAR PROCESSING

Problems associated with InSAR are chiefly (1) shadowing present in the original radar data from topographic relief (particularly when applied to mapping mountainous areas where steep mountains block the inclined radar signal), and (2) decorrelation caused by changes in the imaged area. These changes may be due to freezing, thawing, precipitation, vegetation, wind, motion of water, and man-made changes, such as changes in land-use. Agricultural fields are constantly changing due to vegetation (crop) changes in height and size, and from tilling of fields that may cause significant decorrelation. Vegetated areas may also exhibit decorrelation, due to wind moving vegetation, such as in forests.

Increased time between two radar image acquisitions will result in increased temporal decorrelation and is directly related to ground surface parameters. Zebker and Villasenor (1992) found that increasing the time between acquisitions decreased correlation significantly for lava flows and forests in Oregon; however, the Death Valley, California, valley floor did not experience this correlation decrease. Some geographic areas typically have low temporal decorrelation, including many desert and low-vegetation-density areas; high-temporal-decorrelation areas include many moderately to highly vegetated and/or forested areas, active agricultural lands, and other areas subject to surface disturbance. A relatively new technique utilizing point scatterers may be used to match common points between radar images, such as the centers of pivoting agricultural sprinklers, reflective metallic objects that may act as near-corner reflectors, or other stationary reflective objects.
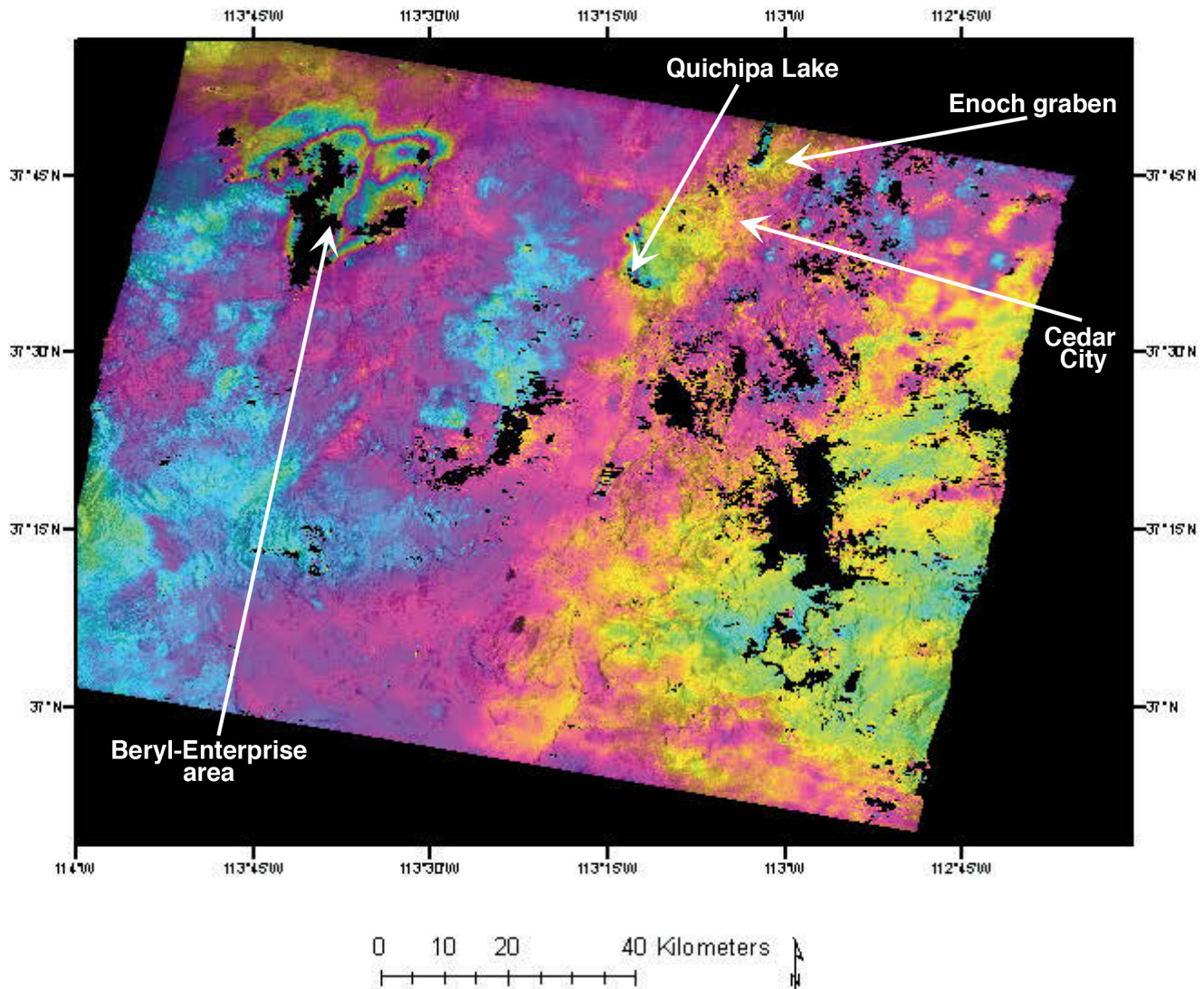
Figure F3. *Unwrapped interferogram of an entire Envisat frame, processed by the UGS, covering the time period of August 11, 2009, to August 31, 2010, showing significant subsidence near Quichapa Lake, Enoch graben, and the Beryl-Enterprise area resulting from groundwater withdrawal. Each specific color cycle represents 3 cm of deformation; the variable colors in the rest of the image are the result of incomplete removal of topography and/or atmospheric noise in the data. Area outside the Envisat frame shown in black on the edges; black areas within interferogram denote areas of no data from shadowing or from no correlation between the two images used to create the interferogram. Envisat data ©2009, 2010 European Space Agency.*

SAR DATA AVAILABILITY AND PROCESSING

SAR data suitable for use in differential interferometric processing is available for the many areas in Utah from ESA satellites (ERS-1, ERS-2, and ENVISAT). Commercial purchases of ERS-1, ERS-2, and ENVISAT data in the existing ESA data archive cost approximately $560 per scene.

Due to the large amount of data generated by a radar system, available satellite on-board data storage, and high power (electrical) use of a radar system, radar data is not continuously acquired as in other imaging satellites, such as the Landsat series (1-7). Rather, specific, pre-determined areas of the Earth surface are imaged on each path of the satellite within the power and data storage capabilities of the satellite. These pre-determined areas are based on requirements of the satellite program, scientific investigator requests, and commercial purchases. In many cases, radar data are downlinked to ground stations within radio receiving range (ground station mask), so additional data may be acquired beyond the limits of on-board data storage, or are transmitted to a satellite communications network that in turn transmits to ground stations. This pre-planning and equipment adds additional cost to new data acquisitions, which is reflected in the higher cost of new acquisitions to the end-user.

REFERENCES

Alaska Satellite Facility, undated, ASF station mask: Online, http://www.asf.alaska.edu/sites/all/files/images/ASF_mask_horizon.jpg, accessed September 3, 2013.

Avery, T.E., and Berlin, G.L., 1992, Fundamentals of remote sensing and airphoto interpretation, fifth edition: New York, Macmillan Publishing Company, 472 p.

Canadian Space Agency, 2010, Satellites—earth-observation satellites: Online, http://www.asc-csa.gc.ca/eng/satellites/, accessed October 18, 2010.

Canadian Space Agency, 2013, RADARSAT—seventeen years of technological success: Online, http://www.asc-csa.gc.ca/eng/media/news_releases/2013/0509.asp, accessed September 3, 2013.

European Space Agency, 2008, ERS overview: Online, http://www.esa.int/esaEO/SEMGWH2VQUD_index_0_m.html, accessed October 18, 2010.

European Space Agency, 2010, ENVISAT history: Online, http://earth.esa.int/category/index.cfm?fcategoryid=87, accessed October 18, 2010.

European Space Agency, 2012, ESA declares end of mission for Envisat: Online, https://earth.esa.int/web/guest/news/-/asset_publisher/G2mU/content/good-bye-envisat-and-thank-you, accessed September 3, 2013.

European Space Agency, 2012, ERS satellite missions complete after 20 years: Online, https://earth.esa.int/web/guest/missions/esa-operational-eo-missions/ers/news/-/asset_publisher/T7aX/content/ers-satellite-missions-complete-after-20-years-7895?p_r_p_564233524_assetIdentifier=ers-satellite-missions-complete-after-20-years-7895&redirect=%2Fc%2Fportal%2Flayout%3Fp_l_id%3D66101, accessed March 15, 2012.

Gabriel, A.K., Goldstein, R.M., and Zebker, H.A., 1989, Mapping small elevation changes over large areas—Differential radar interferometry: Journal of Geophysical Research, v. 94, p. 9183–9191.

German Aerospace Center, 2009, TerraSAR-X—Germany's radar eye in space: Online, http://www.dlr.de/eo/en/desktopdefault.aspx/tabid-5725/9296_read-15979/, accessed March 15, 2012.

German Aerospace Center, 2010, TanDEM-X—a new high resolution interferometric SAR mission: Online, http://www.dlr.de/hr/desktopdefault.aspx/tabid-2317/3669_read-5488/, accessed September 3, 2013.

Goldstein, R., Englehardt, H., Kamb, B., and Frohlich, R.M., 1993, Satellite radar interferometry for monitoring ice sheet motion—Application to an Antarctic ice stream: Science, v. 262, p. 525–1530.

Graham, L.C., 1974, Synthetic interferometer radar for topographic mapping: Institute of Electrical and Electronics Engineers, Proceedings of the IEEE, v. 62, no. 6, p. 763–768.

Hanssen, R.F., 2001, Radar interferometry—Data interpretation and error analysis: Dordrecht, The Netherlands, Kluwer Academic Publishers, 308 p.

Japan Aerospace Exploration Agency, 2010a, Japanese earth resources satellite "FUYO-1" (JERS-1): Online, http://www.jaxa.jp/projects/sat/jers1/index_e.html, accessed October 18, 2010.

Japan Aerospace Exploration Agency, 2010b, Advanced land observing satellite "DAICHI": Online, http://www.alos-restec.jp/aboutalos_e.html, accessed October 25, 2010.

Japan Aerospace Exploration Agency, undated, ALOS-2-the advanced land observing satellite-2 "DAICHI-2": Online, http://www.jaxa.jp/pr/brochure/pdf/04/sat29.pdf, accessed September 3, 2013.

Jet Propulsion Laboratory, 2010a, Shuttle Radar Topography Mission, The mission to map the world: Online, http://www2.jpl.nasa.gov/srtm/, accessed October 18, 2010.

Jet Propulsion Laboratory, 2010b, SIR-C/X-SAR flight 1 statistics: Online, http://southport.jpl.nasa.gov/sir-c/html/mission.html, accessed October 18, 2010.

Madsen, S.N., and Zebker, H.A., 1998, Imaging radar interferometry, in Henderson, F.M., and Lewis, A.J., editors, Principals & applications of imaging radar, third edition, volume 2: New York, John Wiley & Sons, p. 359–380.

Richman, D., 1971, Three dimensional azimuth-correcting mapping radar: United Technologies Corporation, variously paginated.

Rosen, P.A., Hensley, S., Joughin, I.R., Li, F., Madsen, S.N., Rodriquez, E., and Goldstein, R.M., 2000, Synthetic aperture radar interferometry: Institute of Electrical and Electronics Engineers, Proceedings of the IEEE, v. 88, n. 3.

Zebker, H.A., and Goldstein, R.M., 1986, Topographic mapping from interferometric synthetic aperture radar observations: Journal of Geophysical Research, v. 91, p. 4993–4999.

Zebker, H.A., Rosen, P.A., Goldstein, R.M., Gabriel, A., and Werner, C.L., 1994, On the derivation of coseismic displacement fields using differential radar interferometry—The Landers earthquake: Journal of Geophysical Research, v. 99, no. B10, p. 19,617–19,634.

Zebker, H.A., and Villasenor, J., 1992, Decorrelation in interferometric radar echoes: IEEE Transactions on Geoscience and Remote Sensing, v. 30, no. 5, p 950–959.

APPENDIX G

LiDAR BACKGROUND AND APPLICATION

by Steve D. Bowman

INTRODUCTION

Light detection and ranging (LiDAR) technology uses transmitted and reflected laser pulses to measure the distance to an object. LiDAR transmitted from an airborne platform (fixed-wing aircraft or helicopter) is commonly used to determine ground surface elevations to create highly accurate, bare-earth digital elevation models (DEM). A LiDAR instrument can send many thousands of laser pulses at a rapid rate, which allows a high point spacing density, much greater than is possible using traditional surveying methods. Landslides, fault scarps, earth fissures, and other features that are difficult to detect visually because of vegetation, access, or other issues, may often be clearly shown in LiDAR data.

Unlike radar interferometry (InSAR), most LiDAR data are acquired by private aerial imaging and mapping firms. In 1996, only one vendor was selling commercial LiDAR systems (Baltsavias, 1999); today there are numerous commercial vendors producing LiDAR scanning systems including Leica Geosystems, Toposys (now Trimble), Optech, and Riegl. Most of these systems are small and light enough to be installed and operated in small, single-engine aircraft.

LiDAR BACKGROUND AND PROCESSING TECHNIQUES

First developed in the 1960s with early laser components (Miller, 1965; Shepherd, 1965), LiDAR has evolved from simple electronic distance measurement systems used in surveying (Shan and Toth, 2009) into a sophisticated surface mapping technique on multiple platforms. LiDAR may be applied using one of two general methods: profiling or scanning. Profiling involves acquiring elevation data along a single flight path of the platform. Scanning involves acquiring elevation data along a swath parallel to the flight path of the platform, or in the case of terrestrial scanners, along a path parallel to the angular rotation path of the stationary scanner. In addition, the reflected light backscatter, intensity, and other parameters can be measured for additional applications. LiDAR can measure the ground surface with accuracies of a few inches horizontally and a few tenths of inches vertically (Carter and others, 2001) and can penetrate thick vegetation canopies as shown

on figure G1 from the Snowbasin, Utah, area.

LiDAR may be acquired from three different platforms: (1) spaceborne, (2) airborne, and (3) terrestrial. The most common acquisition platform is airborne, with the LiDAR unit mounted in the floor of an airplane or helicopter (figure G2). As terrestrial systems are not applicable to investigating land subsidence and earth fissures they will not be discussed further here.

Due to the long path length of emitted and reflected laser light, spaceborne LiDAR systems require high-power lasers with high electrical input requirements. Consequently, few spaceborne LiDAR systems are in use, with the exception of profiling systems, which typically are employed for atmospheric and/or ocean monitoring and research, such as the NASA IC-ESat satellite (NASA, 2010).

LiDAR systems typically use either a neodymium-doped yttrium aluminum garnet (Nd:YAG) or gallium arsenide (GaAs) laser (Shan and Toth, 2009) driven by a power source and sophisticated electronics, and are coupled with a GPS or more recently, a Global Navigation Satellite System (GNSS) inertial measurement unit (IMU) to determine precise three-dimensional position information. The position information is used during processing raw sensor data to point cloud and to bare-earth data to correct for aircraft flight path drift (yaw, pitch, and roll) and other irregularities.

While scanning systems generally comprise a laser aimed at a rotating mirror, various manufacturers use different methods, including standard rotating mirrors (Optech and Leica Geosystems ALS scanners); rotating optical polygon scanners (Reigl scanners); Palmer scanning with a wobbling mirror (NASA Airborne Topographic Mapper [ATM] and Airborne Oceanographic LiDAR [AOL] scanners [figure G3]); and tilted, rotating mirrors with a fiber optic array (Toposys scanners) (Leica Geosystems, 2008a; National Oceanic and Atmospheric Administration, 2008; Shan and Toth, 2009).

LiDAR data acquired from the reflected laser pulses (figure G4) are converted to raw point cloud data—a collection of range measurements (straight-line distance from platform system to the imaged ground surface) and sensor orientation pa-
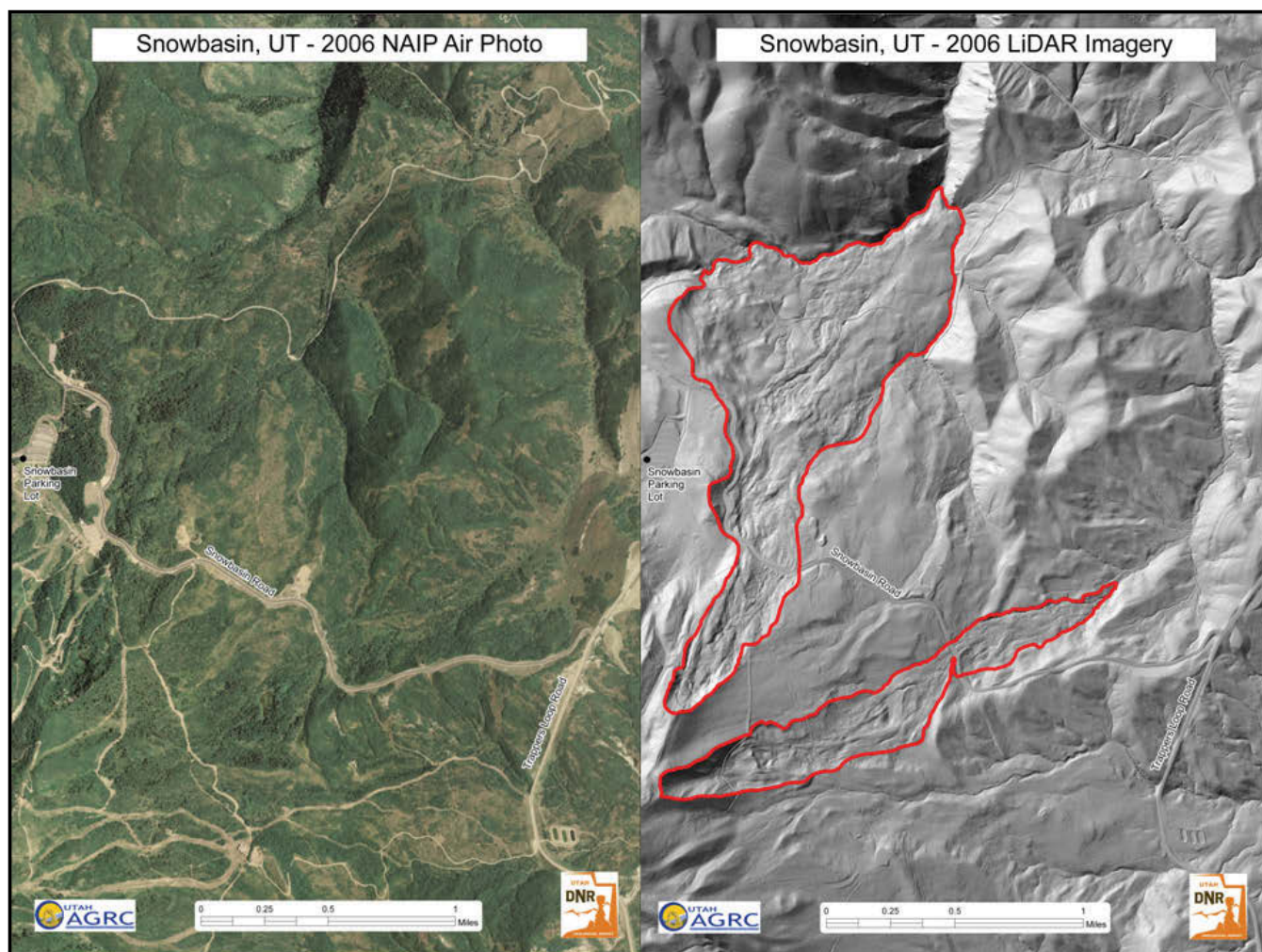
Figure G1. *Comparison of 2006 National Agriculture Imagery Program (NAIP) 1-meter color orthophoto imagery (left) and 2006 2-meter airborne LiDAR imagery (right) in the Snowbasin area, Weber County, Utah. Red lines outline the Green Pond and Bear Wallow landslides that are clearly visible in the LiDAR imagery, but barely visible to undetectable in the NAIP imagery. Data from the Utah Automated Geographic Reference Center (AGRC) (2006a, 2006b), and graphics generated by the Utah Geological Survey, Geologic Hazards Program, undated.*

rameters (Fernandez and others, 2007) in the LiDAR system. For use in elevation studies, the point cloud data must first be converted to bare-earth data that have vegetation removed, and then be georeferenced to a coordinate system. The point cloud data are converted by using the range and orientation of each laser shot (pulse) to place the shot in a three-dimensional reference frame (Fernandez and others, 2007). The intensity of returned laser pulses can also be used to determine general surface texture, although ground surface classification is difficult. Bare-earth LiDAR data may then be processed by a variety of remote sensing image software to develop digital elevation models (DEM), shaded-relief images at various sun (illumination) angles, or a combination of these image types.

ISSUES WITH LiDAR PROCESSING

Variable vegetation and tree canopy cover density and thickness and/or steep, mountainous terrain can result in difficult

post-acquisition processing of the raw LiDAR data to bare-earth data. Vegetation-related issues can introduce additional height error and may cause additional scattering of the transmitted laser pulse, resulting in less laser energy reflected back to the receiving sensor. Various laser backscatter methods may be used to resolve canopy height issues. These issues are typically addressed by the data acquisition vendor, during the post-acquisition processing of raw point cloud data to bare-earth data, and should be checked during a quality control process by the data purchaser before final data acceptance.

LiDAR DATA AVAILABILITY AND PROCESSING

Unlike SAR data, which are available over a wide area of Utah and for multiple time periods, LiDAR data for Utah are limited. The only currently available LiDAR data for Cedar Val-
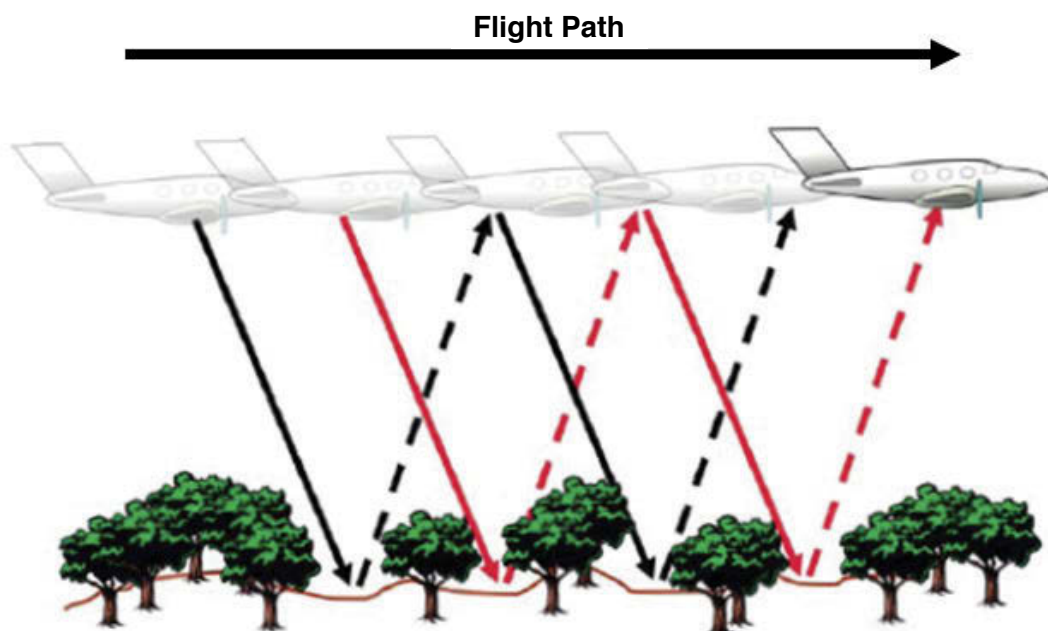
Flight Path

Figure G2. *General imaging geometry of an airborne LiDAR instrument. Dashed lines indicate reflected laser pulses that may be detected if sensor crosses the reflected path (modified from Leica Geosystems, 2008b).*
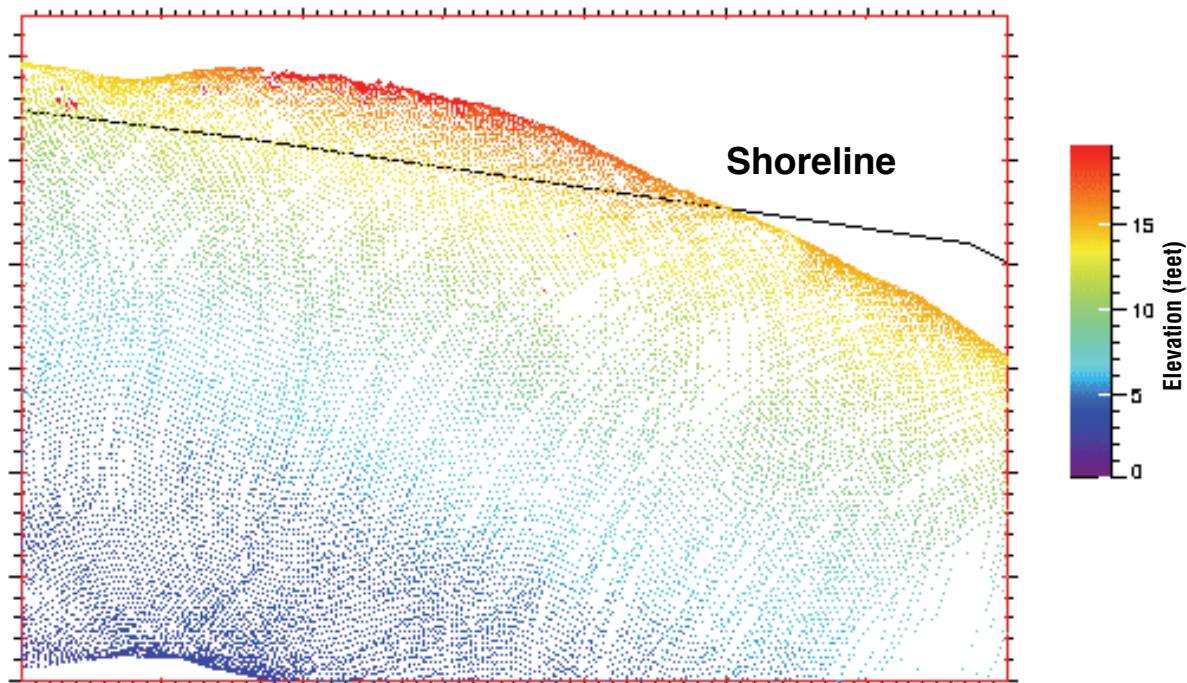

Figure G3. *Scanning swath from the ATM-2 LiDAR scanner showing oscillating scanning motion (modified from National Oceanic and Atmospheric Administration, 2008). Individual laser data points are shown as colored points.*
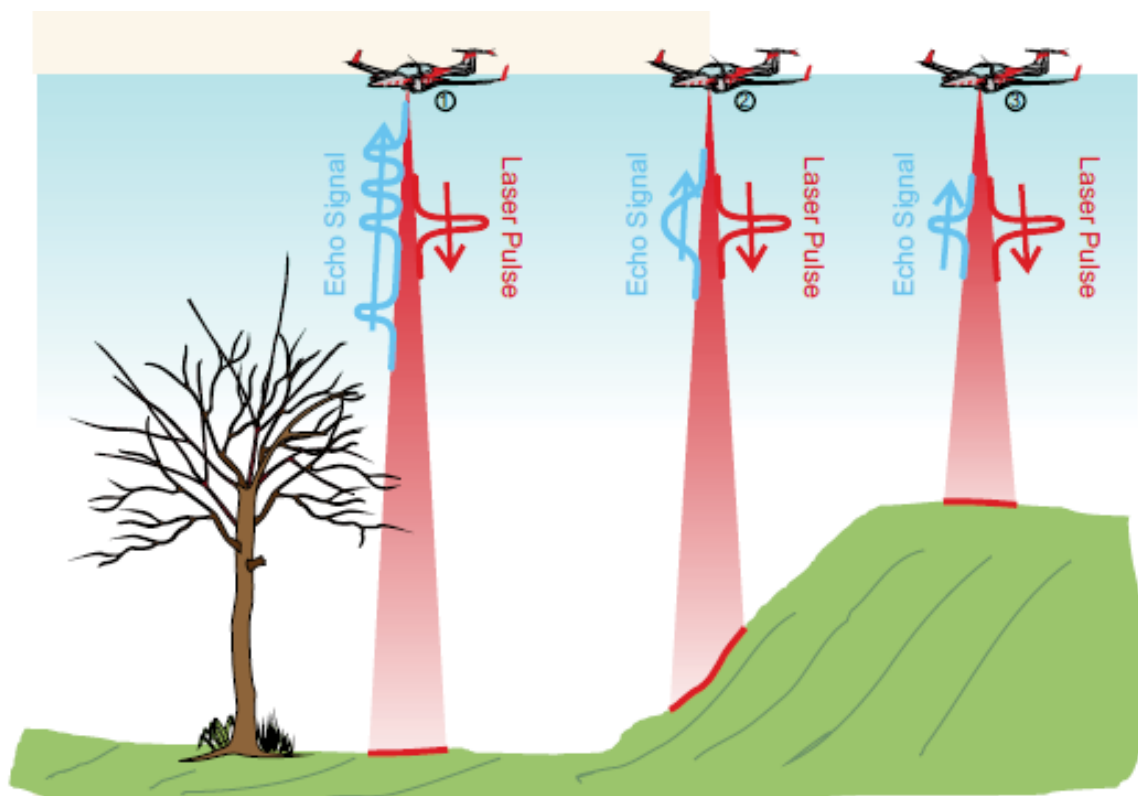
Figure G4. *Typical LiDAR transmitted and received pulses for flat, but partially obscured; sloping; and flat, smooth terrain from left to right (modified from Riegl Laser Measurement Systems GmbH, 2010).*

ley known to the UGS were acquired in 2009, by Aero-graphics, Inc. for Cedar City Corporation as part of a flood-hazard mapping study, and in 2011, by Utah State University, LASSI Service Center (LASSI) for the UGS as part of geologic-hazard mapping activities. The 2009 data cover approximately 78 square miles of Cedar Valley, out of a total area of approximately 270 square miles (Lowe and others, 2010). These data do not cover most of the area in Cedar Valley or the Enoch graben where land subsidence and subsidence-related earth fissures have been documented (Knudsen and others, 2012). Vertical accuracy of the data ranges from a minimum of -3.35 inches (-85.0 mm) to a maximum of 1.67 inches (42.4 mm), with an average of -0.37 inches (-9.4 mm), based on comparison with surveyed monuments (Aero-graphics, 2009). Data acquisition cost Cedar City Corporation $30,000 (Kit Wareham, Cedar City Corporation, written communication, 2010), or approximately $384 per square mile, a cost within typical LiDAR cost ranges. The 2011 data cover approximately 498 square miles of Cedar and Parowan Valleys, including fissure and subsidence areas. Fundamental vertical accuracy of the data is 1.97 inches (50 mm), based on comparison with surveyed monuments (LASSI, 2011). Similar LiDAR data were recently used by the UGS to identify several strands of the West Valley fault zone near Salt Lake City, Utah, where surface offsets were not easily visible or locatable in the field (figure G5).

UGS LiDAR DATA

The UGS acquires LiDAR data with its partners in support of various geologic mapping and research projects. In 2011, approximately 1902 square miles (4927 km2) of 1-meter LiDAR data was acquired for the Cedar and Parowan Valleys, Great Salt Lake shoreline/wetland areas, Hurricane fault zone, Lowry Water, Ogden Valley, and North Ogden, Utah. These datasets were funded by the UGS, with the exception of the Great Salt Lake area, which was funded by the U.S. Environmental Protection Agency and the UGS, and the North Ogden area, which was funded by the Utah Division of Emergency Management (UDEM), Floodplain Management Program. In late 2013, the UGS and its partners acquired 0.5-meter LiDAR of Salt Lake and Utah Valleys, and along the entire length of the Wasatch fault zone. For more information about UGS LiDAR acquisitions and data, see http://geology.utah.gov/databases/LiDAR/LiDAR.htm.

The 2011 LiDAR acquisition was performed by Utah State University, LASSI Service Center through a partnership with the Utah Automated Geographic Reference Center (AGRC) and the UGS. The 2013 LiDAR acquisition was performed by Watershed Sciences, Inc. through a partnership with AGRC, U.S. Geological Survey, Salt Lake County Surveyors Office, and UDEM.
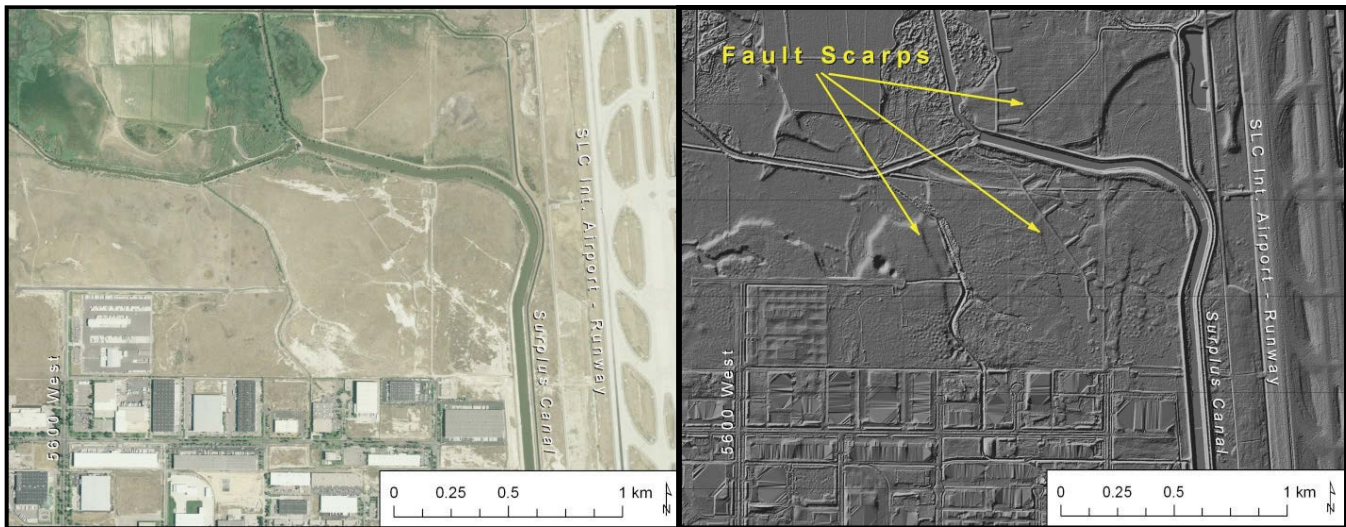
Figure G5. *Comparison of 2009 high-resolution orthophotography (HRO) 1-foot color imagery (left) and 2006 2-meter airborne LiDAR imagery (right) in the International Center area, Salt Lake City, Utah. Fault scarps indicated by yellow arrows show traces of the Granger fault, West Valley fault zone that are clearly visible in the LiDAR imagery, but barely visible to undetectable in the HRO imagery. Salt Lake International Airport visible to the right on each image. Data from the AGRC (2006b, 2009), and graphics generated by Mike Hylland, Utah Geological Survey, Geologic Hazards Program, 2010.*

The 2011 datasets include raw LAS (industry standard LiDAR format), LAS, DEM, digital surface model (DSM), and metadata (XML metadata, project tile indexes, and area completion reports) files. This LiDAR data is available from the AGRC Raster Data Discovery Application (DEM data and metadata only, http://mapserv.utah.gov/raster), is included in the U.S. Geological Survey National Elevation Dataset (http://ned.usgs.gov/) that is part of The National Map (DEM data and metadata only, http://nationalmap.gov/viewer.html), and OpenTopography (all data and metadata, http://www.opentopography.org/id/OTLAS.042013.26912.1), a National Science Foundation-supported portal to high-resolution topography data and tools. LiDAR data are not directly viewable without suitable software, such as Global Mapper, 3DEM, and ESRI ArcGIS. The datasets acquired by the UGS and its partners are in the public domain and can be freely distributed with proper credit to the UGS and its partners.

LiDAR data can be used to create DEMs, and subsequently to determine ground subsidence and for ground surface modeling. At least one repeat data acquisition is required to determine the magnitude of ground subsidence using LiDAR data. However, several repeat acquisitions would be necessary to determine the ongoing rate of ground subsidence over a specified time period. These acquisitions must be timed correctly to avoid snow cover and to have similar vegetation coverage conditions to ensure similar data processing of each LiDAR acquisition. LiDAR data are typically acquired by private aerial mapping vendors that supply bare-earth georeferenced data.

Once two or more DEMs are available over an area, they can be subtracted from each other to determine the change in elevation over a given time period. By using three or more DEMs and the corresponding elevation differences, an estimate of the rate of change in elevation can be determined. The rate of change may also be influenced by seasonal changes in groundwater levels and ground temperature that may overprint ground subsidence changes, as soil material volume changes result in an inflation or deflation signal. The major drawbacks to this method are the relatively high cost of LiDAR data when used in a repeat acquisition application and the variable vertical accuracy of the data, which can be significant if data acquisition is not carefully controlled.

REFERENCES

Aero-graphics, 2010, Cedar City LiDAR, Collection—October, 2009: Salt Lake City, unpublished consultant's report for Michael Baker Jr., Inc. (Cedar City Corporation), variously paginated.

Baltsavias, E.P., 1999, Airborne laser scanning—Existing systems and firms and other resources: ISPRS Journal of Photogrammetry & Remote Sensing, v. 54, p. 164–198.

Carter, W., Shrestha, R., Tuell, G., Bloomquist, D., and Sartori, M., 2001, Airborne laser swath mapping shines new light on Earth's topography: EOS, Transactions, v. 82, no. 46, p. 549–555.

Fernandez, J.C., Singhania, A., Caceres, J., Slatton, K.C., Starek, M., and Kumar, R., 2007, An overview of LiDAR point cloud processing software: Geosensing Engineering and Mapping, Civil and Coastal Engineering Department, University of Florida, 27 p.

Knudsen, T., Inkenbrandt, P., Lund, W., and Lowe, M., 2010, Investigation of land subsidence and earth fissures in Cedar Valley, Iron County, Utah: Utah Geological Survey contract report prepared for the Central Iron County Water Conservancy District, 118 p.

Leica Geosystems, 2008a, Leica ALS60 airborne laser scanner: Online, http://www.leica-geosystems.com/common/shared/downloads/inc/downloader.asp?id=10325, accessed November 18, 2010.

Leica Geosystems, 2008b, Leica ALS Corridor Mapper, Airborne laser corridor mapper product specifications: Online, http://www.leica-geosystems.com/common/shared/downloads/inc/downloader.asp?id=9035, accessed November 18, 2010.

Lowe, M., Wallace, J., Sabbah, W., and Kneedy, J.L., 2010, Science-based land-use planning tools to help protect groundwater quality, Cedar Valley, Iron County, Utah: Utah Geological Survey Special Study 134, 6 plates, 125 p.

Miller, B., 1965, Laser altimeter may aid photo mapping: Aviation Week & Space Technology, v. 88, i. 13, p. 60–65.

National Aeronautics and Space Administration, 2010, ICESat & ICESat-2, Cryospheric Sciences Branch, Code 614.1: online, http://icesat.gsfc.nasa.gov/, accessed November 18, 2010.

National Oceanic and Atmospheric Administration, 2008, Topographic LiDAR—An emerging beach management tool, data collection animations: Online, http://www.csc.noaa.gov/beachmap/html/animate.html, accessed November 18, 2010.

Riegl Laser Measurement Systems GmbH, 2010, Long-range airborne scanner for full waveform analysis, LMS-Q680i: Online, http://www.riegl.com/uploads/tx_pxprieglldownloads/10_DataSheet_LMS-Q680i_20-09-2010.pdf, accessed November 18, 2010.

Shan, J., and Toth, C.K., 2009, Topographic laser ranging and scanning, principals and processing: Boca Raton, Florida, CRC Press, 590 p.

Shepherd, E.C., 1965, Laser to watch height: New Scientist, v. 26, no. 437, p. 33.

Utah Automated Geographic Reference Center, 2006a, 2006 NAIP 1 meter color orthophotography: online, http://gis.utah.gov/naip2006, accessed November 18, 2010.

Utah Automated Geographic Reference Center, 2006b, 2 meter LiDAR: Online, http://gis.utah.gov/elevation-terrain-data/2-meter-LiDAR, accessed November 18, 2010.

Utah Automated Geographic Reference Center, 2009, 2009 HRO 1 foot color orthophotography: Online, http://gis.utah.gov/aerial-photography/2009-hro-1-foot-color-orthophotography, accessed December 8, 2010.

Utah Automated Geographic Reference Center, 2013, 1 meter LiDAR elevation data (2011): Online, http://gis.utah.gov/data/elevation-terrain-data/2011-LiDAR/, accessed September 3, 2013.

Utah Geological Survey, 2013, LiDAR elevation data: Online http://geology.utah.gov/databases/LiDAR/LiDAR.htm, accessed September 3, 2013.

Utah State University, LASSI Service Center, 2011, Cedar Valley, Hurricane fault, Ogden Valley, and Lowry Water LiDAR acquisition; Iron, Emery, Sanpete, Washington, and Weber Counties, Utah; Completion report: Logan, unpublished consultant's report for the Utah Automated Geographic Reference Center (Utah Geological Survey), 27 p.: Online, http://geology.utah.gov/databases/LiDAR/pdf/LiDAR_Report.pdf.

APPENDIX H

RECOMMENDED GUIDELINES FOR INVESTIGATING LAND-SUBSIDENCE AND EARTH-FISSURE HAZARDS

by William R. Lund

These guidelines provide professional geologists with standardized minimum recommended guidelines for investigating land-subsidence and earth-fissure hazards, particularly in areas known or suspected to be subsiding due to aquifer overdraft (groundwater mining). The guidelines do not include systematic descriptions of all available investigative techniques or topics, nor is it suggested that all techniques or topics are appropriate for every project. Variations in site conditions, project scope, economics, and level of acceptable risk may require that some topics be addressed in greater detail than is outlined in these guidelines. However, all elements of these guidelines should be considered in all comprehensive land-subsidence- and earth-fissure-hazard investigations, and may be applied to any project site, large or small.

These guidelines are largely modified from existing guidelines for preparing engineering geologic reports in Utah (Utah Section of the Association of Engineering Geologists, 1986), guidelines for evaluating surface-fault-rupture and land-subsidence hazards in Nevada (Nevada Earthquake Safety Council, 1998), and guidelines for evaluating surface-fault rupture in California (California Geological Survey, 2002) and Utah (Christenson and others, 2003).

I.   DISCLAIMER

Land subsidence and earth fissures caused by groundwater pumping in excess of recharge are human-induced geologic hazards that typically affect a broad area, and that will continue to occur and expand as long as groundwater mining continues. Additionally, subsidence may continue in a diminished fashion for some time after groundwater mining has ceased. The fact that land subsidence is not currently occurring in an area experiencing groundwater mining provides no guarantee that subsidence will not commence there in the future. Likewise, the absence of detectable earth fissures at the ground surface in a subsiding area provides no assurance that fissures are not present in the shallow subsurface or will not form in the future. As long as groundwater mining continues, land subsidence and earth fissures present long-term hazards to infrastructure that a hazard investigation, no

matter how detailed, can only partially identify and mitigate. To ensure the safety of existing infrastructure and future development in subsiding areas, it is necessary to bring aquifer discharge and recharge into balance so that subsidence stops and hazards dissipate.

Other geologic and human-induced phenomena (such as near-surface soil desiccation [giant desiccation cracks], collapsible soil, highly organic soil, sinkhole formation, soil piping, and underground mining) can also cause subsidence and earth fissures. These guidelines apply specifically to land subsidence and earth fissures related to groundwater mining, but may be applicable when investigating other causes of land subsidence and earth fissures as well.

II.   WHEN TO PERFORM A SUBSIDENCE/FISSURE HAZARD INVESTIGATION

An investigation of potential land-subsidence and earth-fissure hazards should be made for all proposed development in areas of known or suspected land subsidence resulting from groundwater mining. Additionally, a land-subsidence and earth-fissure hazard investigation may become necessary for existing infrastructure in or adjacent to areas known or suspected to be subsiding.

The level of investigation conducted for a particular project depends on several factors, including site-specific geologic and hydrologic conditions, type of proposed or existing development, level of risk acceptable to property owners, and requirements of permitting and regulatory agencies or other governmental entities. A land-subsidence- and earth-fissure-hazard evaluation may be conducted separately or as part of a comprehensive geologic-hazard and/or geotechnical site investigation.

III.   INVESTIGATION DESCRIPTION

A.   Minimum Qualifications of Investigator

Geologic studies of land-subsidence and earth-fissure hazards performed before the public (Utah Code, Title 58, Chapter 76, Section 102 [3]) shall be conducted by

or under the direct supervision of a Utah licensed Professional Geologist, who must sign and seal the final geologic and/or geotechnical report. The evaluation of land-subsidence and earth-fissure hazards is a specialized area within the practice of engineering geology, requiring expertise and knowledge of techniques not commonly used in other geologic disciplines. In addition to meeting the qualifications for geologist licensure in Utah, minimum recommended qualifications of the engineering geologist in charge of a land-subsidence- and earth-fissure-hazard investigation should include five years of experience in a responsible position in the field of engineering geology. This experience should include an in-depth familiarity with local geology and hydrology, and direct knowledge of appropriate techniques for performing land-subsidence- and earth-fissure-hazard investigations.

Geologists performing land-subsidence- and earth-fissure-hazard investigations are ethically bound to protect public safety and property, and as such must adhere to the highest ethical and professional standards in their investigations. Conclusions, drawn from information gained during the investigation, should be consistent, objective, and unbiased. Relevant information gained during an investigation may not be withheld. Differences in opinion regarding conclusions and recommendations and perceived levels of risk may arise between geologists performing investigations and agency-employed or retained geologists working as reviewers for a public agency. Adherence to these minimum guidelines should reduce differences of opinion and simplify the review process.

Detailed investigation and mitigation of land-subsidence and earth-fissure hazards in complex or high-risk situations are best accomplished through an interdisciplinary approach involving the expertise of several professional disciplines (e.g., engineering geology, civil and geotechnical engineering, hydrology, land surveying, geophysics). Engineering and land surveying activities performed as part of a land-subsidence and earth-fissure hazards investigation performed before the public shall be conducted under the direct supervision of a Utah licensed Professional Engineer or Utah licensed Professional Land Surveyor, who must sign and seal the final investigation report.

B.   Literature Review

The following published and unpublished information (as available) should be reviewed as part of the investigation:

   a.   Published and unpublished geologic and engineering literature, maps, and records relevant to the site and site region's geology and hydrology, and past history of land subsidence and earth-fissure formation. The UGS web page for consultants and design professionals (http://geology.utah.gov/ghp/consultants/index.htm) contains relevant information for many locations in Utah.

   b.   Survey data that may indicate past land subsidence, particularly as-built plans of linear infrastructure such as roads, canals, dams, airport runways, and levees for historical elevation data, or as-built design grades that can be compared to current elevations. Be aware of any historical vertical datum changes and/or shifts, including geoid changes.

   c.   Maintenance records of nearby wells for signs of subsidence-related damage.

   d.   Water-level data and subsurface geologic units from nearby water well and geotechnical borehole logs (if available). Water-level data may be available from the U.S. Geological Survey National Water Information System (http://waterdata.usgs.gov/nwis) and UGS Groundwater Monitoring Data Portal (http://geology.utah.gov/databases/groundwater/projects.php). The UGS GeoData Archive System (https://geodata.geology.utah.gov) contains scanned geotechnical and other reports that may contain water-level data for many areas in Utah.

   e.   Borehole geophysical data, if available, from deep wells in the area.

   f.   Pumping history of nearby water wells.

C.   Analysis of Remote Sensing Data

Analysis should include interpretation of aerial photographs, and if available, interferometric synthetic aperture radar (InSAR), light detection and ranging (LiDAR) imagery, and other remotely sensed images for evidence of land subsidence and fissure-related lineaments, including vegetation lineaments, gullies, and vegetation/soil contrasts. Where possible, the analysis should include both stereoscopic low-sun-angle and vertical aerial photography. Examination of repeat aerial photographs and/or LiDAR imagery from multiple years may show fissure growth. The area interpreted should extend sufficiently beyond the site boundaries to identify off-site subsidence areas or fissures that might affect the site.

Aerial photography of Utah is available from the online UGS Aerial Imagery Collection application at http://geology.utah.gov/databases/imagery/. LiDAR data for Utah are available from the UGS at http://geology.utah.gov/databases/LiDAR/LiDAR.htm, the Utah Automated Geographic Reference Center at http://gis.utah.gov/data/elevation-terrain-data/, and OpenTopography at http://opentopo.sdsc.edu/gridsphere/gridsphere?cid=datasets.

The best possible understanding and characterization of subsidence is critical to land-subsidence- and earth-fissure-hazard investigations. The importance of satellite-based InSAR data to achieving that understanding cannot be overemphasized. Where ground surface conditions are

compatible with the technology, InSAR data can depict recent subsidence patterns and magnitudes over large areas, and (if archived data are available) has the potential to map subsidence back to about 1992. InSAR's potential has been demonstrated by the Arizona Department of Water Resources (ADWR, 2010). ADWR processes InSAR data and makes subsidence results available for several actively subsiding basins in Arizona. Additionally, examples from Utah showing land subsidence in southwest Utah measured with InSAR (Forster, 2006, 2012; Katzenstein, 2013) can be found at http://geology.utah.gov/ghp/consultants/pubs/iron.htm. Appendix F presents additional information about the InSAR technique, satellite imagery acquisition and processing, and cost.

D. Surface Investigation

Surface investigation should include mapping of geologic and soil units, fissures, faults or other geologic structures, geomorphic features and surfaces, vegetation lineaments, animal burrowing patterns, and deformation of engineered structures both on and beyond the site, as appropriate. Special attention should be paid to linear infrastructure such as roadway pavements, canals, dams, levees, airport runways, etc. Level surveys of linear infrastructure and comparison with as-built elevations may be appropriate to detect the presence or absence of measurable subsidence, and in the case of dams, levees, and other fluid conveyance and retention facilities, should be mandatory to determine if infrastructure integrity and safety have been compromised. Observed features should be documented with detailed photographs, including metadata (date, location, feature observed, etc.).

E. Subsurface Investigation

Earth fissures tend to be vertical to near-vertical features extending to depths typical for most subsurface investigative techniques. In an uneroded state, the aperture of an earth fissure may be 0.25 to 1 inch (4 to 25 mm) or less, and may be open or filled. Situations may arise where surficial expression of earth fissures is lacking, but the presence or absence of shallow subsurface earth fissuring that could lead to future surface expression needs to be assessed. Lateral subsurface investigation methods such as trenching or shallow geophysics (see Section F) tend to be most effective in these situations. Subsurface characterization may be especially important when assessing whether subsurface conditions are consistent with a surface feature being a subsidence-related earth fissure or a giant desiccation crack. Subsurface investigation techniques may include, but are not limited to:

a. Trenching or test pits with appropriate logging and documentation to permit detailed and direct observation of continuously exposed geologic units, soils, fissures, and other geologic features. This includes trenching across known earth fissures or suspicious zones to determine the location

and width of fissures and fissure zones, general fissure geometry and depth, and displacement, if any, across fissures. When uneroded or filled, earth fissures are often very subtle features, so logging should be performed in sufficient detail to detect these features. Considerable cleaning of loose materials associated with the excavation process from trench and test pit walls may be required to adequately expose fissures and other features of subsurface geology.

Excavating to appropriate investigation depths may necessitate the use of stepped excavations and/or shoring to provide safe access for cleaning and preparing trench and test pit walls for detailed investigation and logging. See Occupational Safety and Health Administration Technical Manual Section V, Chapter 2 (http://www.osha.gov/dts/osta/otm/otm_v/otm_v_2.html) and applicable federal, state, and local excavation regulations for guidance.

b. Boreholes and cone penetrometer testing (CPT) soundings to permit collection of data on geologic units and groundwater and to verify fissure plane geometry. Vertically focused investigation methods such as boreholes or CPT technologies are useful for general subsurface characterization in a potential fissure zone; however, an uneroded earth fissure in the subsurface is a very small target for vertically directed investigation methods. Data points should be sufficient in number and adequately spaced to permit reliable correlations and interpretations. However, it will likely not be possible to observe an earth fissure in a borehole.

CPT soundings should be done in conjunction with continuously logged boreholes to correlate CPT data with the physical characteristics of subsurface geologic units. The number and spacing of CPT soundings and boreholes should be sufficient to adequately interpret site stratigraphy. The existence and location of fissures based on CPT data are interpretive.

F. Geophysical Investigations

Geophysical investigations are indirect, non-destructive methods that can be reliably interpreted when site-specific surface and subsurface geologic conditions are known. Geophysical methods should seldom be employed without knowledge of site geology; however, where no other subsurface geologic information is available, geophysical methods may provide the only economically viable means to perform deep geologic reconnaissance.

Although geophysical methods can be used to detect the presence and location of shallow earth fissuring, such methods alone never prove the absence of a fissure or

fault at depth. Geophysical methods can provide critical information concerning subsidence potential, especially compressible basin-fill and bedrock geometry that may not otherwise be available. Geophysical techniques used may include, but are not limited to, high-resolution seismic reflection, ground penetrating radar, seismic refraction, magnetic profiling, electrical resistivity, and gravity.

Rucker and Fergason (2009) presented the results of a recent subsidence and earth-fissure investigation that demonstrates the integrated application of InSAR, gravity, electrical resistivity, and refraction microtremor (ReMi) seismic methods for site characterization (http://www.eegs.org/fasttimes/files/ft1401_mar2009_low.pdf). A case study by the Laboratory for Advanced Subsurface Imaging (2009) employed side-by-side testing of shallow seismic refraction, ground penetrating radar, electromagnetic resistivity/conductivity, and magnetic profiling for site characterization at both a subsidence-related earth fissure and a giant desiccation crack in an alluvial basin setting (http://www.lasi.arizona.edu/GEN%20416%20 2009%20Final%20Report.doc). For fissure and desiccation crack analysis, it was found that many geophysical methods were useful in areas near open fissures, but where there was no obvious sign of a fissure at the surface. Magnetic surveys provided strong correlations with suspected fissures. With good three-dimensional processing, ground penetrating radar proved reliable for finding fissures and desiccation cracks. Seismic studies were promising for identifying fissures, but did not appear to pick out shallower desiccation cracks.

G. Other Methods

Other methods should be incorporated when conditions permit or requirements for critical structures or facilities require more intensive investigation or monitoring over extended time periods. Possible methods may include, but are not limited to:

a. Aerial reconnaissance flights, including high-resolution aerial photography when applicable.

b. Installation of piezometers.

c. High-precision surveying or geodetic measurements, including comparison surveys with infrastructure design grades and long-term monitoring employing repeat surveys. Highly stable survey monuments are required, such as those developed by UNAVCO; see http://facility.un-avco.org/kb/questions/104/UNAVCO+Resour ces%3A+GNSS+Station+Monumentation for details.

d. Strain (displacement) measurement both at the surface and in boreholes as part of a long-term monitoring program (Galloway and others, 1999).

e. Geochronologic analysis, including but not lim-ited to radiometric dating (e.g., ^{14}C, $^{40}Ar/^{39}Ar$), optically stimulated luminescence or thermoluminesence techniques, soil-profile development, fossils, tephrochronology, and dendrochronology.

IV. RECOMMENDED OUTLINE FOR A LAND-SUBSIDENCE- AND EARTH-FISSURE-HAZARD INVESTIGATION REPORT

A recommended minimum outline for land-subsidence- and earth-fissure-hazard investigation reports is presented below. The report should be prepared, stamped, and signed by a Utah licensed Professional Geologist with experience in conducting land-subsidence- and earth-fissure-hazard investigations. Reports co-prepared by a Utah licensed Professional Engineer or Utah licensed Professional Land Surveyor should include the engineer's and/or surveyor's stamp and signature.

A.   Text

a. Purpose and scope of investigation, including a description of the proposed project.

b. Geologic and hydrologic setting, including previous land subsidence and earth fissures on or near the site.

c. Site description and conditions, including dates of site visits and observations. Include information on geologic and soil units, hydrology, topography, graded and filled areas, vegetation, existing structures, presence of fissures on or near the site, evidence of land subsidence, and other factors that may affect the choice of investigative methods and interpretation of data.

d. Methods and results of investigation.

   1. Review of published and unpublished maps, literature, and records regarding geologic units, faults, geomorphic features, surface water and groundwater, previous land subsidence and earth fissures.

   2. Interpretation of remote sensing imagery including stereo aerial photographs, and LiDAR and InSAR images.

   3. Results of surface investigation including mapping of geologic and soil units, faults, fissures, and other geomorphic features.

   4. Results of subsurface investigation including test pits, trenching, boreholes, CPT soundings, and geophysical investigations.

e. Conclusions

   1. Location and existence (or absence) of land subsidence and earth fissures on or adjacent to the site and existing/proposed infrastructure.

2. Statement of relative risk that addresses the probability or relative potential for future earth fissure formation or growth of existing fissures and the rate and amount of anticipated land subsidence. This may be stated in semi-quantitative terms such as low, moderate, or high as defined within the report, or quantified in terms of fissure growth rates or land subsidence rates.

3. Degree of confidence in, and limitations of, the data and conclusions. Evidence on which the conclusions are based should be clearly stated and documented in the report.

f. Recommendations

1. Setback distances from fissures or areas of anticipated fissure growth, including justification for the setback chosen with supporting data.

2. Mitigation measures to control fissure growth and reduce structural damage, such as preventing surface water from entering fissures, strengthening structures that must bridge fissures, and using flexible utility connections in subsidence areas or where utilities cross fissures displaying differential displacement.

3. Limitations on the investigation and recommendations for additional investigation to better understand or quantify the hazard.

4. Construction testing, observation, inspection, and long-term monitoring.

B. References

a. Literature and records cited or reviewed; citations should be complete.

b. Remote sensing images interpreted; list type, date, project identification codes, scale, source, and index numbers.

c. Other sources of information, including well records, personal communication, and other data sources.

C. Illustrations

a. Location map – showing site location and significant physiographic and cultural features.

b. Site development map – showing site boundaries, existing and proposed structures, graded and filled areas (including engineered and non-engineered fill), streets, exploratory test pits, trenches, boreholes, and geophysical traverses.

c. Geologic map(s) – showing distribution of bedrock and unconsolidated geologic units, faults or other geologic structures, geomorphic features,

earth fissures, areas of subsidence, and, if available, InSAR results. For large projects (dams, canals, pipelines, etc.), a regional geologic map and regional InSAR results also may be required to adequately depict all important geologic features and recent land subsidence trends.

d. Geologic cross sections, if needed, to provide three-dimensional site representation.

e. Logs of exploratory trenches, test pits, CPT soundings, and boreholes – showing details of observed features and conditions. Logs should not be generalized or diagrammatic. Trench and test pit logs should show geologic features at the same horizontal and vertical scale.

f. Geophysical data and interpretations.

g. Photographs that enhance understanding of site surface and subsurface (trench and test pit walls) conditions with applicable metadata.

D. Appendices

Supporting data not included in the body of the report (e.g., water-well data, survey data, etc.).

E. Authentication

Report signed and sealed by a Utah licensed Professional Geologist in principal charge of the investigation. Reports co-prepared by a Utah licensed Professional Engineer or Utah licensed Professional Land Surveyor must include the engineer's or surveyor's stamp and signature.

V. ACKNOWLEDGMENTS

VI. REFERENCES

Arizona Department of Water Resources, 2010, Interferometric Synthetic Aperture Radar, Hydrology, Geophysics Surveying Unit: Arizona Department of Water Resources: Online, http://www.azwater.gov/AzDWR/Hydrology/Geophysics/InSAR.htm, accessed October 23, 2010.

California Geological Survey, 2002, Guidelines for evaluating the hazard of surface fault rupture: California Geological Survey Note 49, 4 p

Christenson, G.E., Batatian, L.D., and Nelson, C.V., 2003, Guidelines for evaluating surface-fault-rupture

hazards in Utah: Utah Geological Survey Miscellaneous Publication 03-6, 14 p.

Forester, R.R., 2006, Land subsidence in southwest Utah from 1993 to 1998 measured with Interferometric Synthetic Aperture Radar (InSAR): Utah Geological Survey Miscellaneous Publication 06-5, 35 p.

Forster, R.R., 2012, Evaluation of interferometric synthetic aperture radar (InSAR) techniques for measuring land subsidence and calculated subsidence rates for the Escalante Valley, Utah, 1998 to 2006: Utah Geological Survey Open-File Report 589, 25 p.

Galloway, D.L., Jones, D.R., and Ingebritsen, S.E., editors, 1999, Land subsidence in the United States: U.S. Geological Survey Circular 1182, variously paginated.

Katzenstein, K., 2013, InSAR analysis of ground surface deformation in Cedar Valley, Iron County, Utah: Utah Geological Survey Miscellaneous Publication 13-5, 43 p.

Laboratory for Advanced Subsurface Imaging, 2009, Geophysical investigation of subsidence fissures near Wilcox, Arizona: University of Arizona 2009 Geophysics Field Camp, LASI 09-1: Online, http://www.lasi.arizona.edu/GEN%20416%202009%20Final%20Report.doc, accessed October 23, 2010.

Nevada Earthquake Safety Council, 1998, Guidelines for evaluating potential surface fault rupture/land subsidence hazards in Nevada: Nevada Earthquake Safety Council, 7 p

Rucker, M.L. and Fergason, K.C., 2009, Geophysics in geotechnical investigations and mitigations of distressed flood control dams: FastTimes, v. 14, no. 1, p. 33–42.

Utah Section of the Association of Engineering Geologists, 1986, Guidelines for preparing engineering geologic reports in Utah: Utah Geological and Mineral Survey Miscellaneous Publication M, 2 p.